LOAN DOCUMENT

AD-A252 128

DTIC ACCESSION NUMBER

PHOTOGRAPH THIS SHEET

LEVEL

INVENTORY

(1)

Proceedings of the 15th Annual Gravity Gradiometry Conference Vol. 1

DOCUMENT IDENTIFICATION

11-13 Feb 87

DISTRIBUTION STATEMENT A

Approved for public release;
Distribution Unlimited

DISTRIBUTION STATEMENT

ACCESSION FOR

NTIS GRA&I ☒
DTIC TRAC ☐
UNANNOUNCED ☐
JUSTIFICATION

BY

DISTRIBUTION/

AVAILABILITY CODES

DISTRIBUTION	AVAILABILITY AND/OR SPECIAL	
A-1		

DISTRIBUTION STAMP

DTIC
ELECTE
JUN 2 4 1992
S C D

DATE ACCESSIONED

DATE RETURNED

92

DATE RECEIVED IN DTIC

92-16509

REGISTERED OR CERTIFIED NUMBER

PHOTOGRAPH THIS SHEET AND RETURN TO DTIC-FDAC

HANDLE WITH CARE

DTIC FORM JUN 90 70A

DOCUMENT PROCESSING SHEET

PREVIOUS EDITIONS MAY BE USED UNTIL STOCK IS EXHAUSTED

LOAN DOCUMENT

AD-A252 128

Proceedings

of the

Fifteenth Annual Gravity Gradiometry Conference

United States Air Force Academy
Colorado Springs, Colorado

11-13 February, 1987

VOLUME I

Compiled By:

Capt Vishnu V. Nevrekar, USAF
Earth Sciences Division
USAF Geophysics Laboratory
Hanscom AFB, MA 01731

A MERCURY MANOMETER GRAVITY GRADIOMETER

by

G. Ian Moore
Frank D. Stacey
Gary J. Tuck

Department of Physics
University of Queensland
Brisbane, Australia

ABSTRACT

We present the design of a gravity gradiometer based on the principles of a mercury manometer. The gradiometer consists of two identical manometers separated vertically by 1 meter. The pressure difference required to support the mercury columns is maintained in gas chambers above pools at each end of the mercury columns and is servoed to keep the lower column height constant. A change in the vertical gravity gradient leads to a change in the upper column height. The column heights are monitored using capacitance micrometry. Using the lower manometer as a pressure reference and servoing to a constant pressure removes the requirements of absolute temperature stability and dimensional stability of the pressure chambers.

A Mercury Manometer Gravity Gradiometer

G. Ian Moore, Gary J. Tuck, Barry D. Goodwin and Frank D. Stacey.

Department of Physics

University of Queensland,

Brisbane Australia.

Inroduction:

The gravity group at the Physics Department of the University of Queensland is currently developing a gradiometer based on the principles of a mercury manometer. The design has the advantage of using relatively simple technology and has a target sensitivity useful in both geophysical surveying and fundamental gravitational experiments.

Design principle:

The principle of the gradiometer design is based on the simple relationship between the height of a mercury column and the hydrostatic pressure difference between the two mercury surfaces. By way of introduction, consider a manometer as shown in Fig 1. This consists of two mercury pools, separated by 0.5m and connected by a fine capillary tube. The pressure difference required to support the height of the mercury column is maintained in the gas chambers above each pool and is simply given by,

$$\Delta P = P_L - P_U = \rho g H \qquad ---(1)$$

where ρ is the density of the mercury, g the acceleration due to gravity

and H the column height. Generally a manometer is used to detect changes in the pressure difference, however we are interested in keeping the pressure difference constant and observing small changes in the local gravitational acceleration by way of a change in the column height. Small changes in this height can be monitored using capacitance micrometry to measure the changes in the gap between each mercury surface and a stainless steel electrode fixed above it on the supporting framework. Provided the requirement of constant pressure difference can be met, the manometer can be used as a simple vertical axis accelerometer or gravimeter. A simple calculation shows that the absolute temperature must be maintained to the same precision as that desired for the gravimeter. For an instrument capable of detecting changes as small as 10^{-10} of g (the effect due to a gradient of 1 E over a distance of 1 metre), this is clearly impractical. Even to match the sensitivity of commonly used gravimeters (10 μGal) requires a stability of order micro degrees Kelvin which is extremely difficult.

The requirements for a very stable absolute temperature, a high degree of dimensional stability in the gas chambers and perfect gas seals make a useable gravimeter based on this principle impractical. Fortunately these problems can be greatly reduced in the design of a gradiometer.

The gradiometer is formed by coupling two single manometers as shown in Fig 2. The lower chambers of each manometer are connected by a small tube as are the upper chambers. The pressure difference across the pairs of chambers is servoed by means of an adjustable bellows to maintain the lower column height constant. Any change in the gravity difference acting on the two columns due to a change in vertical gravity gradient will lead to a small change in the height of the upper column.

Since the lower manometer now forms a precise pressure reference the absolute temperature of the instrument is no longer important. It is only necessary that temperature gradients along the length of the instrument be kept small. Also, since the pressure chambers of the manometers are directly coupled, any slight leak or dimensional change in any gas chamber becomes a common mode signal and is removed by the pressure servo.

Design details:

I. Sensitivity:

As a basis for the design we take a target sensitivity of 1 $\mathring{E}$, equal to that generally accepted as useful in terms of geophysical surveying.

For a column height of 0.5 m and a separation of 1 m between corresponding pools of the coupled manometers as shown in Fig 2, a change in gradient of 1 $\mathring{E}$ gives rise to a change in the upper column height of 0.05 nm or half of this as the detectable change in the level of a pool. This displacement comes close to the observable limit of the capacitance micrometry technique used. This technique will be discussed in more detail in part IV of this section.

The mercury pools act as pistons as the column heights change, varying the gas volume and hence the supporting pressure. This effect tends to stabilize the column heights against perturbations and therefore would reduce the sensivity of a single manometer to gravitational changes. However, in a differential instrument this problem does not arise because

we are concerned with height differences of mercury columns subjected to a common pressure difference.

II. Thermal stabilization:

There are two requirements of the thermal stabilization of the instrument. First, to maintain a stable absolute temperature and second, to maintain a constant (preferably zero) temperature gradient along the length of the instrument.

The thermal expansion of the mercury dominates the stability problem because we are concerned with thermal changes in its density relative to the thermal expansion of the stainless steel framework of the instrument. The relevant parameter is $(\alpha_{Hg} - \alpha_{ss})$ where $\alpha_{Hg} \simeq 2 \times 10^{-4}\ K^{-1}$ is the volume expansion coefficient for mercury and $\alpha_{ss} \simeq 1.7 \times 10^{-5}\ K^{-1}$ is the linear coefficient for the stainless steel. If it were necessary to obtain absolute accuracy of 1 part in 10^{10} in a single manometer then absolute temperature stability of 0.5 μK would be required and this cannot be realized. In a differential mode we formally require this precision in the temperature difference between manometers and the thermal stabilization system described below is targetted on this accuracy. This looks a difficult target but we have an internal check on strong temperature gradients, because levels in all four mercury pools are monitored. The instrument can actually measure the thermal expansion of the mercury (relative to the plastic pools and the stainless steel) in each manometer independently, although it is not clear that this will be directly useful and further developments to reduce thermal sensitivity are under consideration.

There is a residual thermal problem if the two manometers are slightly different dimensionally, but assuming matched lengths of the stainless steel spacing rods to better than 1 part in 10^4, which is easily achieved, 0.05 K absolute temperature stability suffices to avoid this problem.

The temperature stabilization system which we propose to use to achieve the above requirements is shown in Fig 3. This consists of a double circulated water jacket, the temperature of the water being controlled at a point just prior to the entry into the instrument jacket by means of a heater and thermistor feedback. The water first circulates down the inner jacket and then back up the outer jacket. The outer casing is covered with closed cell insulation and the wall between the inner and outer jackets is also well insulated. The instrument itself is housed inside an inner casing. In principle it should be possible to achieve temperature gradients of less than 2×10^{-6} K over the length of the instrument at the inner water jacket for an external temperature controlled to within 1 K. The final passive shield consisting of a layer of insulation over the copper instrument case should reduce this to less than the required 5×10^{-7} K over the length of the instrument. A completely passive thermal shield (relying on thermal conduction rather than a circulating media) which would achieve a similar result is totally impractical because of the large surface area to cross section ratio of the shielding tubes.

III. <u>Servo Bellows</u>:

The servo bellows is currently driven in two stages. Firstly with a coarse motor driven differential thread and secondly with a piezo-stack

for fine control. This is a temporary arrangement and the final servo is to be driven using an "inch-worm" device which will give fine control over a range of 6mm and remove the problems of backlash etc associated with the mechanical drive. The large force exerted by the bellows on its drive is overcome by placing the servo bellows in a chamber pressurised to very nearly the same pressure as the lower manometer chambers to which the bellows is connected.

IV. Detection System:

Between each pool and its corresponding gas chamber is an arrangement of stainless steel electrodes, detailed in Fig 4. This forms a fixed capacitance gap against which the capacitance between the mercury surface and the central electrode is compared. The technique of capacitance micrometry[1] is described with reference to Fig 5. The upper, fixed electrode and the mercury are excited in antiphase with 3 kHz (3 Vpeak) signals derived from a switchable ratio transformer. The resulting 3 kHz signal on the central electrode is detected synchronously with the excitation signal. The ratio transformer switch setting is adjusted until the detected signal is a null. The switch setting then gives a direct reading of the ratio of the two gaps. The mercury gap is then calculated from this ratio and the known fixed gap. Only the first five digits of the ratio are obtained from the ratio transformer; three more digits are obtained by measuring the out of balance signal at the final ratio transformer setting. Thus with capacitance gaps of 0.2 mm the detector sensitivity is better than 10^{-7} of this or <0.02 nm. This corresponds approximately with the expected change in a single gap for a change in gradient of 1 É.

An automatic ratio transformer bridge samples the four channels corresponding to the upper and lower pools of each manometer under computer control. The computer controls the pressure servo feedback loop and provides automatic readout of the gaps and column heights.

V. Mercury Pool Floats:

Potentially the most significant problem and one which is currently being addressed is that of rippling of the mercury surface when the instrument is vibrated. This rippling causes two problems: First, slight impurities in the mercury make the mercury stick to the stainless steel electrodes when the gap is very small. Second, and more importantly from a fundamental view point is that this rippling causes a bias in the measured capacitance gaps. This is due to the fact that the average reciprocal gap is measured and this is biased from the reciprocal of the average gap when the mercury surface is not flat as shown Fig 6.

To overcome this problem, we intend to use stainless steel floats on the mercury pools. These will be constrained by flat stainless steel springs to prevent them drifting to one side. The proposed arrangement is shown in Fig 7. The springs are etched from 0.001" sheet (Fig 8) and are designed to have a large compliance to motions perpendicular to their plane and retain a high stiffness to motions in their plane. The floats are rebated in order to avoid possible interference between the spring leaves and their lower faces.

The floats rest on supports until the mercury pools are filled and the spring anchors are machined so that the desired working gaps are

obtained with zero extension of the springs. This is important for two reasons. First, the stiffness of the springs rises rapidly with large extensions and very compliant springs are required if the sensitivity of the instrument is not to be reduced. Second, the natural bouyancy level of the floats must not be significantly altered by the springs. In the absence of springs the floats would always float at the same level in the mercury regardless of the gravitational acceleration. Since the springs may exert a non-zero force in the vertical direction, this will no longer be true as illustrated in Fig 9.

$$\delta = \frac{M}{A(\rho_{Hg}-\rho_{ss})} + \frac{ks}{gA(\rho_{Hg}-\rho_{ss})} \qquad \text{---(2)}$$

where...

δ is the flotation level of a float

M is the mass of a float

A is the cross sectional area of a float

ρ_{Hg} and ρ_{ss} are the desities of mercury and stainless steel

s is the effective operating extension of the paired springs

k is the effective spring constant of the paired springs

Hence if the gravitational field changes (for example with a gain in altitude) the level at which the floats ride in the mercury will change for each individual float, thereby voiding the measurements. Assuming a change in gravity of one part in 10^4 and requiring the natural flotation level of the floats to remain constant within the tolerance implied by the target sensivity gives the following condition,

$$\frac{ks}{gA(\rho_{Hg}-\rho_{ss})} \times 10^{-4} < 0.2 \times 10^{-10} \text{ m} \qquad \text{---(3)}$$

Assuming the operating extension of the spring can be kept to less than 0.1 mm this gives an upper limit on the spring constant of 0.14 Nm^{-1}. So the springs must be extremely compliant, at least over the very limited range of extensions expected during operation.

References:

1: STACEY, F.D., RYNN, J.M.W., LITTLE, E.C. and CROSKELL, C. Displacement and tilt transducers of 140 dB range. *J. Sci. Instrum.* Series 2, 2, 945-949 (1969).

Figure captions:

Figure 1.

Basic schematic of a single mercury manometer.

Figure 2.

Schematic of a double manometer showing interconnections of pressure chambers and servo bellows.

Figure 3.

Proposed temperature shield consisting of a double, insulated, circulated water jacket with heater and thermistor feedback. The instrument is housed inside a final passive thermal shield consisting of a layer of insulation around a heavy copper casing. The whole assembly operates in an environment stabilized to within 1 K.

Figure 4.

Stainless steel electrode configuration used to measure small changes in the height of the mercury column by the technique of capacitance micrometry.

Figure 5.

General schematic of electronics used for capacitance micrometry.

Figure 6.

Diagramatic view of rippling on the mercury surface. In general the average reciprocal gap measured by the capacitance micrometry is less than the reciprocal of the average gap.

GRADIO ACCELEROMETER

◇ Design based on **ONERA** experience in :

- ***micro-accelerometry in space :*** ***CACTUS accelerometer***
  (CASTOR-D5B satellite)

- ***three-axles accelerometer for inertial navigation***

◇ Principle :

Three-axles electrostatic suspension of a proofmass

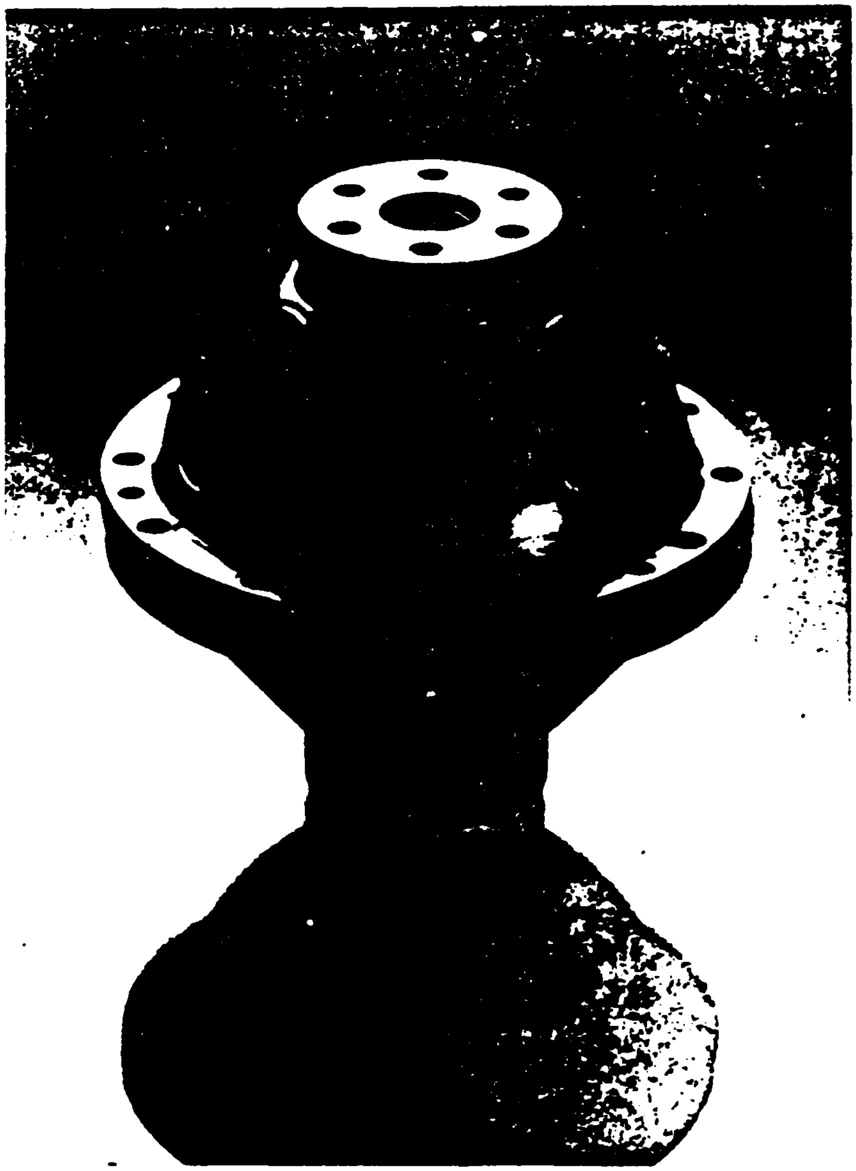

Figure 7.

Proposed arrangements of stainless steel boats and constraining springs intended to overcome the problem of rippling of the mercury surface.

Figure 8.

Detail of spring shape. These are etched from 0.001" stainless steel sheet and have a very high compliance in a direction perpendicular to the plane of the spring.

Figure 9.

The effect of a spring on the natural bouyancy of a float. The flotation level is no longer independent of g and the spring constant must be very small.

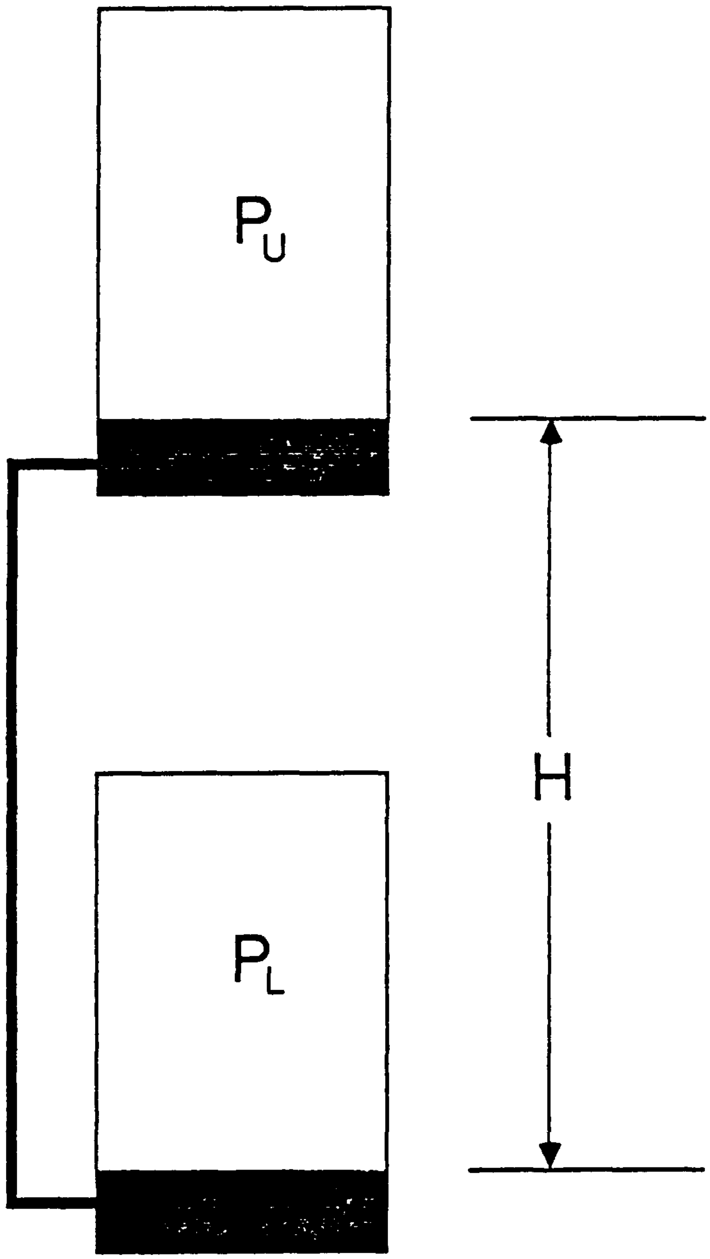

$$\Delta P = P_L - P_U = \rho \, g H$$

Fig. 1

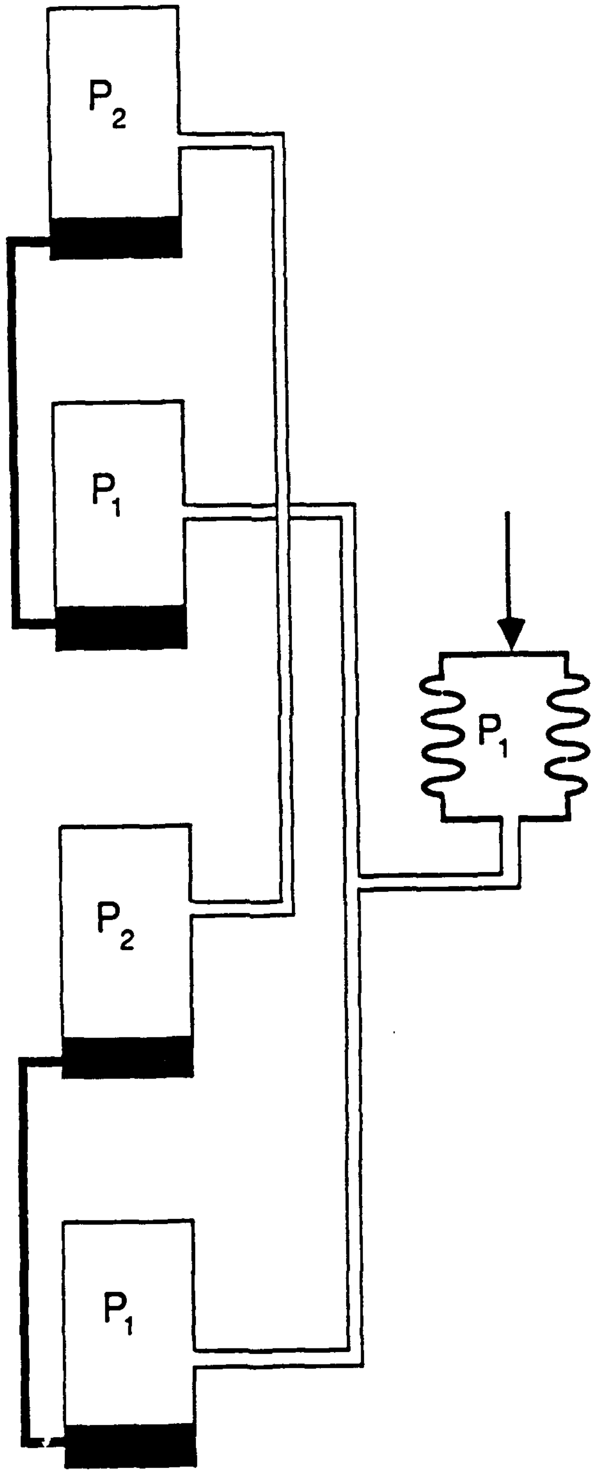

Fig 2

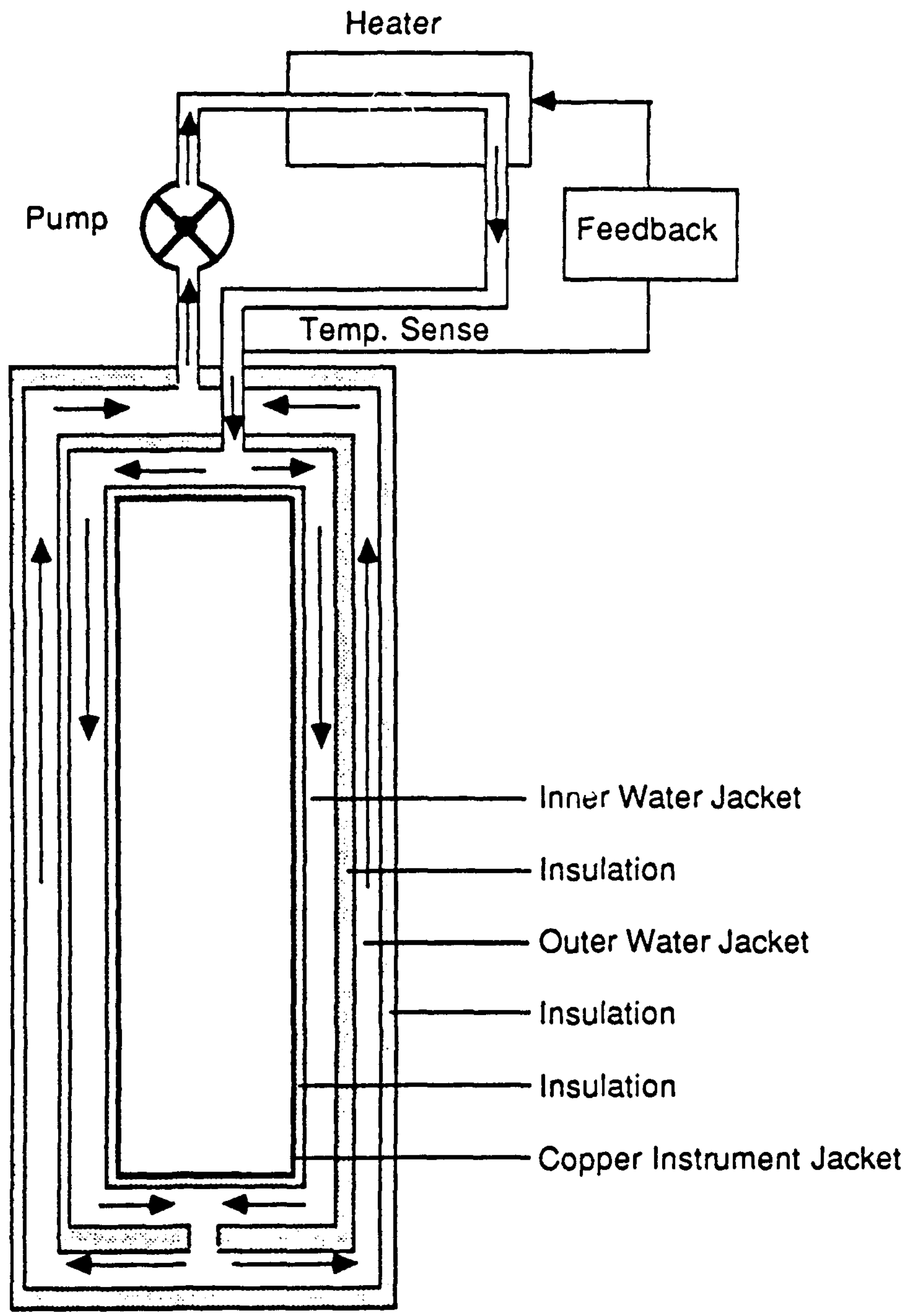
Heater
Pump
Feedback
Temp. Sense
Inner Water Jacket
Insulation
Outer Water Jacket
Insulation
Insulation
Copper Instrument Jacket

Fig. 3

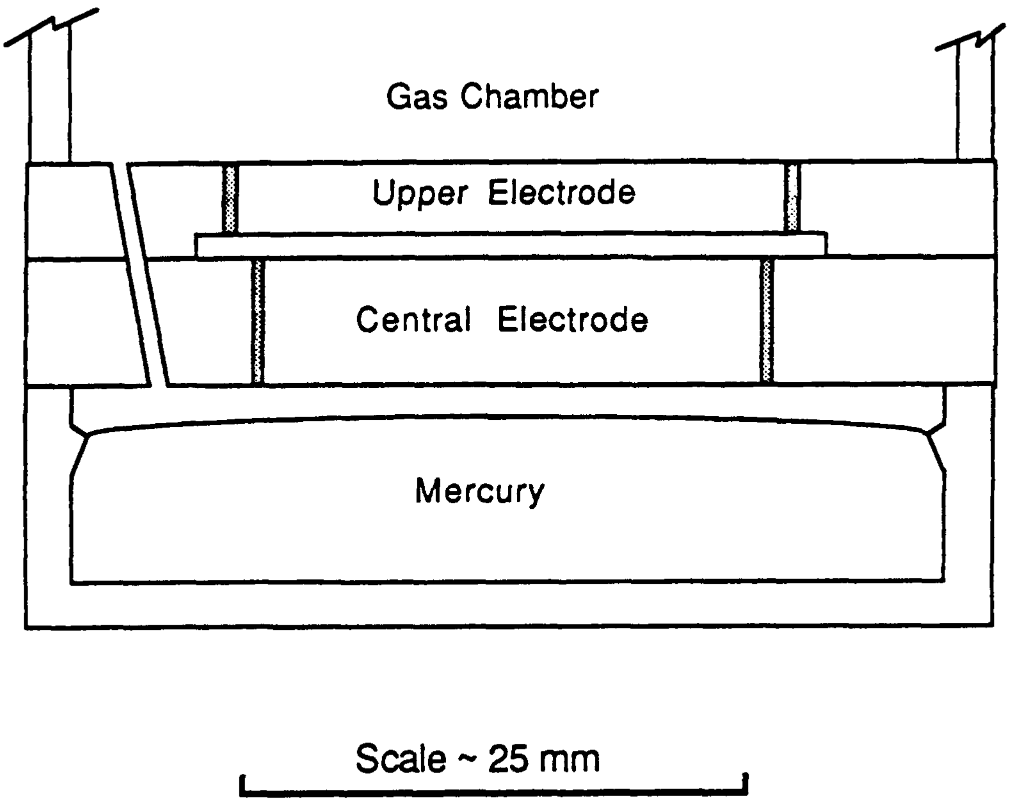

Electrode Configuration

Fig. 4

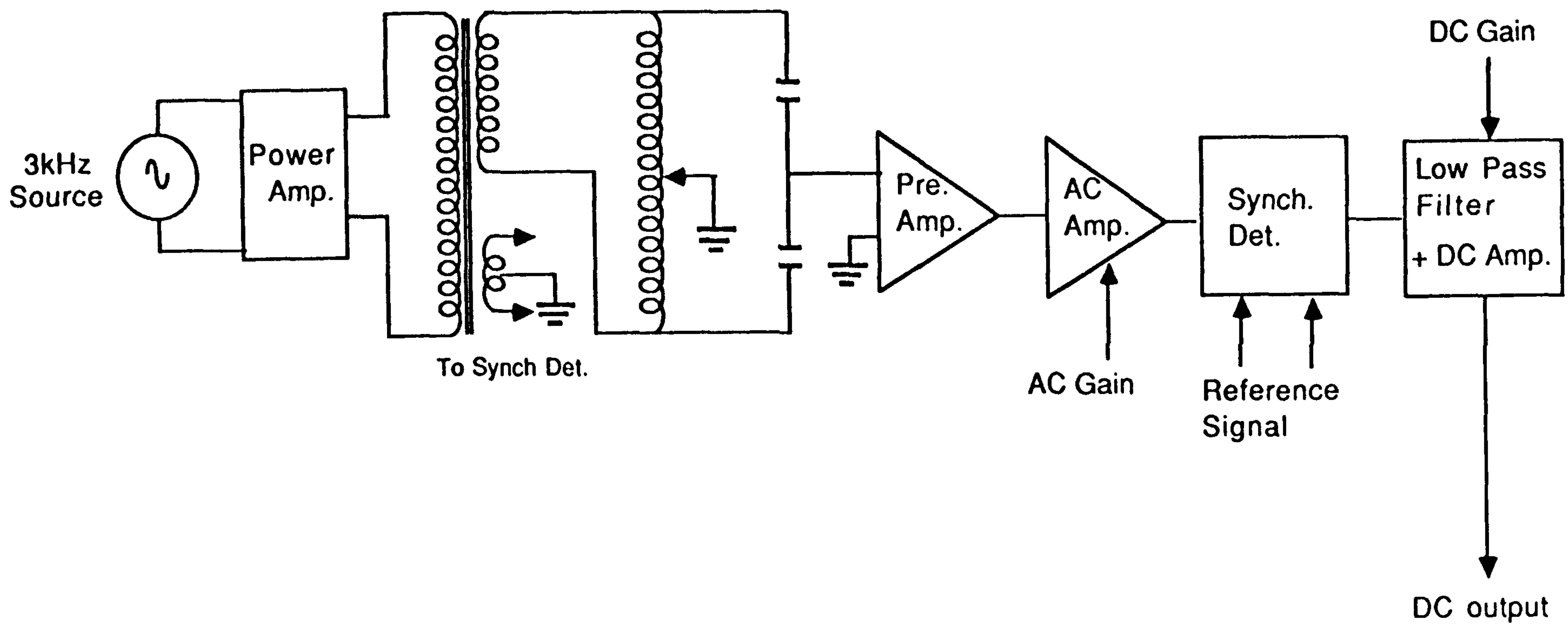
3kHz Source
Power Amp.
To Synch Det.
Pre. Amp.
AC Amp.
AC Gain
Synch. Det.
Reference Signal
DC Gain
Low Pass Filter + DC Amp.
DC output

Fig. 5

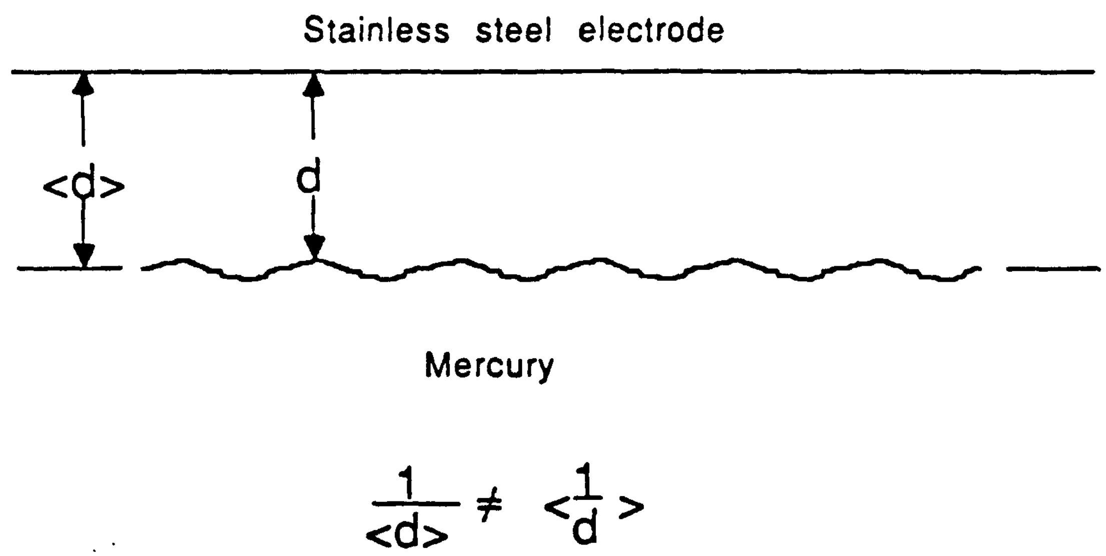

Fig. 6

GRADIOMETRY

Error budget for attitude, attitude rate and orbital position.

→ Angular and common mode acceleration rejection ratio = 10^{-5} (100 dB)
(alignment + scale factor matching)

→ Ω_0 = orbital angular frequency = 10^{-3} rd/s

For diagonal components :

$$\delta T_{xx} \simeq 2\,\Omega_0\,\Delta\Omega_y + 3\,\frac{GM}{r^3}\,\frac{\delta r}{r} + 10^{-5}\left(\mathring{\Omega} + \text{drag}\right)$$

$$\delta T_{yy} \simeq 3\,\frac{GM}{r^3}\,\frac{\delta r}{r} + 10^{-5}\left(\mathring{\Omega} + \text{drag}\right)$$

$$\delta T_{zz} \simeq 2\,\Omega_0\,\Delta\Omega_y - 3\,\frac{GM}{r^3}\,\frac{2\delta r}{r} + 10^{-5}\left(\mathring{\Omega} + \text{drag}\right)$$

Requirements : for $\delta T_{ii} < 10^{-3}$ E.U.

In the gradiometer bandwidth = 3×10^{-3} Hz − 3.10^{-1} Hz

- $\mathring{\Omega} < 10^{-7}$ rd/s² to be achieved by S.A.C.
- Accuracies of measurements :

	δT_{xx}	δT_{yy}	δT_{zz}
$\Delta\Omega_y$	5×10^{-10} rd/s	—	5×10^{-10} rd/s
δr	1.5 m	1.5 m	0.75 m

+ $\Delta\Omega_x$ and $\Delta\Omega_z$ < 10^{-6} rd/s
+ attitude = $\Delta\theta < 2\times10^{-4}$ rd
+ along track position < 1 km

GRAVITY GRADIOMETER

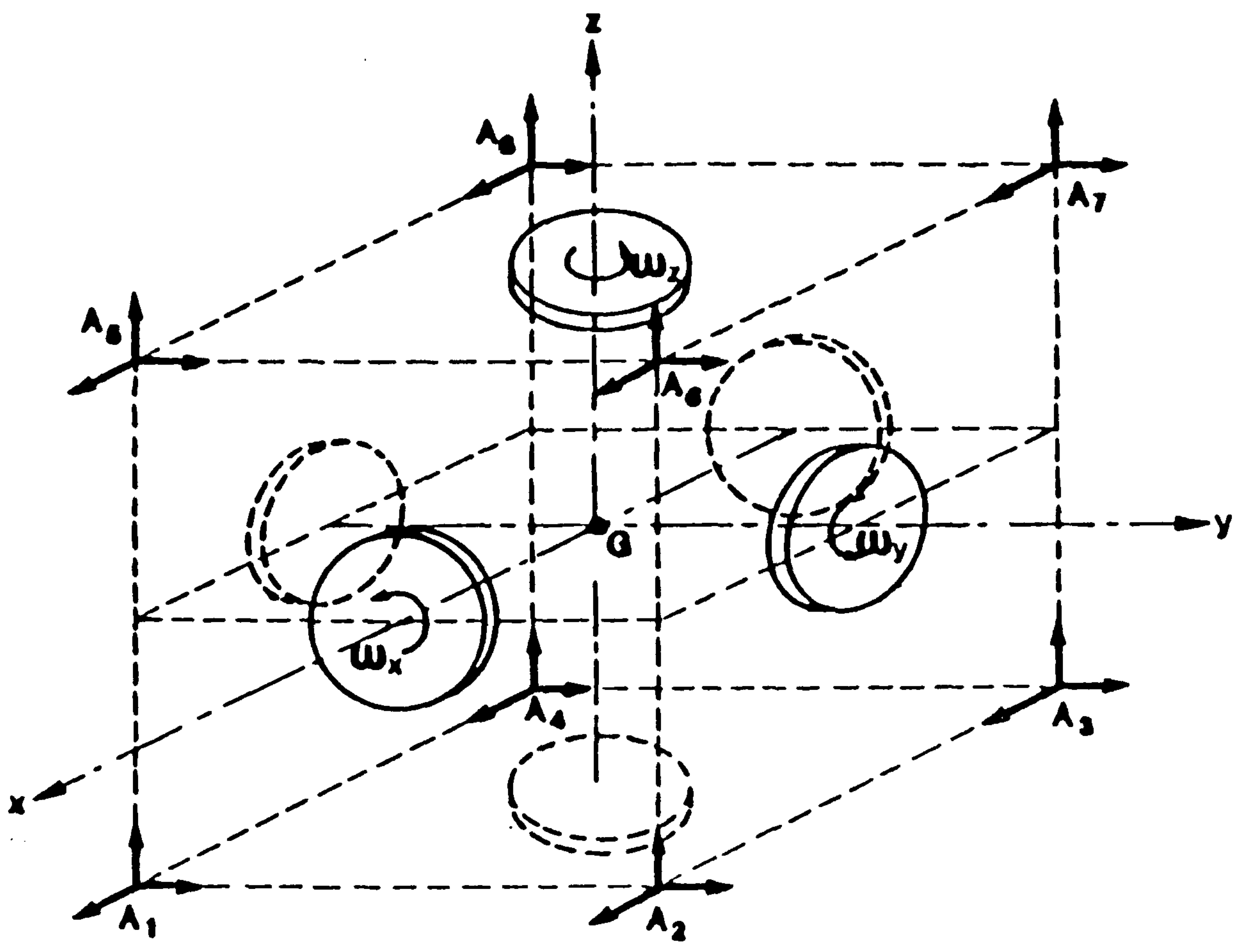

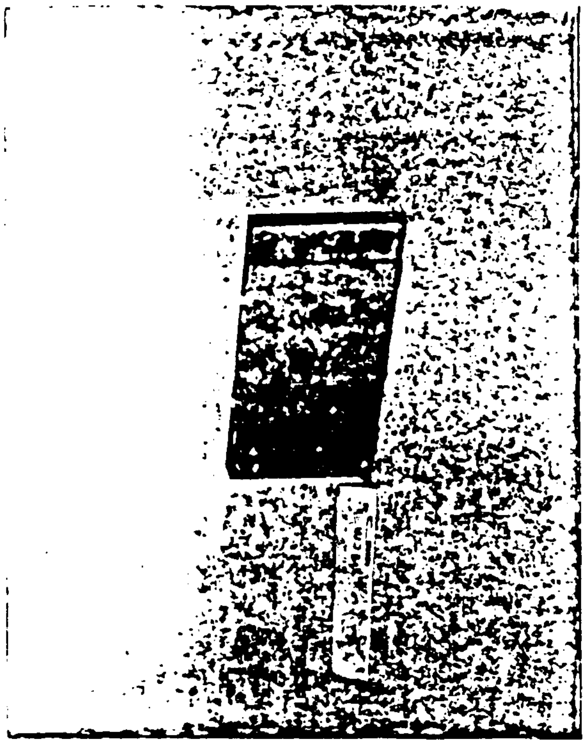

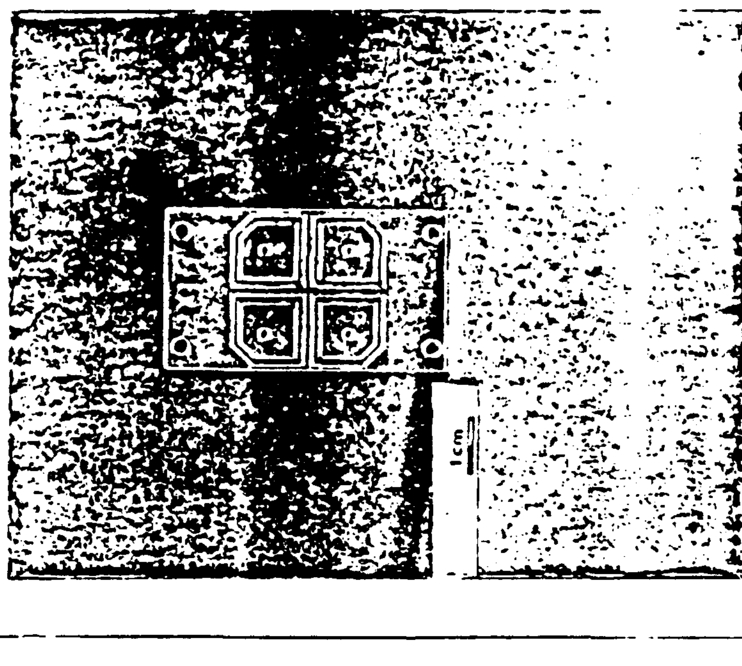

ELECTRODES

Pattern is obtained by ultra-sonic machining, then grinding

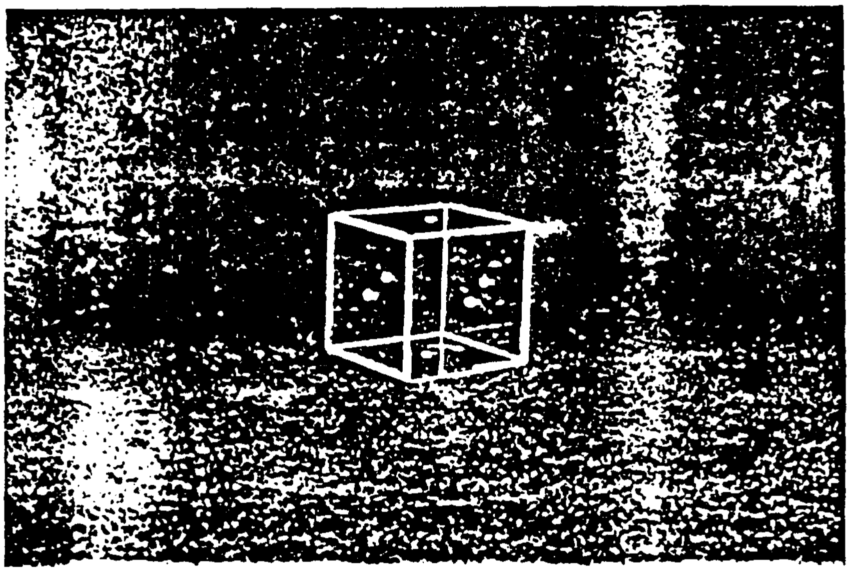

Proof mass empty silicium cube

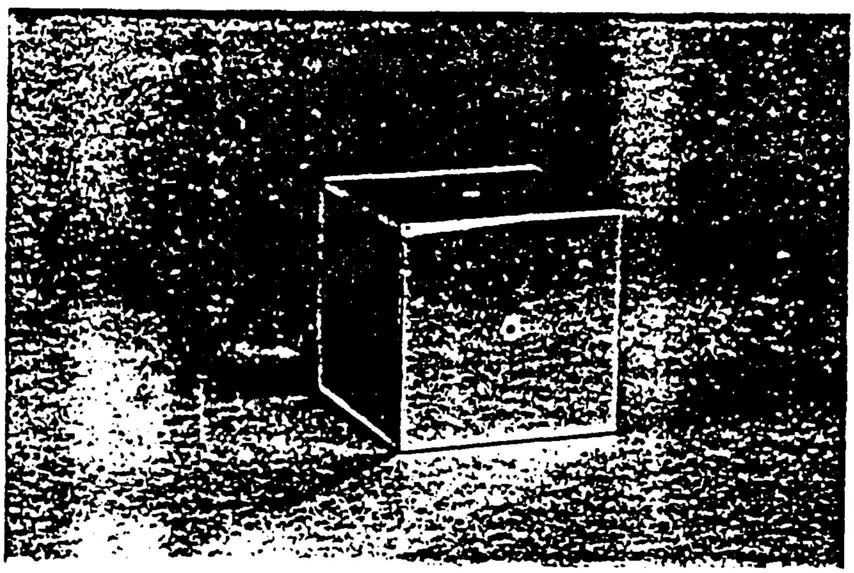

Proof mass full silicium cube

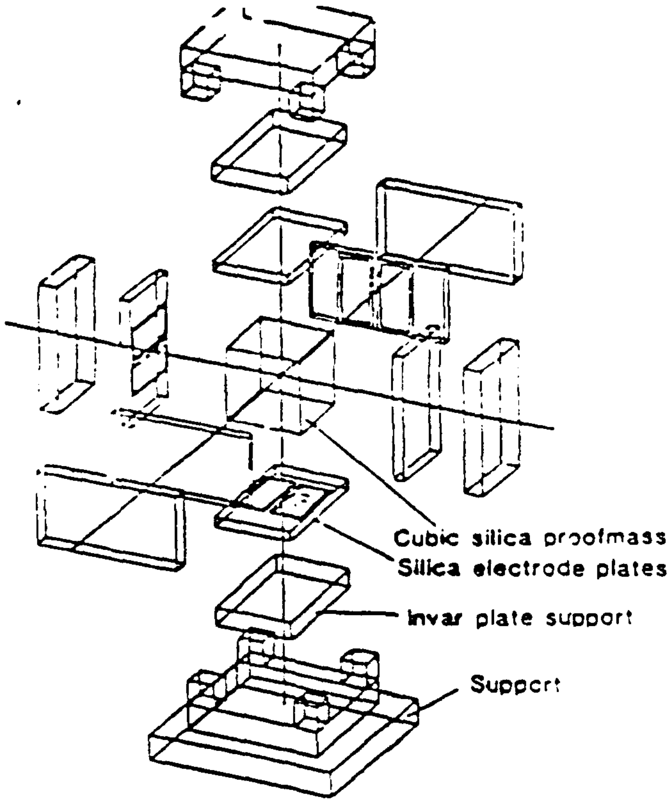

- Gradio accelerometer : arrangement of [illegible]

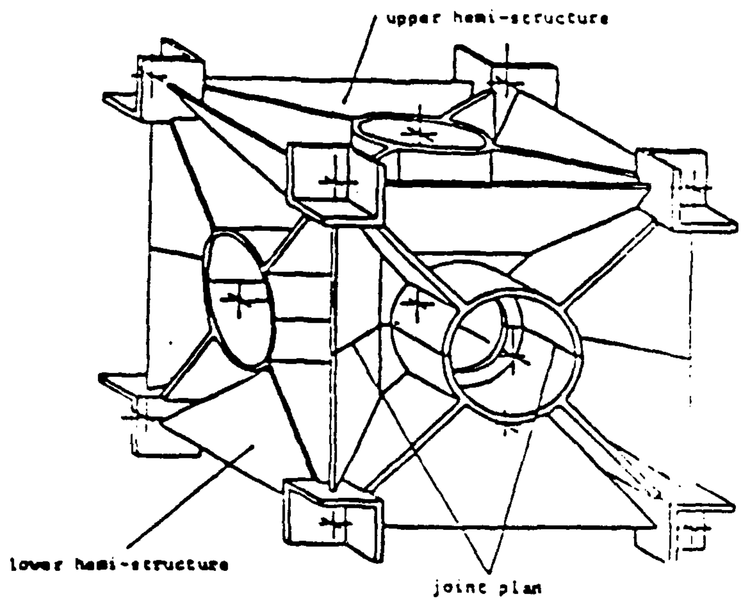

SATELLITE REQUIREMENTS

- SUNSYNCHRONOUS ORBIT, ALTITUDE 230KM, LH = 18^{H} A.N
- RESULTING OF THE FOLLOWING TRADE-OFF

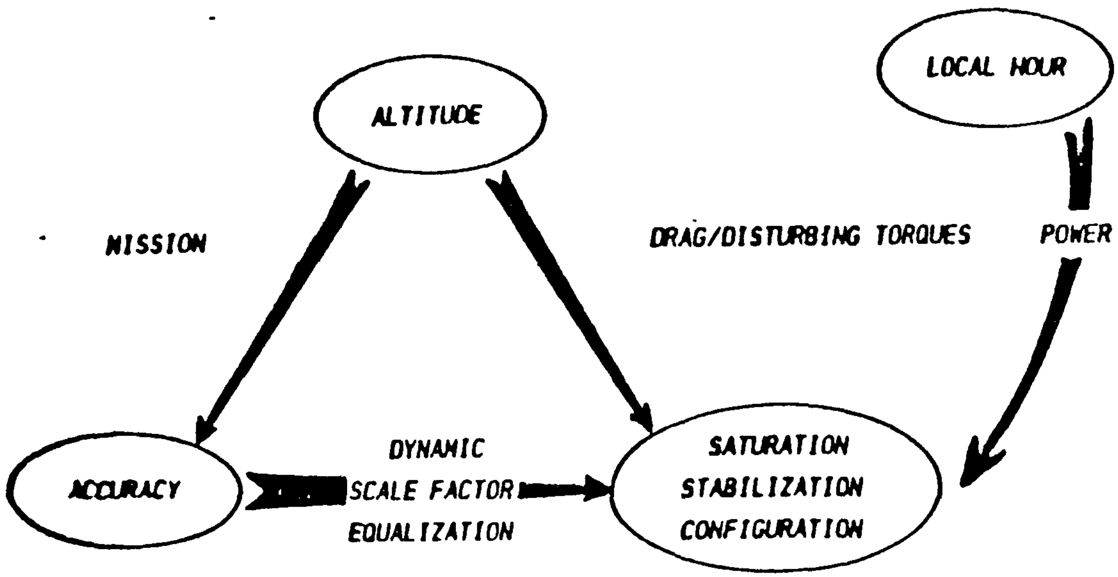

- MISSION LIFETIME 6 MONTHS
- DUAL LAUNCH WITH SPOT 4 UNDER SHORT SPELDA (REDUCTION OF LAUNCH COST) 820KM - $22^{H}30$ A.N

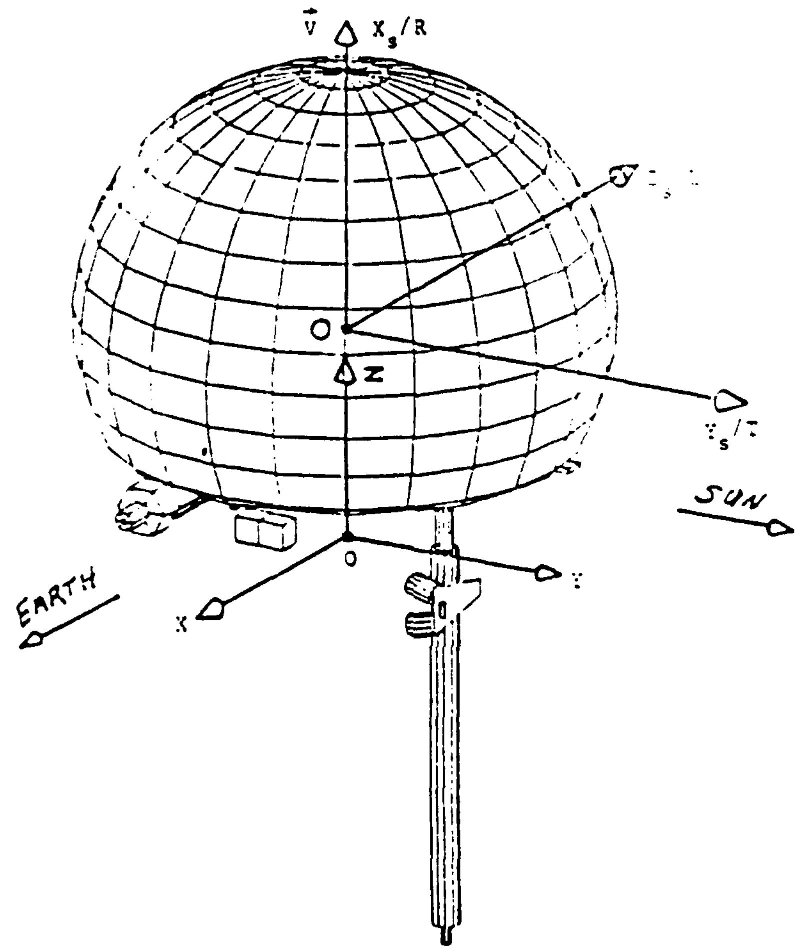

- Velocity vector : $\vec{V}$

- Satellite frame : X_S, Y_S, Z_S, R, T, L
  O_S orbital configuration satellite C.O.G.

- Structure frame : X, Y, Z
  O : launch interface center (J 1497)

(used for mathematical modelization)

MECHANICAL ARCHITECTURE

- DISTURBANCE TORQUES AS LOW POSSIBLE
  - . MAXIMA INERTIA
  - . SPHERICAL CONFIGURATION AROUND VELOCITY VECTOR (DRAG EFFECT)
  - . COINCIDENCE OF GEOMETRIC CENTER AND GRAVITY CENTER
- PAYLOAD SETTLED INSIDE THE CENTRAL TUB (MECHANICAL AND THERMAL UNCOUPLING)
- EQUIPEMENTS SHAPED ON AN EXTERNAL DECK AND THE INTERNAL DECK ON TOP OF THE TUBE UNDER THE SPOILER
- CELLS STICKEN TO THE SPOILER ON ALUMINIUM HONEYCOMB SANDWICH PANELS (PENTAGONAL AND HEXAGONAL SHAPED)
- FOUR TANKS LOADED WITH UP TO 1000 KG OF BILIQUID PROPELLANT
- MAGNETOMETRIC PAYLOAD SETTLED ON A MAST AFT ALIGNED WITH THE VELOCITY VECTOR (SEE CONFIGURATION)

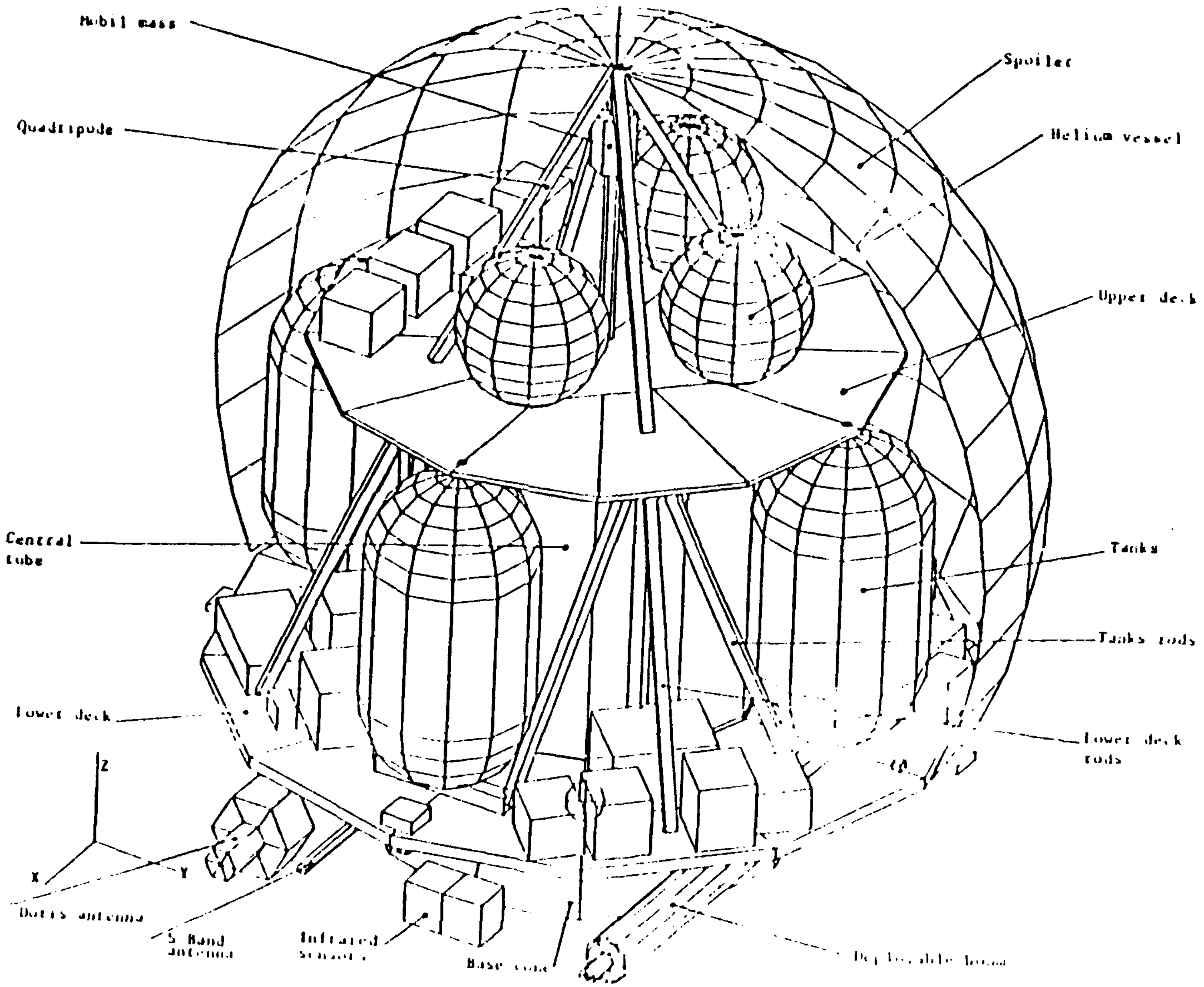

Mobil mass
Quadripode
Central tube
Lower deck
Z
X
Y
Doris antenna
S Band antenna
Infrared sensors
Base cone
Spoiler
Helium vessel
Upper deck
Tanks
Tanks rods
Lower deck rods

cnes

LAUNCH CONFIGURATION

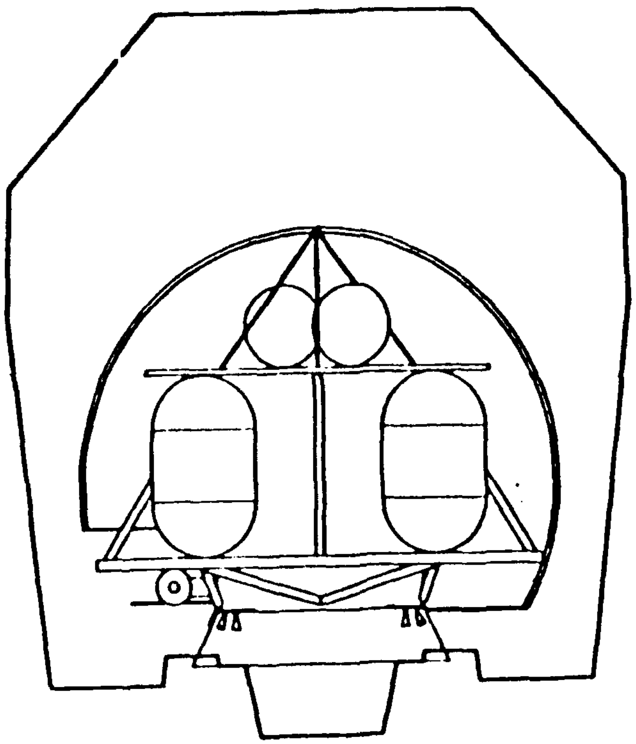

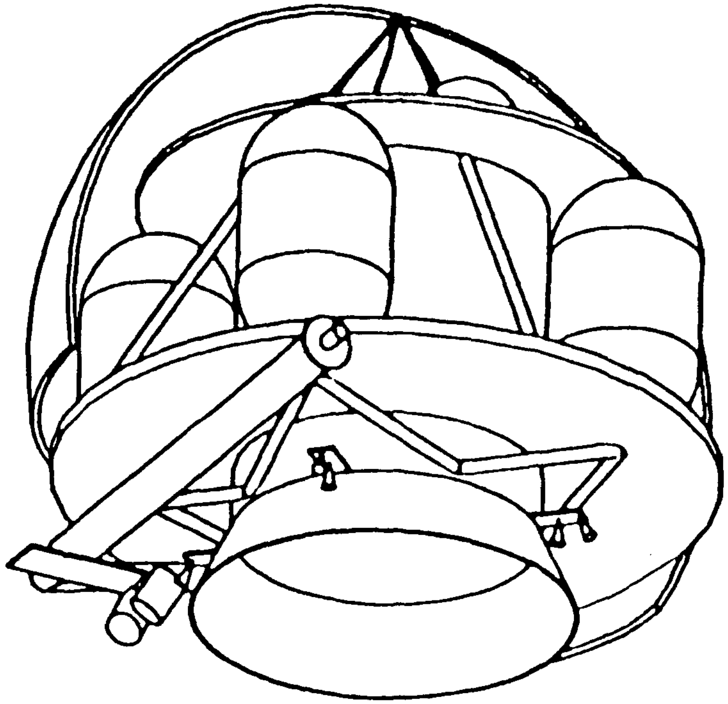

GRADIO - MAGNOLIA - MASS AND POWER BUDGETS

	MASS (KG)	POWER (W)
DRY SPACECRAFT	730*	410
PLATFORM	490	220
. STRUCTURE, SPOILER/CELLS AND THERMAL CONTROL	200	20
. POWER SUPPLY, DATA HANDLING, TTC, AOCS	150	170
. TANKS, PROPULSION (BILIQUID)	120	10
. DORIS LOCALIZATION SYSTEM	20	20
PAYLOAD	180	150
. GRADIO	130	100
. MAGNOLIA	50	50
MARGIN (10 %)	60	40
PROPELLANTS	1 000	

MAX LAUNCH CAPACITY WITH AR 44 L/SHORT SPELDA DUAL LAUNCH (SPOT 4) - 1980 KG

GRADIO - MAGNOLIA - PROPELLANTS BUDGET

TOTAL ΔV CAPACITY..	2 500 M/S
(INITIAL MASS OF PROPELLANTS = 1 000 KG)	
GRADIO ORBIT TRANSFER....................................	760 M/S
(830 KM ; $10^{30}/22^{30}$ ⟶ 230 KM ; $06^{00}/18^{00}$)	
DRIFT (6 MONTH ⟶ WEST)................................	300 M/S
FINAL ORBIT INSERTION..................................	460 M/S
GRADIO ORBIT CONTROL (6 MONTH)..........................	1 040 M/S*
(2 TIMES A DAY ; ΔH < 7 KM)	

*FOR M_{MIN} > 675 KG. $\left[\dfrac{M_{MIN}\ (KG)}{S\ (M^2)} > 110 \right]$.

ΔV AVAILABLE FOR MAGNOLIA MISSION.......................	700 M/S
(ORBIT ALTITUDE > 1 000 KM)	

GRADIO

DORIS

IMPLANTATION SCHEME OF DORIS STATIONS

GRADIO ALTITUDE : 200 KM - 15 DEGREES ELEVATION

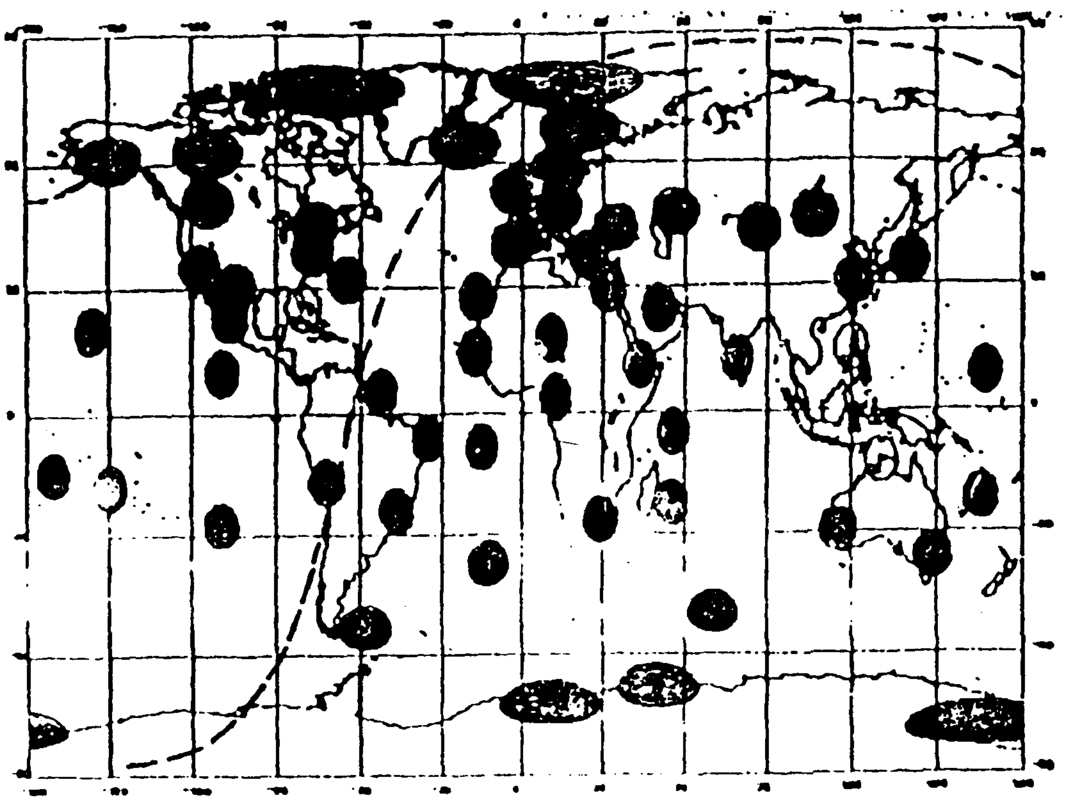

Attitude Control of the inner stage with/without GRADIO as an angular acceleration sensor

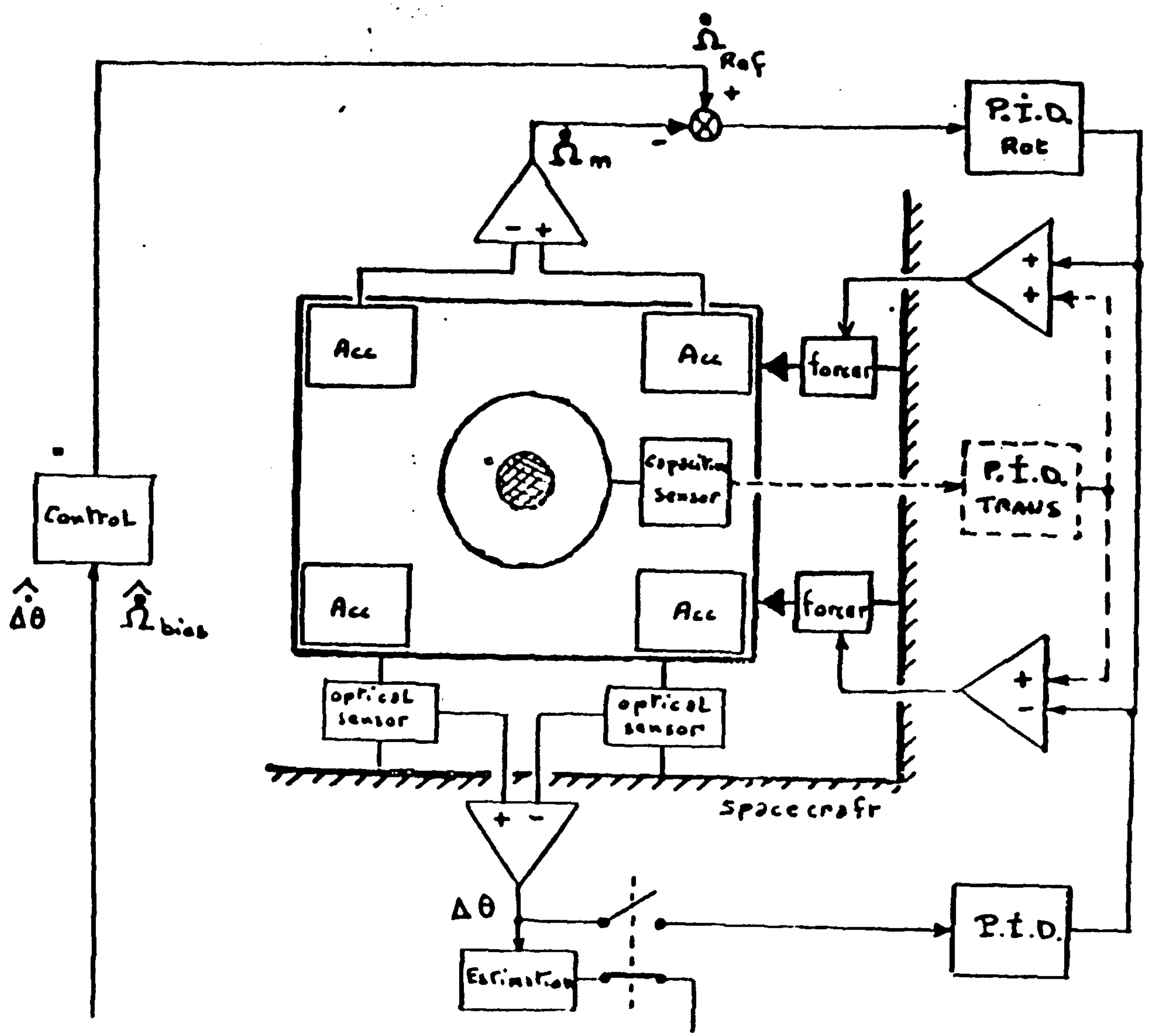

TITLE OF PAPER: GRADIO Project: High Sensitivity Electrostatic Accelerometers For Spaceborne Gradiometry

SPEAKER: Georges Balmino

QUESTIONS AND COMMENTS:

1. Question: Ho Jung Paik

   Could you go over how you get Ω out of the cross components? You have $\Omega\Delta\Omega$, but do you know $\Delta\Omega$?

   Response:

   We use star trackers and gyros for that.

2. Question: Jean-Paul Richard

   Accuracy of star trackers?

   Response:

   Star trackers accuracy = 0.01 sec of arc/sec

ELECTROSTATIC SUSPENSION

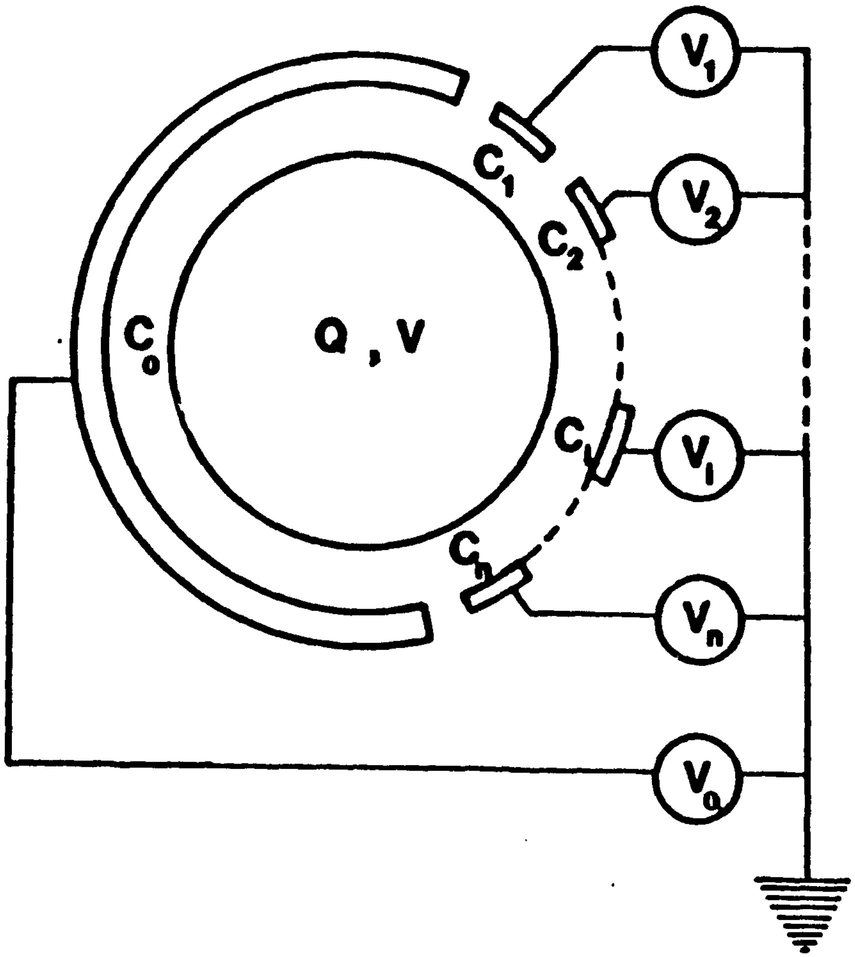

$$V = \frac{Q + \sum_{i=1}^{n} C_i V_i}{C_0 + \sum_{i=1}^{n} C_i}$$

$$\vec{F} = \frac{1}{2} \sum_{i=0}^{n} \vec{\nabla} C_i (V - V_i)^2$$

ELECTROSTATIC SUSPENSION OF A CUBE

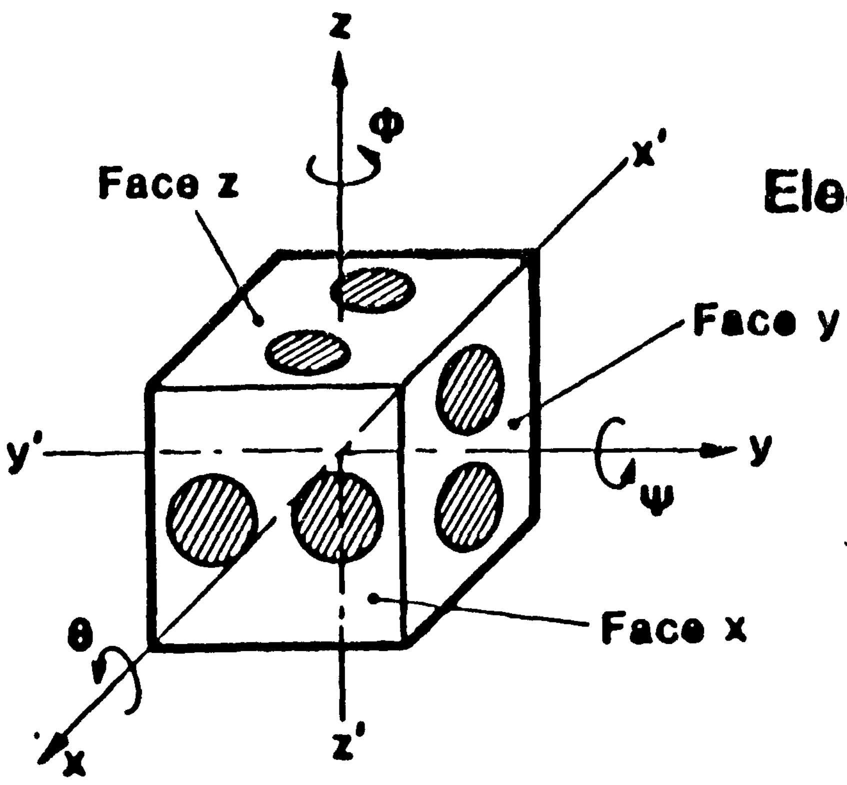

Electrodes

X	Translation	x
	Rotation	$\Phi / \vec{z}$
Y	Translation	y
	Rotation	$\theta / \vec{x}$
Z	Translation	z
	Rotation	$\psi / \vec{y}$

ELECTROSTATIC FORCE AND TORQUE

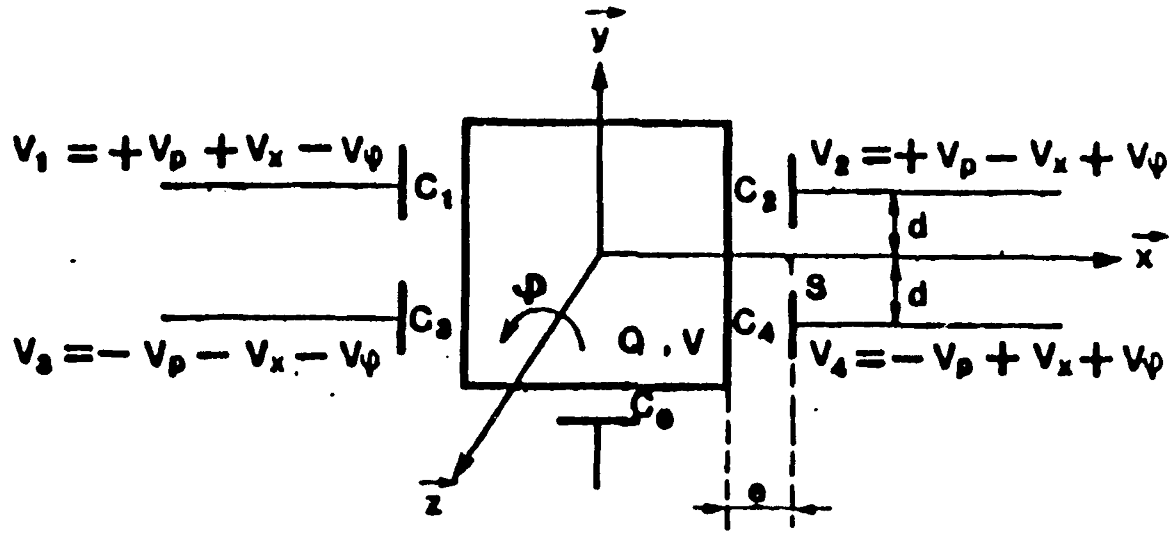

Force / $\vec{x}$: $F_x = -\dfrac{4\varepsilon S}{e^2} V_p V_x$

Torque / $\vec{z}$: $N = -\dfrac{4\varepsilon S}{e^2} d\, V_p V_\varphi$

CUBE MOTION DETECTION

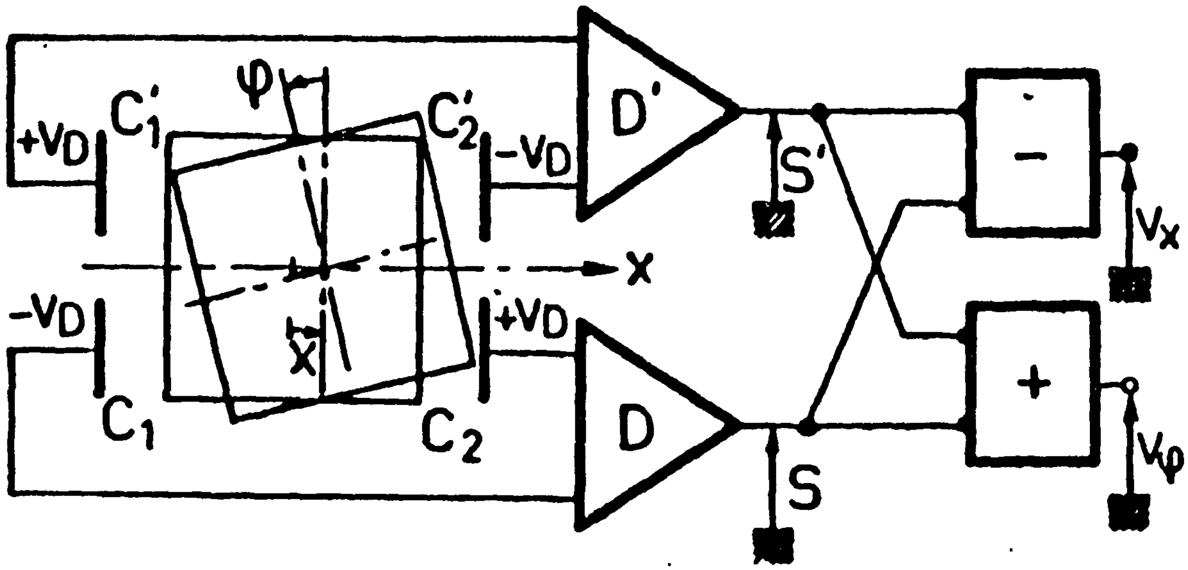

$\Delta C_1 = -ax - b\varphi$

$\Delta C_2 = +ax + b\varphi$

$\Delta C'_1 = -ax + b\varphi$

$\Delta C'_2 = +ax - b\varphi$

$$D \longrightarrow S = (\Delta C_2 - \Delta C_1) = 2\,[+ax + b\varphi]$$

$$D' \longrightarrow S' = -(\Delta C'_2 - \Delta C'_1) = 2\,[-ax + b\varphi]$$

Translation : $S - S' = 4ax$

Rotation : $S + S' = 4b\varphi$

ACCELEROMETER RESOLUTION

(Typical values)

For low frequencies (<1 Hz) :

$$\Gamma_b = \frac{4 \varepsilon S}{m e^2} \left[V_p^2 + V_{D_{eff}}^2 \right] \frac{x_b}{e} \quad ms^{-2} / \sqrt{Hz}$$

x_b resolution of capacitive position sensing :

$$x_b \simeq \frac{3.10^{-18}}{V_{D_{eff}}} \quad \frac{e^2}{2 \varepsilon S}$$

$V_p \simeq V_D \simeq 5V$	Polarization and detection voltages
$m \simeq 70$ g	Cubic proof-mass (3 cm side)
$e \simeq 300$ µm	Gap between proof-mass and electrodes
$S \simeq 2.5$ cm^2	Surface of one electrode

▶ $x_b \simeq 10^{-5}$ µm$/\sqrt{Hz}$ ▶ $\boxed{\Gamma_b \simeq 10^{-12} \ ms^{-2} / \sqrt{Hz}}$

DATA PROCESSING

Accelerometer i output :

$$\overrightarrow{V_i} = (I + [\varepsilon_i])\overrightarrow{\Gamma} + \overrightarrow{b_i} + \overrightarrow{b}_{noise}$$

$$[\varepsilon_i] \begin{cases} \text{diagonal} & : \text{ scale factor errors} \\ \text{non-diagonal} & : \text{ coupling factors} \end{cases}$$

$\overrightarrow{b_i}$: bias

Three operations must be performed :

- ◇ *digitalization*
- ◇ *alignment of the accelerometers*
- ◇ *scale factor equalization*

DIGITIZATION

* Accelerometer range : $\dfrac{10^{-4}\ ms^{-2}}{10^{-12}\ ms^{-2}} = 10^{8}$
* A / D converter : 16 bits $\longrightarrow 10^{5}$ ONLY

Use of voltage to frequency conversion :

$10^{-4}\ ms^{-2} \longrightarrow 10$ MHz

$10^{-12}\ ms^{-2} \longrightarrow 0.1$ Hz

One channel only,for each accelerometer axis, provides :

. One measurement every 10 s :

Resolution $10^{-12}\ ms^{-2}$

(10^{-3} E.U. for a 1 m base line)

. The necessary data for calibration processing

(simple dedicated algorithms)

ACCELEROMETER SCALE FACTOR AND CROSS-COUPLING COEFFICIENTS

$$\underbrace{\frac{\vec{F_i}}{m_i}}_{\text{restoring acc.}} = \underbrace{\vec{\Gamma}}_{\text{common mode}} + \underbrace{\vec{\Gamma_i}}_{\text{differential}}$$

Measure : $\vec{\gamma_i} = (I + \varepsilon_i)(\vec{\Gamma} + \vec{\Gamma_i}) + \vec{b_i} + \text{noise}$

$$\varepsilon_i = \begin{pmatrix} \varepsilon_{ix} & \varepsilon_{ix}^{y} & \varepsilon_{ix}^{z} \\ \varepsilon_{iy}^{x} & \varepsilon_{iy} & \varepsilon_{iy}^{z} \\ \varepsilon_{iz}^{x} & \varepsilon_{iz}^{y} & \varepsilon_{iz} \end{pmatrix}$$

Diagonal terms : *Error on sensitivity coefficients* : $\varepsilon_i < 10^{-2}$

Non-diagonal terms : *Cross coupling coefficients* : $\varepsilon_i^j < 10^{-3}$

$\vec{b_i}$ = Bias *(Including satellite attraction)*

COMMON MODE SINE-WAVE ACCELERATION PRODUCTION

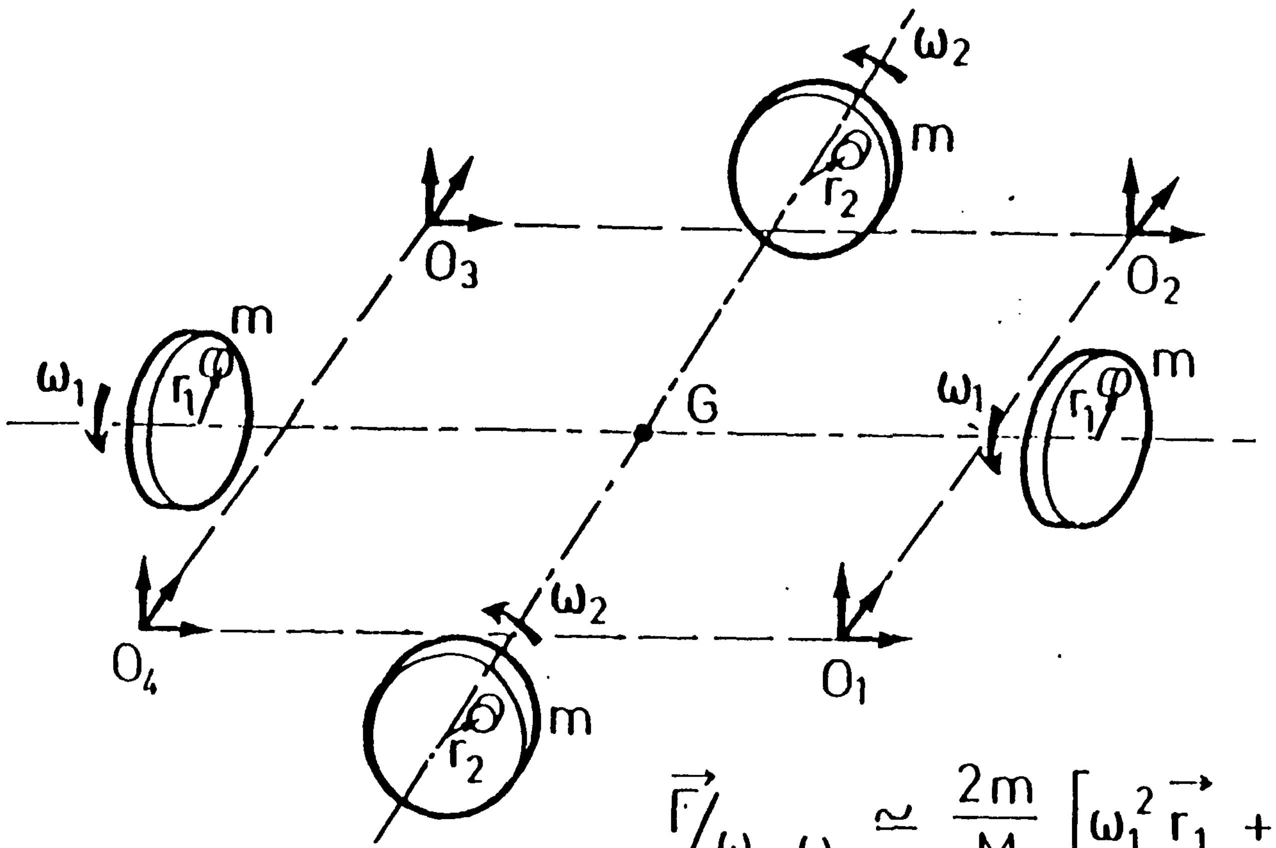

$$\vec{\Gamma}/_{\omega_1,\omega_2} \simeq \frac{2m}{M}\left[\omega_1^2\,\vec{r_1} + \omega_2^2\,\vec{r_2}\right]$$

ALIGNMENT AND SCALE FACTOR MATCHING : PRINCIPLE

* *Calibrating acceleration*

(provided by wheels of axis $\vec{x}$) $\longrightarrow$ Accelerometer measurement

$$2\,\frac{\delta m}{M}\,r\omega_x^2 \begin{pmatrix} 0 \\ \cos\omega_x t \\ \sin\omega_x t \end{pmatrix} \longrightarrow 2\,\frac{\delta m}{M}\,r\omega_x^2 \begin{pmatrix} \varepsilon_x^y \cos\omega_x t + \varepsilon_x^z \sin\omega_x t \\ (1+\varepsilon_y)\cos\omega_x t + \varepsilon_y^z \sin\omega_x t \\ (1+\varepsilon_z)\sin\omega_x t + \varepsilon_z^y \cos\omega_x t \end{pmatrix}$$

SYNCHRONOUS DEMODULATION AT ω_x :

For $\vec{x}$:
- in phase (cos) $\longrightarrow \varepsilon_x^y$
- in quadrature (sin) $\longrightarrow \varepsilon_x^z$

$\longrightarrow$ $\boxed{\vec{x} \text{ ALIGNMENT}}$

For $\vec{y}$: – in phase (cos)

For $\vec{z}$: – in quadrature (sin)

$$\longrightarrow \frac{1+\varepsilon_y}{1+\varepsilon_z} \longrightarrow \boxed{\vec{y} \text{ and } \vec{z} \text{ SCALE FACTOR MATCHING}}$$

▶ *In these demodulations , phase shifts give second order errors only*

ACCELEROMETERS : SENSITIVITY ERRORS

Measurement : $\overrightarrow{\gamma_i} = ([I] + [\varepsilon])\left\{([-T] + [\Omega^2] + [\dot{\Omega}])\,\overrightarrow{OO_i} + \overrightarrow{\Gamma_c}\right\}$

Sensitivity errors: $[\varepsilon] = \underbrace{\begin{bmatrix} \varepsilon_x & & 0 \\ & \varepsilon_y & \\ 0 & & \varepsilon_z \end{bmatrix}}_{\text{Diagonal}} + \underbrace{\begin{bmatrix} 0 & & \varepsilon_{AS} \\ & 0 & \\ -\varepsilon_{AS} & & 0 \end{bmatrix}}_{\text{Antisymmetric}} + \underbrace{\begin{bmatrix} 0 & & \varepsilon_S \\ & 0 & \\ \varepsilon_S & & 0 \end{bmatrix}}_{\text{Symmetric}}$

	Diagonal	Antisymmetric	Symmetric
	SCALE FACTORS	*COUPLING*	
Errors of :	Calibration $\varepsilon_{x,y,z} < 10^{-2}$	Alignment $\varepsilon_{AS} < 10^{-3}$	Proof-mass geometry —
	Requirement : $\varepsilon < 10^{-5}$		
	Scale factor matching	Alignment	Optical cube

Continuous calibration + data processing

CALIBRATING SYSTEM

- *The axes of the wheels determine the axes of the gradiometer :*
  Required orthogonaly : better than 10^{-5} rd.
- *For each pair, the two wants of balance have to turn in phase in two parallel planes at equal distances with respect to the satellite center of mass.*

▶Imperfections of :

$$\left.\begin{array}{l} \#\ \text{Phase}\ (\varphi) \\ \#\ \text{Centering}\ (\vec{E}) \end{array}\right\} \longrightarrow \mathring{\Omega} \text{ at } w_x, w_y, w_z$$

▶Every defect of the wheels acts as the resultant of :

a phase difference φ
a satellite off-centering $\vec{E}$.

SENSITIVITIES TO DISPLACEMENTS

In a spherical approximation and local orbital axes :

$$[T]_L \simeq \frac{GM}{r^3} \begin{bmatrix} -1 & & \\ & -1 & \\ & & 2 \end{bmatrix}$$

◇ $$\frac{\partial T_{ij}}{\partial r} = \frac{\partial T_{ij}}{\partial \lambda} = \frac{\partial T_{ij}}{\partial \Phi} = 0$$

◇ $$\frac{\partial T_{ii}}{\partial \lambda} = \frac{\partial T_{ii}}{\partial \Phi} = 0$$

◇ $$\boxed{\frac{\partial T_{ii}}{\partial r} = -\frac{3}{r} T_{ii}}$$

➡ *Gravity gradient components are not sensitive to horizontal displacements*

TRANSFORMATION OF COORDINATES : SPACECRAFT TO LOCAL ORBITAL AXES

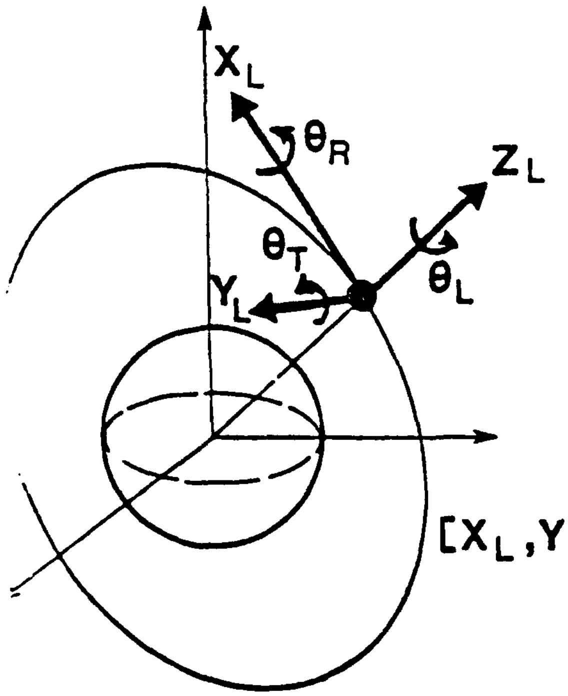

$$[X_L, Y_L, Z_L] \xrightarrow{\theta_T/\vec{y},\ \theta_L/\vec{z},\ \theta_R/\vec{x}} [x,y,z]$$

◇ Uncertainty due to errors $\delta\theta_T$, $\delta\theta_L$,$\delta\theta_R$:

$$[T]_L \simeq 3\frac{GM}{r^3}\begin{bmatrix} 0 & 0 & \delta\theta_T + \sin\theta_L\,\delta\theta_R \\ & 0 & -\delta\theta_L \sin\theta_T - \delta\theta_R \cos\theta_L \cos\theta_T \\ & & 0 \end{bmatrix}$$

◇ Earth pointing (θ_T ,θ_L ,θ_R <<1) :

T_{ij} are not sensitive to $\delta\theta_L$

(rotation about the vertical axis)

◇ Altitude 200 Km :

$\delta\theta_T$ = 1 arc sec ➔ $\delta T_{xz} \simeq 2\times10^{-2}$ E.U.

SENSITIVITIES TO ERRORS ON THE SPACECRAFT ORIENTATION AND POSITION

Measurement with an Earth pointing ($\theta_T , \theta_L , \theta_R << 1$) :

$$\hat{M}^T [T]_S \hat{M} + \frac{3\,GM}{r^4} \begin{bmatrix} +\partial r & 0 & r\partial\theta_T \\ 0 & +\partial r & -r\partial\theta_R \\ r\partial\theta_T & -r\partial\theta_R & -2\partial r \end{bmatrix}$$

- Measurements of :

$(T_{xx} - T_{yy})$, $(2T_{xx} + T_{zz})$, $(2T_{yy} + T_{zz})$ and T_{xy}

are not sensitive to orientation and position

- Measurements of :

◇ T_{xz} and T_{yz} are useful for the estimation of the orientation

◇ T_{xx} , T_{yy} and T_{zz} are useful for navigation (Estimation of ∂r)

GRADIOMETRY THROUGH DIFFERENTIAL ACCELEROMETRY (SUMMARY)

Earth pointing

$$\vec{\Omega} = [\Delta\Omega_x \quad \Omega_0+\Delta\Omega_y \quad \Delta\Omega_z]^T \qquad \textit{with} \qquad \Omega_0 \simeq 10^{-3}\ rad s^{-1}, \quad \Delta\Omega_{x,y,z} < 10^{-6}\ rad\ s^{-1}$$

▷ From the SYMMETRIC part of the accelerometric measurement :

$$[A_S]_L \simeq \underbrace{\hat{M}^T [T]_S \hat{M}}_{[\hat{T}]_L} + \underbrace{\begin{bmatrix} \Omega_0^2+2\Omega_0\Delta\Omega_y & -\Omega_0\Delta\Omega_x & 0 \\ -\Omega_0\Delta\Omega_x & 0 & -\Omega_0\Delta\Omega_z \\ 0 & -\Omega_0\Delta\Omega_z & \Omega_0^2+2\Omega_0\Delta\Omega_y \end{bmatrix}}_{\textit{kinematic acceleration}} + \underbrace{\frac{3GM}{r^4}\begin{bmatrix} \delta r & 0 & r\delta\theta_T \\ 0 & \delta r & -r\delta\theta_F \\ r\delta\theta_T & -r\delta\theta_R & -2\delta r \end{bmatrix}}_{\textit{position and orientation}}$$

▷ From the ANTISYMMETRIC part of the accelerometric measurement :

$$[A_{AS}] \simeq -[\mathring{\Omega}]$$

▷ From the DIAGONAL components :

Trace free tensor ➜ $\| \vec{\Omega} \|^2$

▷ + independant observations

⟹ *GRAVITY GRADIENT , ORIENTATION , POSITION*

Fifteenth Gravity Gradiometer Conference
United States Air Force Academy
Colorado Springs, Colorado

CONFERENCE AGENDA

Tuesday, 10 February 1987

1900 - 2200 - Pre-Conference Get-Together at Hilton Inn
Early Registration

Wednesday, 11 February 1987

0700 - Depart Hilton Inn for Fairchild Hall

0730 - Registration - 3rd floor Fairchild Hall, South End

0745 - Welcome/Introduction - Capt Terry J. Fundak

0815 - Presentation by Dr. Georges Balmino of the ONERA (Office National d'Etudes et de Recherches Aerospatiales).

"GRADIO Project: A SGG Mission Based on Microaccelerometers"

0845 - Presentation by Dr. G. Ian Moore of the University of Queensland.

"A Mercury Manometer Gravity Gradiometer"

0900 - Presentation by Mr. Ernest H. Metzger of Bell Aerospace Textron.

"Bell Aerospace Gravity Gradiometer Survey System (GGSS) - Program Review"

0925 - Presentation by Dr. Frank J. van Kann of the University of Western Australia.

"A Prototype Superconducting Gravity Gradiometer for Geophysical Exploration"

0952 - Presentation by Dr. Warren G. Heller of The Analytic Sciences Corp.

"Gravity Gradiometer Survey System (GGSS) Data Processing and Data Use"

1016 - Break

1035 - Presentation by Mr. Al Jircitano of Bell Aerospace Textron.

"Self-Gradient Calibration of the GGSS in a C-130 Aircraft"

1058 - Presentation by Dr. Sam C. Bose of Applied Sciences Analytics, Inc.

"Gravity Gradiometer Data Processing Using the Karhunen-Loeve Method"

1120 - Presentation by Mr. David M. Gleason of the Air Force Geophysics Laboratory.

"Numerically Deriving the Kernels of an Integral Predictor Yielding Surface Gravity Disturbance Components from Airborne Gradient Data"

1130 - Presentation by Mr. Al Jircitano of Bell Aerospace Textron.

"Stage II Simulation Results Using the NSWC Synthetic Gravity Field"

1150 - Depart Fairchild Hall for USAFA Noncommissioned Officers' (NCO) Club

1200 - Lunch - USAFA NCO Club

1245 - Depart NCO Club for Fairchild Hall

1330 - Presentation by Dr. Richard H. Rapp of Ohio State University.

"Gradient Information in New High Degree Spherical Harmonic Expansions"

1354 - Presentation by Mr. John J. Graham of the Defense Mapping Agency Aerospace Center.

"The Effect of Topography on Airborne Gravity Gradiometer Data"

1357 - Presentation by Mr. Mike Sideris of the University of Calgary.

"Effect of Terrain Representation, Grid Spacing, and Flight Altitude on Topographic Corrections for Airborne Gradiometry"

1417 - Presentation by Dr. Rene Forsberg of Geodetic Institute (Denmark) (Currently at the University of Calgary, Canada).

"Topographic Effects in Airborne Gravity Gradiometry"

1434 - Presentation by Dr. Alan H. Zorn of Dynamics Research Corporation.

"Observability of Laplace's Equation Using a Torsion-Type Gravity Gradiometer"

1510 - Break

1530 - Presentation by Dr. Carl Bowin of Woods Hole Oceanographic Institute.

"Ratios of Gravity Gradient, Gravity, and Geoid for Determination of Crustal Structure"

1550 - Presentation by Dr. Rene Forsberg of Geodetic Institute (Denmark).

"Combining Gravity Gradiometry with Other Exploration Methods for Geophysical Prospecting"

1600 - Presentation by Dr. Rene Forsberg of Geodetic Institute (Denmark).

"Computation of the Gravity Vector from Torsion Balance Data in S. Ohio"

1615 - Presentation by Dr. Hans Baussus von Luetzow of the U.S. Army Engineer Topographic Laboratories.

"Estimation of Gravity Vector Components from Bell Gravity Gradiometer and Auxiliary Data under Consideration of Topography and Associated Analytical Upward Continuation Aspects"

1635 - Depart Fairchild Hall for the Hilton Inn

1700 - Reception - Hilton Inn

Thursday, 12 February 1987

0700 - Depart Hilton Inn for Fairchild Hall

0755 - Presentation by Dr. M. Vol Moody of the University of Maryland.

"Development of A Three-Axis Superconducting Gravity Gradiometer and a Six-Axis Superconducting Accelerometer"

0835 - Presentation by Dr. Bahram Mashhoon of the University of Missouri-Columbia.

"The Gravitational Magnetic Field of the Earth and the Possibility of Measuring It Using an Orbiting Gravity Gradiometer"

0905 - Presentation by Dr. Ho Jung Paik of the University of Maryland.

"Tests of General Relativity in Earth Orbit Using a Superconducting Gravity Gradiometer"

0928 - Presentation by Dr. Dave Sonnabend of Jet Propulsion Laboratory.

"Magnetic Isolation - Closing the Loop"

0941 - Presentation by Dr. Dan Long of Eastern Washington University.

"Laboratory G(R) Experiment - Progress Report"

1004 - Break

1030 - Cheyenne Mountain Complex Overview
Briefing by Maj Bill Carver, USAF
(Chief, NORAD Presentations Division).

1110 - Form Groups A & B

1115 - Depart Fairchild Hall for USAFA NCO Club

1130 - Lunch - USAFA NCO Club

1200 - Depart USAF Academy for Falcon Air Force Station

1245 - Arrive Falcon AFS for briefing on 2nd Space Wing
Tour of the Consolidated Space Operations Center (CSOC)

(Group A)

1415 - Depart CSOC for Cheyenne Mountain Complex (CMC)

1500 - Arrive CMC

1505 - Security in-processing and process through metal detector

1525 - Travel

1530 - Tour NORAD Command Post
Tour Industrial Area

1620 - Travel/question and answer session

1630 - Depart for Hilton Inn

1715 - Arrive Hilton Inn

(Group B)

1415 - Depart USAF Academy for Peterson Air Force Base (AFB)

1445 - Arrive Peterson AFB museum

1600 - Depart Peterson AFB for Hilton Inn

1630 - Arrive Hilton Inn

Friday, 13 February 1987

0800 - Tour of JILA, Boulder, Colorado

Papers included in VOLUME I of the Conference Proceedings

1. *Dr. Georges Balmino, C.N.E.S./Bureau Gravimetrique International, France
Dr. Alain Bernard, ONERA (Office National d'Etudes et de Recherches Aerospatiales, France)
Dr. Pierre Touboul, ONERA, France

"GRADIO Project: A SGG Mission Based on Microaccelerometers"

2. *Dr. G. Ian Moore, University of Queensland, Australia
Dr. Frank D. Stacey, University of Queensland, Australia
Dr. Gary J. Tuck, University of Queensland, Australia
Dr. Barry D. Goodwin, University of Queensland, Australia

"A Mercury Manometer Gravity Gradiometer"

3. Mr. Louis L. Pfohl, Bell Aerospace Textron
*Mr. Ernest Metzger, Bell Aerospace Textron

"Bell Aerospace Gravity Gradiometer Survey System (GGSS) - Program Review"

4. *Dr. Frank J. van Kann, et al, University of Western Australia

"A Prototype Superconducting Gravity Gradiometer for Geophysical Exploration"

5. *Dr. Warren G. Heller, The Analytic Sciences Corporation

"Gravity Gradiometer Survey System (GGSS) Data Processing and Data Use"

6. Dr. W. John Hutcheson, Bell Aerospace Textron
(Paper presented by Mr. Al Jircitano of Bell Aerospace Textron)

"Self-Gradient Calibration of the GGSS in a C-130 Aircraft"

7. *Dr. Sam C. Bose, Applied Science Analytics, Inc
Mr. Glenn E. Thobe, Applied Science Analytics, Inc

"Gravity Gradiometer Data Processing Using the Karhunen-Loeve Method"

* Denotes Speaker at Conference

8. *Mr. David M. Gleason, Air Force Geophysics Laboratory

"Numerically Deriving the Kernels of an Integral Predictor Yielding Surface Gravity Disturbance Components from Airborne Gradient Data"

9. Dr. W. John Hutcheson, Bell Aerospace Textron (Paper presented by Mr. Al Jircitano of Bell Aerospace Textron)

"Stage II Simulation Results Using the NSWC Synthetic Gravity Field"

10. *Dr. Richard H. Rapp, Ohio State University

"Gradient Information in New High Degree Spherical Harmonic Expansions"

* Denotes Speaker at Conference

Papers included in VOLUME II of the Conference Proceedings

1. *Mr. John J. Graham, Defense Mapping Agency Aerospace Center
   Mr. Joseph L. Toohey, Defense Mapping Agency Aerospace Center

   "The Effect of Topography on Airborne Gravity Gradiometer Data"

2. Dr. Klaus-Peter Schwarz, University of Calgary, Canada
   *Mr. M.G. Sideris, University of Calgary, Canada
   Dr. I.N. Tziavos, University of Calgary, Canada
   (Dr. Tziavos on leave from the University of Thessaloniki, Greece)

   "Effect of Terrain Representation, Grid Spacing, and Flight Altitude on Topographic Corrections for Airborne Gradiometry"

3. *Dr. Rene Forsberg, Geodaetisk Institut, Denmark

   "Topographic Effects in Airborne Gravity Gradiometry"

4. *Dr. Alan H. Zorn, Dynamics Research Corporation

   "Observability of Laplace's Equation Using a Torsion-Type Gravity Gradiometer"

5. *Dr. Carl Bowin, Woods Hole Oceanographic Institute

   "Ratios of Gravity Gradient, Gravity, and Geoid for Determination of Crustal Structure"

6. Dr. Anthony A. Vassiliou, University of Calgary, Canada
   (Paper presented by Dr. Rene Forsberg, Geodaetisk Institut, Denmark)

   "Combining Gravity Gradiometry with other Exploration Methods for Geophysical Prospecting"

7. Dr. D. Arabelos, University of Thessaloniki, Greece
   Mr. Christian Tscherning, Geodaetisk Institut, Denmark
   (Paper presented by Dr. Rene Forsberg, Geodaetisk Institut, Denmark)

   "Computation of the Gravity Vector from Torsion Balance Data in Southern Ohio"

* Denotes Speaker at Conference

8\. *Dr. Hans Baussus von Luetzow, US Army Engineer Topographic Laboratory

"Estimation of Gravity Vector Components from Bell Gravity Gradiometer and Auxiliary Data under Consideration of Topography and Associated Analytical Upward Continuation Aspects"

9\. Dr. H. A. Chan, University of Maryland
Dr. Q. Kong, University of Maryland
*Dr. M. Vol Moody, University of Maryland
Dr. H. J. Paik, University of Maryland
Mr. J. W. Parke, University of Maryland

"Development of a Three-Axis Superconducting Gravity Gradiometer and a Six-Axis Superconducting Accelerometer"

10\. *Dr. Bahram Mashhoon, University of Missouri-Columbia

"The Gravitational Magnetic Field of the Earth and the Possibility of Measuring it Using an Orbiting Gravity Gradiometer"

11\. *Dr. Ho Jung Paik, University of Maryland

"Tests of General Relativity in Earth Orbit Using a Superconducting Gravity Gradiometer"

12\. *Dr. Dave Sonnabend, Jet Propulsion Laboratory
Mr. A. Miguel San Martin, Jet Propulsion Laboratory

"Magnetic Isolation-Closing the Loop"

13\. *Dr. Dan Long, Eastern Washington University

"Laboratory G(R) Experiment - Progress Report"

* Denotes Speaker at Conference

PROCEEDINGS

OF THF

FIFTEENTH GRAVITY GRADIOMETRY CONFERENCE

VOL I PAPERS

GRADIO PROJECT:
A SGG MISSION BASED ON MICROACCELEROMETERS

by

Dr. Georges Balmino
C.N.E.S./Bureau Gravimetrique International
18 Ave Edouard Berlin
31055 Toulouse Cedex
FRANCE

Dr. Alain Bernard
Dr. Pierre Touboul
Office National d'Etudes et de Recherches Aerospatiales
BP 72
92322 Chatillon Cedex
FRANCE

ABSTRACT

The status of the satellite gravity gradiometry project is reviewed. Since the first ideas in 1980, technological solutions have ripened and a configuration composed of eight cubic electrostatic microaccelerometers is proposed which should guarantee a signal detection limit of 10^{-2} to 10^{-3} Eotvos. Two basic systems are proposed to fly the instrument: one is a dedicated satellite on which a permanent calibrating device, actually part of the gradiometer, would be implemented; the other would consist of flying the instrument in one of the NASA projects, the GRM drag-free spacecraft, where it would be suspended in the double stage DISCOS system. A laboratory model of the cubic accelerometers is also presented.

GRADIO

A SGG MISSION BASED ON MICROACCELEROMETERS

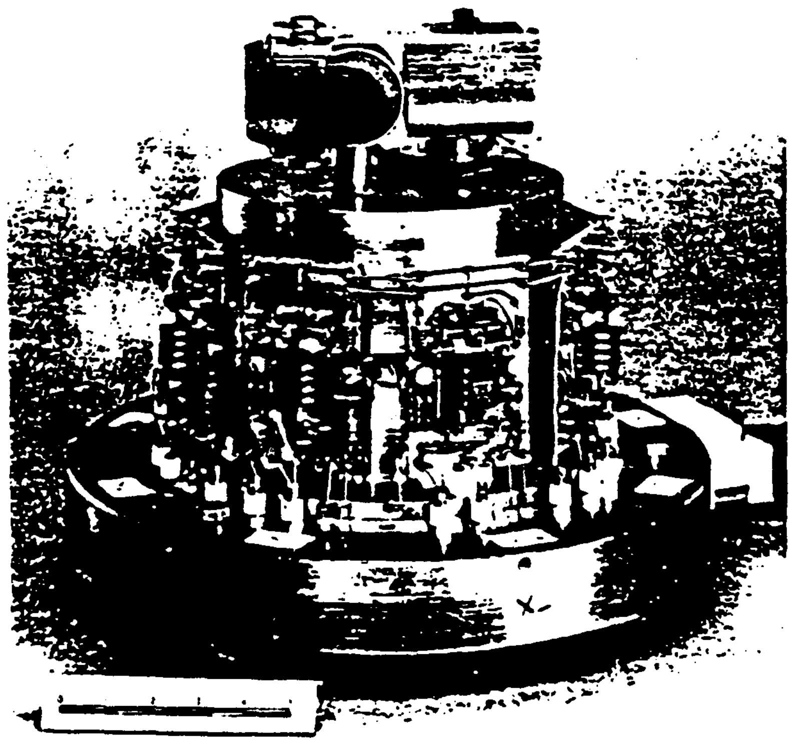

BERNARD A. (ONERA, Chatillon s/Bagneux, France)

TOUBOUL P. (ONERA, id.)

BALMINO G. (CNES, Toulouse, France)

15th GRAVITY GRADIOMETRY CONFERENCE

Feb. 11-13, 1987

(Colorado Springs - USA)

GRAVITY FIELD RESOLUTION EXPECTED FROM SATELLITE GRADIOMETRY

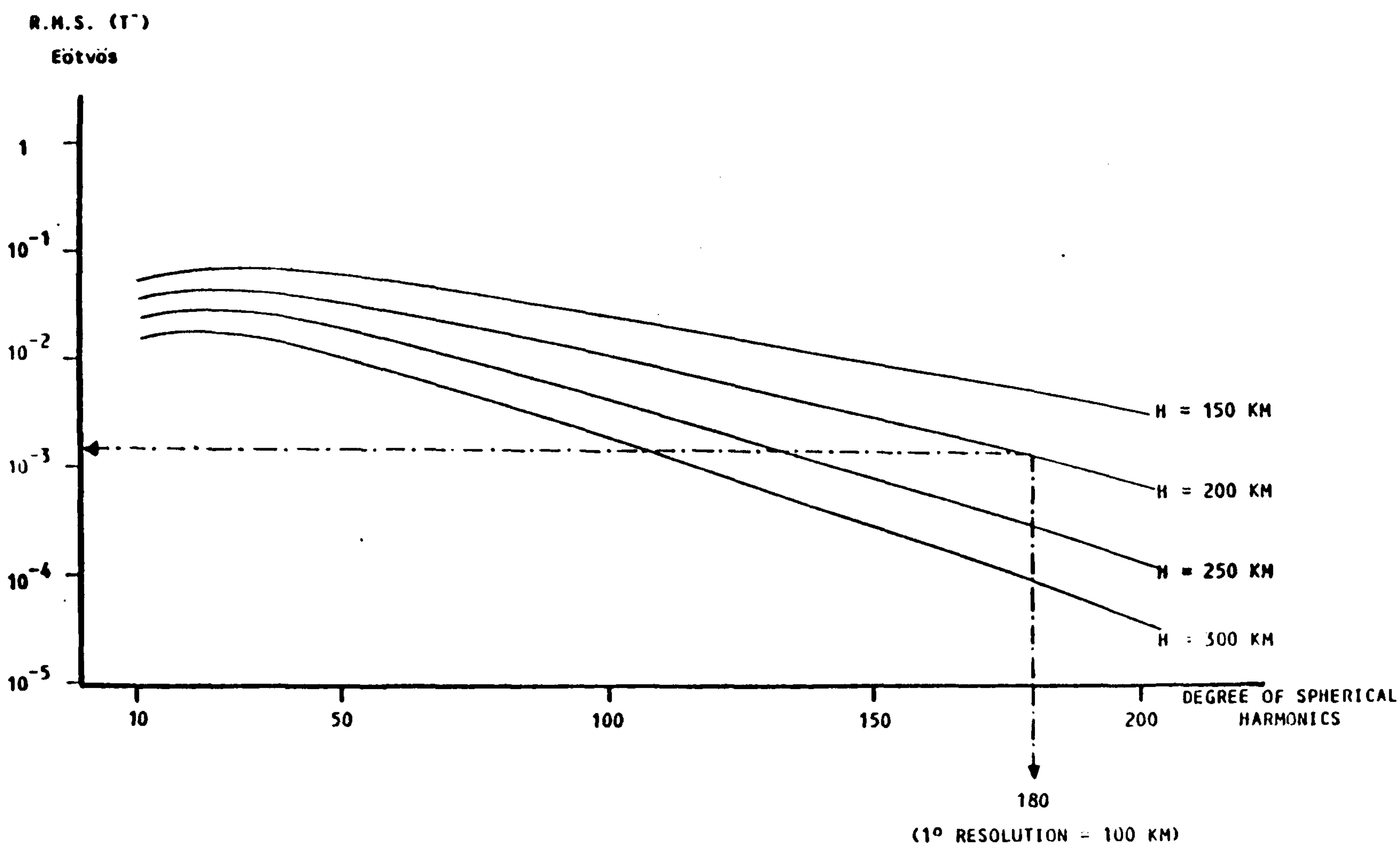

GRADIOMETRY THROUGH DIFFERENTIAL ACCELEROMETRY

Gradiometer purpose : → $T_{ij} = \dfrac{\partial^2 U}{\partial x_i \, \partial x_j}$

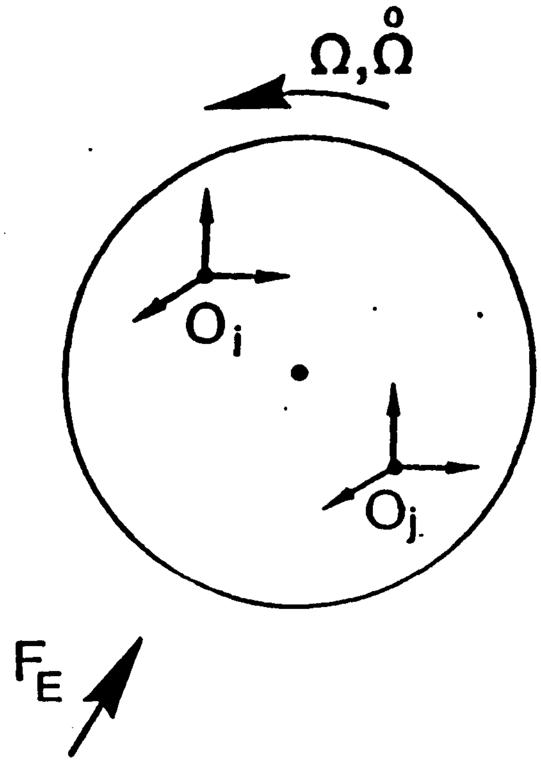

Differential accelerometric measurement :

$$(\Gamma_i - \Gamma_j) = [A](O_i - O_j)$$

with $$[A] = \underbrace{[-T] + [\Omega^2]}_{\text{symmetric}} + \underbrace{[\mathring{\Omega}]}_{\text{antisymmetric}}$$

By use of sets of differential measurements :

$$1/2 \, ([A] - {}^T[A]) = [\mathring{\Omega}]$$

$$1/2 \, ([A] + {}^T[A]) = [-T] + [\Omega^2]$$

→ Ω ***must be controlled and estimated***

GRADIO ACCELEROMETER : SPECIFICATIONS

- △ $T_{ij} \leq 3000$ Eötvös (3×10^{-6} ms^{-2} for 1m base line)
- △ Atmospheric drag : $10^{-5} ms^{-2}$ (200km)

⇨ ***Range :*** $10^{-4} ms^{-2}$ full scale

- △ T_{ij} variations 10^{-2} Eötvös / 10 sec

⇨ ***Resolution :*** $10^{-11} ms^{-2}$ for a bandwidth $< 1 Hz$

- △ Use of a set of differential measurements :
  - ○ *linearity*
  - ○ *low coupling*
  - ○ *scale factors matching*

TRANSFORMATION FROM SPATIAL DOMAIN TO KARHUNEN–LOEVE DOMAIN

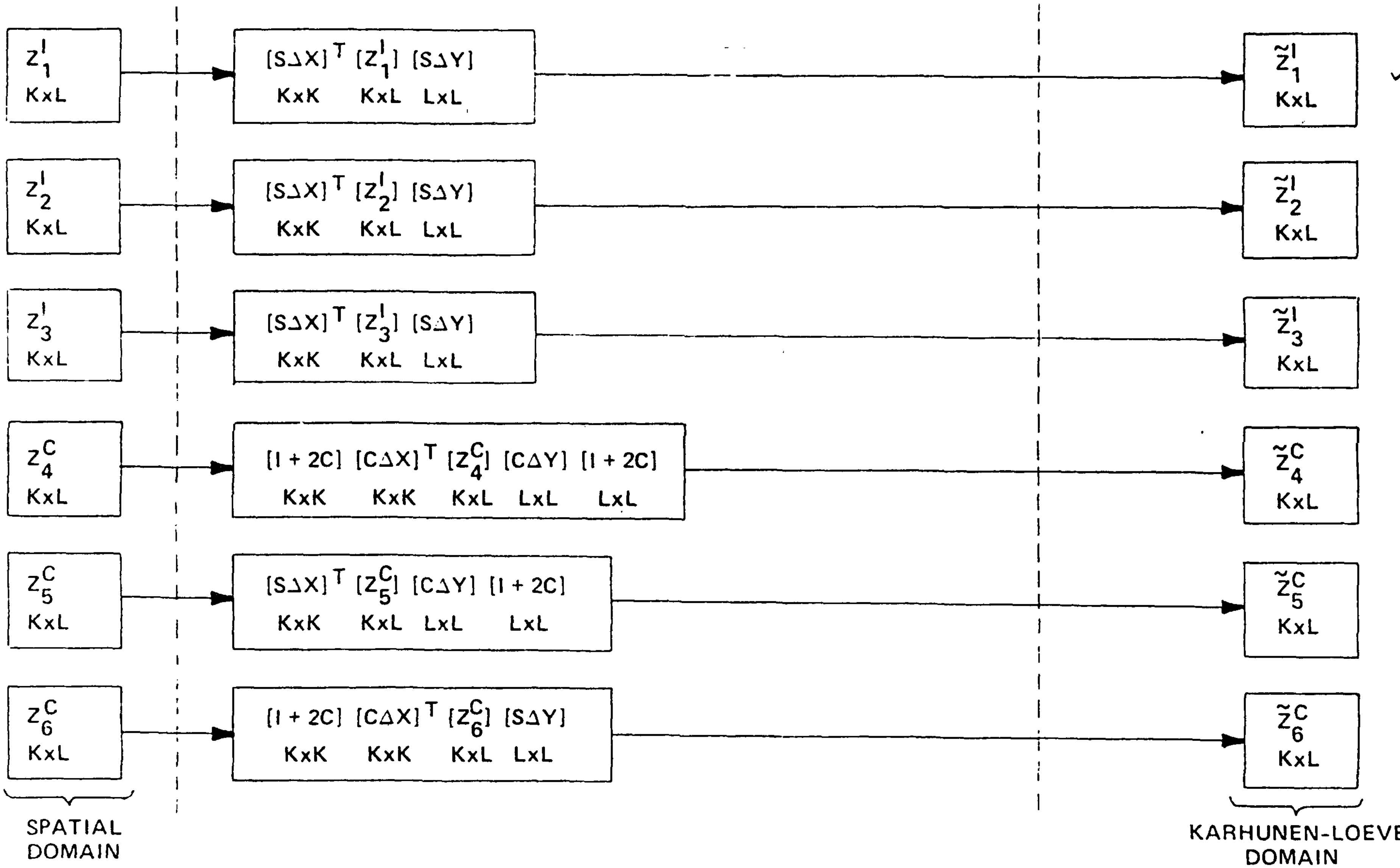

DEFINITION OF TRANSFORMATION MATRICES

$$[S\Delta X] = \begin{bmatrix} \mathrm{SIN}\,\pi\,(1\mathrm{x}1)\,\frac{\Delta X}{A} & \mathrm{SIN}\,\pi\,(1\mathrm{x}2)\,\frac{\Delta X}{A} & \cdots\cdots & \mathrm{SIN}\,\pi\,(1\mathrm{x}K)\,\frac{\Delta X}{A} \\ \mathrm{SIN}\,\pi\,(2\mathrm{x}1)\,\frac{\Delta X}{A} & \mathrm{SIN}\,\pi\,(2\mathrm{x}2)\,\frac{\Delta X}{A} & \cdots\cdots & \mathrm{SIN}\,\pi\,(2\mathrm{x}K)\,\frac{\Delta X}{A} \\ \vdots & & & \\ \mathrm{SIN}\,\pi\,(K\mathrm{x}1)\,\frac{\Delta X}{A} & \mathrm{SIN}\,\pi\,(K\mathrm{x}2)\,\frac{\Delta X}{A} & \cdots\cdots & \mathrm{SIN}\,\pi\,(K\mathrm{x}K)\,\frac{\Delta X}{A} \end{bmatrix}$$

$$[S\Delta X(i,j)] = \mathrm{SIN}\,\pi(i\mathrm{x}j)\,\frac{\Delta X}{A} \quad ; \quad [C\Delta X(i,j)] = \mathrm{COS}\,\pi(i\mathrm{x}j)\,\frac{\Delta X}{A}$$

$$[S\Delta Y(i,j)] = \mathrm{SIN}\,\pi(i\mathrm{x}j)\,\frac{\Delta Y}{B} \quad ; \quad [C\Delta Y(i,j)] = \mathrm{COS}\,\pi(i\mathrm{x}j)\,\frac{\Delta Y}{B}$$

ESTIMATES OF KARHUNEN–LOEVE COEFFICIENTS FROM ALL MEASUREMENTS

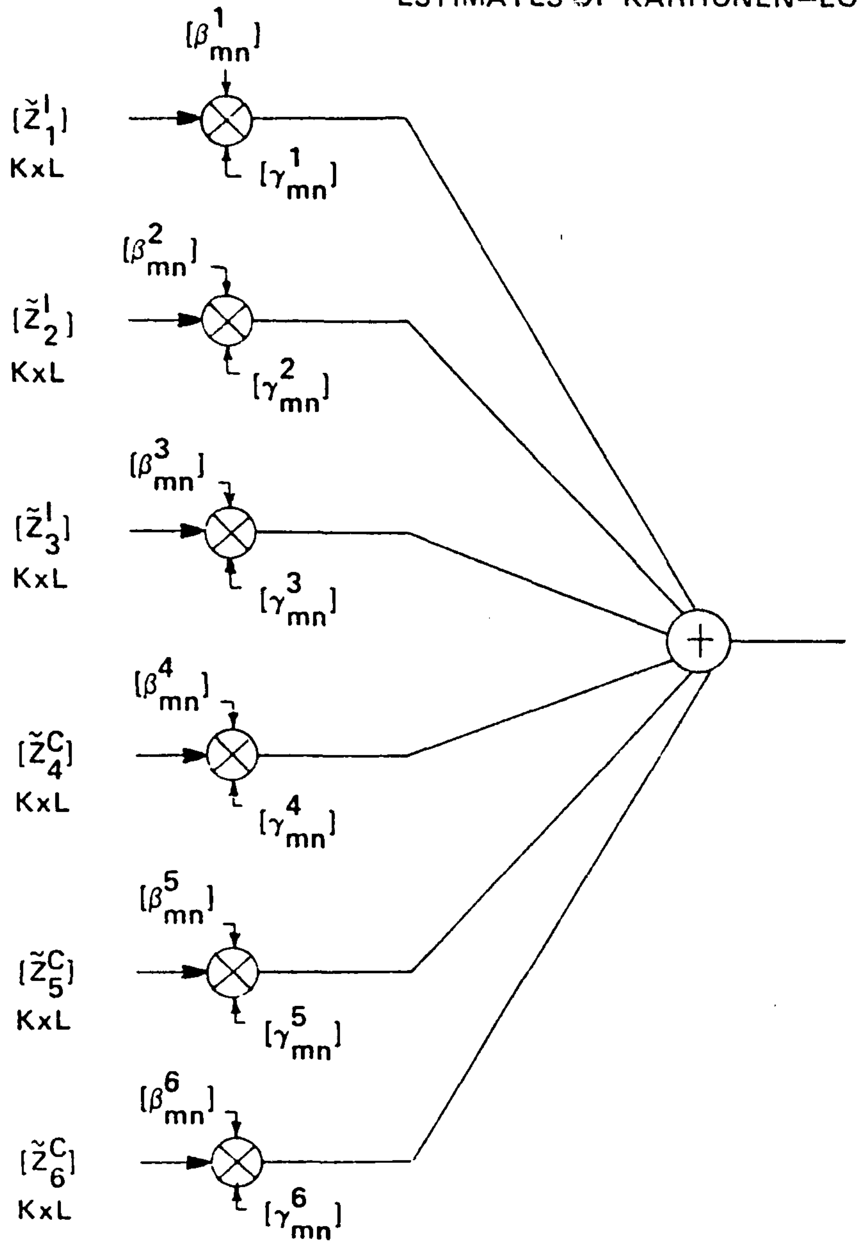

$\otimes$ – POINT-BY-POINT MATRIX MULTIPLICATION (NOT ROW-BY-COLUMN MATRIX MULTIPLICATION)

$\oplus$ – POINT-BY-POINT MATRIX SUMMATION

$[\hat{a}_{mn}]$ KxL – KARHUNEN-LOEVE COEFFICIENT ESTIMATES FROM ALL MEASUREMENTS

$[\beta^i_{mn}]$ KxL – KARHUNEN-LOEVE GAIN MATRIX FOR iTH MEASUREMENT GRID

$[\gamma^i_{mn}]$ KxL – KARHUNEN-LOEVE OBSERVATION MATRIX FOR iTH MEASUREMENT GRID

ESTIMATOR GAINS

- GENERALIZED FORM OF KARHUNEN–LOEVE GAINS

$$\beta^i_{mn} = \frac{\left(\frac{AB}{4}\right) \lambda_{mn} \prod_{\substack{j=1 \\ j \neq i}}^{6} \sigma_i^2}{\prod_{i=1}^{6} \sigma_i^2 + \left(\frac{AB}{4}\right) \lambda_{mn} \left(\sum_{j=1}^{6} \gamma^i_{mn} \prod_{\substack{k=1 \\ k \neq j}}^{6} \sigma_j^2 \right)}$$

σ_i – MEASUREMENT NOISE VARIANCE FOR ITH MEASUREMENT GRID

- GAINS FOR EXAMPLE OF TWO (2) MEASUREMENTS, ONE PERFECT ($\sigma_1 = 0,\ \sigma_2 \neq 0$)

$$\beta^1_{mn} = \frac{\left(\frac{AB}{4}\right) \lambda_{mn} \sigma_2^2}{\sigma_1^2 \sigma_2^2 + \left(\frac{AB}{4}\right) \lambda_{mn} (\gamma^{m1}_{mn} \sigma_2^2 + \gamma^{m2}_{mn} \sigma_1^2)} = \frac{1}{\gamma^{m1}_{mn}} \implies$$ ACCEPTS PERFECT MEASUREMENT WITH PROPER GAIN TO REPRODUCE SIGNAL

$$\beta^2_{mn} = \frac{\left(\frac{AB}{4}\right) \lambda_{mn} \sigma_1^2}{\sigma_1^2 \sigma_2^2 + \left(\frac{AB}{4}\right) \lambda_{mn} (\gamma^{m1}_{mn} \sigma_2^2 + \gamma^{m2}_{mn} \sigma_1^2)} = 0 \implies$$ REJECTS IMPERFECT MEASUREMENT

ABOUT THE GRAVITY GRADIOMETRY CONFERENCE .....

The First Gravity Gradiometry Conference was held at the Air Force Cambridge Research Laboratory (AFCRL, now AFGL) in 1973. Its purpose was to provide a forum to evaluate and compare the efforts of three vendors (Charles Stark Draper Lab, Hughes Research Lab and Bell Aerospace Textron) in still-emerging areas of gravity gradiometry. About 15 people attended, most of them from the companies mentioned above or the Terrestrial Sciences Division at AFCRL. In contrast, the 1987 Conference had a guest list of 70 plus attendees, with participation from academia (foreign and domestic), private industry and government. The papers presented were not restricted to gradiometry alone. Indeed, the scope of this annual event has broadened considerably since 1973.

With the exception of the first two conferences, all the others have been held at the US Air Force Academy in Colorado Springs, Colorado. The Geodesy and Gravity Branch of the Earth Sciences Division of the Air Force Geophysics Laboratory (AFGL), Hanscom AFB, Massachusetts, has always organized the event, which usually takes place around the second week in February. This trend is expected to continue.

If you are not already on our mailing list and would like to attend the 1988 Conference, or if you have any questions, please write to:

Ms Claire McCartney
AFGL/LW
Hanscom AFB, MA 01731

Due to space constraints, we restrict the size of our Conferences to about 75 people. Attendance will generally be on a "first-come, first-served basis" once the completed registration forms are returned to us. We shall mail these forms later this year.

While we have a limited number of copies of the proceedings for non-attendees of the 1987 Conference, copies of proceedings for prior years are not available. Also, we appreciate any comments or suggestions you may have regarding this document.

ABOUT THESE PROCEEDINGS........

Due to the large number of papers presented at the Conference, I have divided the proceedings into two manageable volumes. At the beginning of each volume is a list of all papers contained in both volumes, in actual order of presentation at the Conference. This is also the sequence of the published papers within these proceedings.

For the sake of completeness, both volumes contain the Attendees List, Conference Agenda, Lists of Papers, Conference History, Acknowledgments and this explanation.

Every paper is preceded by an abstract in a standard format. Some papers may also have the original abstract included. Further, you may recall the Q&A session we had at the end of each presentation. In cases where a technical interchange did take place, the questions and answers are documented at the end of each pertinent paper. Every paper did not have a Q&A session, and I have included all Q&A sheets that were handed to me at the end of each presentation. Except for a few minor editorial changes, the information on these sheets has not been significantly altered. Obviously, these sheets are as "good" as the inputs you provided.

In summary, I hope the above explanation was helpful. I have done what I consider to be a thorough job of collecting and checking all the information for these proceedings. Errors will occur, however, and while I will entertain any comments and criticisms on this issue, these proceedings will stand as published.

Thank you for your participation, and your patience!

Capt Vishnu V. Nevrekar
Earth Sciences Division
USAF Geophysics Laboratory
Hanscom AFB, MA 01731

November 1987

ACKNOWLEDGMENTS

We couldn't possibly organize a conference the scope and size of our forum without some very diligent "behind-the-scenes" work by a few outstanding individuals. We would like to recognize their efforts and thank them for their support throughout the planning and execution of the 1987 Gradiometry Conference.

We are indebted to the Directorate of Protocol at the US Air Force Academy for allowing us to host the Conference there these past 13 years. Ms Nancy Gass was the liaison officer from the Directorate, and we gratefully acknowledge her assistance in handling all the conference arrangements, including hotel accomodation for the attendees, transportation for the Conference and NORAD/CSOC tours, luncheons during the conference and the "mixers" later in the evening, all of which were set up with great skill and professionalism.

Also, we acknowledge the outstanding efforts of TSgt Kent Droz, USAF, of the Community Relations Division at HQ NORAD, who arranged tours of the Cheyenne Mountain Complex (CMC) and the Consolidated Space Operations Center (CSOC) at Falcon AFS. These tours gave the conference attendees a first-hand look at the complex space defense environment.

Next, we thank all the speakers for taking the time to compile and present their papers for the benefit of the Conference attendees. As always, the broad mix of topics went a long way towards making the Conference an intellectually stimulating event. Indeed, the high quality of the research material presented "made" this Conference.

Finally, we thank Col J.R. Johnson, Commander, AFGL, Dr Donald H. Eckhardt, Director, Earth Sciences Division and Dr Thomas P. Rooney, Chief, Geodesy and Gravity Branch, without whose support and guidance this Conference could not have been held.

Alphabetical Listing of Conference Participants

Name	Organization
*Georges Balmino	C.N.E.S./Bureau Gravimetrique International (FR)
Anthony Barringer	Barringer Resources, Inc
*Hans Baussus Von Luetzow	US Army Engineer Topographic Laboratory
Don Benson	Dynamics Research Corporation
Ed Biegert	Shell Development Corporation
John Binns	BP Minerals International, Ltd (UK)
*Sam Bose	Applied Science Analytics, Inc
*Carl Bowin	Woods Hole Oceanographic Institution
John Brozena	Naval Research Laboratory
Marcus Chalona	US Naval Oceanographic Office
Lindrith Cordell	US Geological Survey
Ronald Davis	Northrop Electronics Division
Mark Dransfield	University of Western Australia (AUS)
Donald Eckhardt	USAF Geophysics Laboratory
Michael Ellett	USAF Space Division
Harry Emrick	Consultant
John Fett	LaCoste and Romberg Gravity Meters, Inc
Charles Finley	National Aeronautics and Space Administration
Thomas Fischetti	Technology Management Consultants, Inc
James Fix	Teledyne Geotech
Guy Flanagan	Standard Oil Production Company
*Rene Forsberg	Geodetic Institute (DEN)
Capt Terry Fundak	USAF Geophysics Laboratory
*David Gleason	USAF Geophysics Laboratory
Rob Goldsborough	USAF Geophysics Laboratory

Name	Organization
*John Graham	Defense Mapping Agency
Andrew Grierson	Bell Aerospace Textron
Michael Hadfield	Honeywell, Inc
Richard Hansen	Colorado School of Mines
Chris Harrison	Geodynamics Corporation
Ray Hassanzadeh	McDonnell Douglas
*Warren Heller	The Analytic Sciences Corporation
Howard Heuberger	Johns Hopkins University
George Hinton	Consultant
Albert Hsui	USAF Geophysics Laboratory
Gene Jackson	McDonnell Douglas
Christopher Jekeli	USAF Geophysics Laboratory
*Albert Jircitano	Bell Aerospace Textron
Col J.R. Johnson	Commander, USAF Geophysics Laboratory
J. Edward Jones	USAF Intelligence Service
J. Latimer	Johns Hopkins University
Andrew Lazarewicz	USAF Geophysics Laboratory
Thomas Little	US Naval Oceanographic Office
*Dan Long	Eastern Washington University
James Lowery III	Rockwell International
Charles Martin	University of Maryland Research Foundation
*Bahram Mashhoon	University of Missouri
*Ernest Metzger	Bell Aerospace Textron
*M. Vol Moody	University of Maryland
*Ian Moore	University of Queensland (AUS)
1Lt Vishnu Nevrekar	USAF Geophysics Laboratory
*Ho Jung Paik	University of Maryland

Name	Organization
Maj John Prince	USAF Office of Scientific Research
*Richard Rapp	Ohio State University
Richard Reineman	GWR Instruments
*Jean-Paul Richard	University of Maryland
Thomas Rooney	USAF Geophysics Laboratory
Alan Rufty	Naval Surface Weapons Center
Alton Schultz	AMOCO Production Company
*Michael Sideris	University of Calgary (CAN)
Ted Sims	Naval Surface Weapons Center
Randall Smith	Defense Mapping Agency
*David Sonnabend	CALTECH/Jet Propulsion Laboratory
Milton Trageser	Charles Stark Draper Laboratory
Gary Tuck	University of Queensland (AUS)
Herbert Valliant	LaCoste and Romberg Gravity Meters, Inc
Robert Valska	Defense Mapping Agency
*Frank van Kann	University of Western Australia (AUS)
Richard Wold	TerraSense, Inc
Robert Ziegler	Defense Mapping Agency
*Alan Zorn	Dynamics Research Corporation
Paul Zucker	Johns Hopkins University

* Denotes Speaker at Conference

OVERALL DATA PROCESSING SCHEME

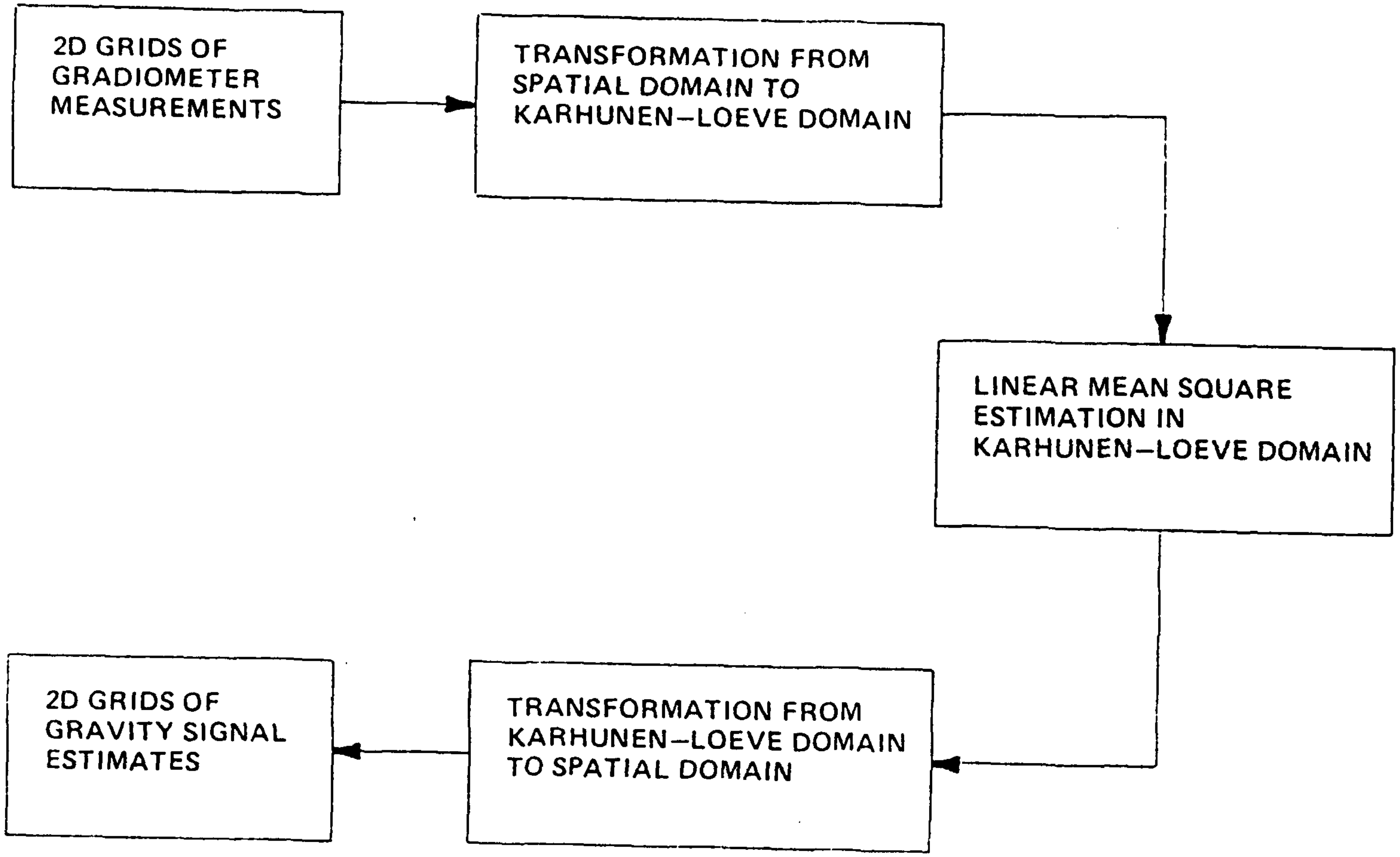

GRADIOMETER INLINE AND CROSSLINE MEASUREMENTS

$$\underbrace{\begin{bmatrix} z_1^I \\ z_2^I \\ z_3^I \\ z_4^C \\ z_5^C \\ z_6^C \end{bmatrix}}_{\text{MEASUREMENT}} = \underbrace{\begin{bmatrix} \frac{1}{2}\left(\frac{\partial^2 T}{\partial x^2} - \frac{\partial^2 T}{\partial y^2}\right) \\ \frac{1}{2}\left(\frac{\partial^2 T}{\partial y^2} - \frac{\partial^2 T}{\partial z^2}\right) \\ \frac{1}{2}\left(\frac{\partial^2 T}{\partial z^2} - \frac{\partial^2 T}{\partial x^2}\right) \\ \frac{\partial^2 T}{\partial x \partial y} \\ \frac{\partial^2 T}{\partial y \partial z} \\ \frac{\partial^2 T}{\partial z \partial x} \end{bmatrix}}_{\text{SIGNAL}} + \underbrace{\begin{bmatrix} \nu_1 \\ \nu_2 \\ \nu_3 \\ \nu_4 \\ \nu_5 \\ \nu_6 \end{bmatrix}}_{\text{NOISE}}$$

GRAVITY GRADIOMETER DATA PROCESSING USING THE KARHUNEN—LOEVE METHOD

by

Dr. Sam C. Bose
Glenn E. Thobe

Fifteenth
Gravity Gradiometer Conference
United States Air Force Academy
Colorado Springs, Colorado

11-12 FEBRUARY 1987

APPLIED SCIENCE ANALYTICS, INC.
7049 OWENSMOUTH AVENUE, CANOGA PARK, CALIFORNIA 91303 • (818) 716-1237

Self Gradient Calibration of GGSS in a C-130 Aircraft

Overview

- DUE TO INVERSE CUBE LAW FOR GRAVITY GRADIENTS, MASSES IN CLOSE PROXIMITY TO GGI ACCELEROMETERS GIVE RISE TO LARGE OUTPUTS WHICH HAVE TO BE COMPENSATED FOR.

- ANALYSIS LEADING TO COMPENSATION HAS TO REFLECT THE FACTS THAT:

  - 3 GGIs MEASURE THE GRADIENTS AT 3 DIFFERENT LOCATIONS.

  - A GGI ACTUALLY MEASURES THE FIELD VARIATION OVER A FINITE DISTANCE, THE VALUE OF THE GRADIENT AT THE GIMBAL CENTER IS INFERRED FROM THESE MEASUREMENTS.

- BELL APPORACH TO SELF GRADIENT CALIBRATION IS TO IDENTIFY THE PARAMETERS OF MASS MODELS REPRESENTING THE GIMBALS, BINNACLE, AND VEHICLE FROM DATA COLLECTED IN THE LABORATORY AND ABOARD THE VEHICLE.

Taylor Series Representation Of GGI Output

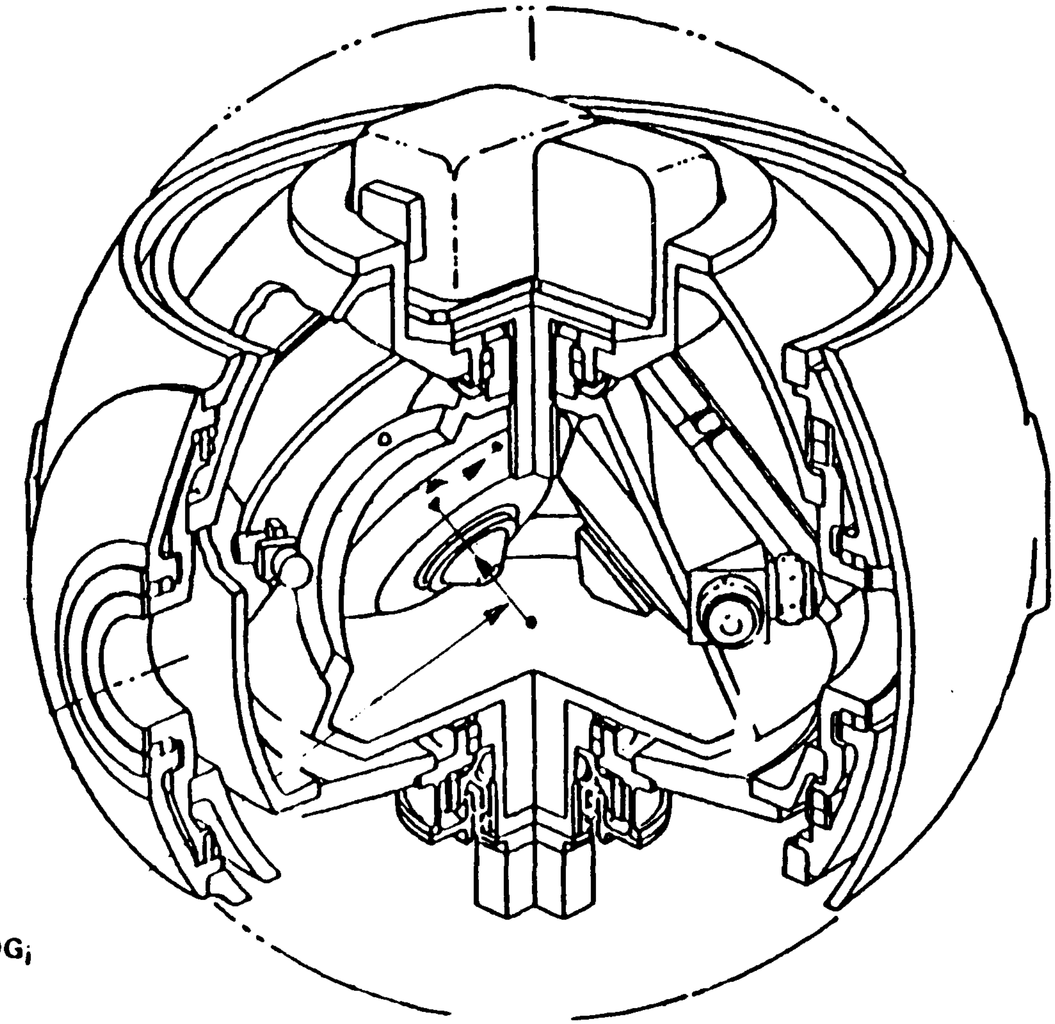

THE OUTPUT OF THE lth ACCELEROMETER IN THE ith GGI CAN BE EXPRESSED AS A TAYLOR SERIES ABOUT THE GIMBAL CENTER.

$$A_{l_j} = \sum_{j=1}^{5} \left[|\underline{S}_l^{M_j}|^T_{\bullet} \nabla W_j + \sum_{k=1}^{K} \frac{1}{k!} |\underline{S}_l^{M_j}|^T \, |\underline{r}_{OP_{il}}^{M_j\,(k)}|^T \, |\nabla^{(k+1)} W_j| \right] \qquad (1)$$

IN EQUATION (1):

$$\nabla \triangleq \begin{bmatrix} \frac{\partial}{\partial x} \\ \frac{\partial}{\partial y} \\ \frac{\partial}{\partial z} \end{bmatrix}$$

THE SUPERSCRIPT (k) DENOTES THE kth KRONECKER POWER, HENCE IF W_j REPRESENTS THE POTENTIAL DUE TO THE jth MASS STRUCTURE THEN $\nabla^{(k+1)} \cdot W_j$ REPRESENTS THE k+1 RANKED MASS TENSOR.

$S_1^{M_j}$ IS THE UNIT VECTOR DEFINING THE SENSITIVE AXIS OF THE 1th ACCELEROMETER IN A GGI EXPRESSED IN A COORDINATE SYSTEM FIXED IN THE jth MASS STRUCTURE.

$$S_1^{M_j} = C_S^{M_j} C_{G_1}^{S} S_1^{G1}$$

WHERE: $$S_1^{G_1} = \begin{bmatrix} -\sin(\Omega t + \phi_1) \\ \cos(\Omega t + \phi_1) \\ 0 \end{bmatrix}$$

WHERE Ωt IS THE WHEEL ANGLE AND ϕ_1 = 0, 90°, 180°, OR 270°

$$\underline{r}^{M_j}_{OP_{ij}} = C^{M_j}_{s} [\underline{r}^{s}_{OG_i} + C^{s}_{Gi} \underline{r}^{Gi}_{G\,Pi}]$$

$C^{M_j}_{s}$ IS THE TRANSFORMATION FROM A SET FIXED IN THE GIMBAL CENTER TO A SET FIXED IN THE jth MASS STRUCTURE (INVOLVING THE GIMBAL ANGLES).

$C^{s}_{G_i}$ IS THE TRANSFORMATION FROM A SET FIXED IN THE ith GGI TO THE SET FIXED IN THE GIMBAL CENTER (INVOLVING THE UMBRELLA GEOMETRY).

$\underline{r}^{s}_{OG_i}$ IF THE CONSTANT VECTOR FROM THE GIMBAL CENTER TO THE ith GGI EXPRESSED IN THE SET FIXED IN THE GIMBAL CENTER.

$\underline{r}^{G_i}_{GP_l}$ IS THE VECTOR FROM THE CENTER OF A GGI TO THE lth ACCELEROMETER EXPRESSED IN THE SET FEXED IN THE ITH GGI.

$$= \begin{bmatrix} d \cos (\Omega t + \phi_l) \\ d \sin (\Omega t + \phi_l) \\ 0 \end{bmatrix}$$

AND d IS THE GGI RADIUS.

THE ith GGI OUTPUT IS THEN

$$y_i^I = a_{1i} + a_{2i} - (a_{3i} + a_{4i}) \Big| \sin (2\Omega t)$$

$$y_i^C = a_{1i} + a_{2i} - (a_{3i} + a_{4i}) \Big| \cos (2\Omega t)$$

THE TOTAL GGSS OUTPUT CAN BE EXPRESSED AS A LINEAR EQUATION IN THE MASS TENSOR ELEMENTS:

$$\underline{y} = H^G \underline{W} = H^G H^1 \underline{W}^1$$

WHERE H^1 IS THE LAPLACIAN CONSTRANT MATRIX.

Mass Structures

LABORATORY:

(1) ROLL GIMBAL
(2) PITCH GIMBAL
(3) BINNACLE & SCORSBY AZIMUTH
(4) SCORSBY PITCH
(5) SCORSBY BASE & LOCAL EARTH

VEHICLE:

(1) ROLL GIMBAL
(2) PITCH GIMBAL
(3) BINNACLE & VAN (& AIRCRAFT)

NUMBER OF VARIABLES PER MASS STRUCTURE

TENSOR RANK	NUMBER OF TENSOR ELEMENTS (3^n)	NUMBER OF GENERIC TENSOR ELEMENTS $(n+1)(n+2)/2$	NUMBER OF LAPLACIAN TENSOR ELEMENTS
2	9	6	5
3	27	10	7
4	81	15	9
5	243	21	11
6	729	28	13
7	2187	36	15
8	6561	45	17

Calibration Overview

DATA SETS:

- LABORATORY SELF GRADIENT DATA CONSISTING OF AVERAGED GGI OUTPUTS TAKEN OVER 280 COMBINATIONS OF SCORSBY AZIMUTH, PITCH AND CAROUSEL ANGLES.
- LABORATORY STEP INDEXING AND CONTINUOUS CAROUSELLED DATA.
- VEHICLE SELF GRADIENT DATA CONSISTING OF AVERAGED GGI OUTPUTS TAKEN OVER APPROXIMATELY 60 COMBINATIONS OF VEHICLE HEADING & PITCH ANGLES.

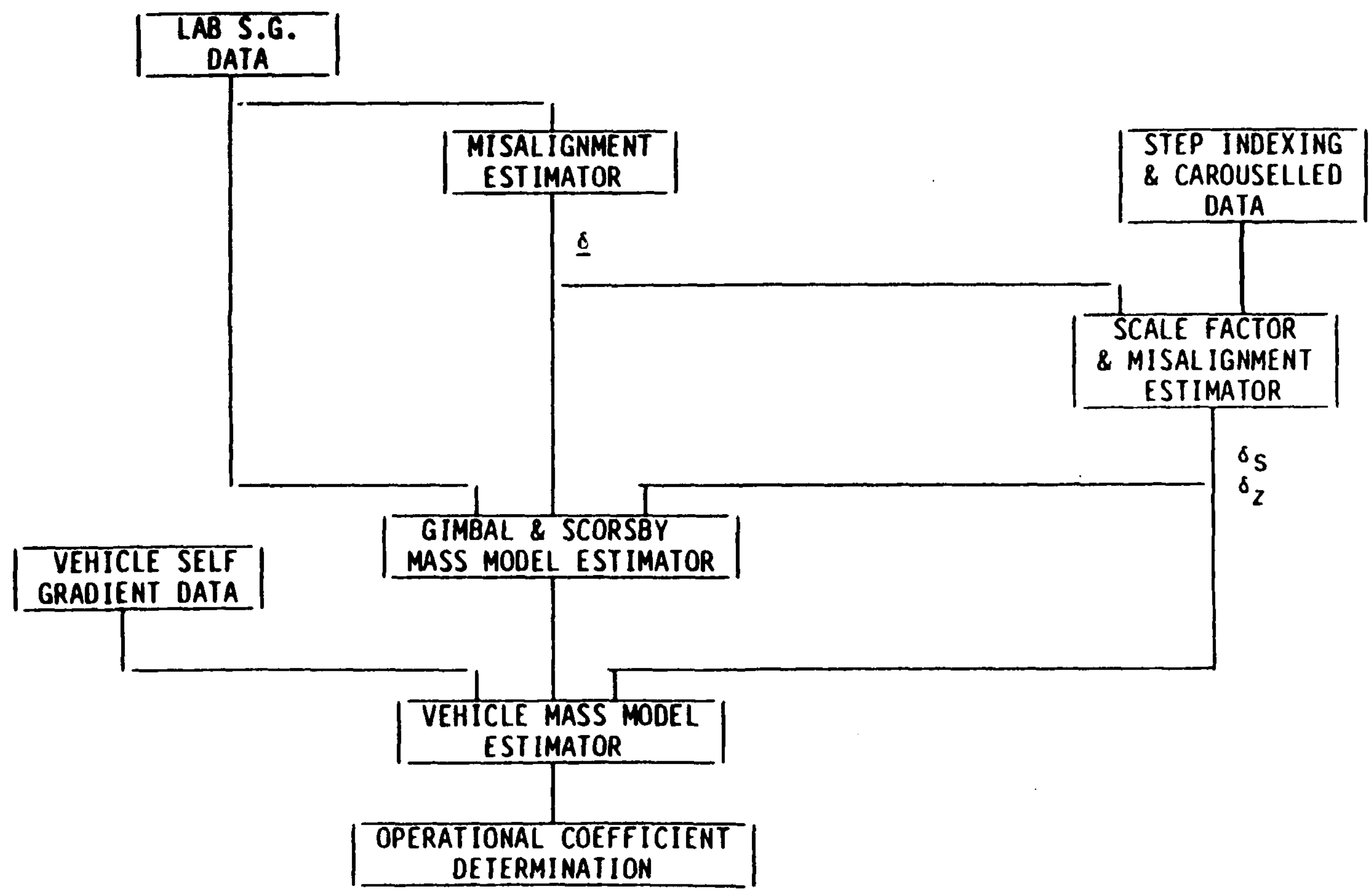

GGSS EXPECTED OUTPUT ERROR WHEN LABORATORY AND VEHICLE

DATA ARE USED FOR SELF GRADIENT CALIBRAION

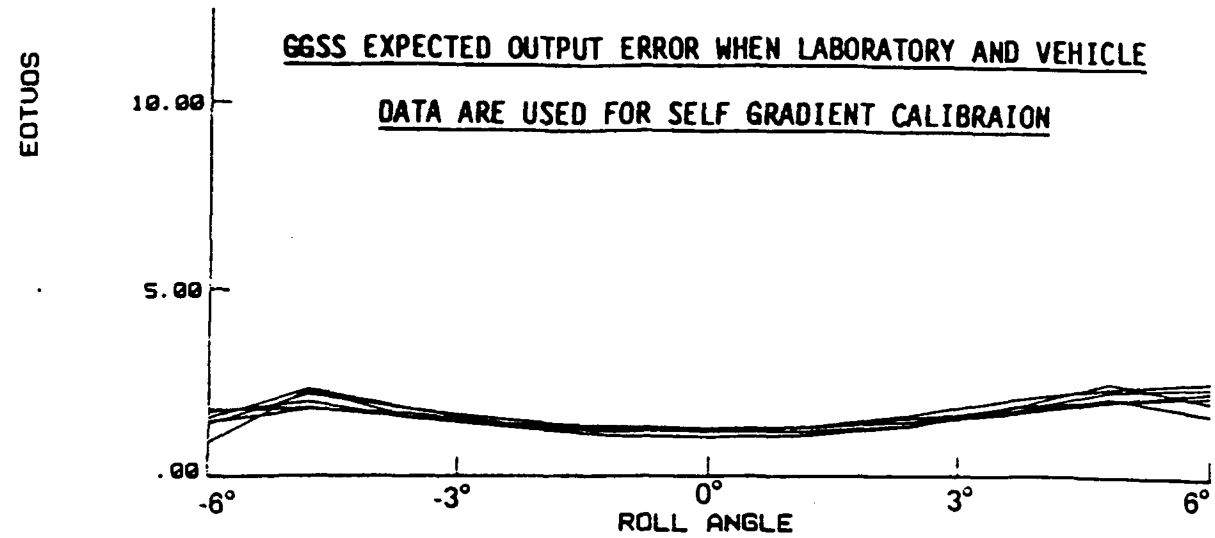

EXPECTED OUTPUT ERROR

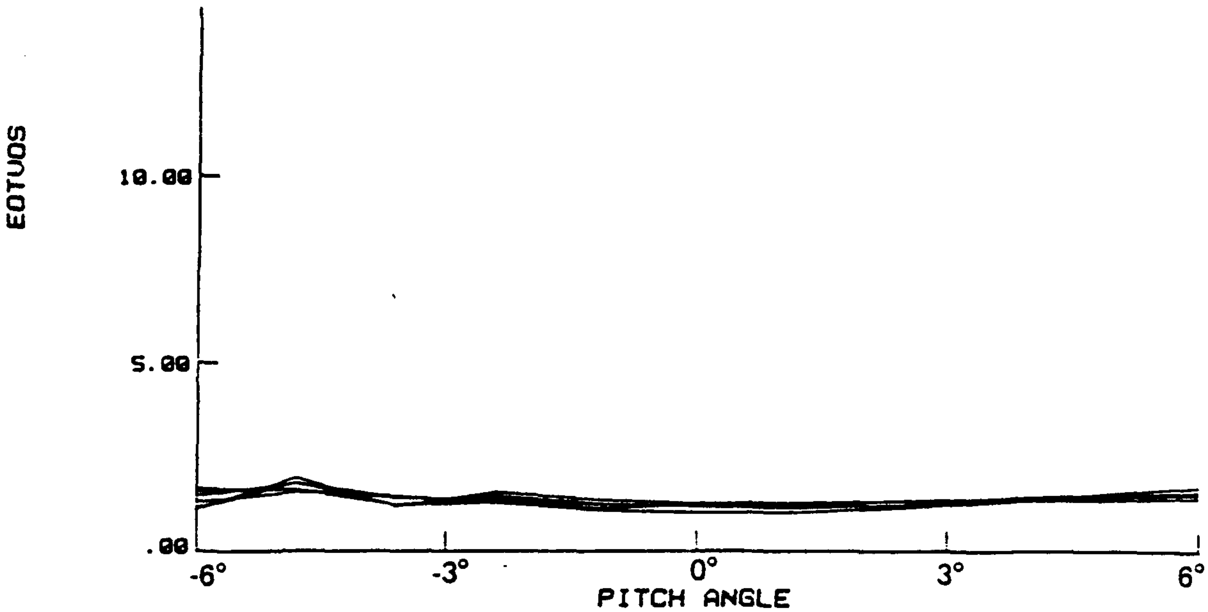

EXPECTED OUTPUT ERROR

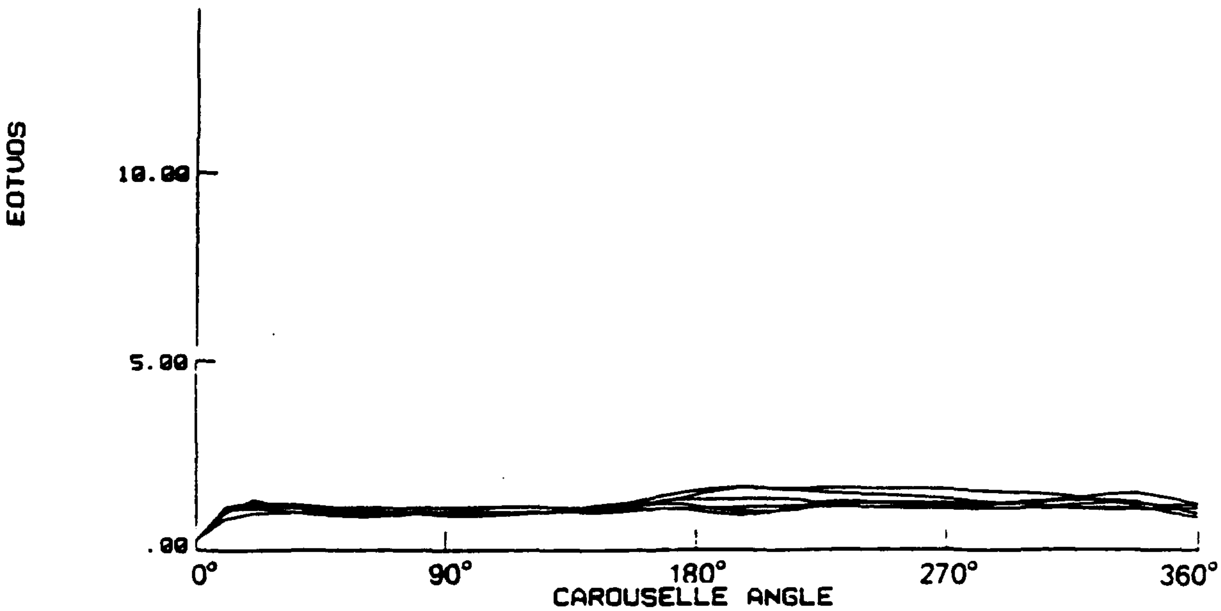

EXPECTED OUTPUT ERROR

GGSS EXPECTED OUTPUT ERROR WHEN AIRCRAFT DATA ONLY IS USED FOR SELF GRADIENT CALIBRATION

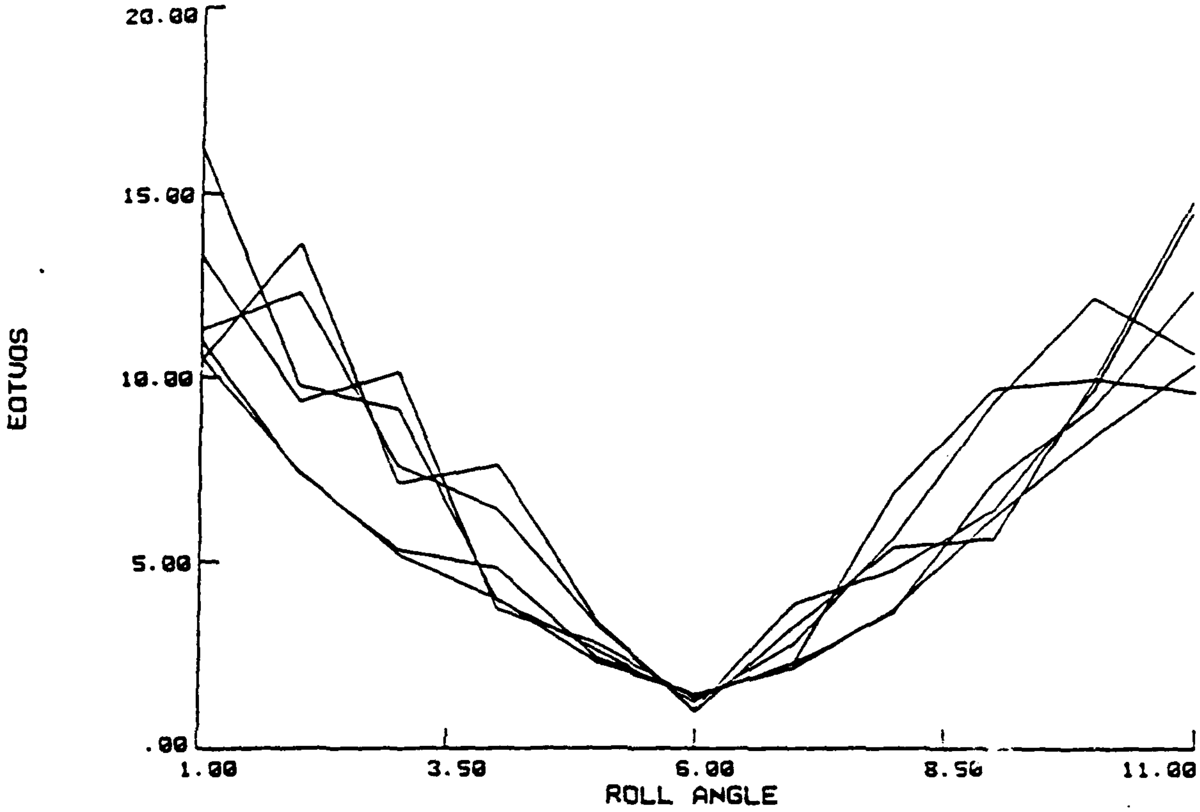

EXPECTED OUTPUT ERROR

07-OCT-86 08:53

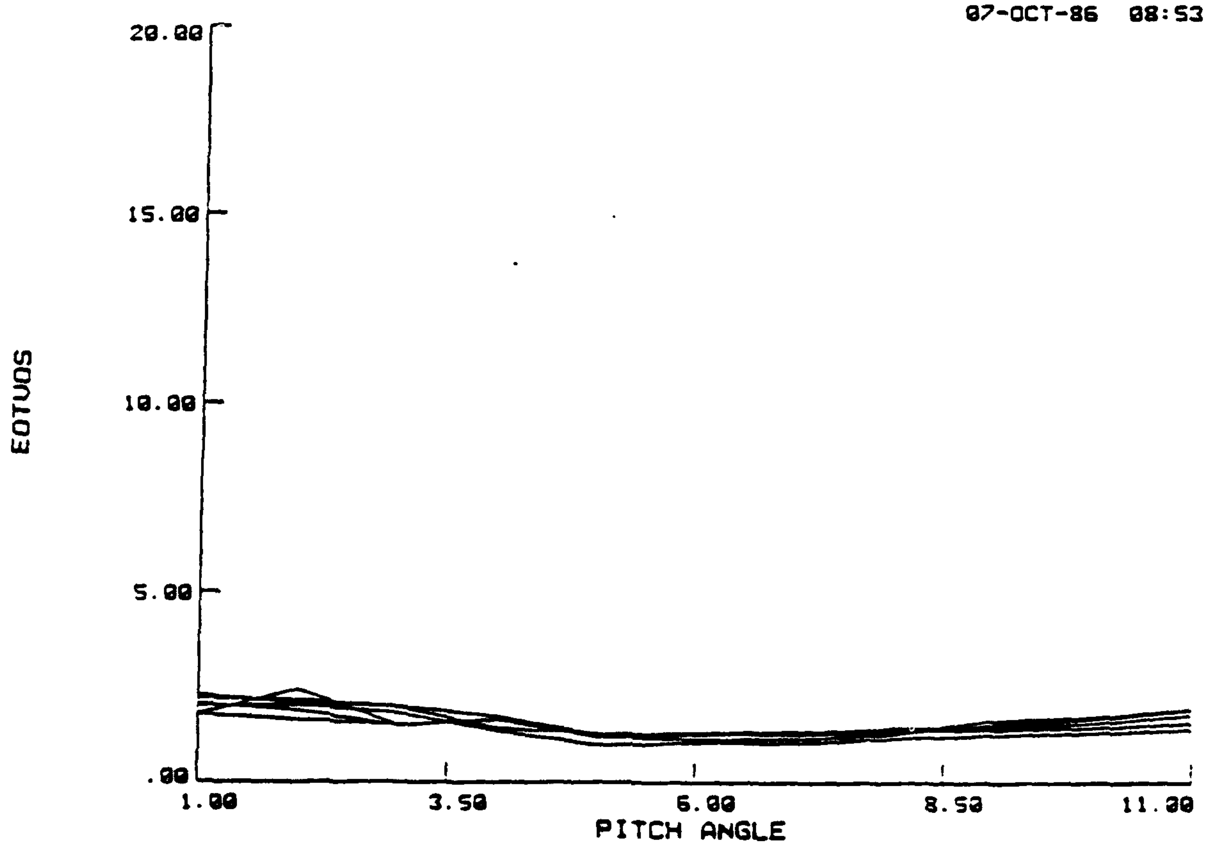

EXPECTED OUTPUT ERROR

GGI #1 OUTPUT DURING LABORATORY CALIBRATION WITH OUTPUT

PREDICTED BY MASS MODEL TAYLOR SERIES

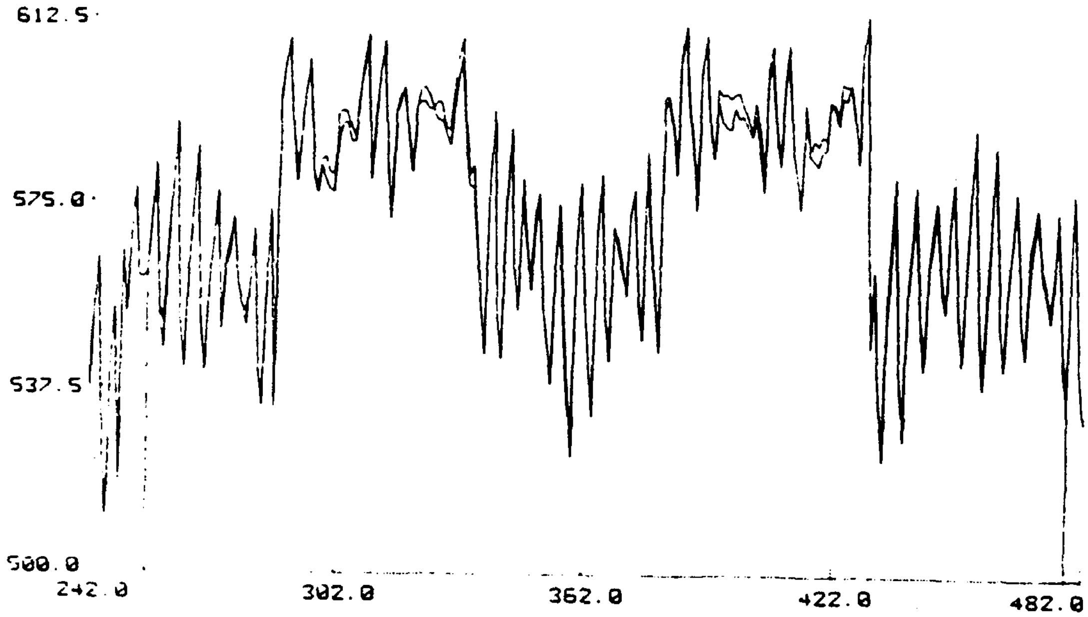

INLINE 1

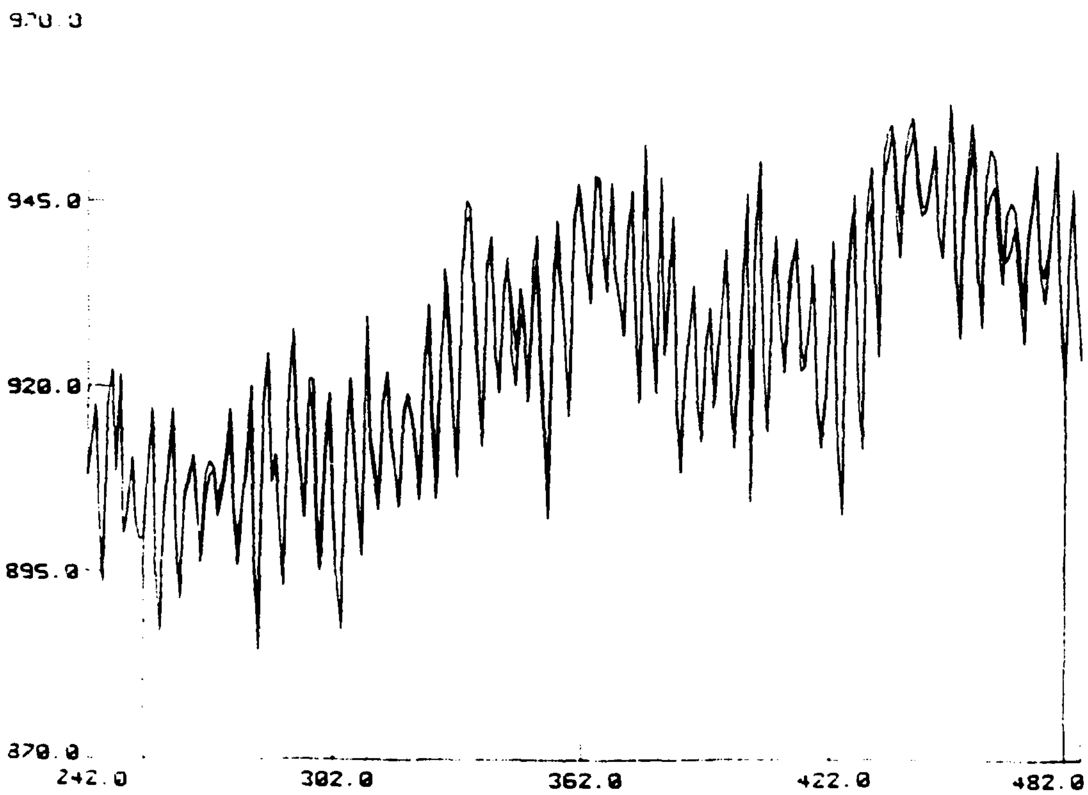

CROSS 1

GGI #2 OUTPUT DURING LABORATORY CALIBRATION WITH OUTPUT

PREDICTED BY MASS MODEL TAYLOR SERIES

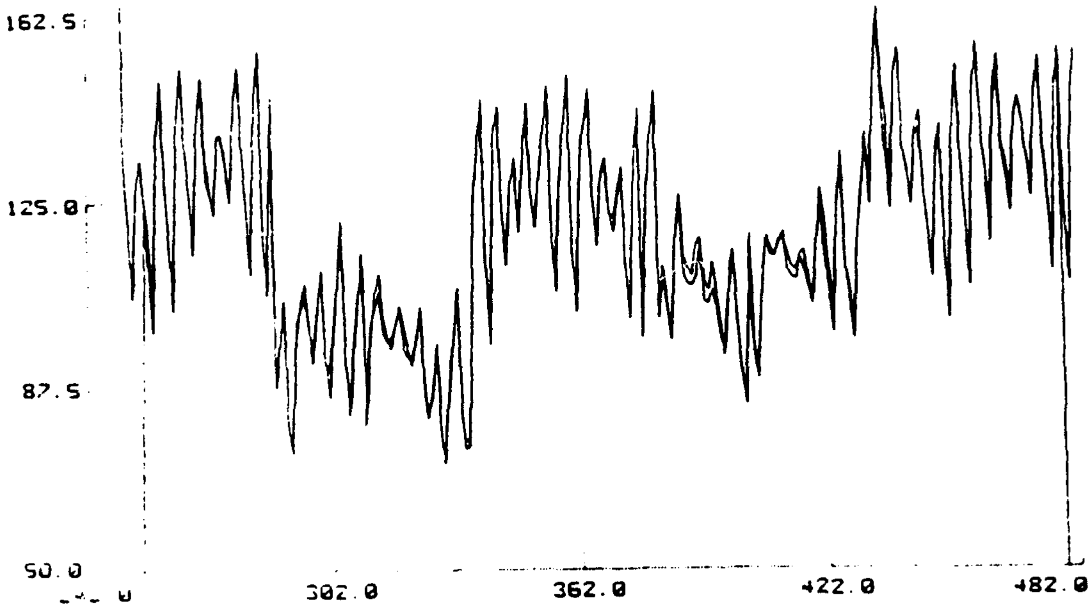

INLINE 2

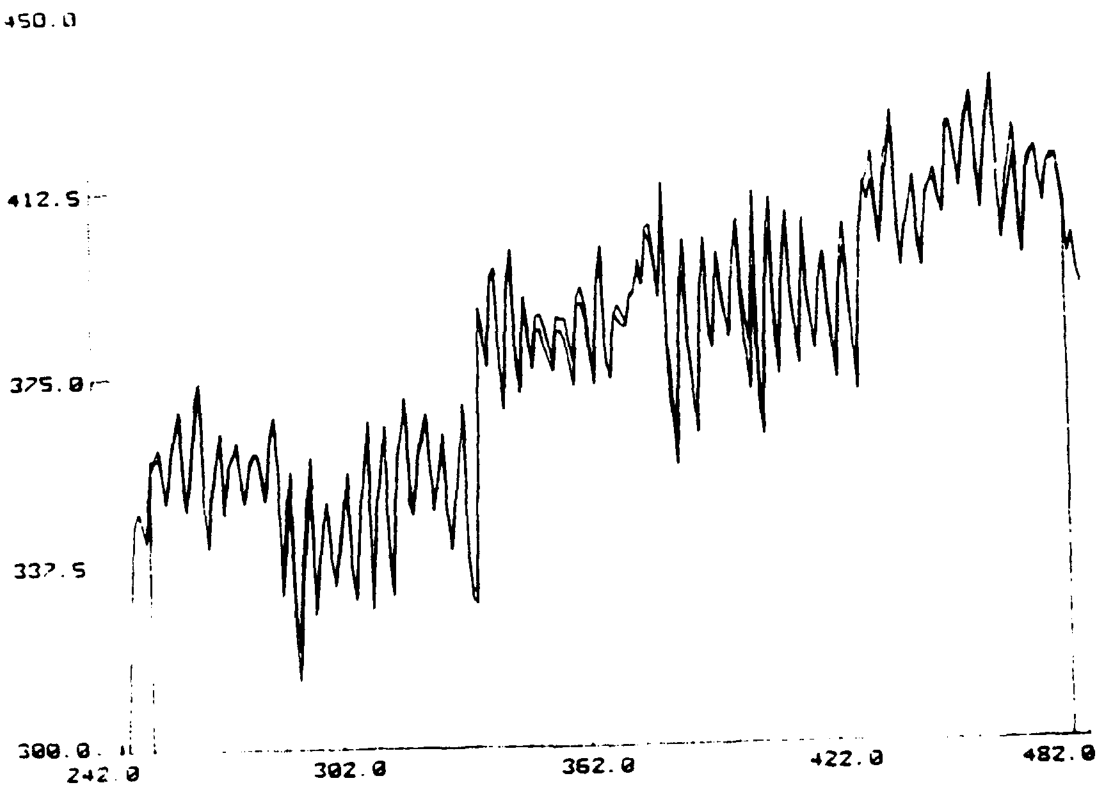

CROSS 2

GGI #3 OUTPUT DURING LABORATORY CALIBRATION WITH OUTPUT PREDICTED BY MASS MODEL TAYLOR SERIES

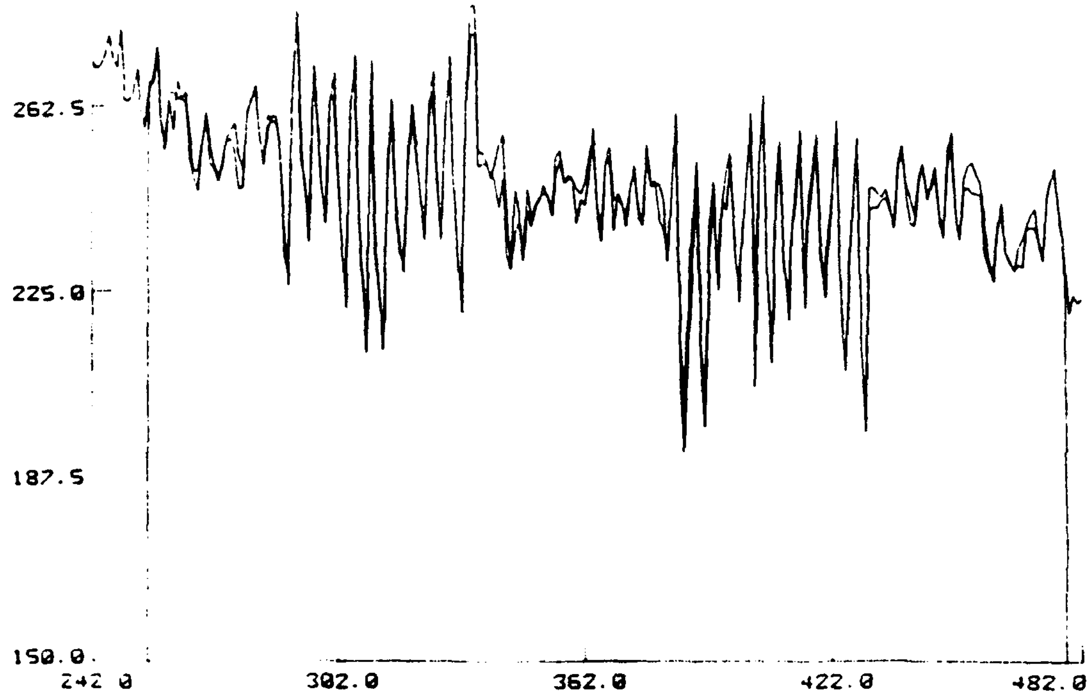

INLINE 3

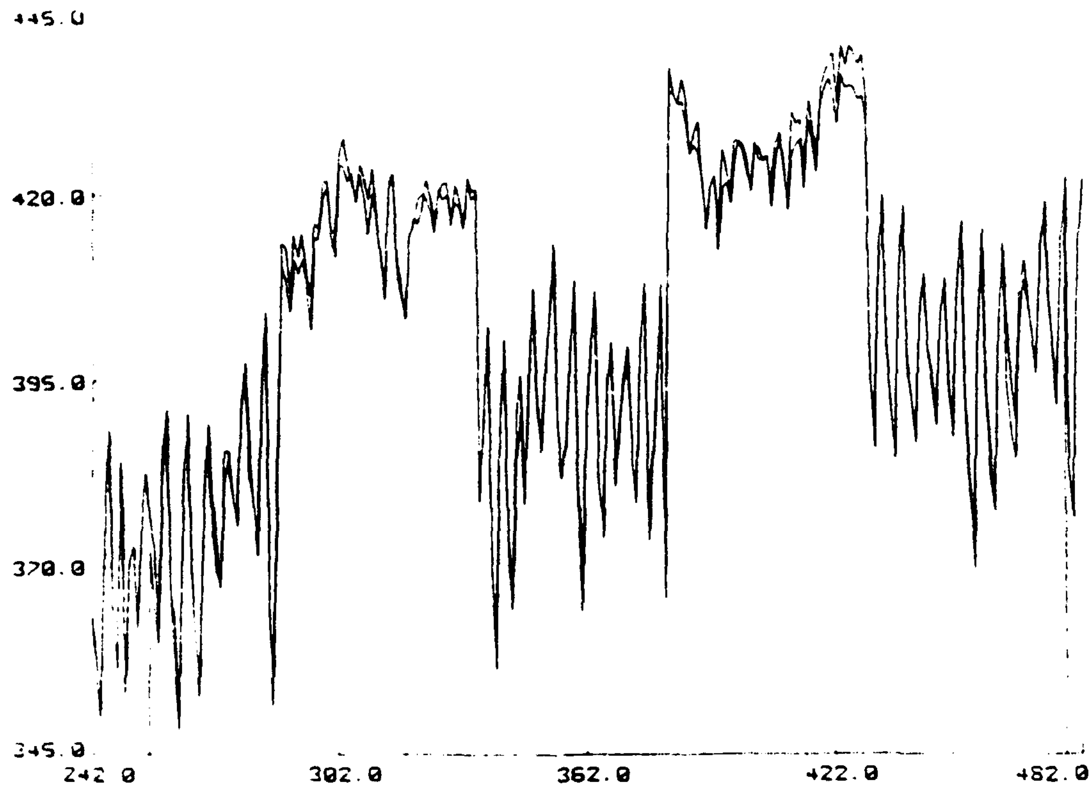

CROSS 3

GGI #1 OUTPUT DURING AIRCRAFT CALIBRATION WITH OUTPUT

PREDICTED BY TAYLOR SERIES

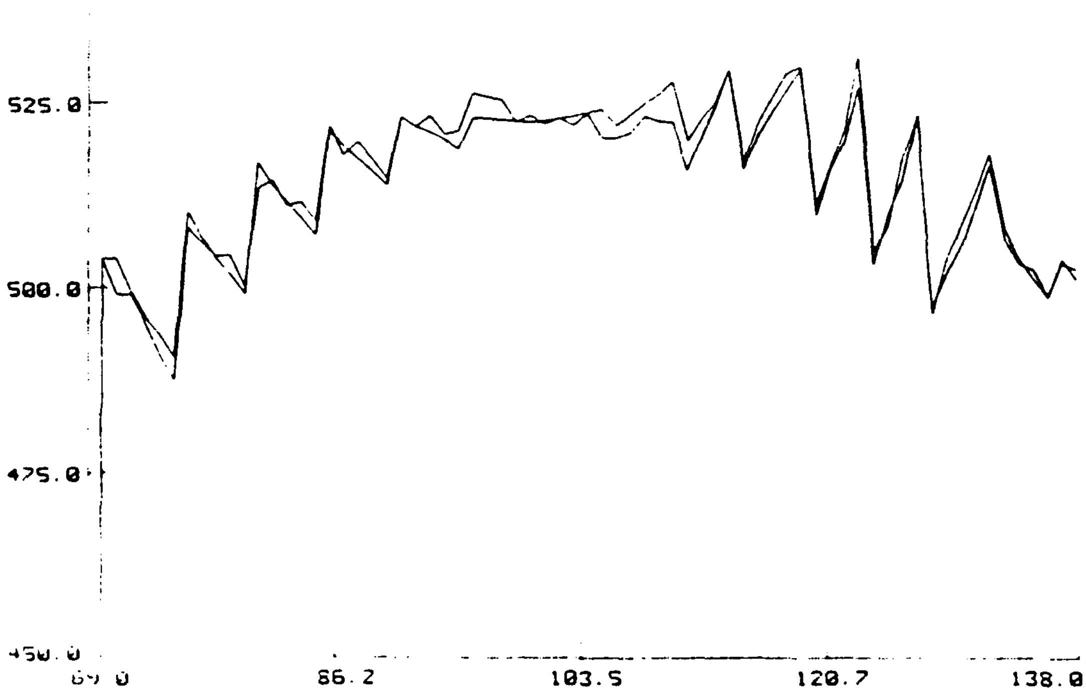

INLINE 1

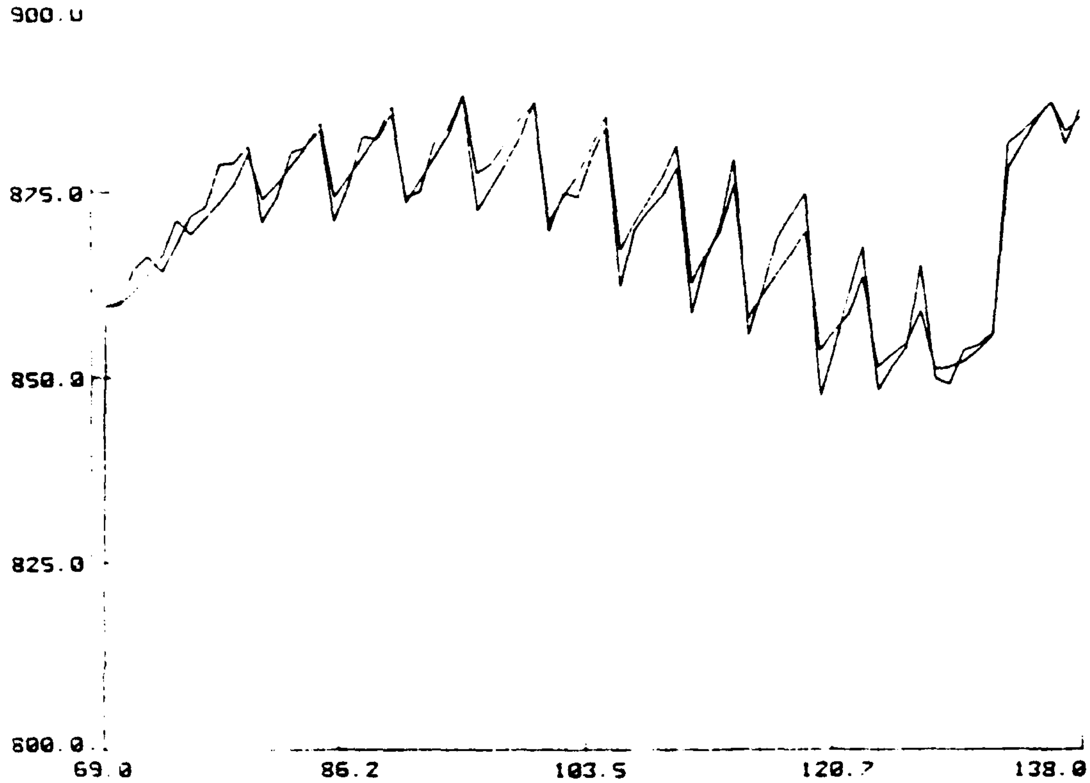

CROSS 1

GGI #2 OUTPUT DURING AIRCRAFT CALIBRATION WITH OUTPUT PREDICTED BY MASS MODEL TAYLOR SERIES

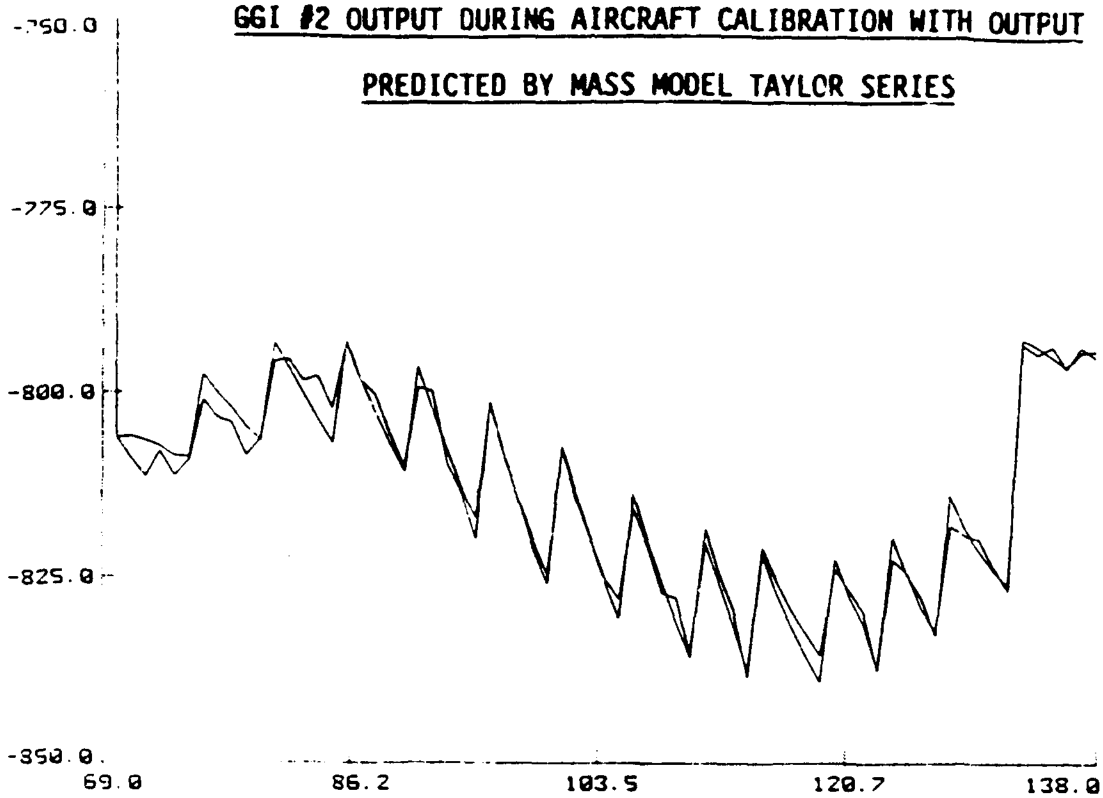

INLINE 2

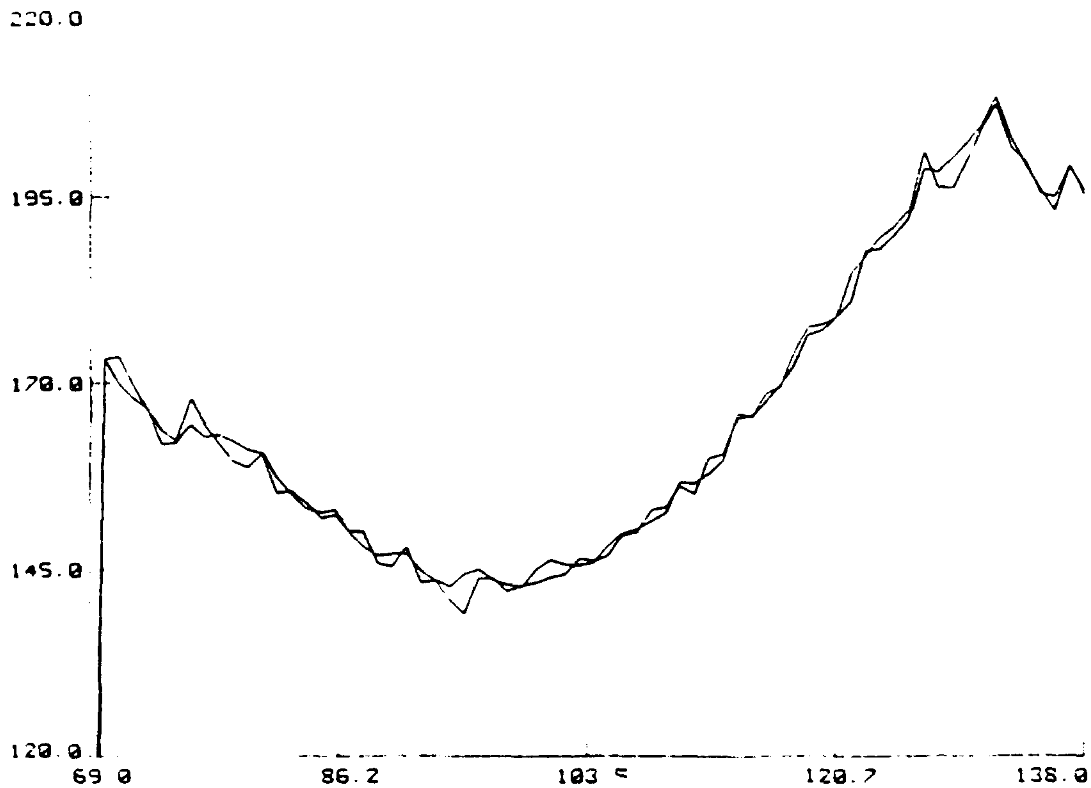

CROSS 2

GGI #3 OUTPUT DURING AIRCRAFT CALIBRATION WITH OUTPUT

PREDICTED BY MASS MODEL TAYLOR SERIES

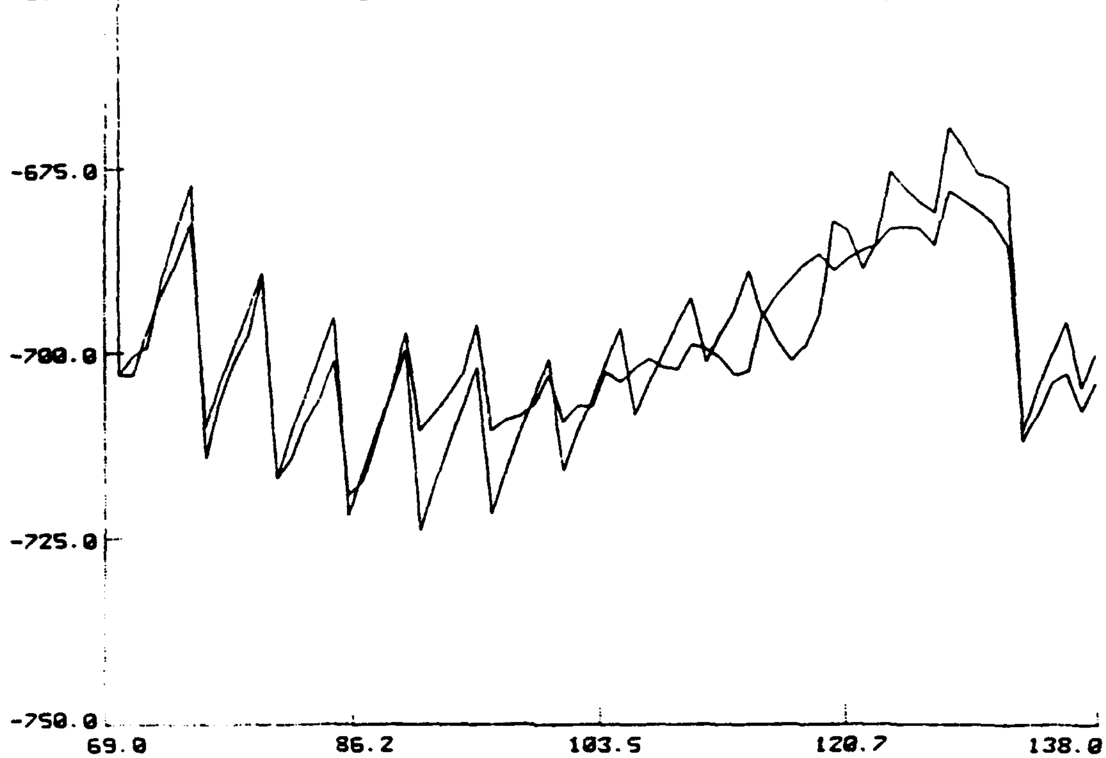

INLINE 3

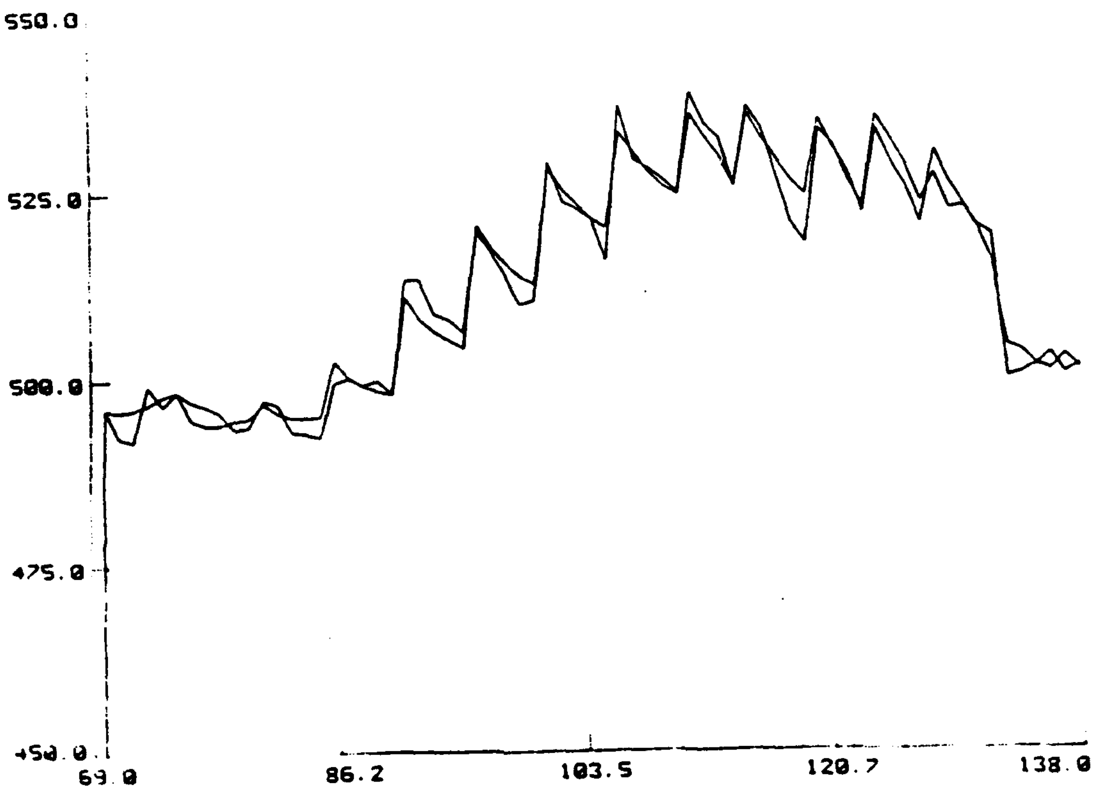

CROSS 3

	I_1	I_2	I_3	C_1	C_2	C_3
RESIDUE S.D. EOTVOS	2.47	2.42	3.67	2.43	3.01	2.64

OUTPUT ERROR STANDARD DEVIATION FOR GIMBAL MASS FILTER

	I_1	I_2	I_3	C_1	C_2	C_3
RESIDUE S.D. EOTVOS	2.05	2.06	5.6	2.65	1.6	2.42

OUTPUT ERROR STANDARD DEVIATION FOR AIRCRAFT MASS MODEL FILTER

SELF GRADIENT CALIBRATION CURVES GGI #3 FOR VARYING ROLL

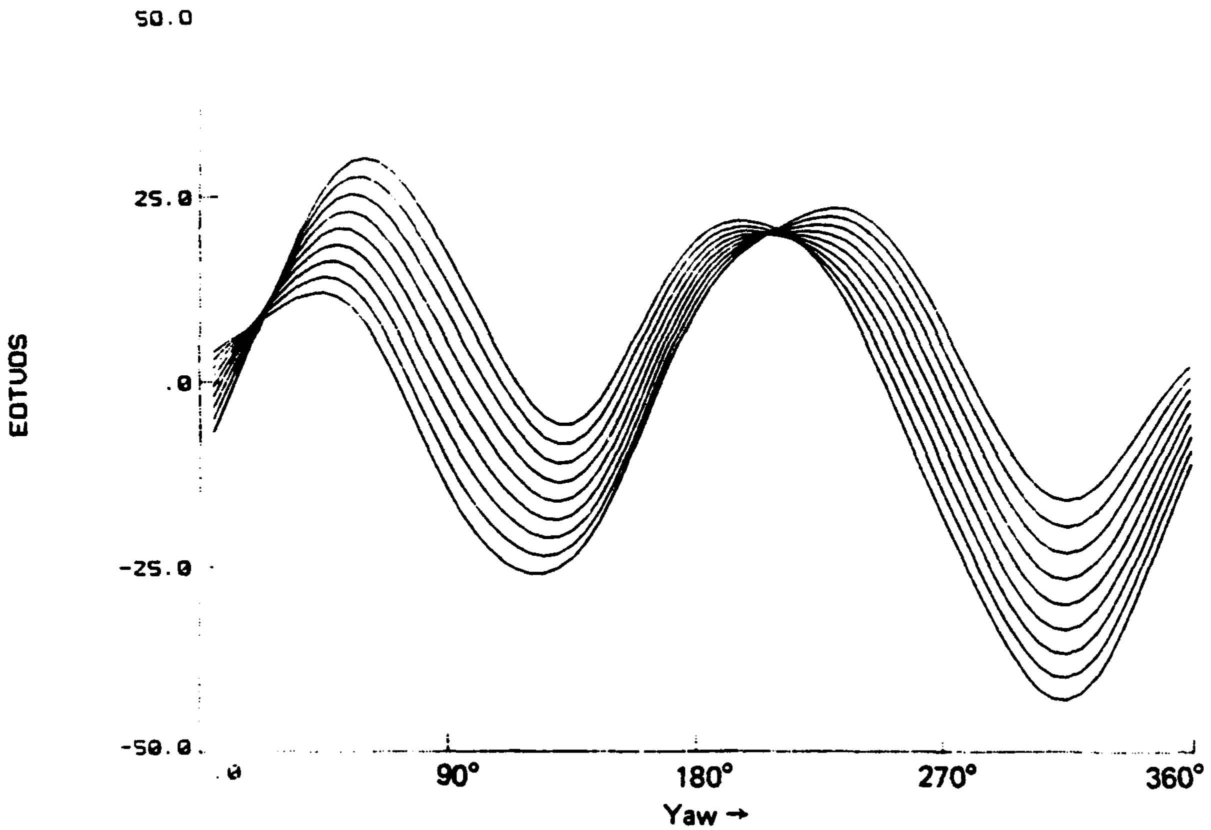

INLINE 3 TOTAL SELF GRADIENT COMPENSATION PITCH -8 +8

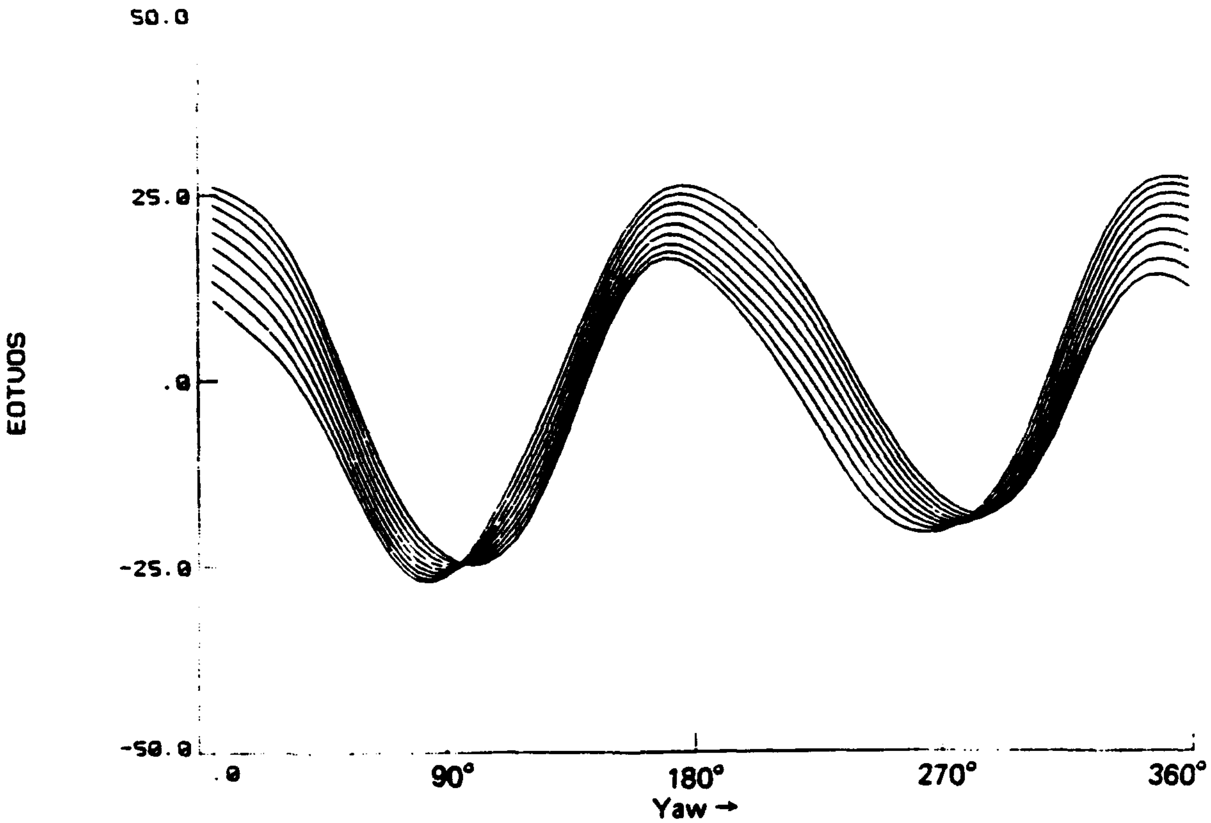

CROSS 3 TOTAL SELF GRADIENT COMPENSATION PITCH -8 +8

SELF GRADIENT CALIBRATION CURVES GGI #3 FOR VARYING PITCH

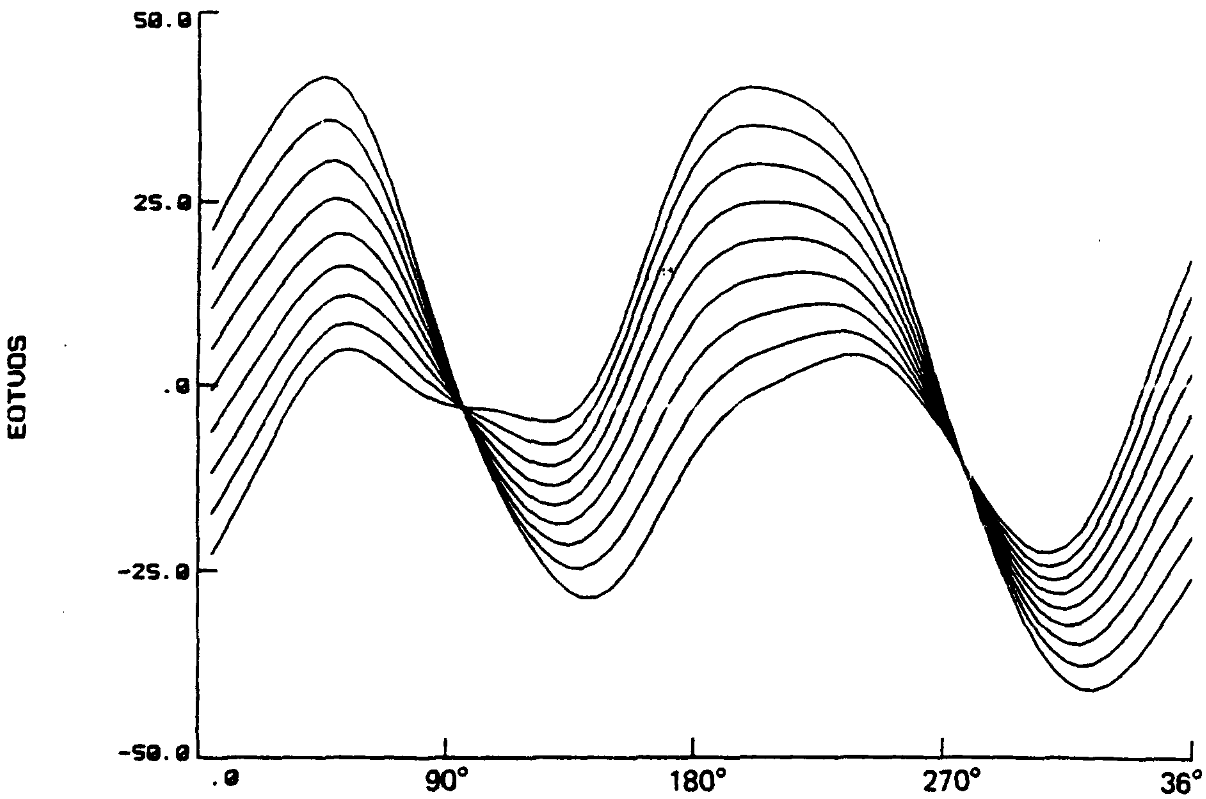

INLINE 3 TOTAL SELF GRADIENT COMPENSATION ROLL -8 +8

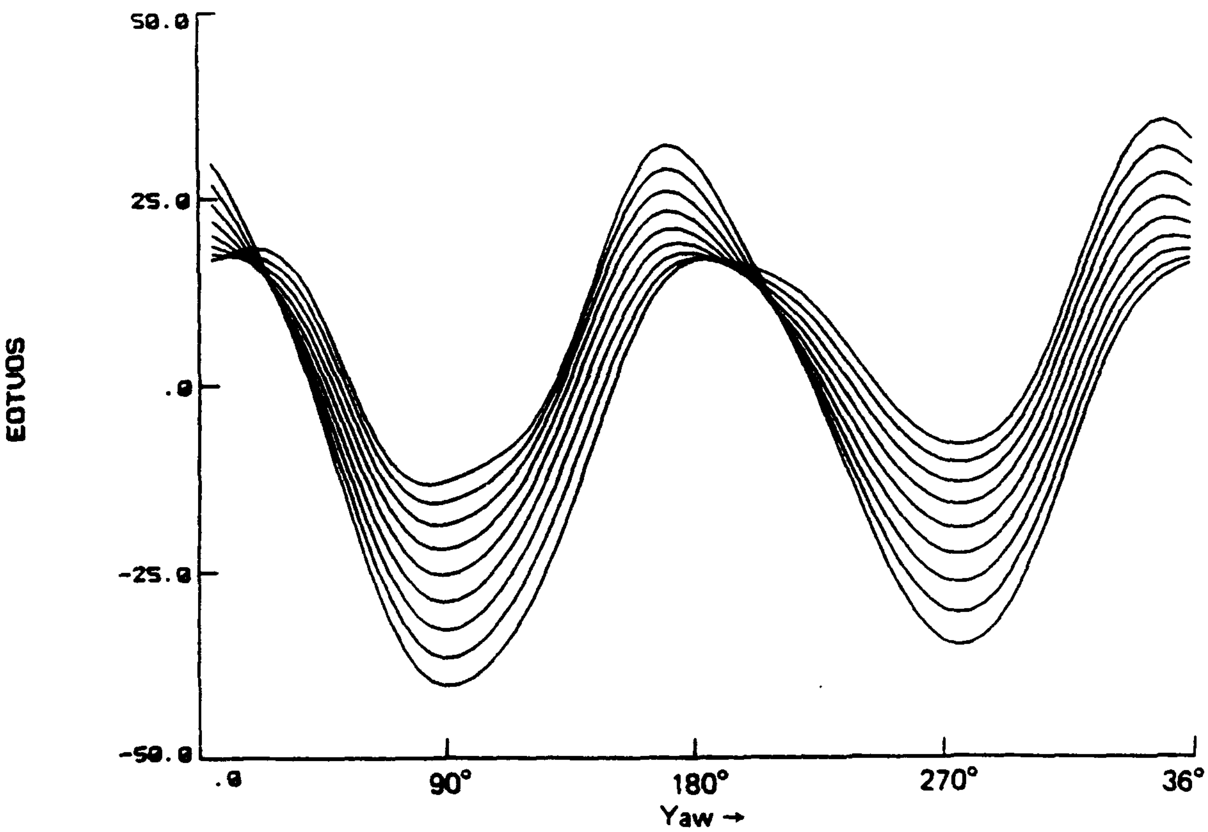

CROSS 3 TOTAL SELF GRADIENT COMPENSATION ROLL -8 +8

TECHNICAL APPROACH

A 45207

- COMPUTE ESTIMATES OF VERY HIGH-FREQUENCY GRAVITY FIELD IN GGSS TEST AREA USING DIGITAL TERRAIN DATA (DTED)
- UPGRADE THE TEXAS ATTENUATED WHITE NOISE (AWN) GRAVITY MODEL TO REFLECT THE HIGH-FREQUENCY TERRAIN EFFECTS IN DIFFERENT LOCATIONS
- USE UPGRADED AWN MODELS TO COMPUTE ALONG-TRACK POWER SPECTRA OF GRAVITY GRADIENTS AS FUNCTION OF ALTITUDE AND LOCATION
- DETERMINE f_{max} BY COMPARING ALONG-TRACK GRADIENT SPECTRUM WITH EXPECTED GGSS NOISE SPECTRUM
- USE $(2f_{max})^{-2}$ AS ESTIMATE OF MEAN-ANOMALY AREA SIZE CONSISTENT WITH GRADIOMETER DATA RESOLUTION ALONG TRACK

TASC

HIGH-FREQUENCY TERRAIN EFFECTS

A 45208

	VERTICAL COMPONENT		NORTH COMPONENT	
	ABSOLUTE MAXIMUM (MGAL)	STANDARD DEVIATION (MGAL)	ABSOLUTE MAXIMUM (MGAL)	STANDARD DEVIATION (MGAL)
NORTH REGION	18.0	3.0	12.2	2.1
SOUTH REGION	2.2	0.6	1.5	0.3

- DEFENSE MAPPING AGENCY DTED (3-arc sec SPACING) USED TO COMPUTE HIGH-FREQUENCY TERRAIN EFFECTS FOR WAVELENGTHS < 10 km
- NUMERICAL QUADRATURE USED TO EVALUATE TERRAIN-EFFECT INTEGRAL AT 262,144 GRID POINTS WITH RMS ERROR LESS THAN 0.15 MGAL

TASC

PRIOR TEXAS GRAVITY MODEL

A-45209

- AWN MODEL FITTED TO
  - WORLD-WIDE GRAVITY DATA (RAPP 180 MODEL)
  - LOCAL 5-km GRIDDED SURFACE DATA FROM NORTH TEXAS PROVIDED BY DMA
- DATA SPACING LIMITED MODEL ACCURACY FOR WAVELENGTHS SHORTER THAN 10 KM

TASC

UPGRADED AWN GRAVITY MODELS FOR BAKER PEAK REGION

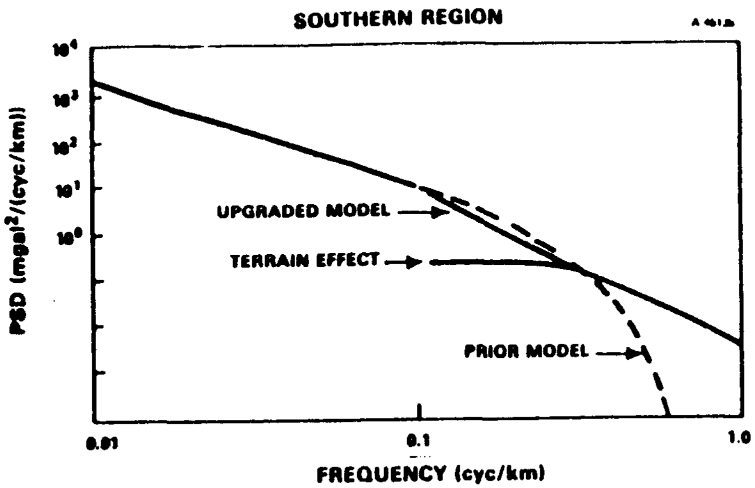

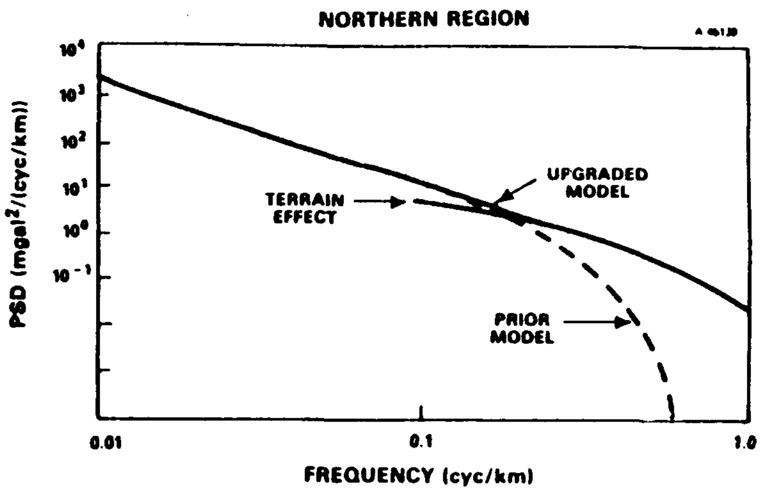

- FIGURES DEPICT ALONG-TRACK VERTICAL DISTURBANCE POWER SPECTRA
- TEXAS MODEL WAS UPGRADED TO BE CONSISTENT WITH COMPUTED TERRAIN EFFECTS
- UPGRADING CONSISTED OF ADDING TWO ADDITIONAL WHITE NOISE LAYERS
- UPGRADED MODELS HAVE SAME HIGH-FREQUENCY POWER AS TERRAIN EFFECTS

NORTH BAKER PEAK MODEL

ALONG-TRACK POWER SPECTRA OF VERTICAL/ALONG-TRACK GRADIENT

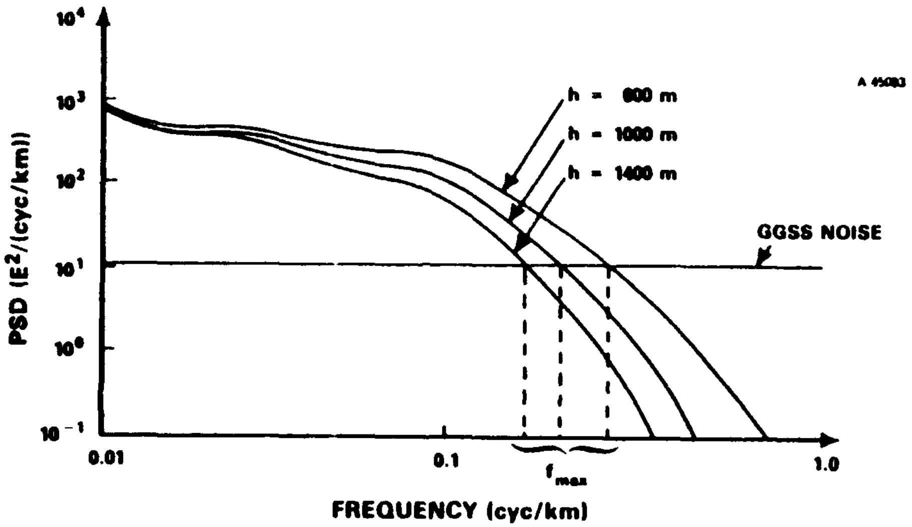

h (m)	f_{max} (cyc / km)	λ_{min} (km)
600	0.37	2.7
1000	0.23	4.3
1400	0.17	6.0

- EFFECTIVE INFORMATION BAND LIMIT, f_{max}, DEPENDS ON SURVEY HEIGHT, h
- APPROPRIATE AVERAGING AREAS FOR SURFACE GRAVITY PRODUCTS ARE ESTIMATED TO BE IN THE RANGE 2 km^2 TO 9 km^2

TASC

SOUTH BAKER PEAK MODEL

ALONG-TRACK POWER SPECTRA OF VERTICAL/ALONG-TRACK GRADIENT

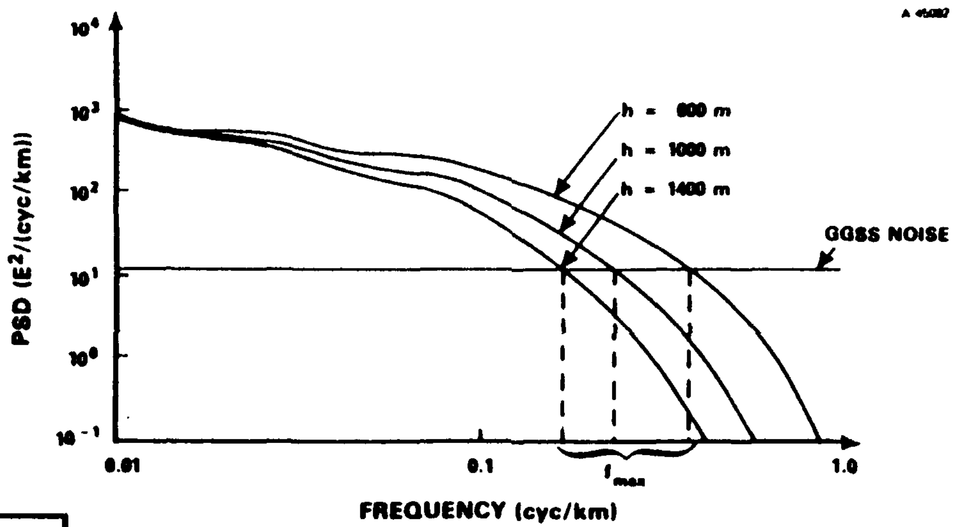

h (m)	f_{max} (cyc / km)	λ_{min} (km)
600	0.25	4.0
1000	0.18	5.6
1400	0.14	7.0

- EFFECTIVE INFORMATION BAND LIMIT, f_{max}, IS REDUCED COMPARED TO NORTH BAKER PEAK REGION
- APPROPRIATE AVERAGING AREA FOR SURFACE GRAVITY PRODUCTS RANGE FROM 4 km^2 TO 12 km^2

SENSITIVITY TO GGSS NOISE

ALONG-TRACK POWER SPECTRA OF VERTICAL/ALONG-TRACK GRADIENT

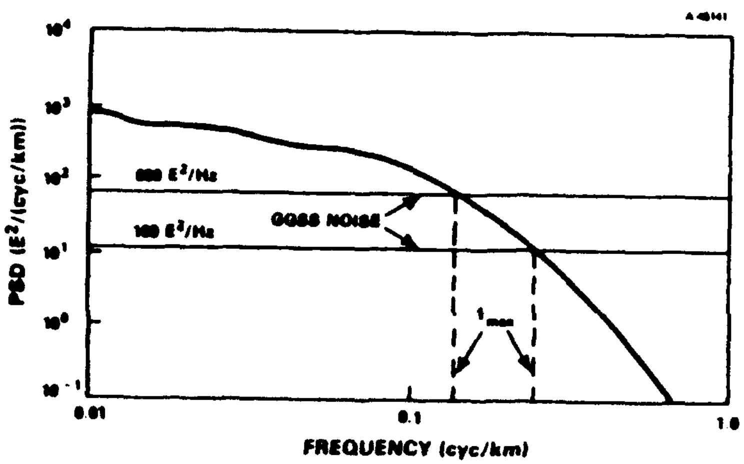

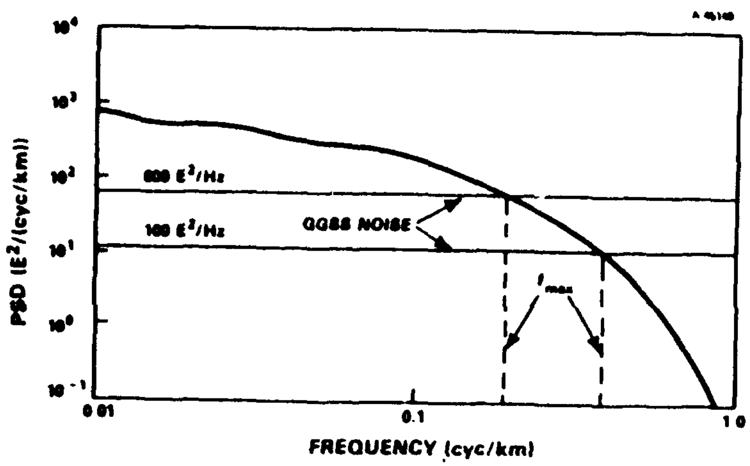

- HIGHER GGSS NOISE LEVEL REDUCES SPATIAL RESOLUTION BY FACTOR OF 1/2

- APPROPRIATE AVERAGING AREAS FOR SURFACE GRAVITY PRODUCTS RANGE FROM 2 km^2 TO 13 km^2

TASC

OBSERVATIONS AND CONCLUSIONS

A-45210

- THE EFFECTIVE BANDWIDTH OF AIRBORNE GRAVITY GRADIOMETER SURVEY DATA DEPENDS ON SURVEY ALTITUDE, GRADIOMETER NOISE, AND THE HIGH FREQUENCY CONTENT OF THE GRAVITY FIELD

- IN THE NORTH BAKER PEAK AREA OF THE GGSS TEST AREA (MODERATELY ROUGH TERRAIN) THE NOMINAL 600-m SURVEY ALTITUDE IMPLIES SHORT WAVELENGTH RESOLUTION OF 2.7 km, USING A GGSS OF EXPECTED ACCURACY. AN APPROPRIATE AVERAGING AREA FOR SURFACE GRAVITY DISTURBANCE QUANTITIES RECOVERED BY THIS SURVEY IS ONE ARC MIN × ONE ARC MIN

- SOUTH OF BAKER PEAK (VERY FLAT TERRAIN) A GGSS SURVEY AT 600 m ALTITUDE WITH GRADIOMETERS OF EXPECTED ACCURACY ENCOUNTERS ITS SHORT WAVELENGTH LIMIT AT 4.0 km.

- THE RECOMMENDED AVERAGING AREAS ARE CONSISTENT WITH ALONG-TRACK BANDWIDTHS

- THE METHODOLOGY MAY BE USED TO DETERMINE THE SIZE OF APPROPRIATE AVERAGING BLOCKS IN OTHER PROSPECTIVE SURVEY AREAS. EXTENSION OF THE METHODOLOGY CAN INCLUDE EFFECTS OF CROSS-TRACK ALIASING.

TASC

TITLE OF PAPER: Gravity Gradiometer Survey System (GGSS) Data Processing and Data Use

SPEAKER: Warren G. Heller

QUESTIONS AND COMMENTS:

1. Question: Unknown

   How big is the test area you used?

   Response:

   300 km on a side, modelled over 40 km.

2. Question: Rene Forsberg

   In fitting your improved AWN covariance model, did you use local gravity data (wavelengths shorter than 10 km) to compare "topographic" and "non-topographic" local gravity power?

   Response:

   No, these data were not available. However, the slope of the refined model seems to fit well with the slope inferred by the original AWN model.

3. Question: Richard Rapp

   What is the accuracy of the recovery of the terrain signal in the block sizes you considered to be the resolution of the system?

   Response:

   The aim is to recover the terrain effects to 0.1 mgal.

4. Question: Chris Jekeli

   Did you use isostatic compensation model for computing terrain effects on deflection of vertical?

   Response:

   No, just used the terrain data.

5. Question: John Brozena

   Did the error model for the gradiometer used in your analysis include environmental noise sources?

   Response:

   Yes.

6. <u>Question:</u> James E. Fix

In analyzing the terrain effect, was a variable density or a constant density used?

<u>Response:</u>

A constant density was used. Density was taken as 2.67 g/cm^3.

7. <u>Question:</u> Sam Bose

How does the performance deteriorate as the averaging size is increased?

<u>Response:</u>

There is no performance degradation provided the averaging size takes into account the maximum bandlimit of the gradiometer signal.

SELF GRADIENT CALIBRATION OF THE GGSS IN A C-130 AIRCRAFT

by

Dr. W. John Hutcheson
Bell Aerospace Textron
P.O. Box One
Buffalo, NY 14240

ABSTRACT

Due to the inverse cube law for gravity gradients, mass structures close to the gradiometer sensing elements produce significant outputs termed self gradients which have to be compensated for in the GGSS Stage I data reduction. In the Bell approach to the self gradient calibration, a mass model representing the mass structures, consisting of the GGSS platform gimbals, servo motors, binnacle and aircraft, is identified using optimal identification techniques and then used to generate the compensation.

This paper contains a brief description of the theory underlying the Bell approach to the self gradient calibration, details of the self gradient calibration of the GGSS, covariance results, GGSS calibration data and the calibration curves representing the combined field of the GGSS, the van and the C-130 aircraft.

MOVING BASE GRAVITY GRADIOMETER REVIEW

Self Gradient Calibration Of GGSS In C-130 Aircraft

AIR FORCE ACADEMY

Report No. 6501-927173 • FEBRUARY 11/12, 1987

Bell Aerospace TEXTRON
Division of Textron Inc

to temperature fluctuations. Improvements to the cryostat have increased the thermal isolation and stability and are expected to reduce noise from this source.

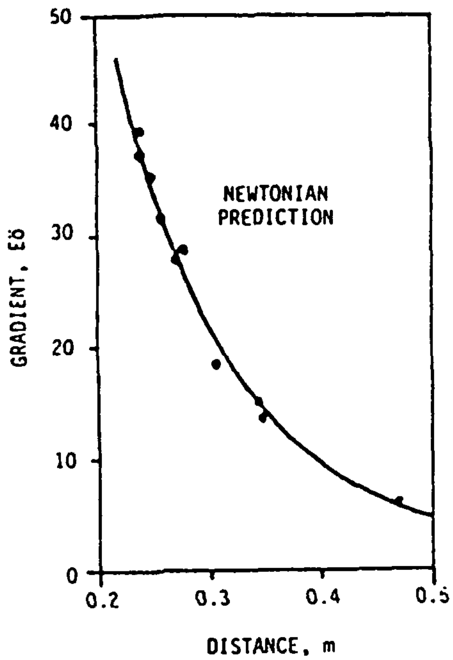

Figure 5 Gradient signal as a function of distance. The observed gradient signal is plotted against the distance between the centres of mass of the gradiometer and the rim of the gradient generator. The solid curve is calculated from its known mass distribution and varies approximately as the inverse cube of the spacing.

Conclusion

The prototype gradiometer has demonstrated that useful gradient sensitivity is attainable and that intrinsic detector noise is unlikely to be a limitation on the development of a practical instrument. However, improvements in multi-axis common mode rejection and rotational stabilization are required. These will be difficult to achieve, but do appear to be practicable.

References

1. S. Hammer and R. Anzoleaga, "Exploring for Stratigraphic Traps with Gravity Gradients", Geophysics 40, p.256, (1975).

2. S.K. Jordan, "Moving-Base Gravity Gradiometer Surveys and Interpretation", Geophysics 43, p.94, 1978.

   See also in "Spaceborne Gravity Gradiometry Workshop", Goddard Space Flight Centre. Greenbelt, Md, (Feb - Mar 1983).

3. E.R. Mapoles, PhD Thesis, Stanford University, (1981).

4. H.J. Paik, "Superconducting Tunable-Diaphragm Transducer for Sensitive Acceleration Measurements", J. Appl. Phys. 47, p1168, (1976).

5. M.V. Moody, H.A. Chan, and H.J. Paik, "Preliminary Tests of a Newly Developed Superconducting Gravity Gradiometer", IEEE Transactions in Magnetics, MAG-19, 461, (1983).

*Research supported by the Australian National Energy Research, Development and Demonstration Program and by B P Australia.

TITLE OF PAPER: A Prototype Superconducting Gravity Gradiometer for Geophysical Exploration

SPEAKER: Frank J. van Kann

QUESTIONS AND COMMENTS:

1. Question: Jean-Paul Richard

What are the mechanical Q, the resonant frequency of test masses and the electrical Q?

Response:

$Q_{mechanical} \cong 10^5$

Frequency of test masses = 30 Hz

$Q_{electrical}$ = not determined

2. Question: Ho Jung Paik

a) What kind of suspension did you use for the gradiometer?
b) Why is it that your noise spectrum does not show resonance peaks of the suspension modes?

Response:

a) It was soft-suspended. And there was some nasty resonance.
b) We used notch filters to remove those peaks.

3. Question: Anthony R. Barringer

What type of rotational stability do you require in the platform for mounting the gradiometer?

Response:

10^{-5} radians per second. It is desirable to have the platform inside the cryostat.

GRAVITY GRADIOMETER SURVEY SYSTEM (GGSS) DATA PROCESSING AND DATA USE

by

Dr. Warren G. Heller
The Analytic Sciences Corp.
100 Walkers Brook Drive
Reading, MA 01867

ABSTRACT

Since the GGSS will be flown at a given altitude, h, (approx. 600m) above the surface, a short wavelength limit is effectively imposed on the information content of the acquired data. This limit is dictated by the noise of the gradiometer instruments and the upward continuation factor, $e^{-2\pi h/\lambda}$, where λ is the gravity disturbance wavelength. Since the information is band limited, it is appropriate to consider representing the downward continued gravity disturbance estimates as area means over a suitably-sized block that retains full data resolution and is easy to incorporate into existing gravity data bases. For a given survey area, the averaging block size increases with flight altitude. This paper 1) describes an analytic technique for determining the shortest wavelength at which information is reliably gathered by an airborne gradiometer, 2) presents the results of applying this technique in the GGSS test area, and 3) discusses the implications of survey altitude on resolution of gravity disturbance recovery by gradiometric surveys in other areas. Video displays are presented which illustrate character of the short wavelength gravity field in the test area.

SP-5362-2

GRAVITY GRADIOMETER SURVEY SYSTEM (GGSS) DATA PROCESSING AND DATA USE

11 February 1987

Prepared for:

Fifteenth Moving Base Gravity Gradiometer Review
United States Air Force Academy
Colorado 80840

THE ANALYTIC SCIENCES CORPORATION
55 Walkers Brook Drive
Reading, Massachusetts 01867

FOREWORD

This document contains material used in a presentation given by The Analytic Sciences Corporation. The material is not intended to be self-explanatory, but rather should be considered in the context of the overall presentation.

ABSTRACT

Gravity Gradiometer Survey System (GGSS)
Data Processing and Data Use

Since the GGSS will be flown at a given altitude, h, (approx. 600 m) above the surface, a short wavelength limit is effectively imposed on the information content of the acquired data. This limit is dictated by the noise of the gradiometer instruments and the upward continuation factor, $e^{-\lambda h}$, where λ is gravity disturbance wavelength. Since the information is band limited, it is appropriate to consider representing the downward continued gravity disturbance estimates as area means over a suitably-sized block that retains full data resolution and is easy to incorporate into existing gravity data bases. For a given survey area, the averaging block size increases with flight altitude. This paper 1) describes an analytic technique for determining the shortest wavelength at which information is reliably gathered by an airborne gradiometer, 2) presents the results of applying this technique in the GGSS test area, and 3) discusses the implications of survey altitude on resolution of gravity disturbance recovery by gradiometric surveys in other areas. Video displays are presented which illustrate the character of the short wavelength gravity field in the test area.

OVERVIEW

A 45204

- BACKGROUND
- STATEMENT OF THE PROBLEM
- TECHNICAL APPROACH
- RESULTS FOR BAKER PEAK AREA
- VIDEO TAPE ILLUSTRATING HIGH-FREQUENCY FIELD

TASC

BACKGROUND

A 45206

- TASC IS UNDER CONTRACT WITH AFGL TO
  - PROVIDE INDEPENDENT ANALYSIS OF THE GGSS
  - REDUCE GRADIOMETER DATA AND ASSESS PERFORMANCE
  - ANALYZE TERRAIN AND OTHER SHORT WAVELENGTH EFFECTS
- FLIGHT ALTITUDE ABOVE SURFACE EFFECTIVELY PRECLUDES VERY SHORT WAVE-LENGTH RECOVERY OF GRAVITY FIELD AT THE SURFACE
- NATURAL QUESTION FOR AIRBORNE GRADIOMETRIC SURVEY OPERATIONS IS:

  "WHAT IS THE APPROPRIATELY-SIZED AVERAGING BLOCK ON WHICH TO REPRESENT SURFACE ESTIMATES OF GRAVITY DISTURBANCE OR GRAVITY ANOMALY WITHOUT SUFFERING ANY EFFECTIVE INFORMATION LOSS?"

TASC

STATEMENT OF PROBLEM

A 45206

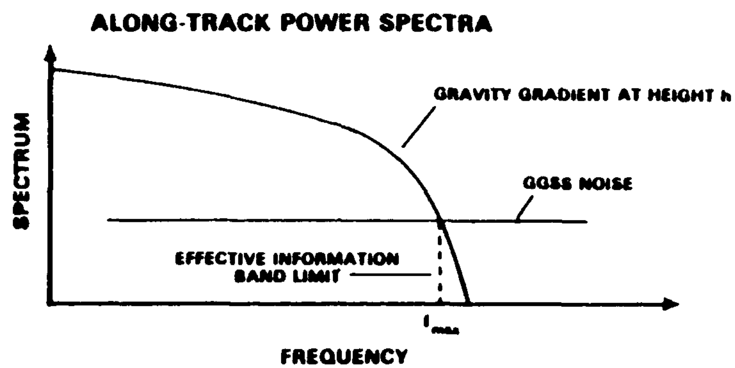

- DETERMINE f_{max}, THE EFFECTIVE INFORMATION BAND LIMIT FOR GGSS DATA
- f_{max} IS FREQUENCY WHERE GRADIENT SPECTRUM CROSSES GRADIOMETER NOISE SPECTRUM (SIGNAL-TO-NOISE RATIO IS UNITY)
- f_{max} DETERMINES AVERAGE SPATIAL RESOLUTION OF AIRBORNE SURVEY DATA ALONG TRACK
- GIVEN f_{max}, ESTIMATE APPROPRIATE AVERAGING AREAS FOR SURFACE GRAVITY PRODUCTS

TASC

Uncorrected Gravity Gradient Measured on GGSS Shakedown Drive

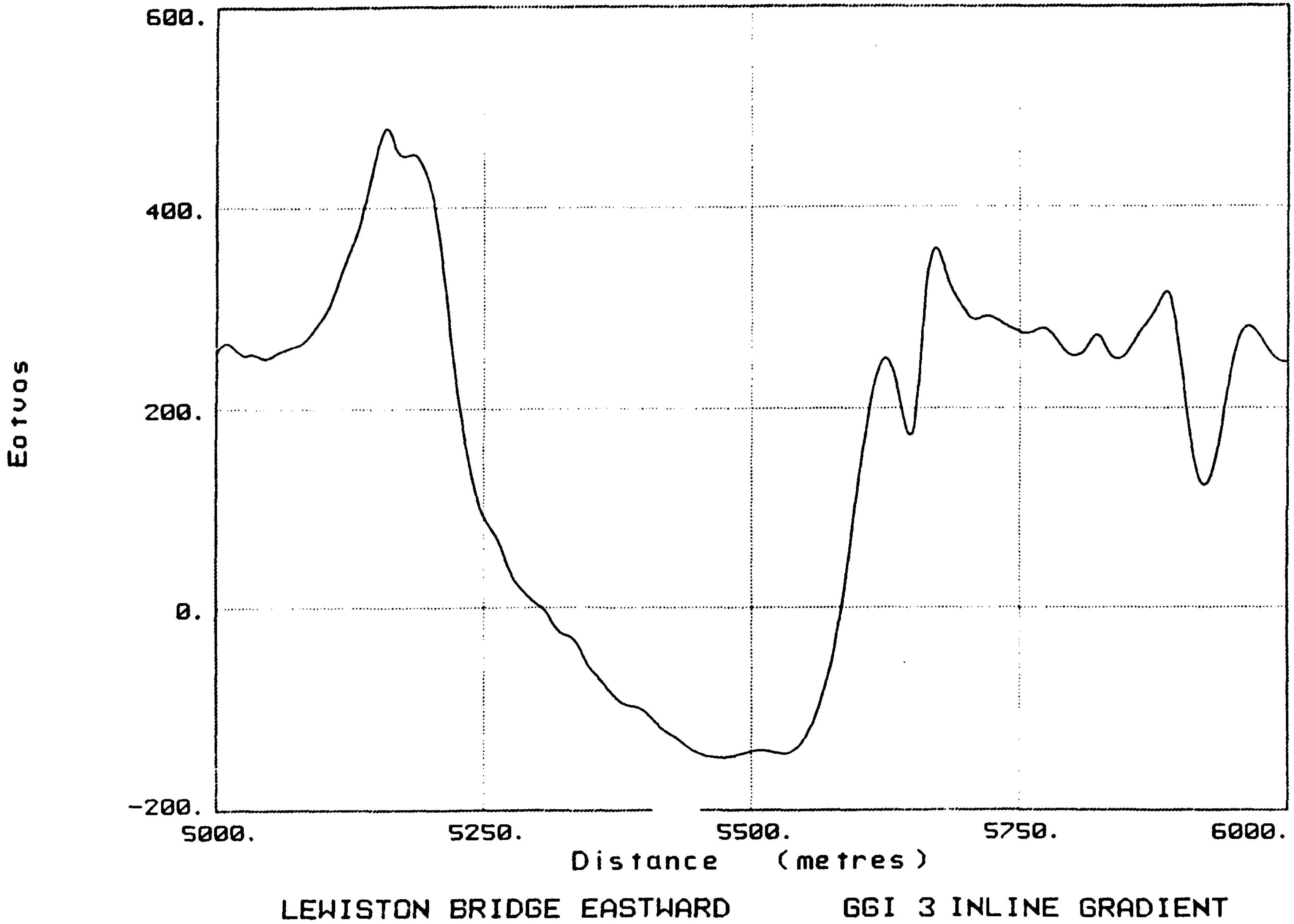

Bell Aerospace TEXTRON

Uncorrected Gravity Gradient Measured on GGSS Shakedown Drive

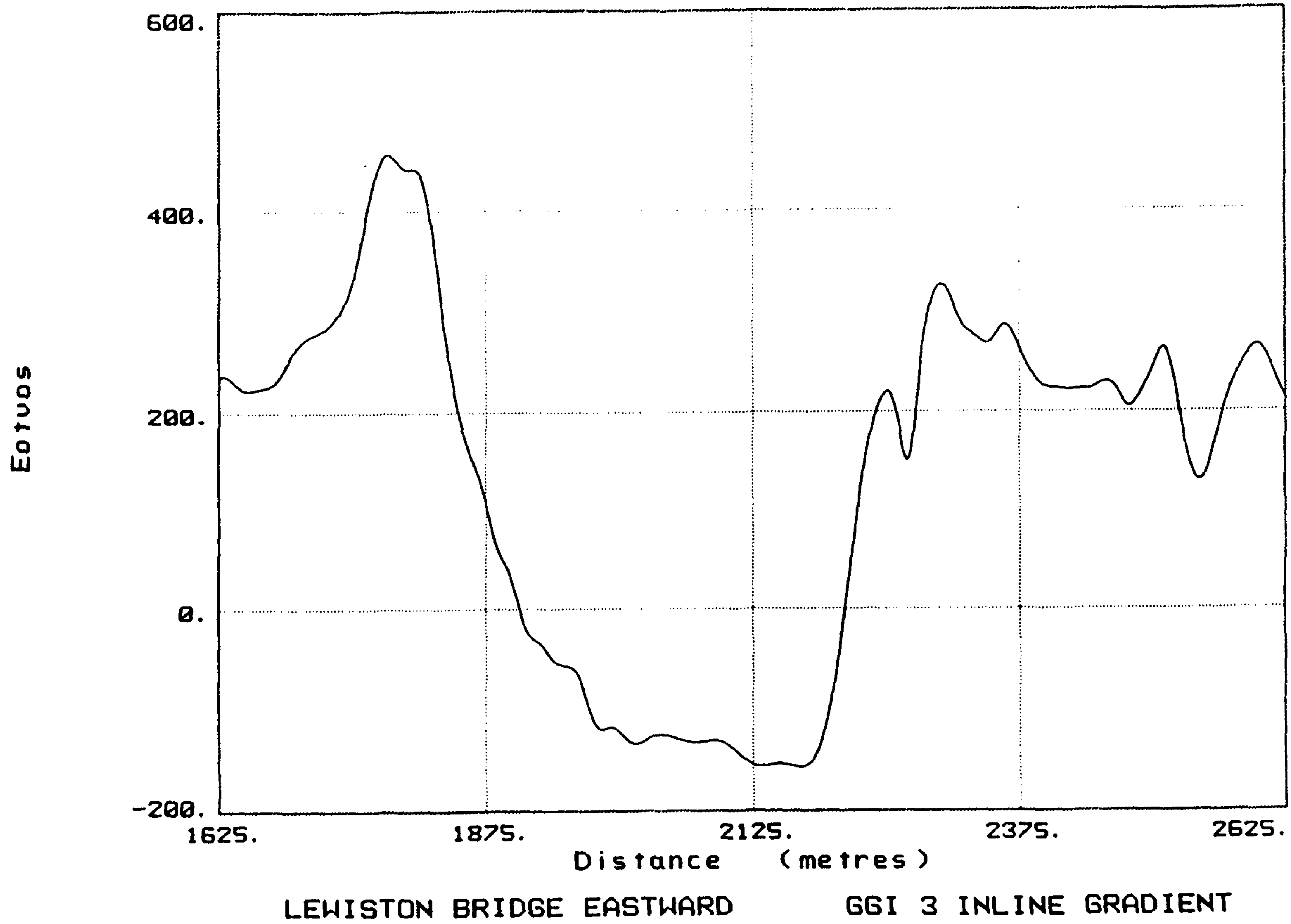

Bell Aerospace TEXTRON

Uncorrected Yaw Angle
Measured On GGSS Shakedown Drive

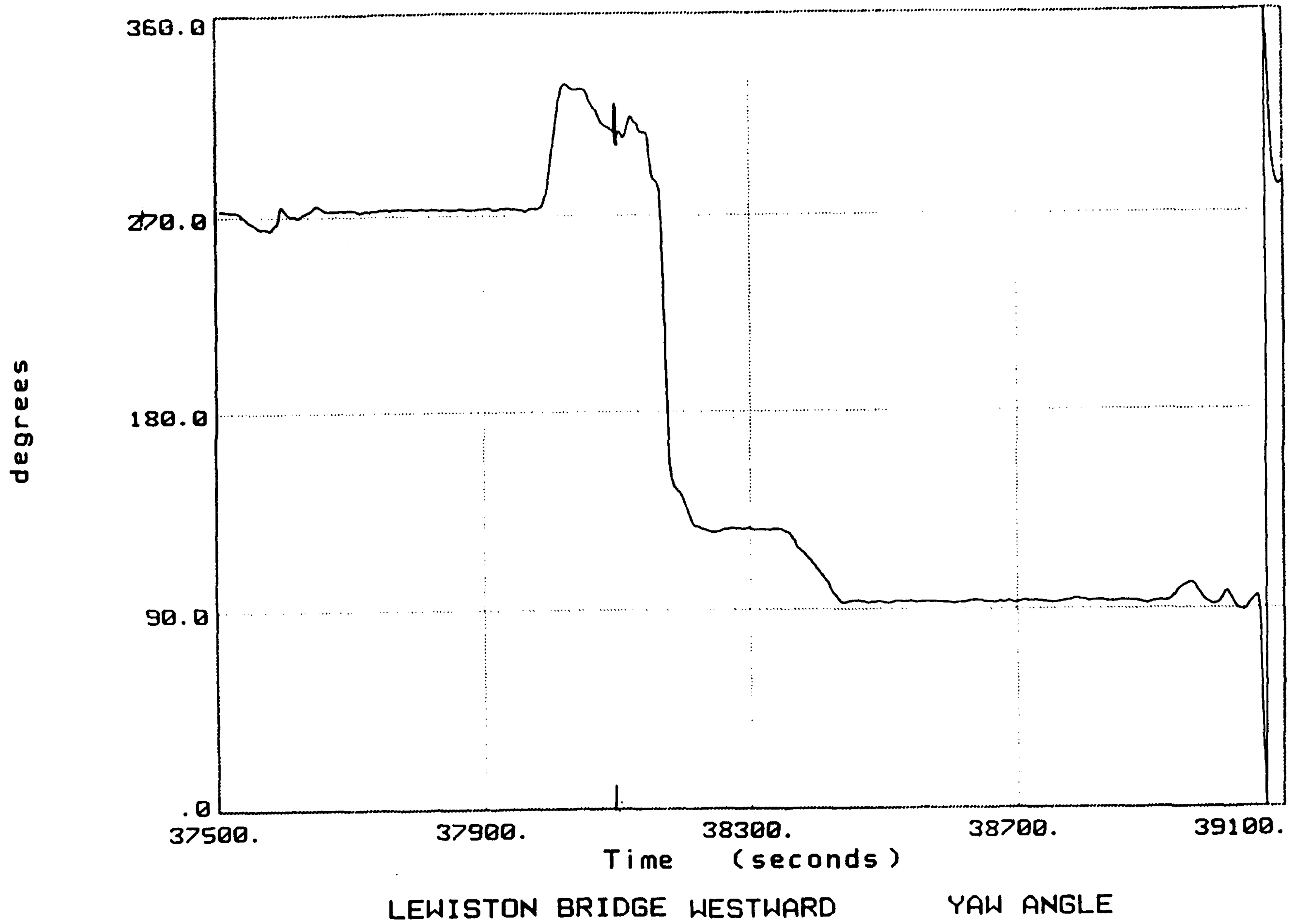

Bell Aerospace TEXTRON

Uncorrected Z-Acceleration Measured On GGSS Shakedown Drive

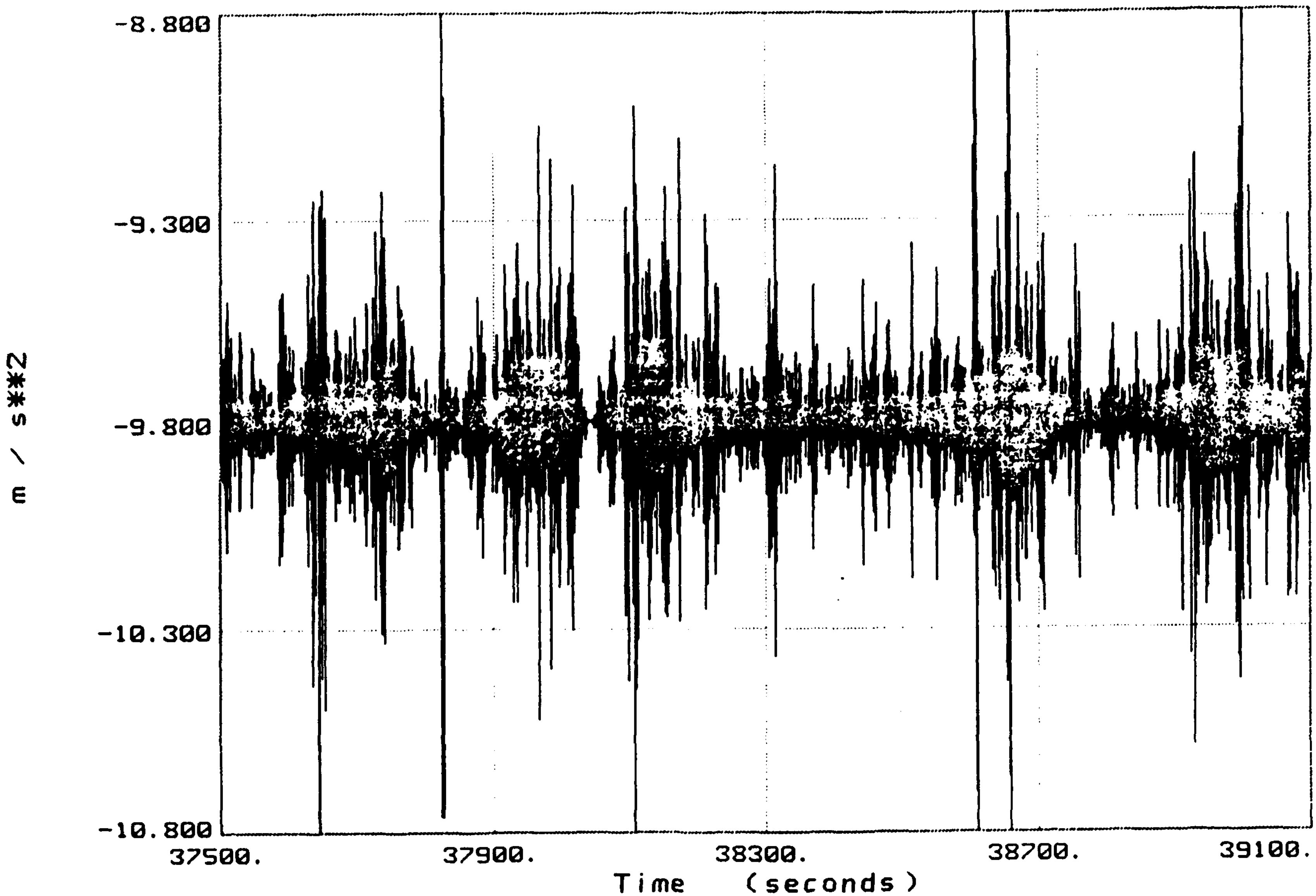

LEWISTON BRIDGE WESTWARD   Z ACCELERATION

Bell Aerospace TEXTRON

Summary

- PRELIMINARY RESULTS FROM SHAKEDOWN DRIVE OF GGSS ARE ENCOURAGING
- FURTHER REDUCTION OF ACCELERATION SENSITIVITIES IN PROGRESS
- ACQUIRING AIRBORNE GRAVITY GRADIENT MEASUREMENTS FOR DERIVATION OF THE DISTURBANCE VECTOR TO 0.2 MGALS IN 1987 IS LIKELY
- ENVIRONMENTAL SENSITIVITIES (ACCELERATION) ARE THE LARGEST ERROR MECHANISM IN MOVING BASE GRAVITY GRADIOMETERS
- THERMAL NOISE IS ONLY A SMALL CONTRIBUTOR TO TERRESTIAL MOVING BASE GRAVITY GRADIOMETERS

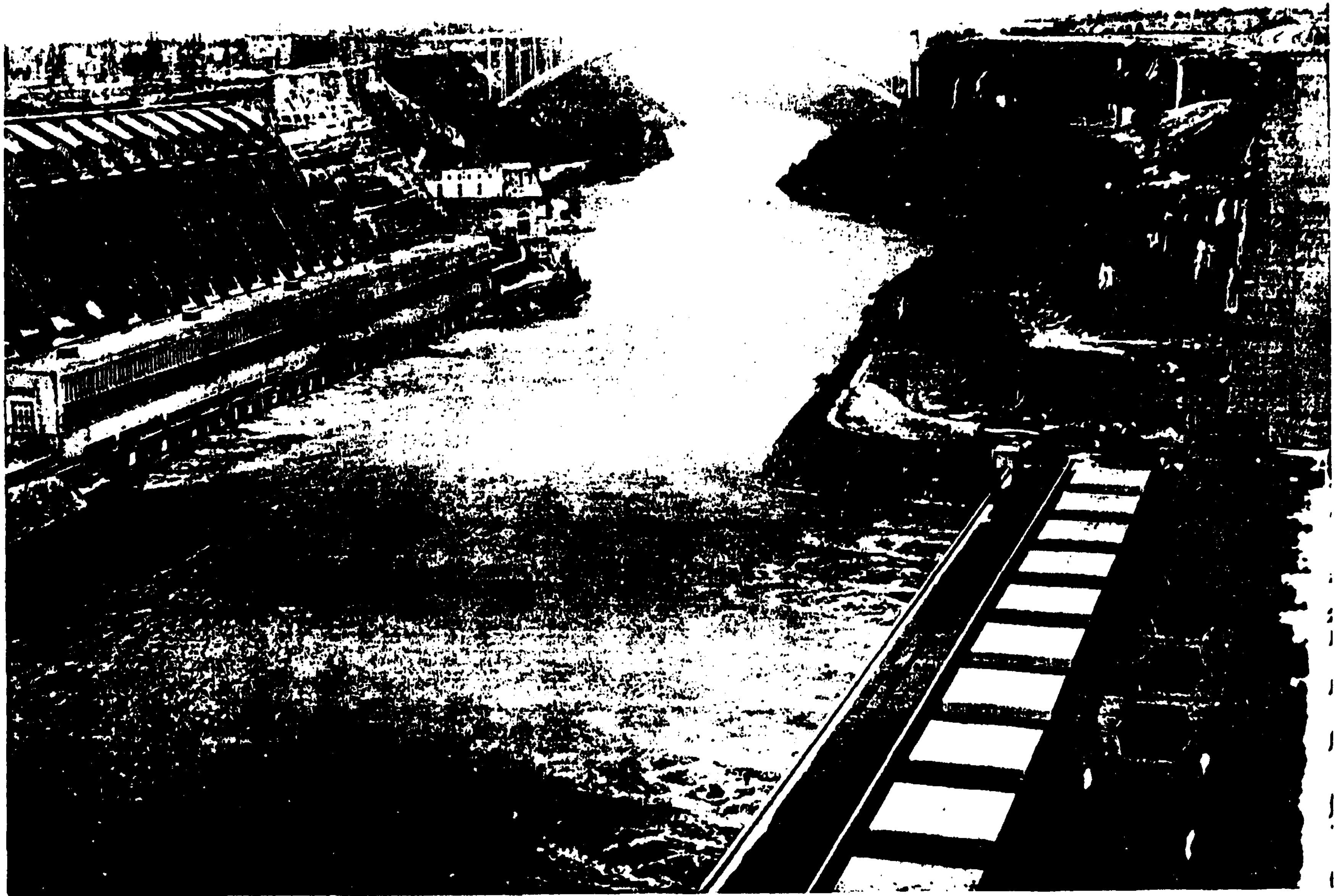

TITLE OF PAPER: Bell Aerospace Gravity Gradiometer Survey System (GGSS) - Program Review

SPEAKER: Ernest H. Metzger

QUESTIONS AND COMMENTS:

1. Question: David Gleason

Does the van have a cruise control system?

Response:

Yes, but the cruise control system will be of assistance only if the van's velocity $\geq$ 20 mph.

2. Question: Anthony R. Barringer

How many satellites did you use for GPS positioning?
Was a ground reference station used?

Response:

Four satellites as a minimum essential. No ground receiver used.

3. Question: Jim Lowery

What was used as an altitude reference on the results shown crossing the gorge?

Response:

GPS aided by barometric altimeter was used as the altitude reference with an accuracy of 7 meters rms to 20 meters rms.

4. Question: Ted Sims

What fraction of a "g" can you reasonably expect the system to experience while in a turn?

Response: .5 g is reasonable.

A PROTOTYPE SUPERCONDUCTING GRAVITY GRADIOMETER FOR GEOPHYSICAL EXPLORATION

by

Dr. Frank J. van Kann, et al
University of Western Australia
Department of Physics
Nedlands, Western Australia 6009

ABSTRACT

A three axis gradiometer, designed to measure the diagonal components of the earth's gravitational gradient tensor, has been built and is being tested in the laboratory. It consists of three pairs of accelerometers. The accelerometers of each pair are mounted with their sensitive axes co-linear and orthogonal to the other pairs. The difference in acceleration for a pair is proportional to the appropriate component of the gradient tensor and is sensed via a displacement which modulates the inductance of a superconducting coil coupled by means of a transformer to an RF biased SQUID with energy sensitivity 3×10^{-29} J/Hz.

Rejection of in-line common mode acceleration is achieved by tuning the natural resonant frequencies of the accelerometers by adjustment of persistent currents stored in the superconducting force coils. A common mode rejection ratio near 100 dB has been achieved in the presence of common mode accelerations approaching 10^{-2} ms^{-2}. This has enabled the detection of a laboratory generated signal as small as 5 Eö at signal frequencies below 1 Hz with signal to noise ratio approaching 10. Above 0.1 Hz, the noise floor of the instrument is about 0.5 Eö / $\sqrt{\text{Hz}}$ under quiet conditions. Below 0.1 Hz it has been limited by thermal drifts but measurements are at present being carried out in a new cryostat with improved temperature stability.

A PROTOTYPE SUPERCONDUCTING GRAVITY GRADIOMETER FOR GEOPHYSICAL EXPLORATION*

F J van Kann, M J Buckingham, M H Dransfield, C Edwards, A G Mann, R D Penny and P J Turner

Physics Department, The University of Western Australia, Nedlands, 6009, Australia.

Abstract

A three axis gradiometer, designed to measure the diagonal components of the earth's gravitational gradient tensor, has been built and is being tested in the laboratory. It consists of three pairs of accelerometers. The accelerometers of each pair are mounted with their sensitive axes co-linear and orthogonal to the other pairs. The difference in acceleration for a pair is proportional to the appropriate component of the gradient tensor and is sensed via a displacement which modulations the inductance of a superconducting coil coupled by means of a transformer to an RF biased SQUID with energy sensitivity 3×10^{-29} J/Hz.

Rejection of in-line common mode acceleration is achieved by tuning the natural resonant frequencies of the accelerometers by adjustment of persistent currents stored in superconducting force coils. A common mode rejection ratio near 100 dB has been achieved in the presence of common mode accelerations approaching 10^{-2} ms^{-2}. This has enabled the detection of a laboratory generated signal as small as 5 Eö at signal frequencies below 1 Hz with signal to noise ratio approaching 10. Above 0.1 Hz, the noise floor of the instrument is about 0.5 Eö/√Hz under quiet conditions. Below 0.1 Hz it has been limited by thermal drifts but measurements are at present being carried out in a new cryostat with improved temperature stability.

Introduction

The form of the earth's gravitational potential function contains a wealth of information of importance in geophysics. For the purposes of geophysical exploration, this has traditionally been exploited through measurement of the first spatial derivatives of the potential – the gravity field. Because of the difficulty of distinguishing spatial variations in gravity from temporal fluctuations of the acceleration of a moving vehicle, these measurements of gravity can be made to sufficient precision only with stationary, earth based instruments. The limitations imposed by translational acceleration can in principle be avoided by measurement of the second derivative of the potential - gravity gradients. Indeed, the discrimination of interesting geological anomalies could be more easily achieved by direct measurements of the gradient[1] rather than gravity itself and under appropriate conditions gradient measurements are less dependent on elaborate corrections for topographical features[2].

To obtain gravity gradient data useful for exploration, a noise level less than 0.1 Eö/√Hz is required, which implies an equivalent acceleration resolution on the order of 10^{-11} ms^{-2} in an instrument of reasonable size and mass. The extremely large common mode rejection ratio (possibly exceeding 200 dB) required to make these measurements in a moving vehicle may be attainable, given a system with adequate linearity and a sufficiently precise and stable method of tuning. However, the finite elastic stiffness of materials gives rise to errors in the gradient

signal which are quadratic in the common mode acceleration. The size of these errors depends on the geometrical shape and the elastic stiffness of the instrument, but for materials with a velocity of sound around 3 km/s and reasonable shape the maximum allowable common mode acceleration is less than 10^{-2} ms^{-2} for a 0.1 Eö error. This sets an exacting requirement for the translational acceleration isolation of the stabilisation system required for any vehicle suitable for use as an exploration platform.

Rotational stabilisation is also required to reduce errors which, for the diagonal components of the gradient tensor, are quadratic in the angular velocity of the instrument. For these errors to be less than 0.1 Eö requires the angular rate to be less than 10^{-5} radian s^{-1} about any axis. Rotation sensors with adequate performance to meet this requirement are currently available. However, these will need to be adapted for low temperature operation, since the innate mechanical elastic compliance of the cryostat imposed by thermal design considerations will require that some rotational stabilisation be implemented inside the cryogenic environment.

The laboratory prototype

The three axis prototype gradiometer uses principles similar to those described by Mapoles[3], Paik[4] and Moody et al[5]. It consists of six essentially identical accelerometers grouped to form three pairs, one for each tensor component to be sensed. The two end faces of each accelerometer can be identified by a letter A, B, C or D so that the two accelerometers for a given pair can be labelled AB and CD respectively. These are selected for matched mechanical resonant frequencies and are mounted with their sensitive axes co-linear and orthogonal to those of the remaining pairs. Each accelerometer consists of a solid niobium cylinder, some 30 mm in diameter, 30 mm in length, and about 300 gm in weight suspended at each end by a thin folded cantilever niobium leaf spring in a niobium housing.

The remote end faces A and D of the pair are parallel and in close proximity to annular, single layer, spiral "pancake" niobium wire coils attached to the ends of the housing. Each of these pancake coils actually consists of a pair of concentric coils; the smaller inner one being used for RF position sensing and the larger outer one forming the force coils for CMRR tuning and feedback. The resonant frequency of the accelerometers is about 25 Hz and can be increased by several percent by means of a persistent current stored in the appropriate force coil. The end face labelled C of accelerometer CD is similarly with another pancake coil mounted on the B end face of the paired accelerometer AB. This coil is coupled to the SQUID by means of a superconducting matching transformer and is used to directly sense the differential motion between the accelerometers.

Common mode acceleration sensing

Accelerations are monitored by sense coils at the ends of the gradiometer housing. Each sense coil is incorporated into the tank circuit of a radio frequency oscillator, whose frequency is modulated by motion of the test mass relative to the housing. This position readout permits preliminary testing of the accelerometers at room temperature and also enables calibration of the primary superconducting differential motion sensing system when cold.

The RF oscillators have been optimised for low power operation, both to permit their use in the highly thermally isolated cryogenic environment and also to minimise SQUID interference. At liquid helium temperature, these provide a stable and sensitive position sensor with 10^{-9} m

resolution while dissipating only 40 μW.

The spring constant of the mechanical springs is augmented as required by means of the magnetic force from a persistent current stored in the force coils. This allows the accelerometers to be precisely matched to achieve high rejection of accelerations along the gradient sensing axis.

The effectiveness of the adjustment of persistent current for CMRR tuning is illustrated in figure 1. Here the natural resonant frequency of the CD accelerometer was about 0.8 Hz below that of AB. The upper two curves in figure 1 show the Fourier spectrum of the response of the two accelerometers from white noise excitation. The peak near 26.5 Hz corrresponds to the natural untuned low frequency normal mode for the coupled oscillators. (The other, high frequency normal mode is above 28 Hz and not visible in this diagram.) The family of curves in the central region of figure 1 shows the spectrum of the transfer function amplitude i.e. the magnitude of the complex ratio of the response of the two accelerometers, for several persistent currents stored in force coils C and D. The lower curves show the corresponding phase of the transfer function.

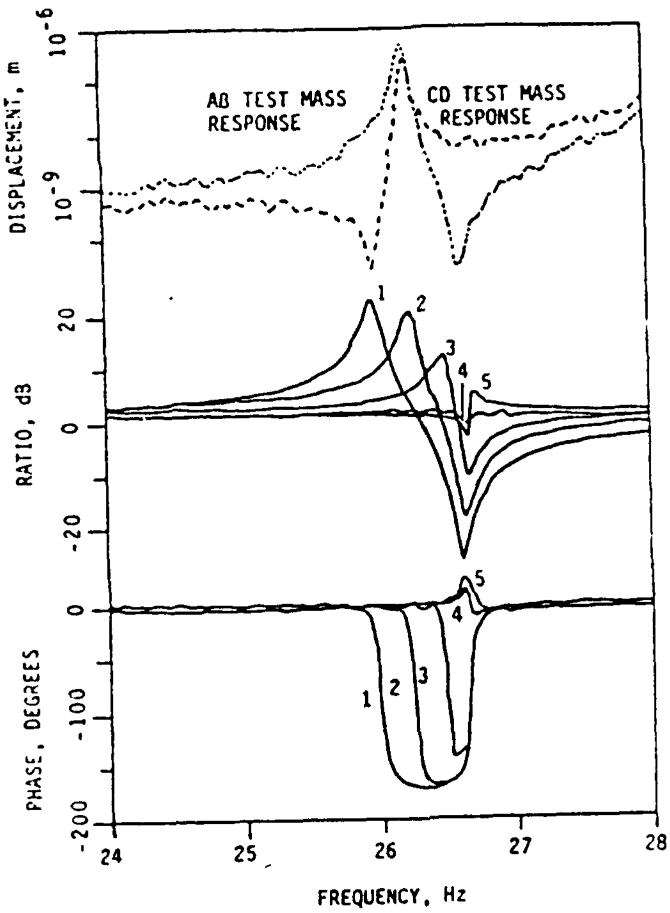

Figure 1 Fourier spectrum of the gradiometer response as a function of tuning current.

The curves 1 to 5 show the resonant frequency of the CD accelerometer, corresponding to the peak in the transfer function amplitude, being increased to match that of AB, corresponding to the dip in amplitude. The accelerometers are matched when these coincide as in curve number 4. In curves 1 to 3, the stored current is too small and the frequency of CD is lower than that of AB. In curve 5, the current is too large and the frequency difference is reversed. In curve 4, the accelerometers are as closely matched as can be determined by this method. More precise tuning is achieved by direct measurement of the differential motion using the SQUID.

Differential mode acceleration sensing

Differential motion between the two accelerometers is measured to extremely high resolution by means of an RF biased SQUID magnetometer, model 330X, manufactured by Biomagnetic Technology Inc. This detects changes in the persistent current trapped in the superconducting differential motion sense coil. Extreme care has been taken in shielding this input circuitry from fluctuations in the ambient magnetic field and also from RF interference which can cause the SQUID to cease functioning.

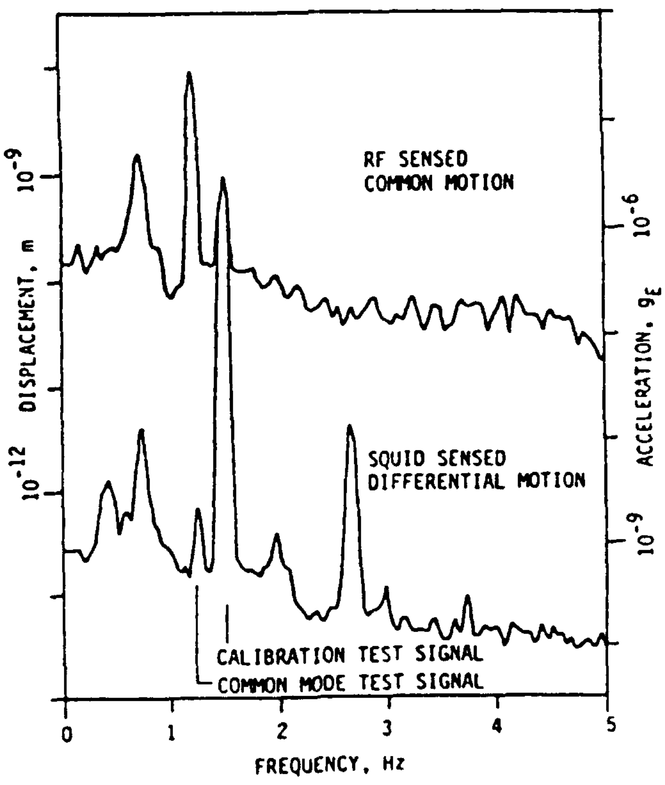

Figure 2 Gradiometer response to applied calibration and common mode rejection test signals.

The differential motion sensitivity is calibrated with respect to the known sensitivity of the RF

position sensor as shown in figure 2. The Fourier components of both the common mode motion, sensed by the RF detector and differential mode motion, sensed by the SQUID are shown as a function of frequency. The vertical scale on the left is labelled with the calibrated displacement scale, while the scale on the right shows the equivalent acceleration amplitude relative to the earth's gravitational acceleration. For the calibration, the CD accelerometer is forced into oscillation at a known amplitude and frequency by means of one of its force coils, which has a trapped persistent current. Although the heat switch which is in parallel with the force coil remains cold, the stray series inductance allows the persistent current to be modulated via the external current leads. Since the forced oscillation is well below the resonant frequency, the resulting motion of the AB accelerometer is small and not detectable above the noise. The CMRR is measured simultaneously by means of a forced common mode oscillation of the entire gradiometer assembly, which itself is suspended inside the dewar on soft coil springs with a resonant frequency of about 1 Hz. The dependance of the CMRR on the trapped current is shown in figure 3. The circles and crosses represent data from two different runs, with $I_0^2 = 100\ A^2$ and $20\ A^2$ respectively. For clarity, some of the data from the latter are omitted and plotted on an expanded scale in the inset. The maximum CMRR achieved is nearly 100 dB.

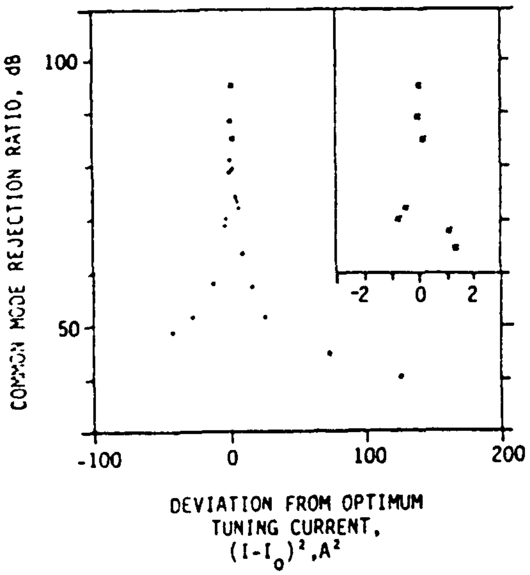

Figure 3 Common mode rejection ratio as a function of the square of the push coil current.

Gravity gradient detection

A gravitational gradient generator was constructed to test the performance of the gradiometer with actual time varying gradients. The generator consists of a 1.2 meter diameter wheel at the periphery of which are attached four lead masses weighing some 65 kg each. The gradient produced by such a mass when placed close (0.3 m) to the gradiometer is some 120 Eö. When the disc is set into rotation by a variable speed drive, it produces an AC gradient with

fundamental Fourier component at four times the rotation frequency, and rms amplitude of about 30 Eö.

The ability of the gradiometer to successfully detect the gravitational gradient of the generator is shown clearly in figure 4. The frequency for the measurement was chosen such that the fundamental rotor frequency (0.077 Hz) and its first few harmonics did not coincide with any natural resonances of the gradiometer suspension or dewar system. The gradient signal at 0.3 Hz has the expected amplitude of approximately 4 Eö rms. This fundamental Fourier component of the gradient produced by the rotor can be quantitatively predicted from its known mass distribution, and serves as a useful check on the gradiometer calibration. The strong signal at 0.53 Hz results from the rocking motion of the gradiometer on its suspension springs and cannot be suppressed by common mode rejection.

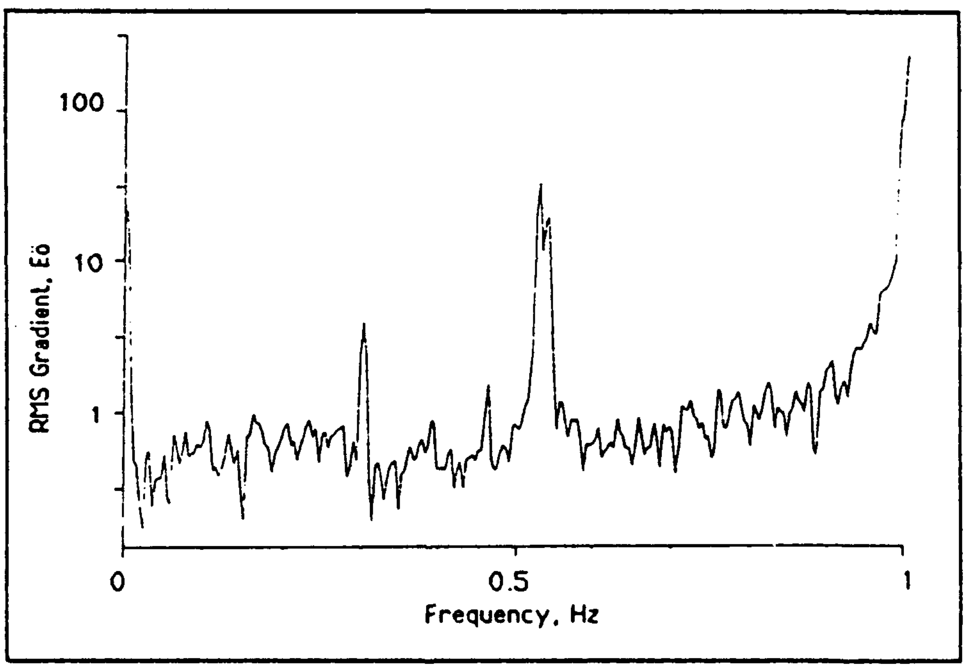

Figure 4 Detection of a gradient signal. This figure shows on a logarithmic scale the Fourier spectrum of the differential motion SQUID signal in response to the four mass gradient generator rotating at 0.077 Hz. The SQUID sensitivity is 2 V/μA and the unfiltered output is used for feedback damping to reduce the accelerometer Q. The signal is processed by an HP 3582A spectrum analyser without any additional filtering.

The distance dependence of the gravity gradient produced by the generator (approximately $1/r^3$ at short distances) is easily calculated and the results are in good agreement with the observed behaviour, as shown in figure 5.

At very low frequency, the gradiometer noise level rises significantly because of the sensitivity

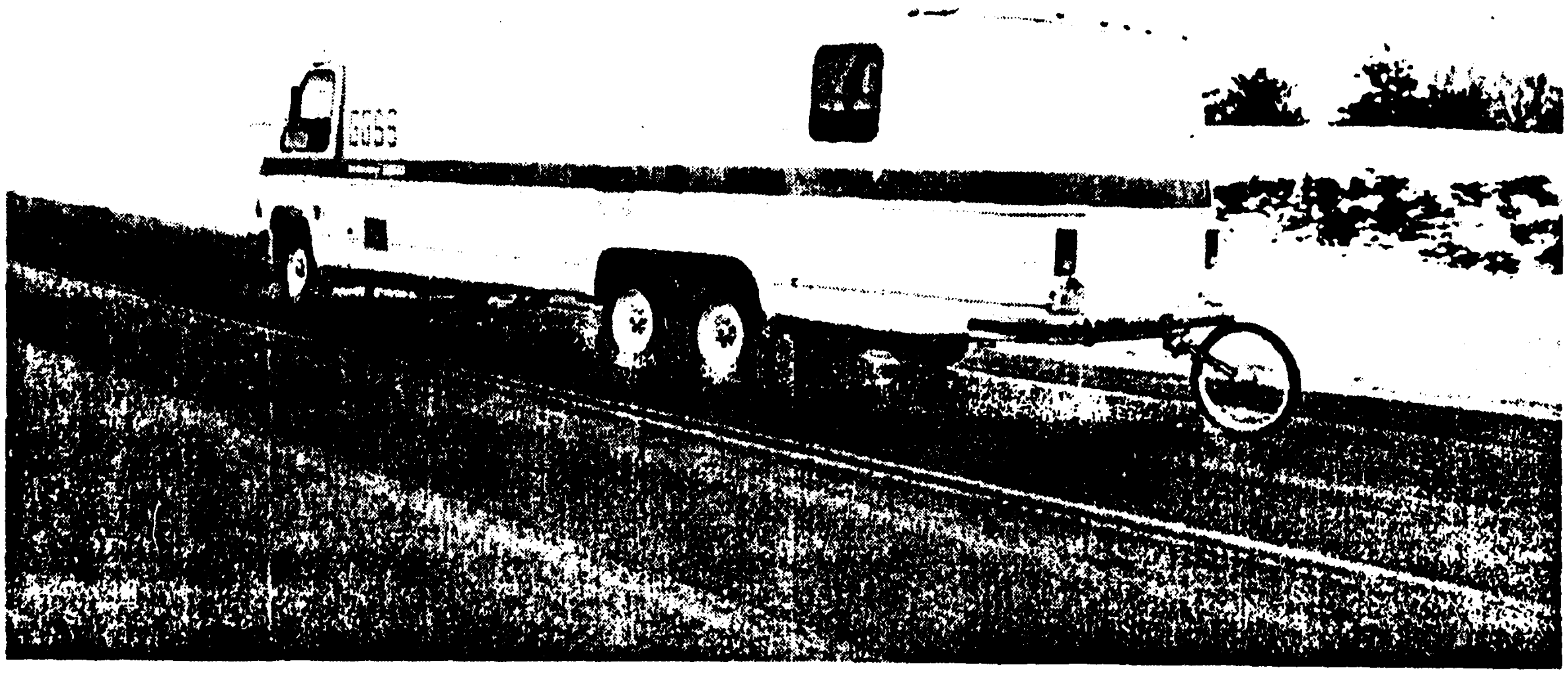

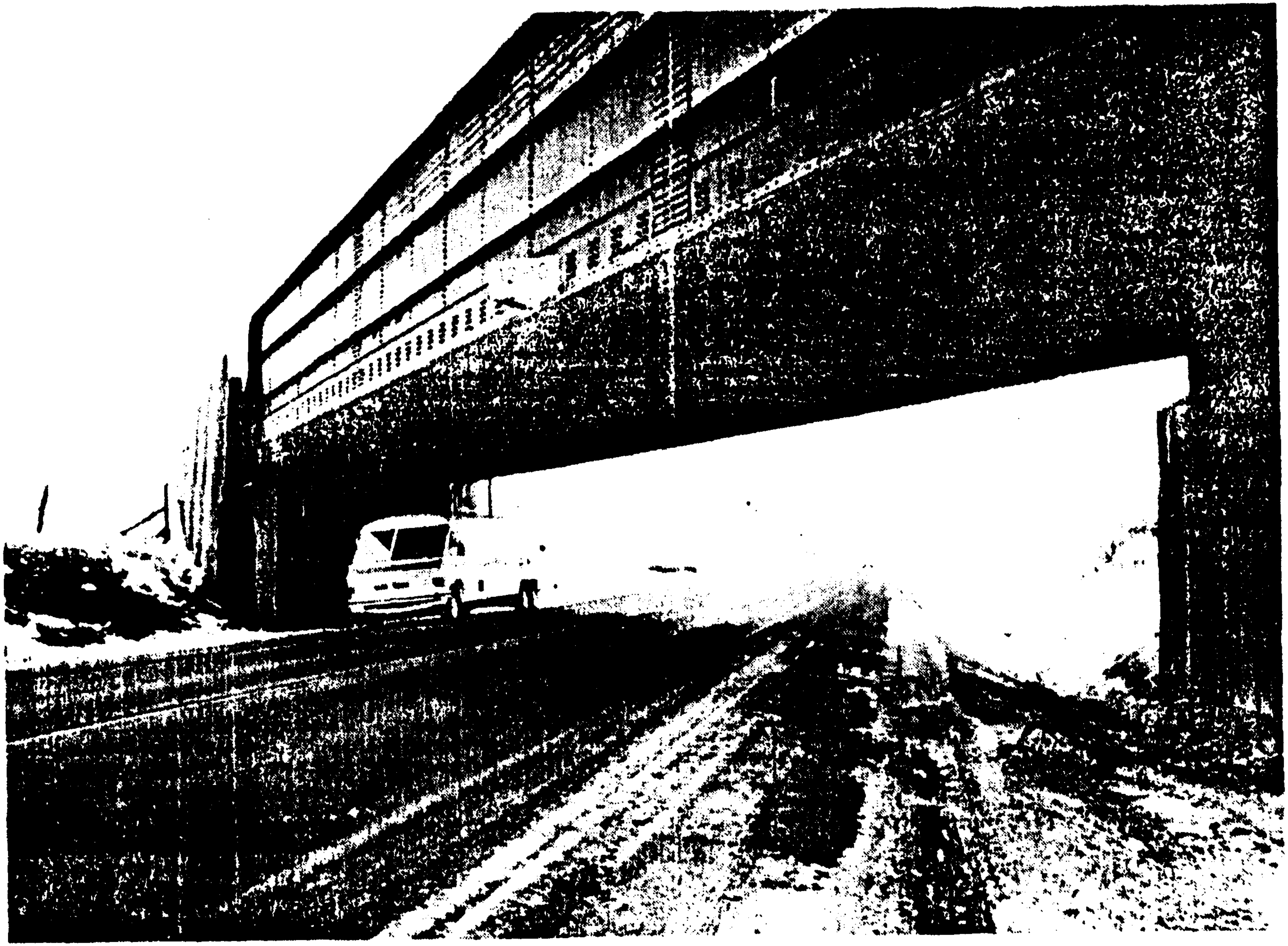

Van Acceleration Power Spectrum

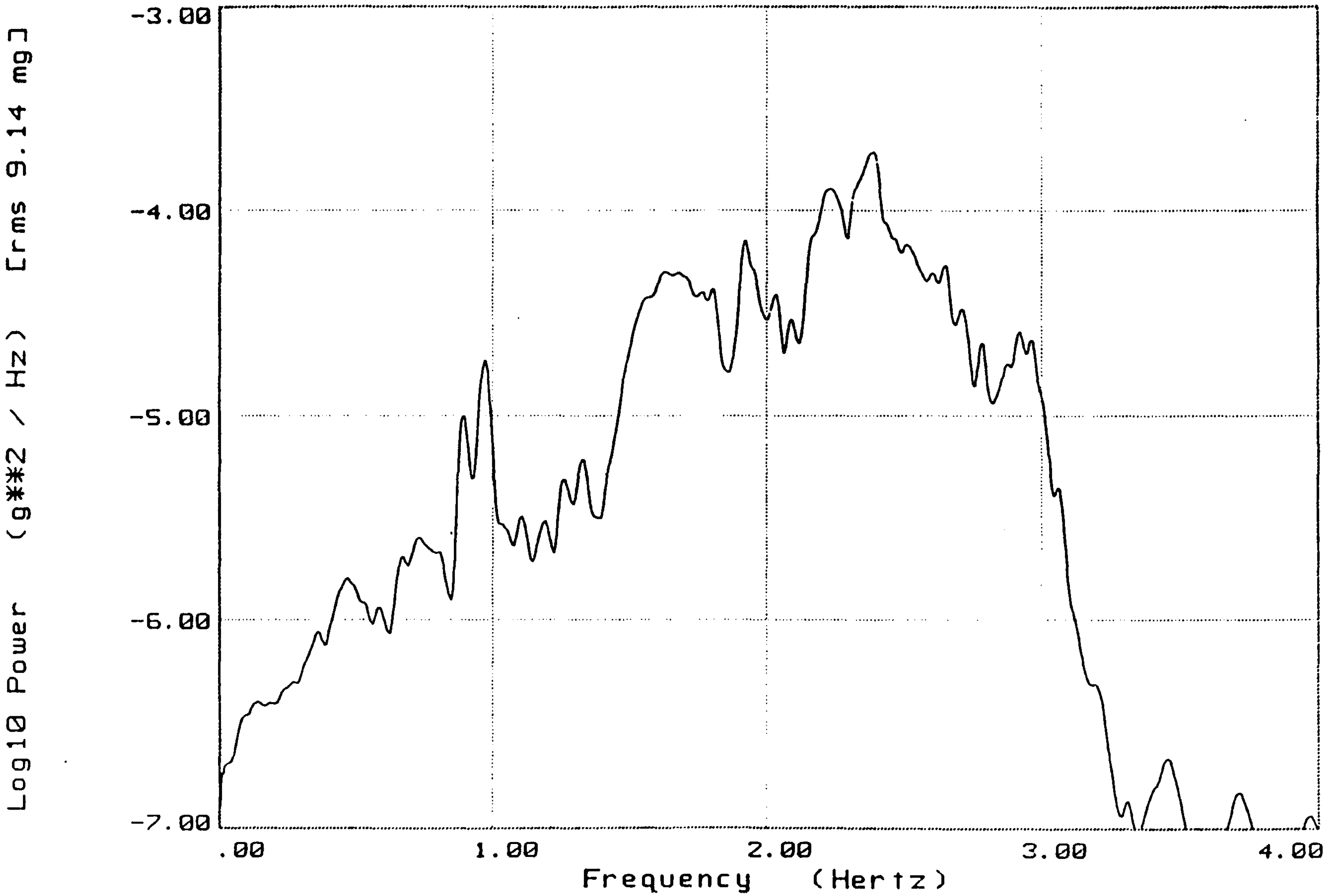

GGSS VAN 22 JAN 87 VERTICAL ACCEL 5 mph

Bell Aerospace TEXTRON

Van Acceleration Power Spectrum

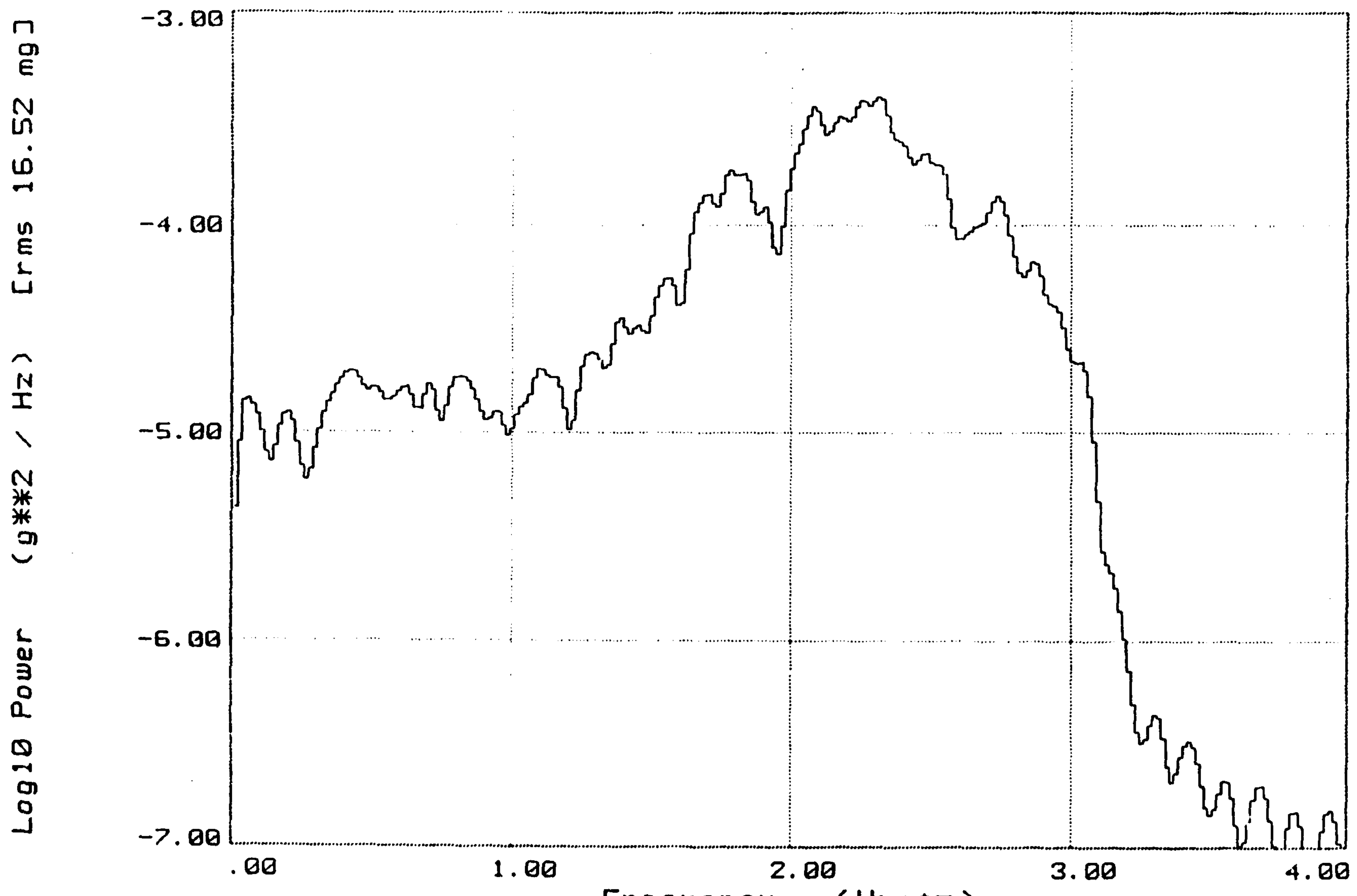

GGSS VAN 22 JAN 87 VERTICAL ACCEL 30 mph

Bell Aerospace TEXTRON

Van Acceleration Power Spectrum

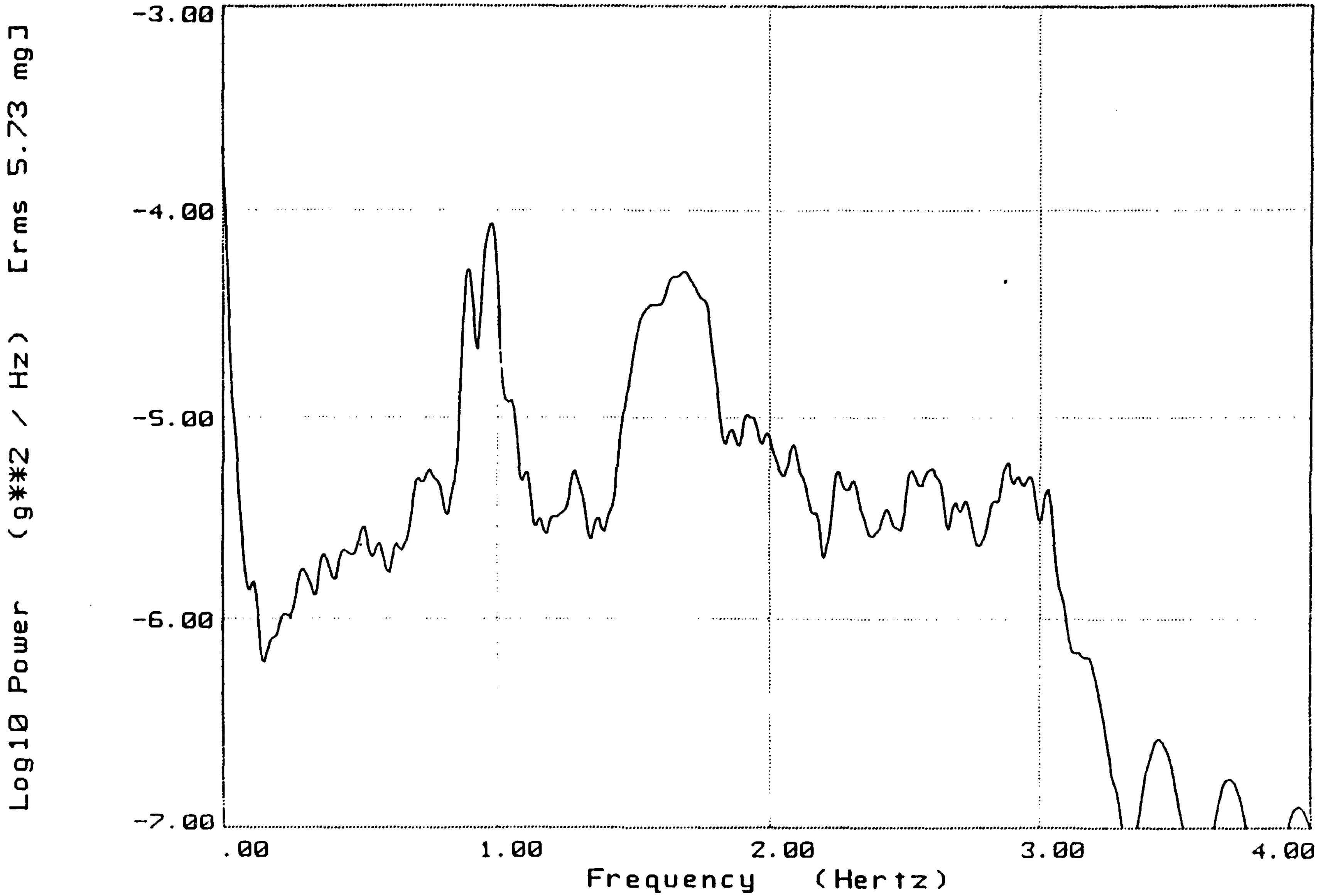

GGSS VAN 22 JAN 87 LONGITUDINAL ACCEL 5 mph

Bell Aerospace TEXTRON

Van Acceleration Power Spectrum

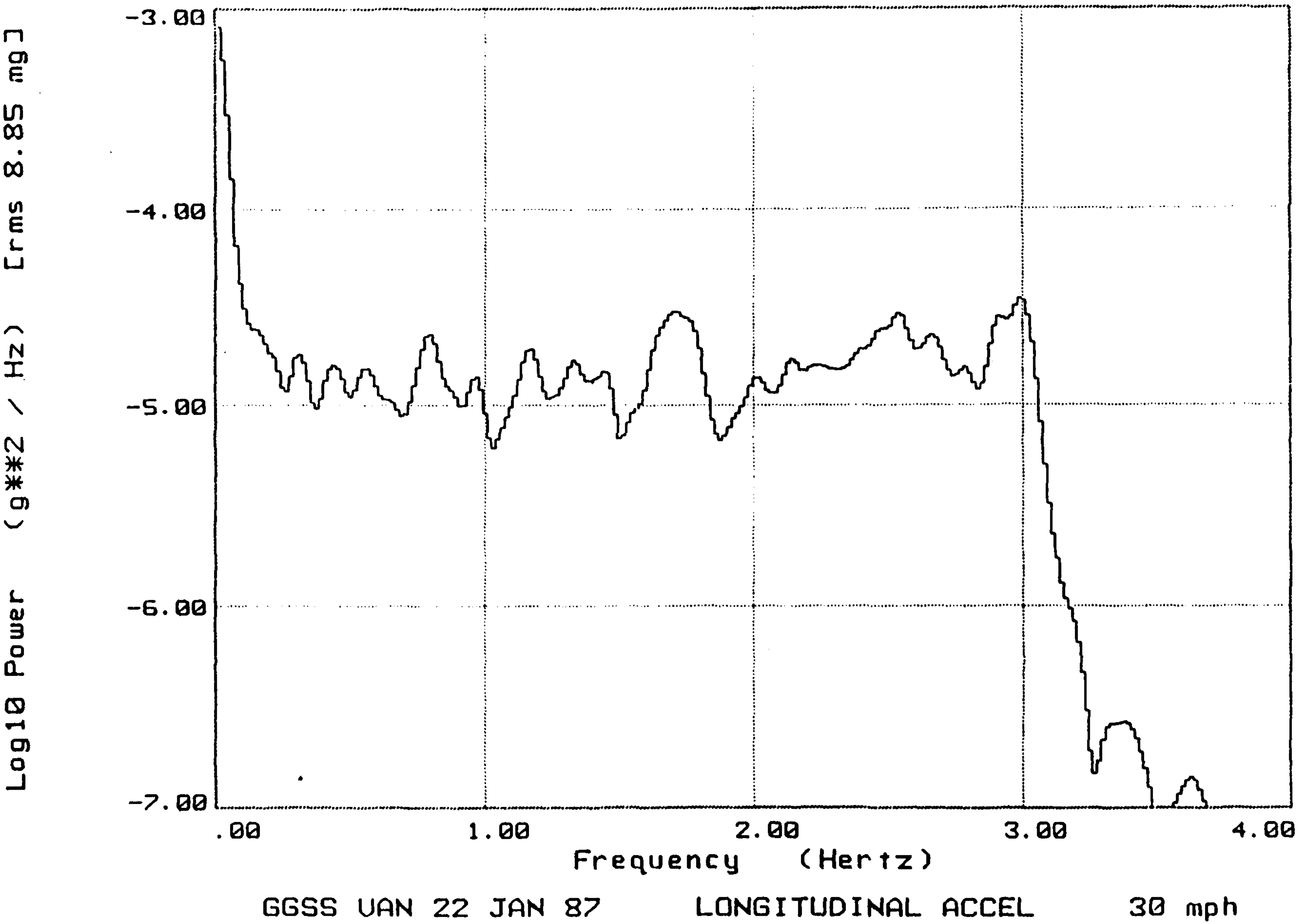

Bell Aerospace TEXTRON

Van Acceleration Power Spectrum

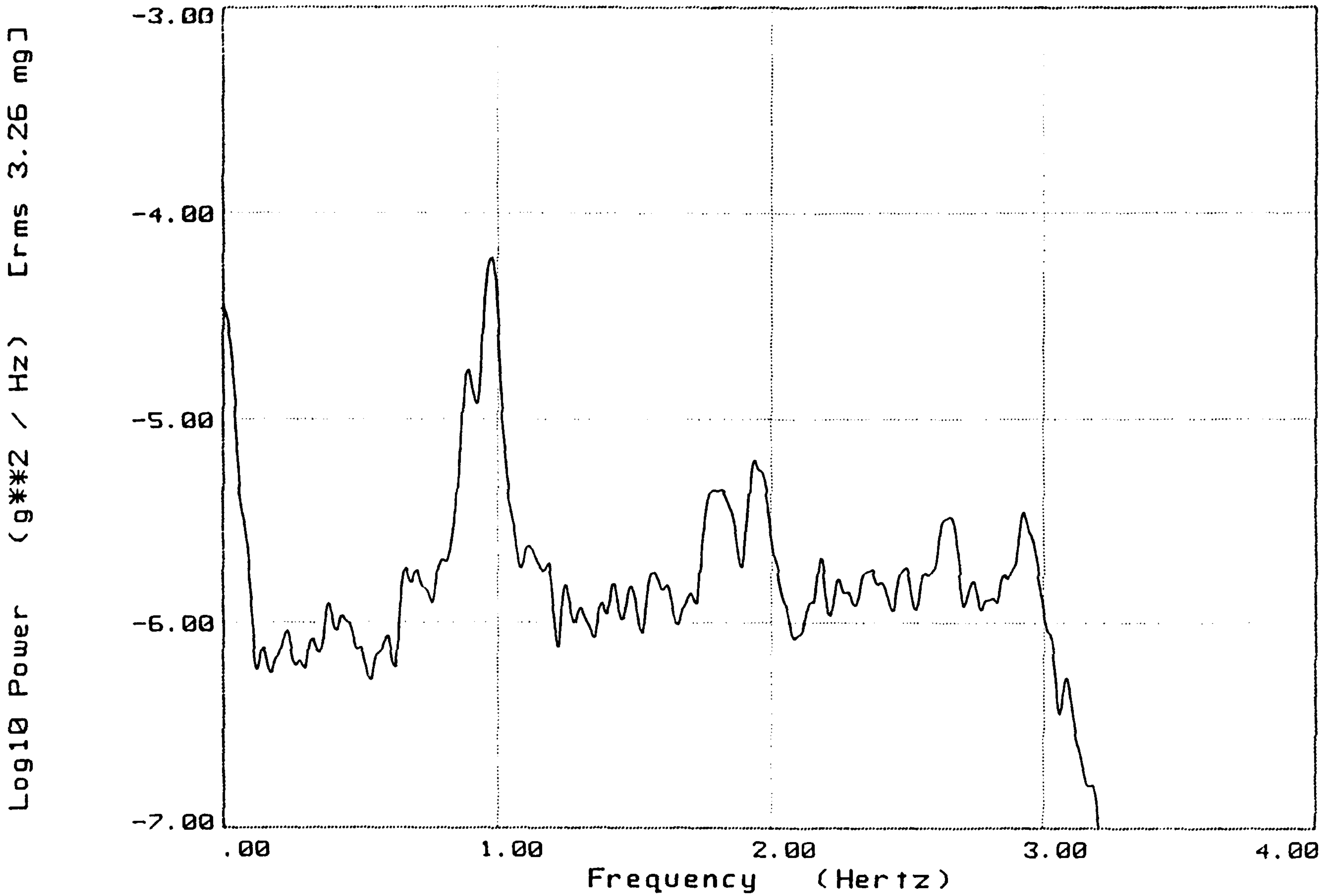

GGSS VAN 22 JAN 87 LATERAL ACCEL 5 mph

Bell Aerospace TEXTRON

Van Acceleration Power Spectrum

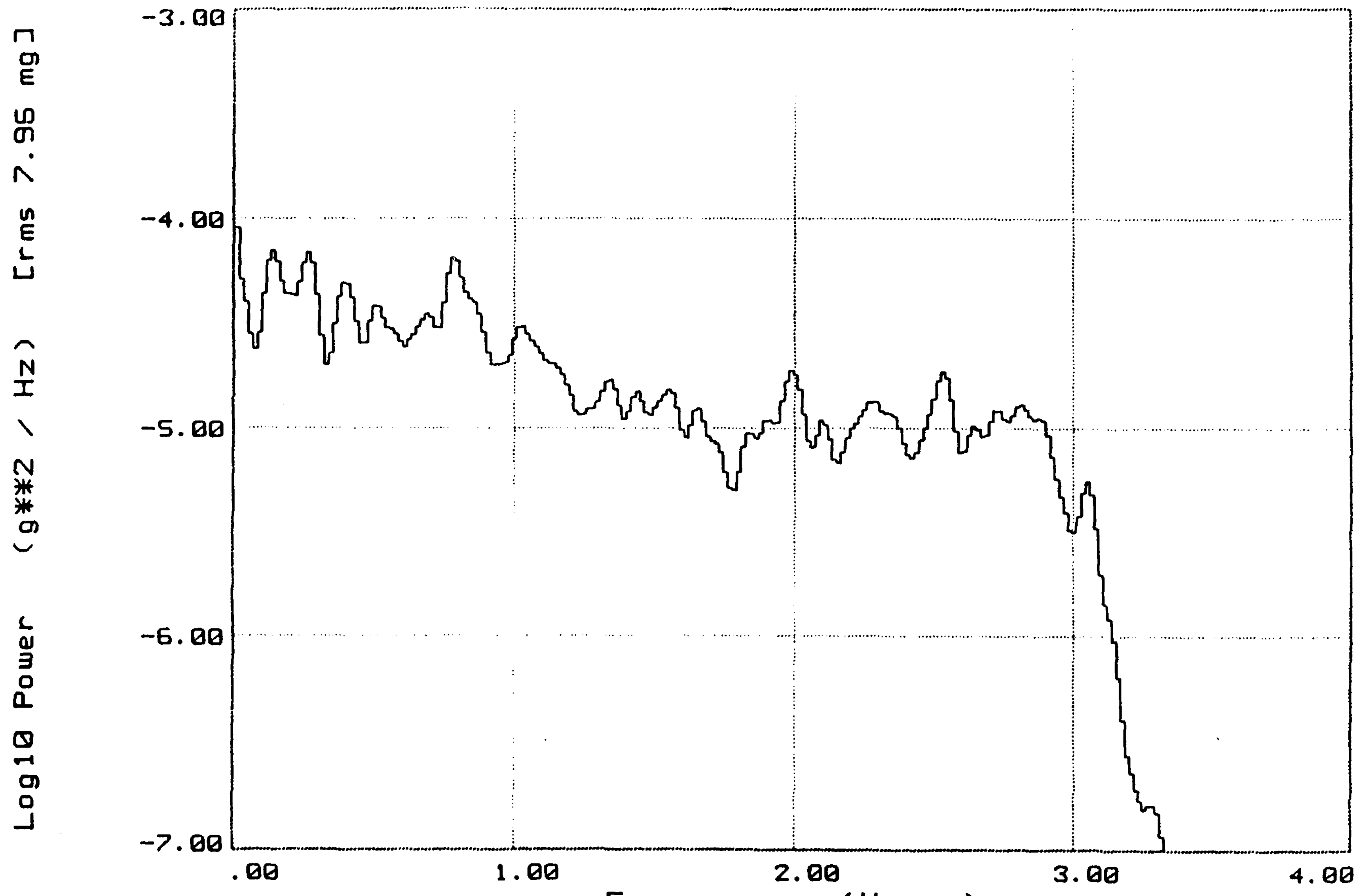

GGSS VAN 22 JAN 87 LATERAL ACCEL 30 mph

Bell Aerospace TEXTRON

Uncorrected Gravity Gradient
Measured on GGSS Shakedown Drive

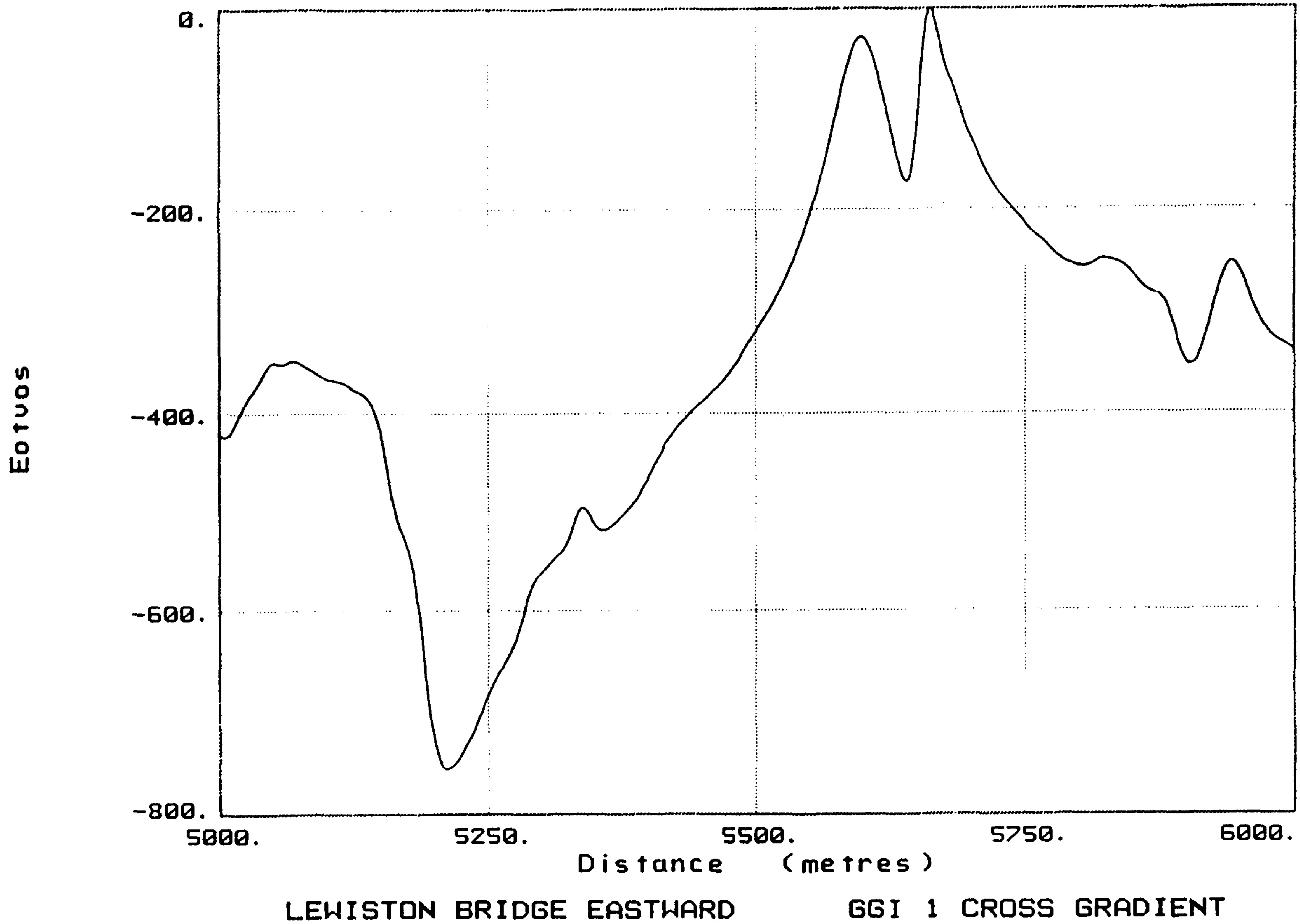

Bell Aerospace TEXTRON

Uncorrected Gravity Gradient Measured on GGSS Shakedown Drive

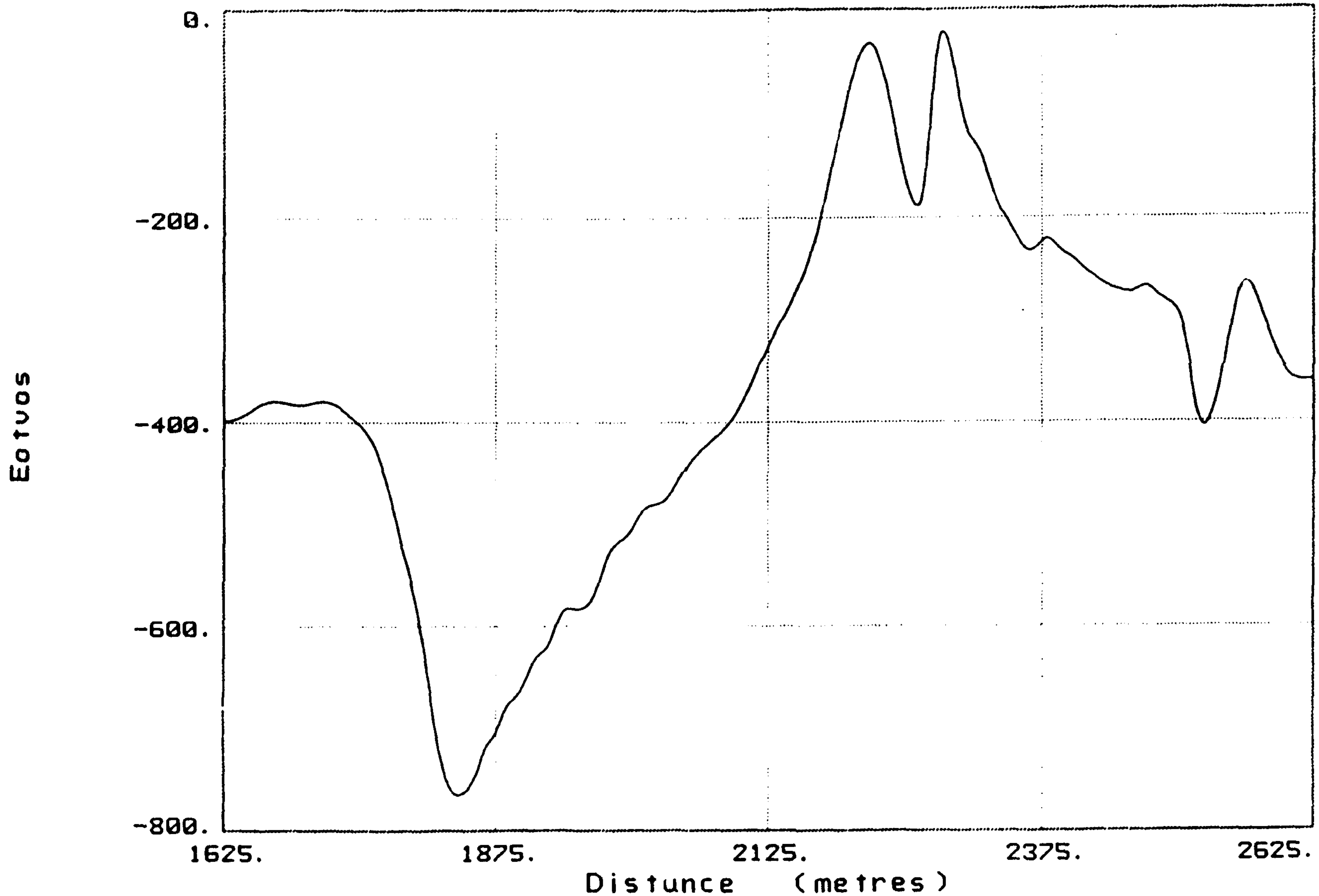

Bell Aerospace TEXTRON

Measured on GGSS Shakedown Drive

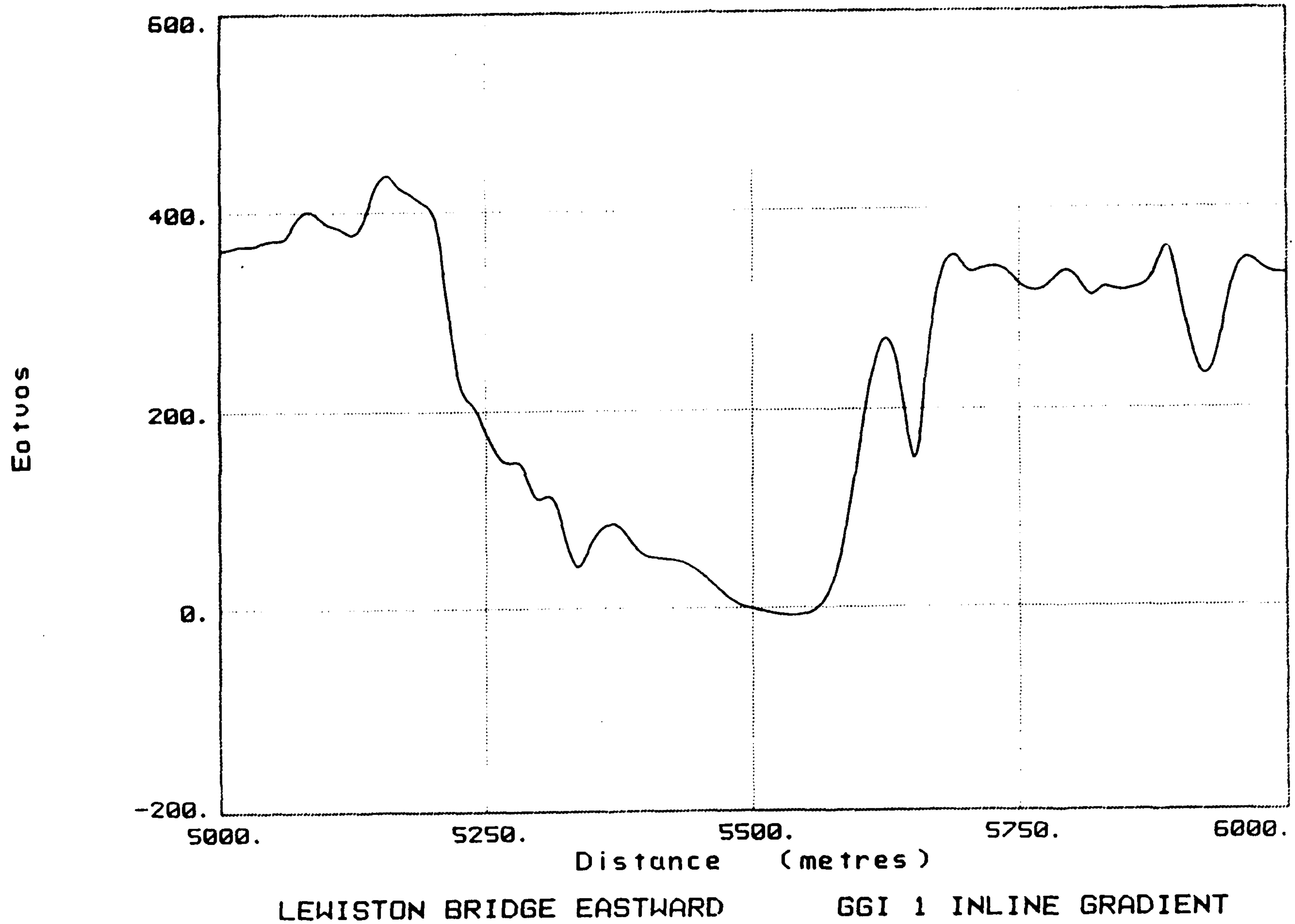

Bell Aerospace TEXTRON

Uncorrected Gravity Gradient Measured on GGSS Shakedown Drive

Bell Aerospace TEXTRON

Uncorrected Gravity Gradient Measured on GGSS Shakedown Drive

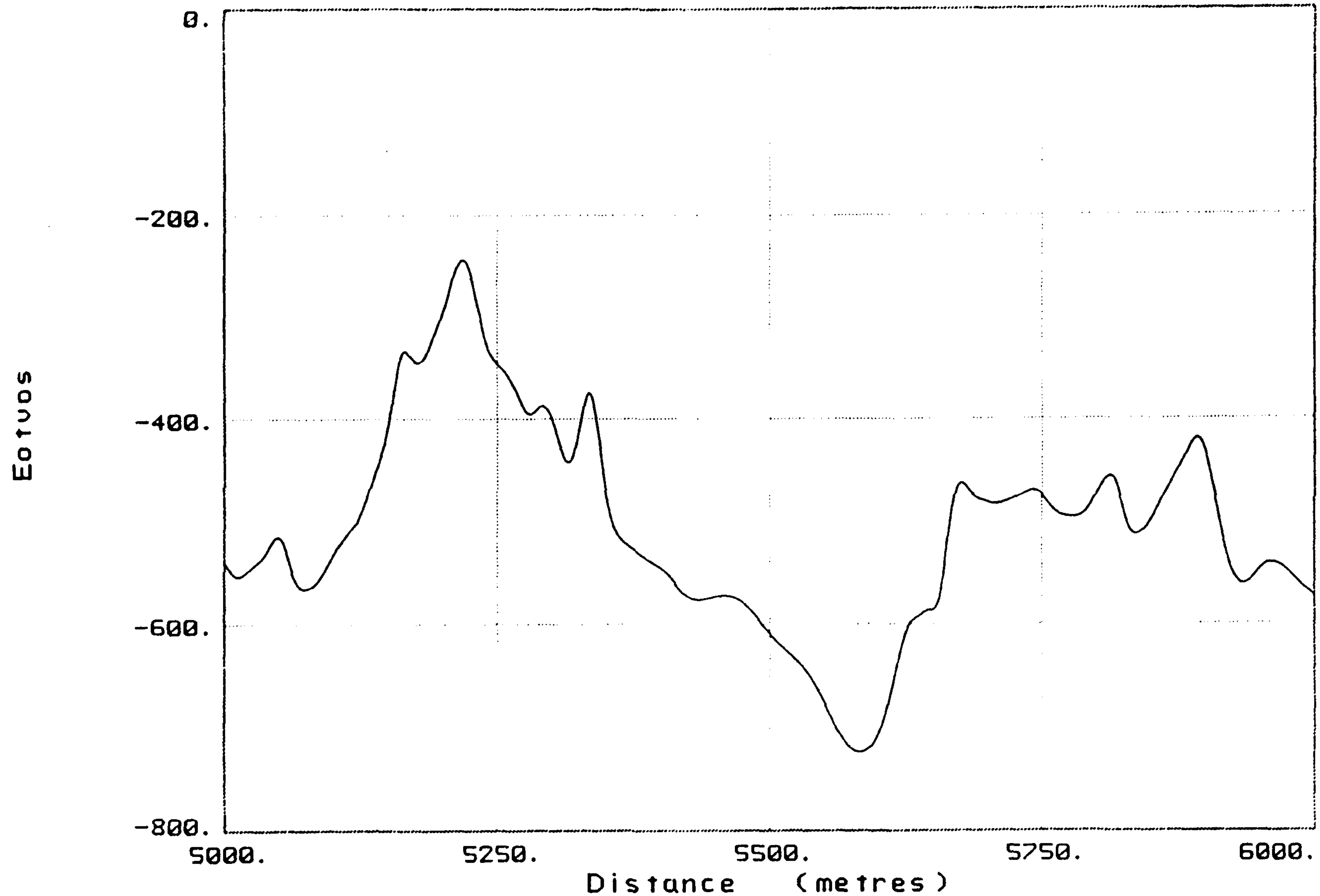

Bell Aerospace TEXTRON

Uncorrected Gravity Gradient Measured on GGSS Shakedown Drive

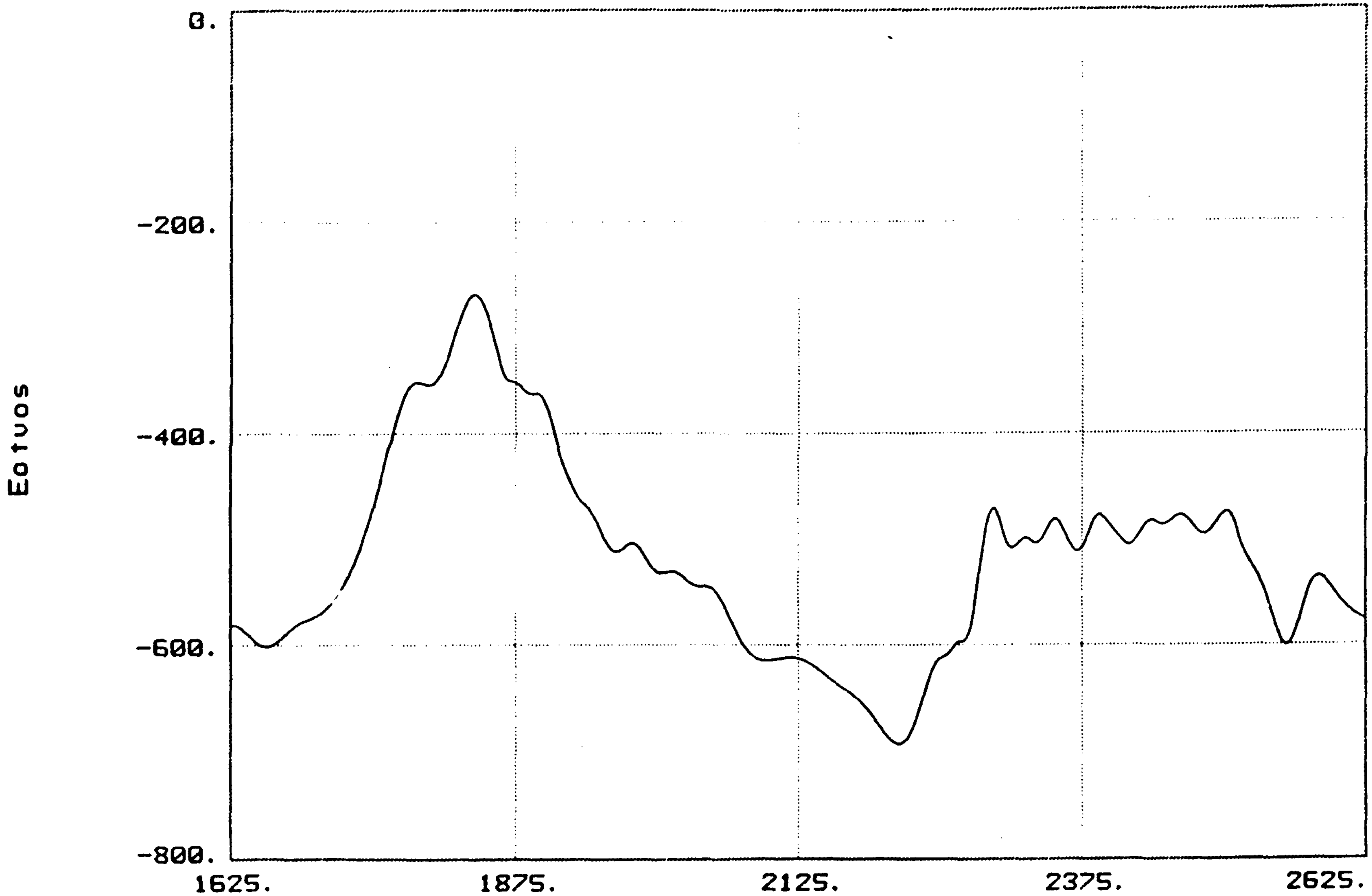

LEWISTON BRIDGE EASTWARD GGI 2 CROSS GRADIENT

Bell Aerospace TEXTRON

Uncorrected Gravity Gradient Measured on GGSS Shakedown Drive

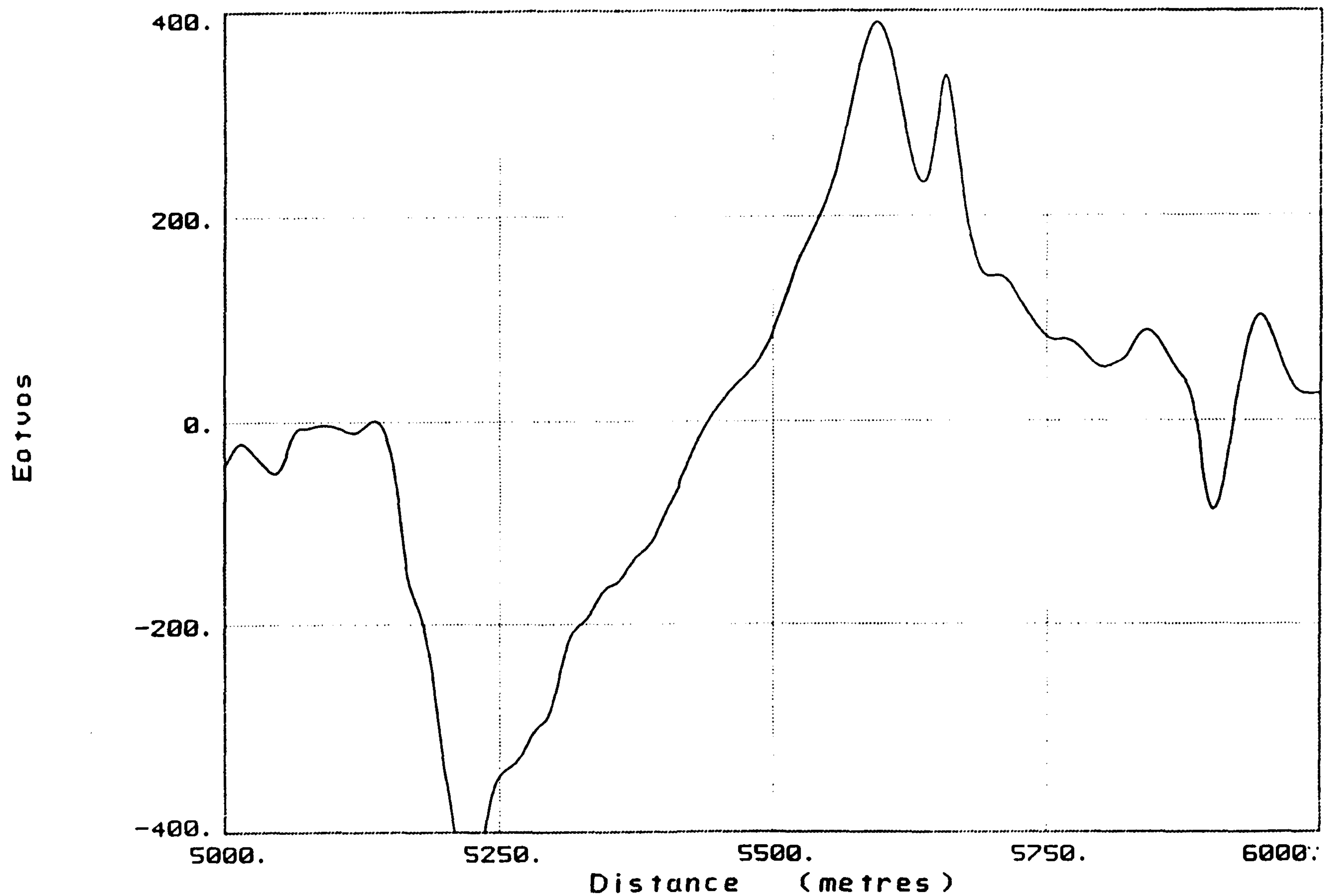

Bell Aerospace TEXTRON

Uncorrected Gravity Gradient Measured on GGSS Shakedown Drive

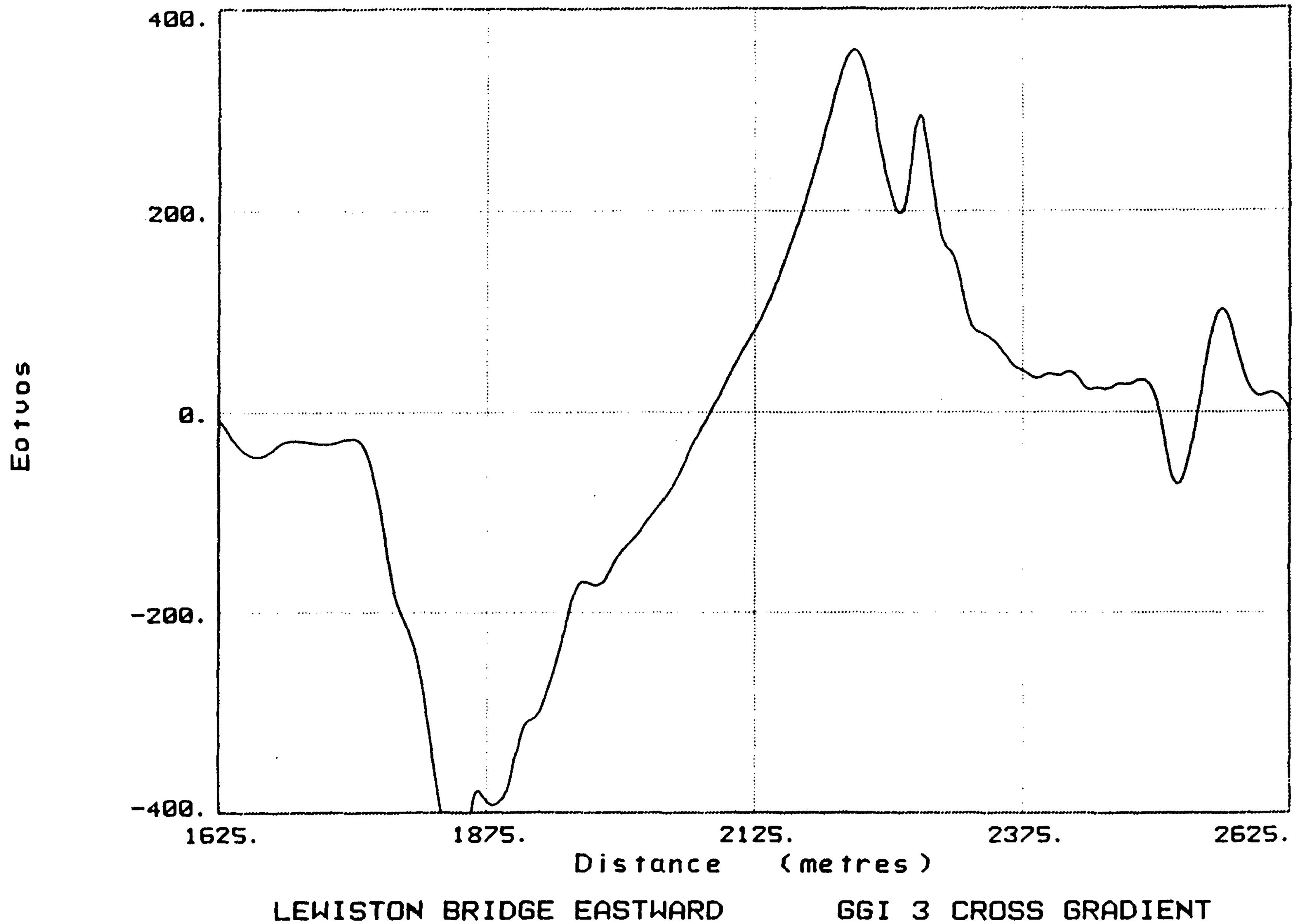

Bell Aerospace TEXTRON

C130 Installation

LOCKHEED L-100-30

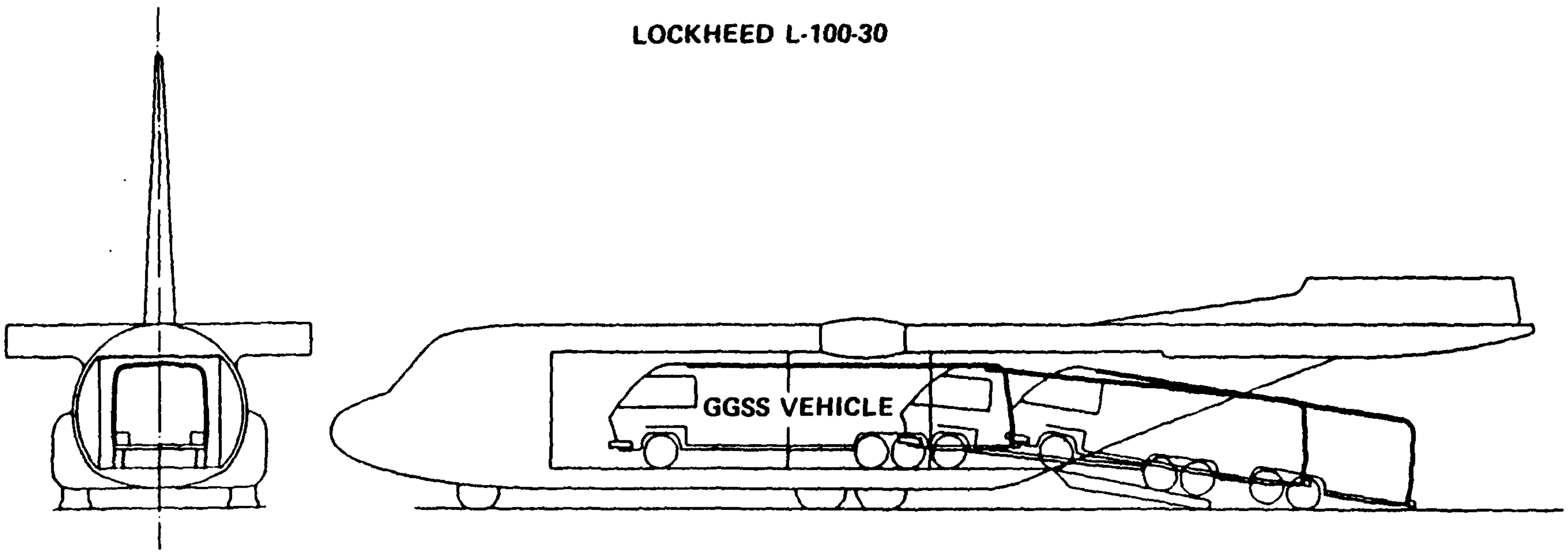

GGSS VEHICLE

APPROXIMATELY 35' LONG & 19,000 POUNDS

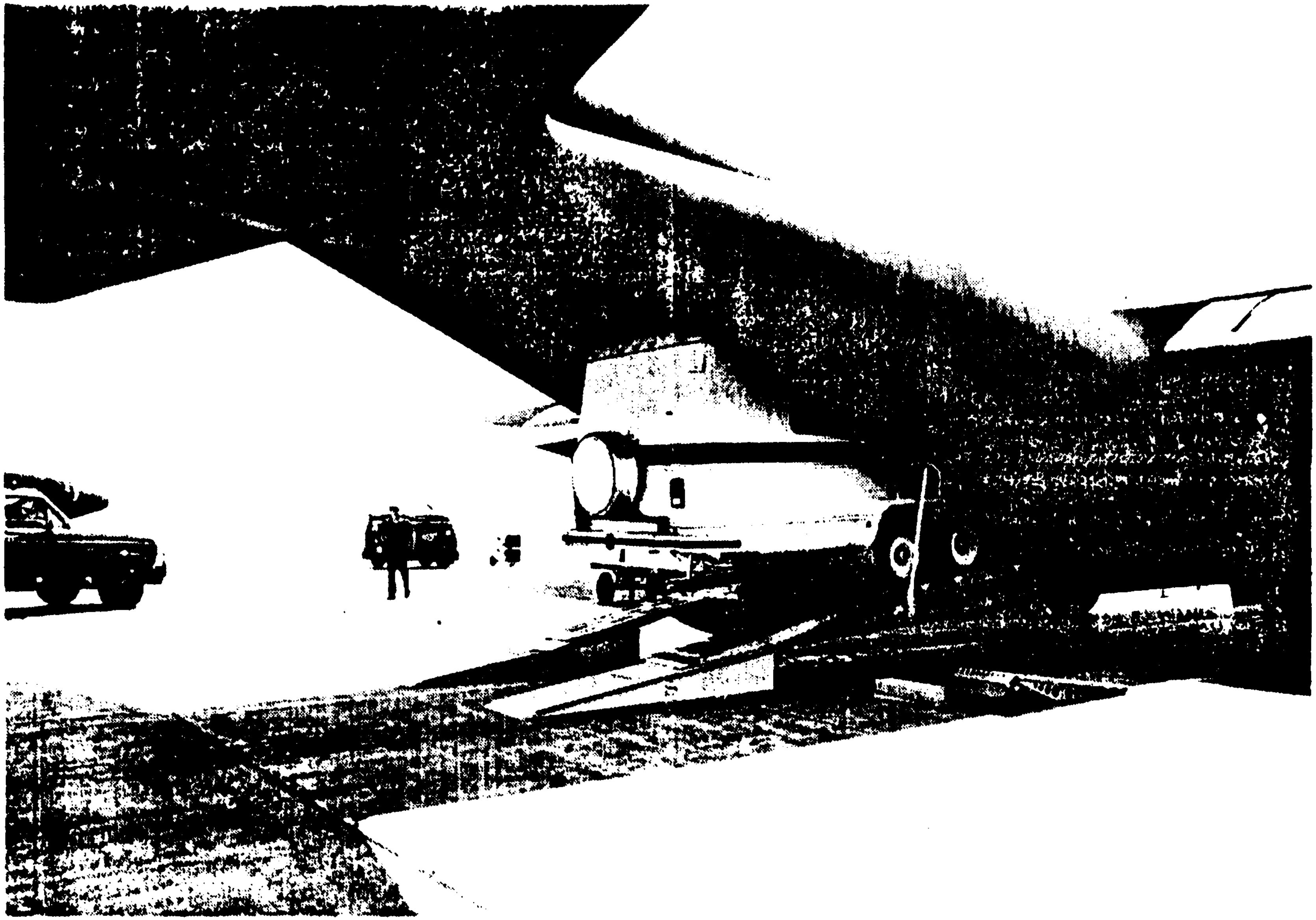

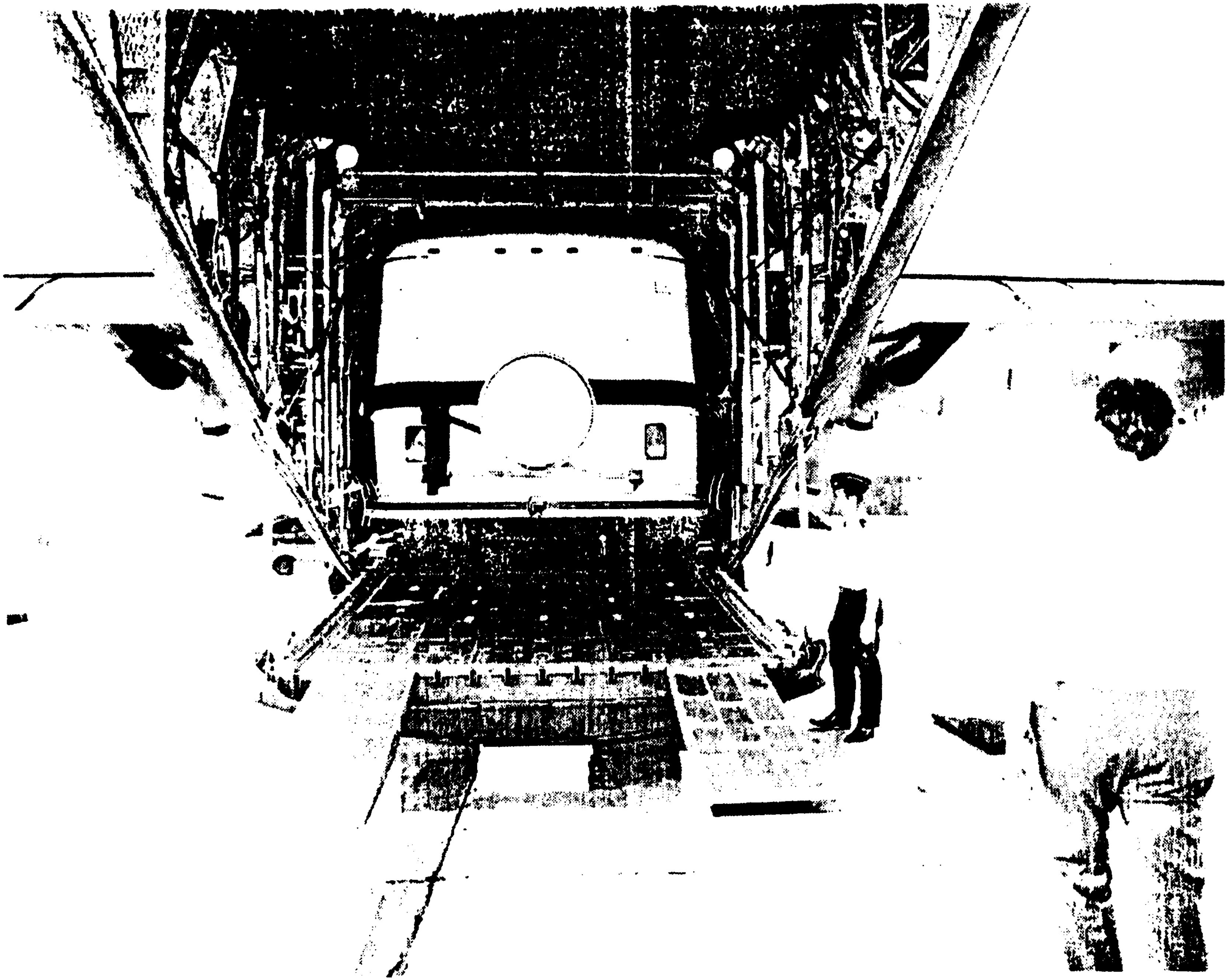

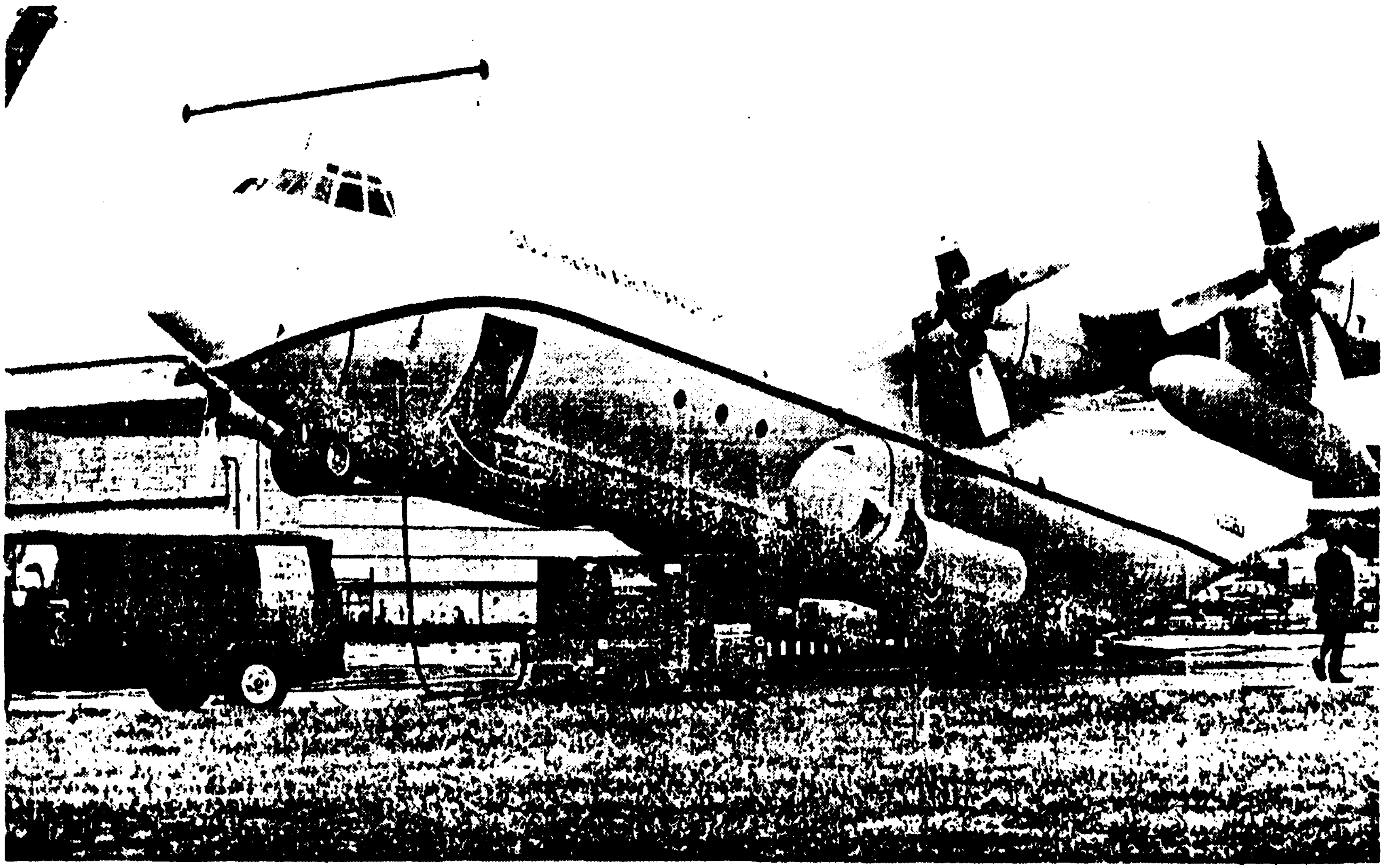

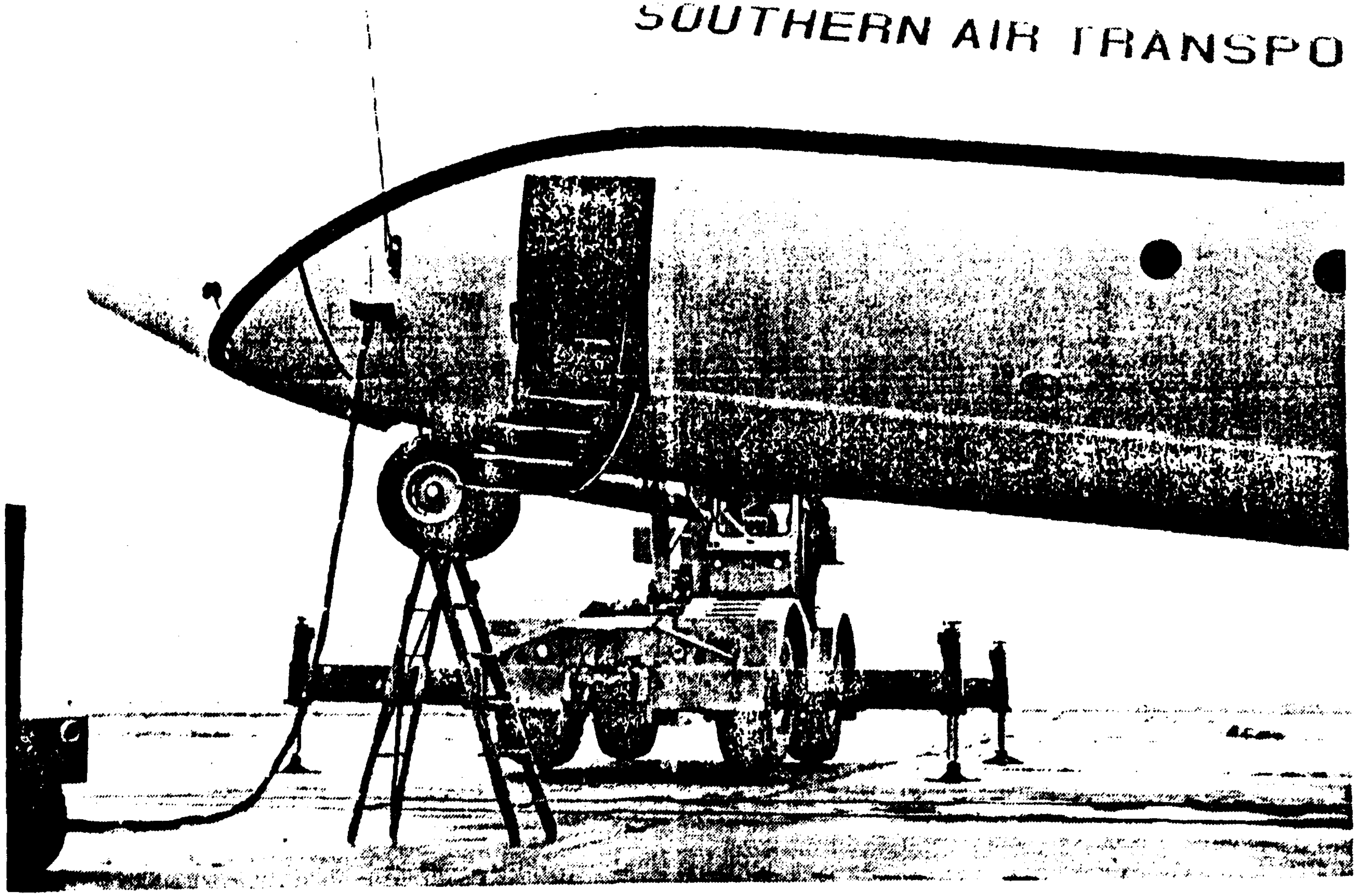
SOUTHERN AIR TRANSPO

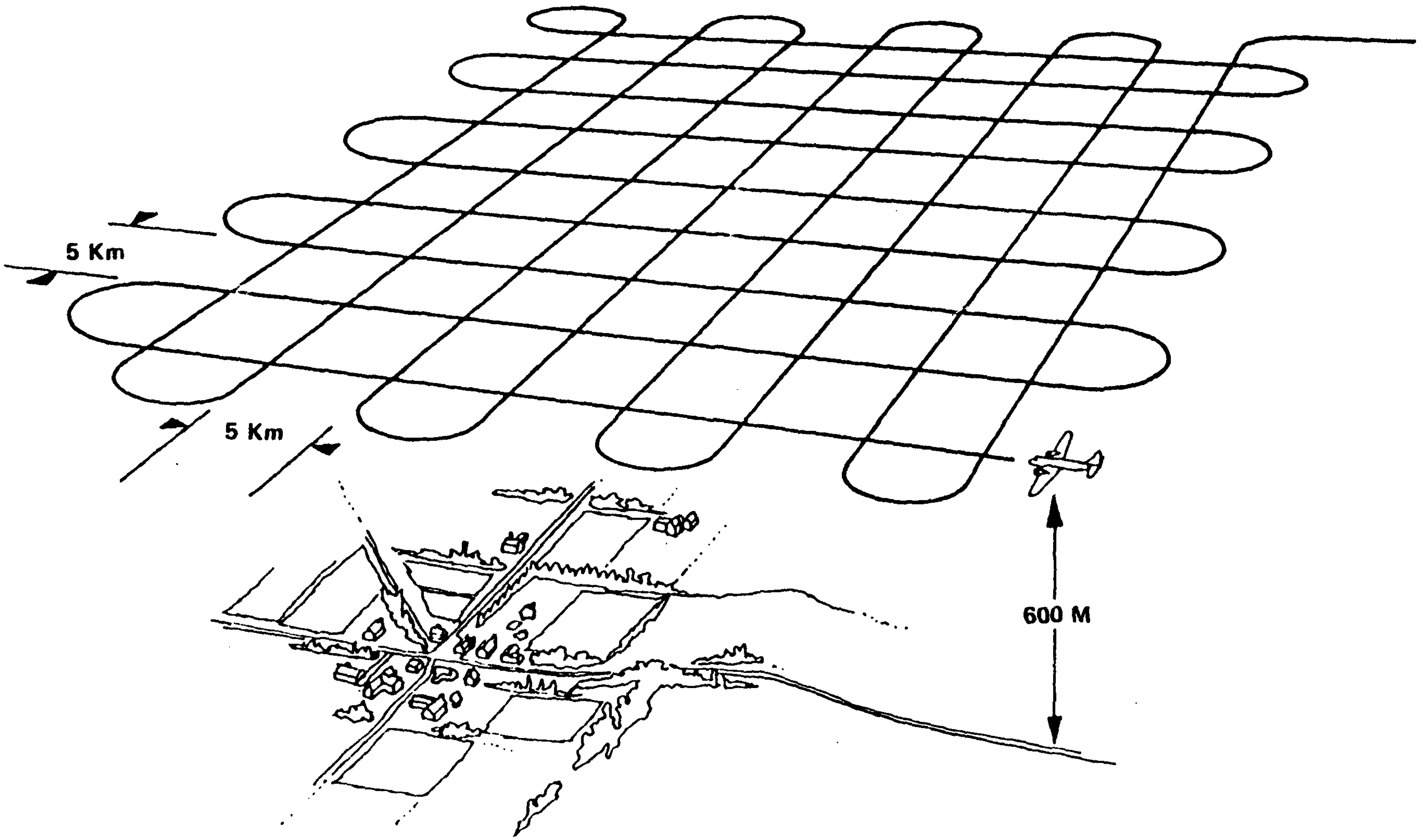
5 Km
5 Km
600 M

C-130 Aircraft Flight Path Between Way Points Under Computer Control

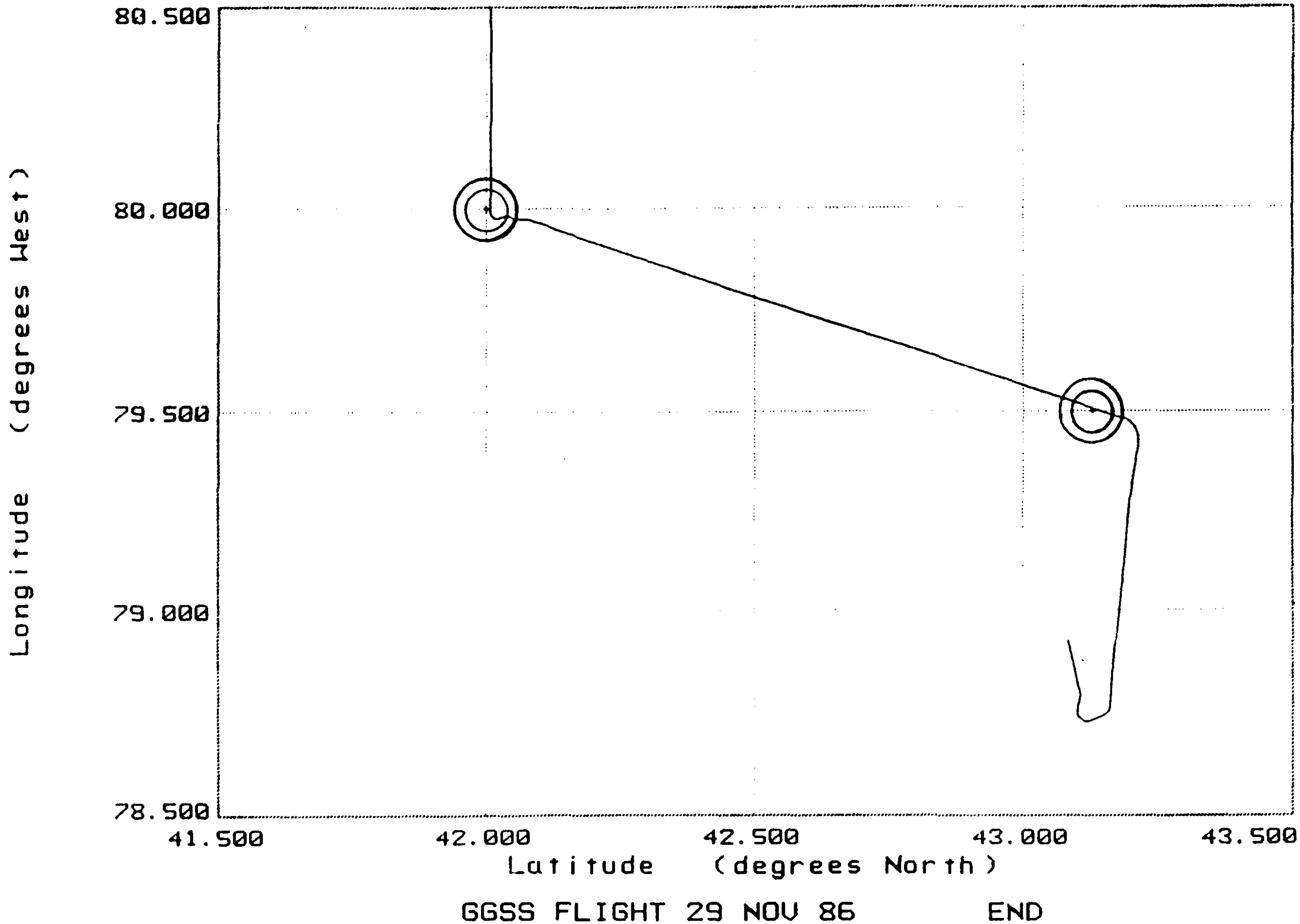

Bell Aerospace TEXTRON

C-130 Aircraft Cross Track Error as a Function of Distance

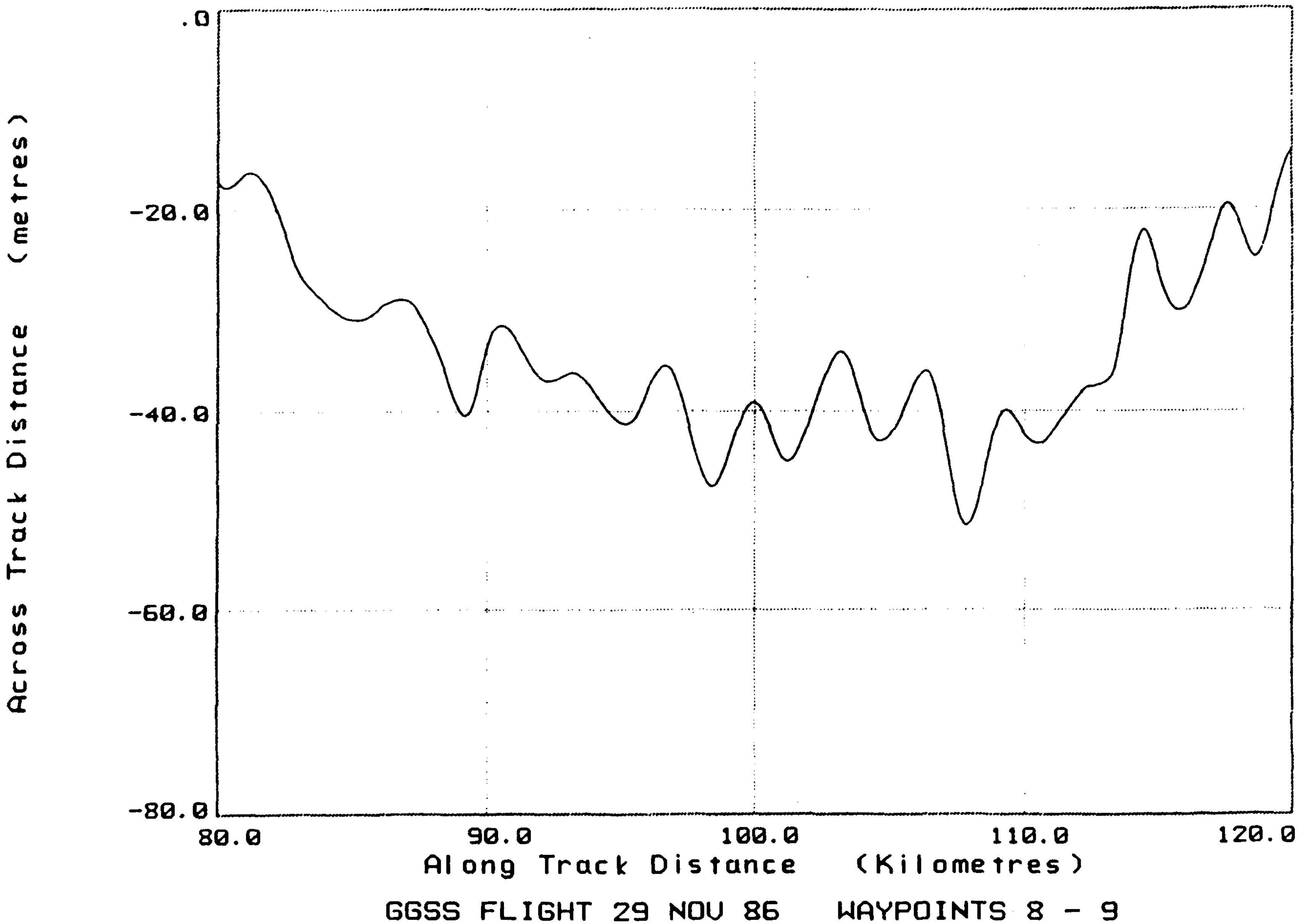

C-130 Aircraft Power Spectrum

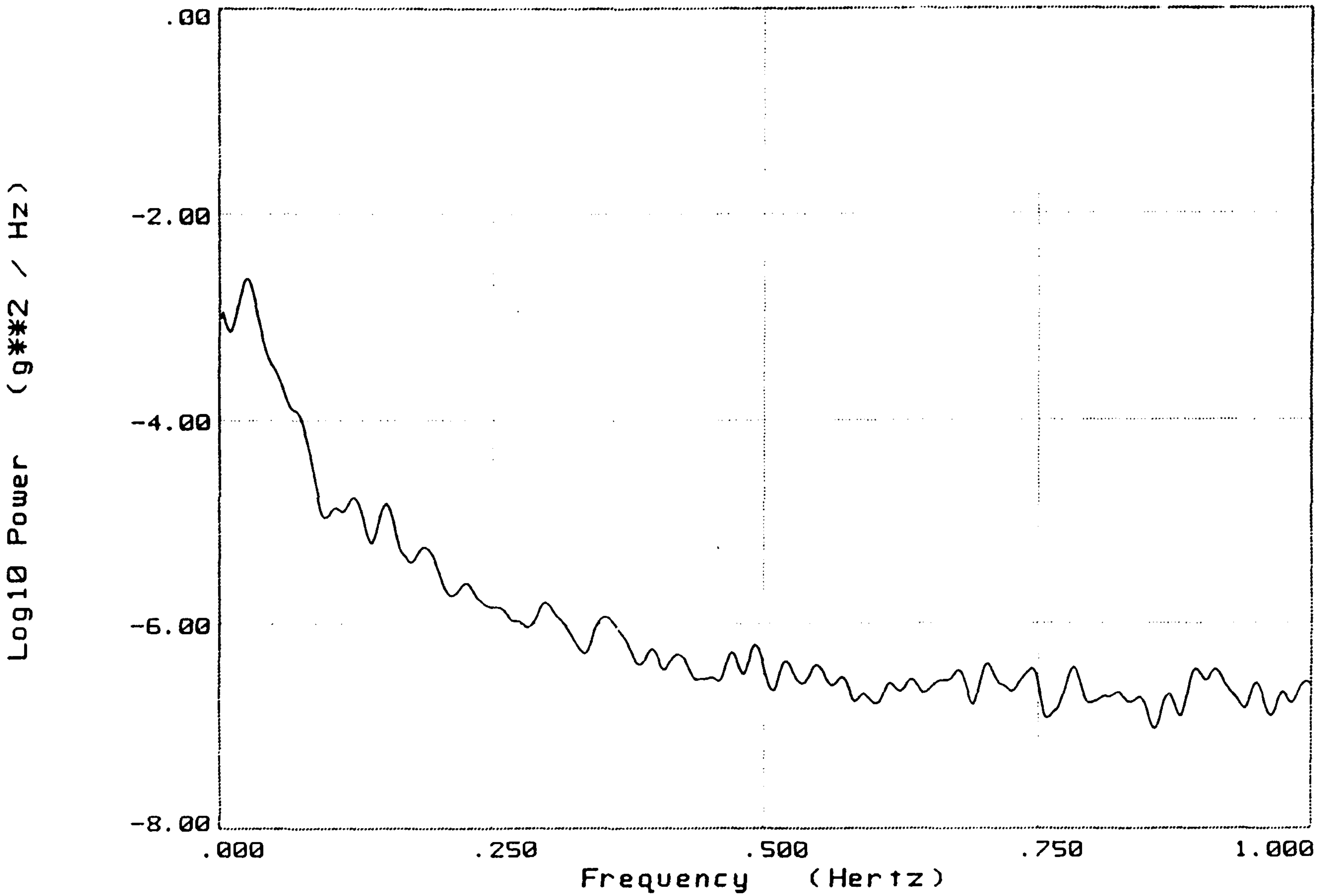

GGSS FLIGHT 29 NOV 86 11550-12600 LONGITUDINAL ACCEL

Bell Aerospace TEXTRON

C-130 Aircraft Power Spectrum

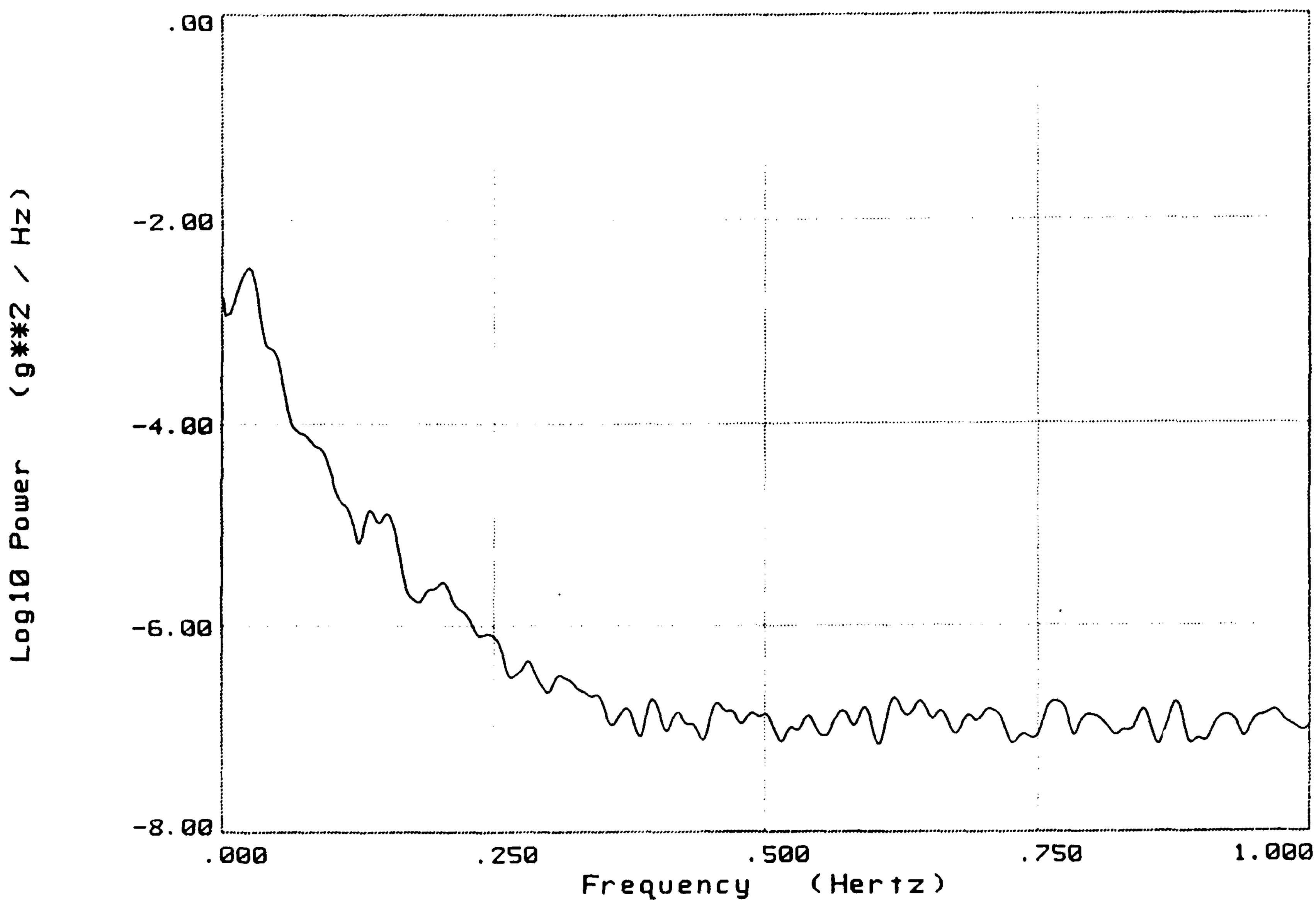

GGSS FLIGHT 29 NOV 86 11550-12600 LATERAL ACCEL

Bell Aerospace TEXTRON

C-130 Aircraft Power Spectrum

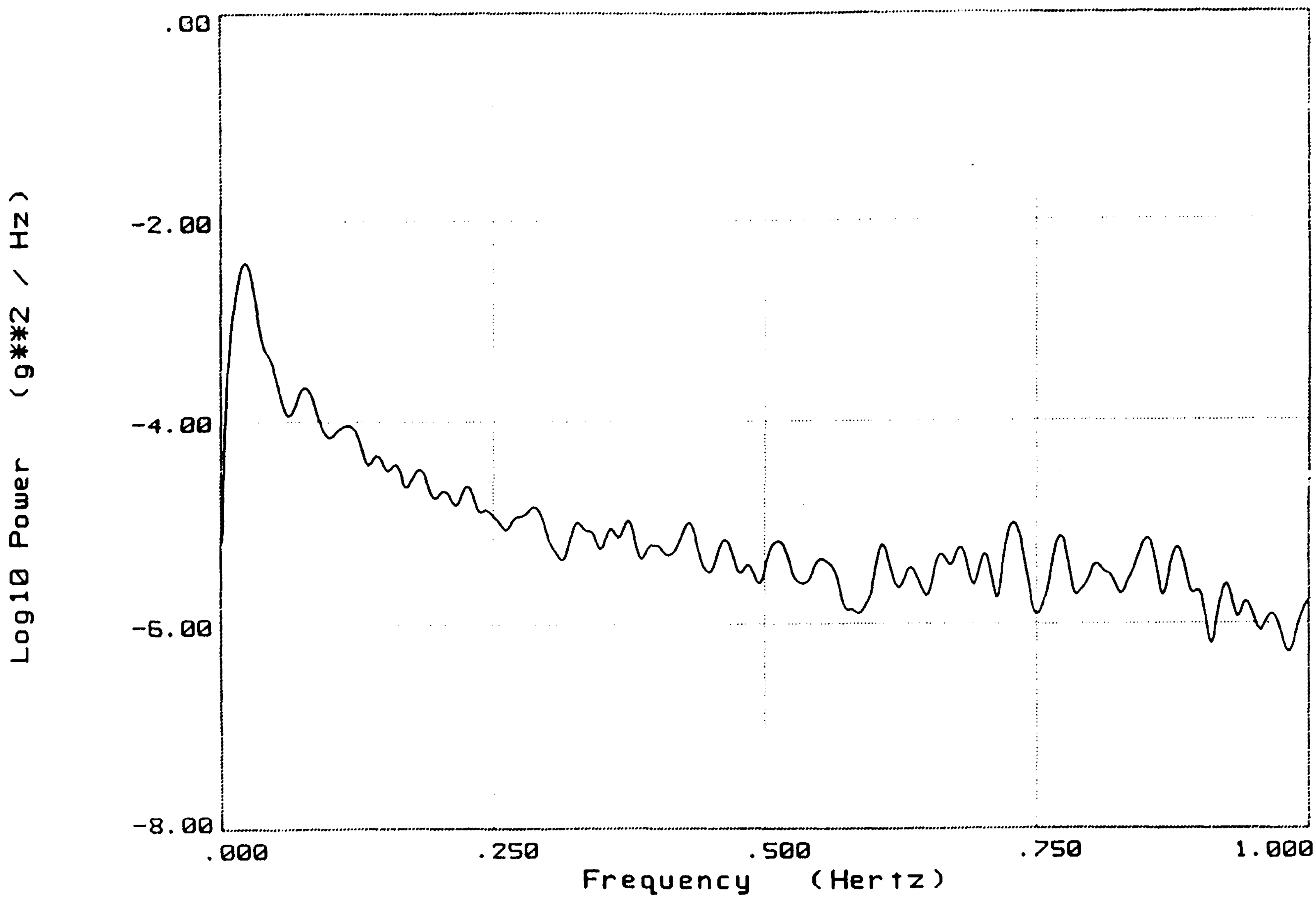

GGSS FLIGHT 29 NOV 86 11550-12600 VERTICAL ACCEL

Bell Aerospace TEXTRON

C-130 Aircraft
Z-Axis Acceleration Time History

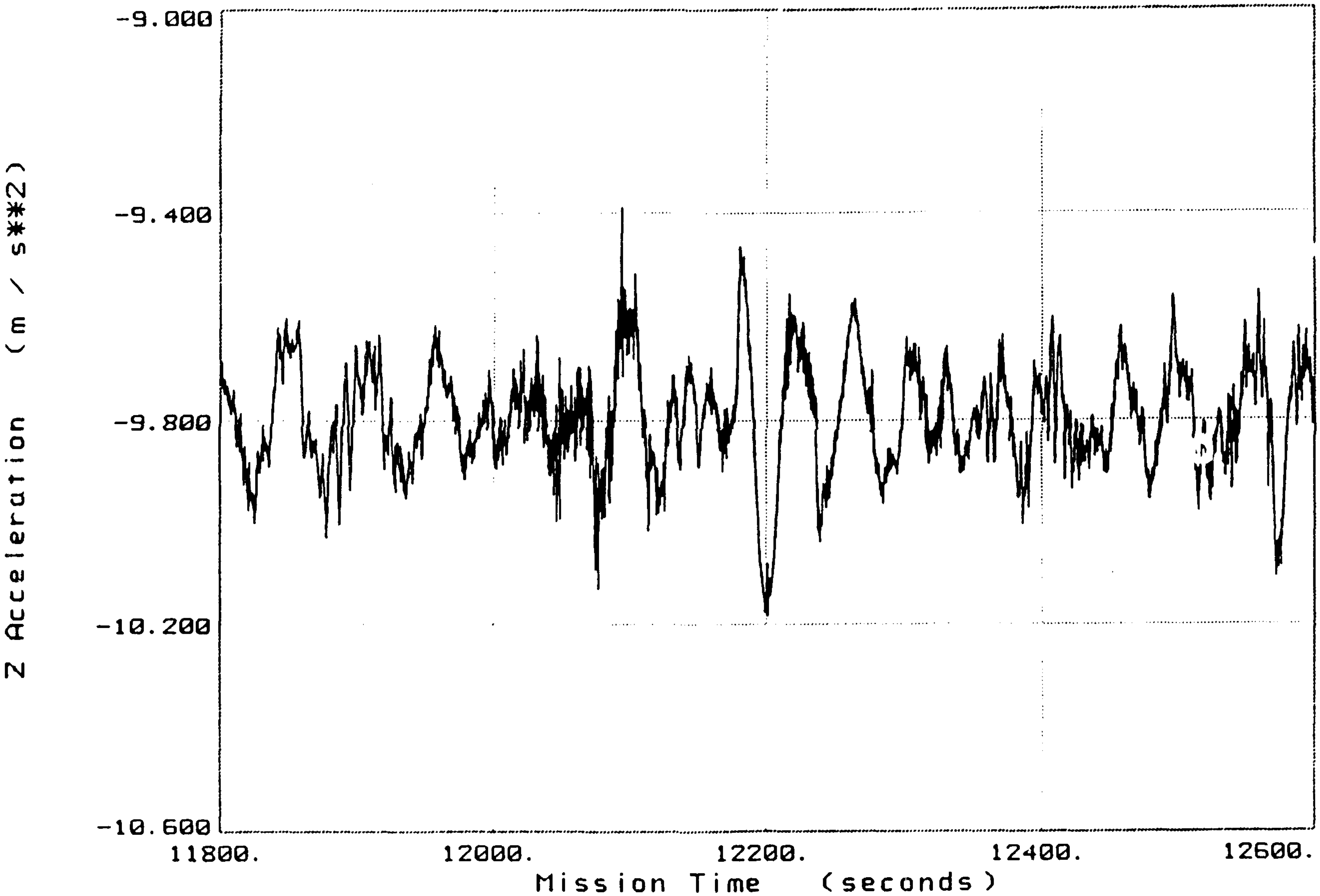

GGSS FLIGHT 29 NOV 86

Bell Aerospace TEXTRON

C-130 Aircraft
Y-Axis Acceleration Time History

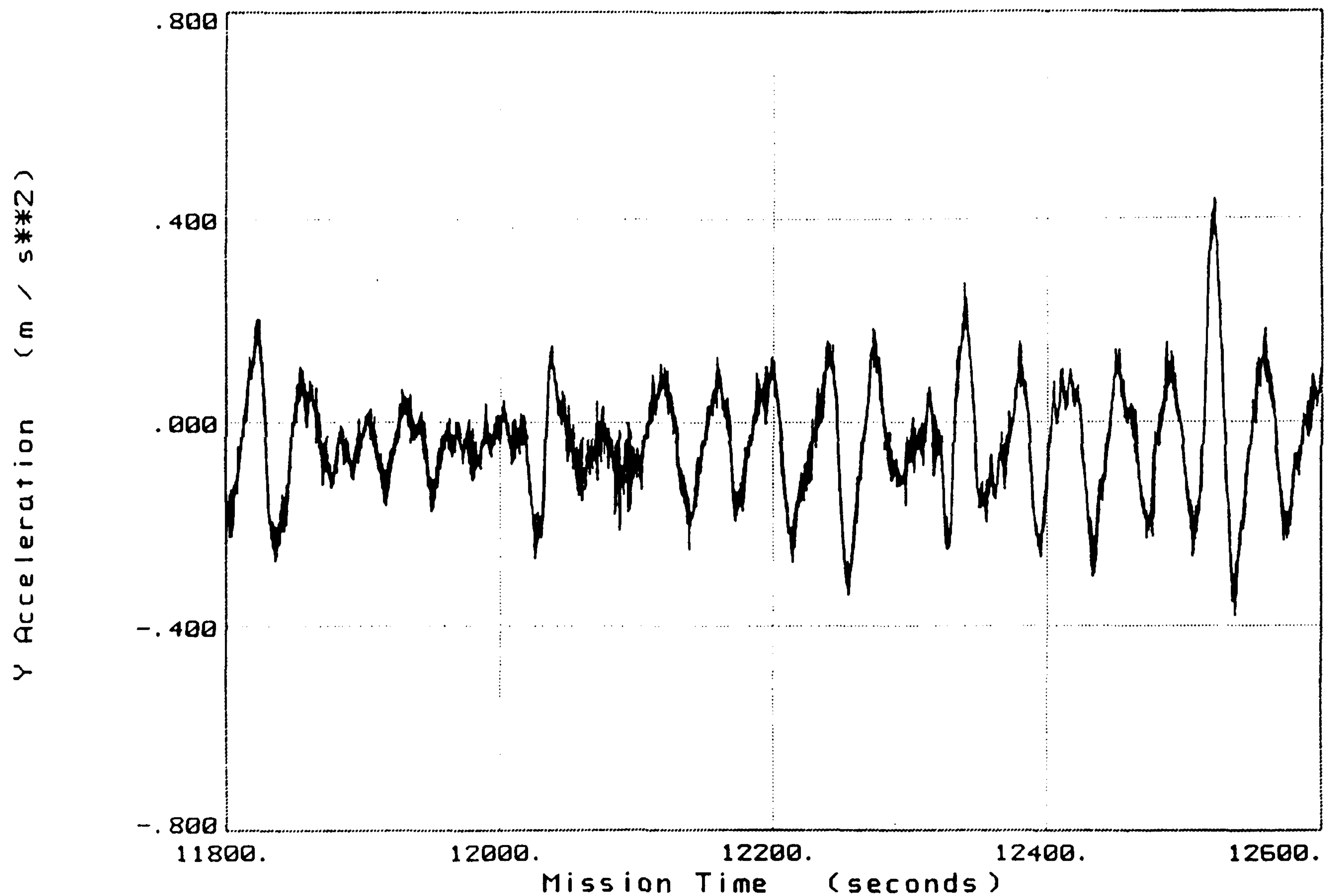

GGSS FLIGHT 29 NOV 86

Bell Aerospace TEXTRON

Land Vehicle Shake Down Drives
December Until Present

- REPLACE REVCON SUSPENSION SYSTEM
- INSTALL FIFTH WHEEL
- MEASURE LINEAR ACCELERATION CHARACTERISTICS VS SPEED
- TRIM ACCELERATION SENSITIVITY COMPENSATION FOR EVEN ORDER ERROR COEFFICIENTS
- IMPLEMENT ACCELERATION SENSITIVITY FOR THIRD ORDER ERROR COEFFICIENTS
- CONDUCT SHAKE DOWN DRIVES

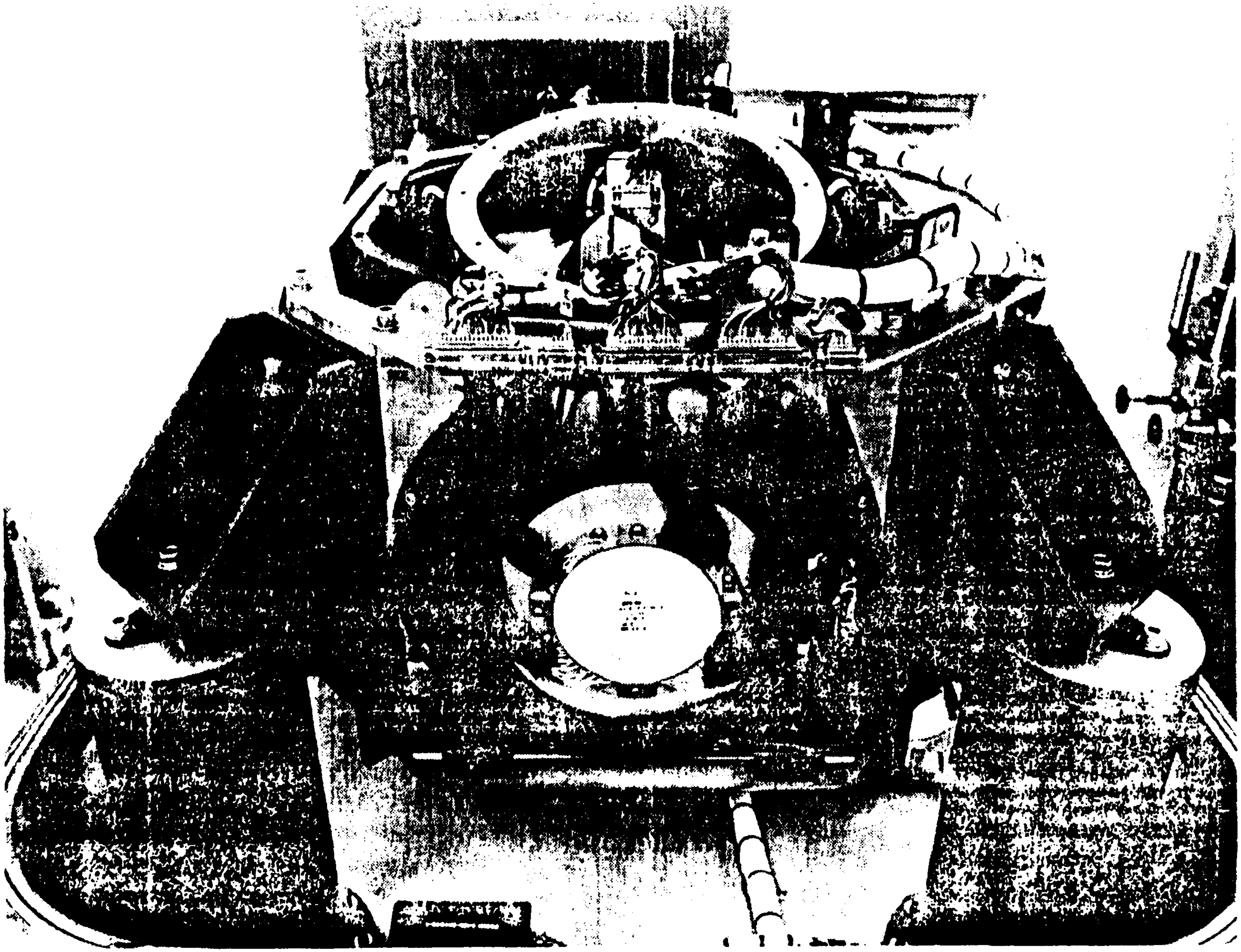

Orientation Of GGIs

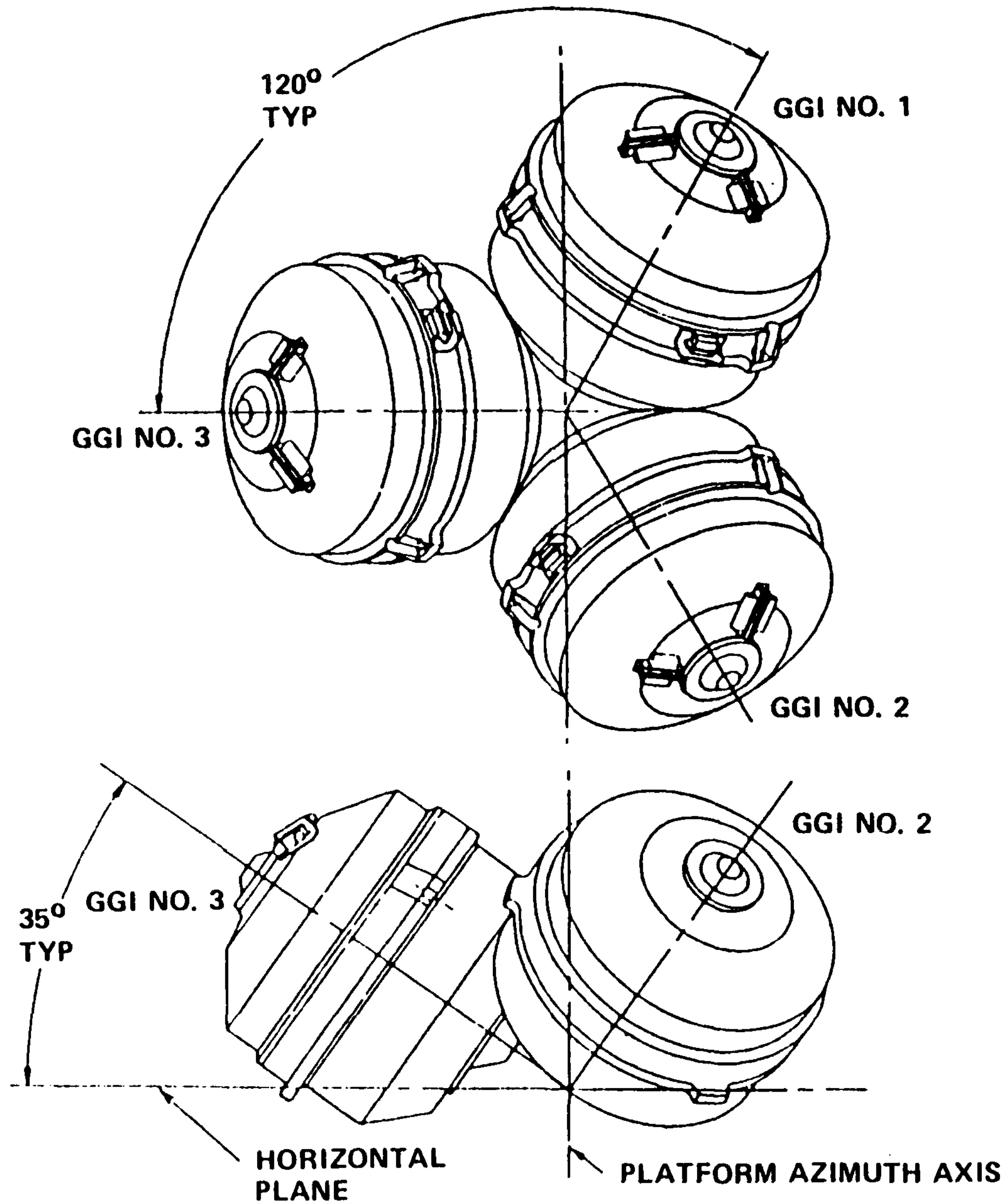

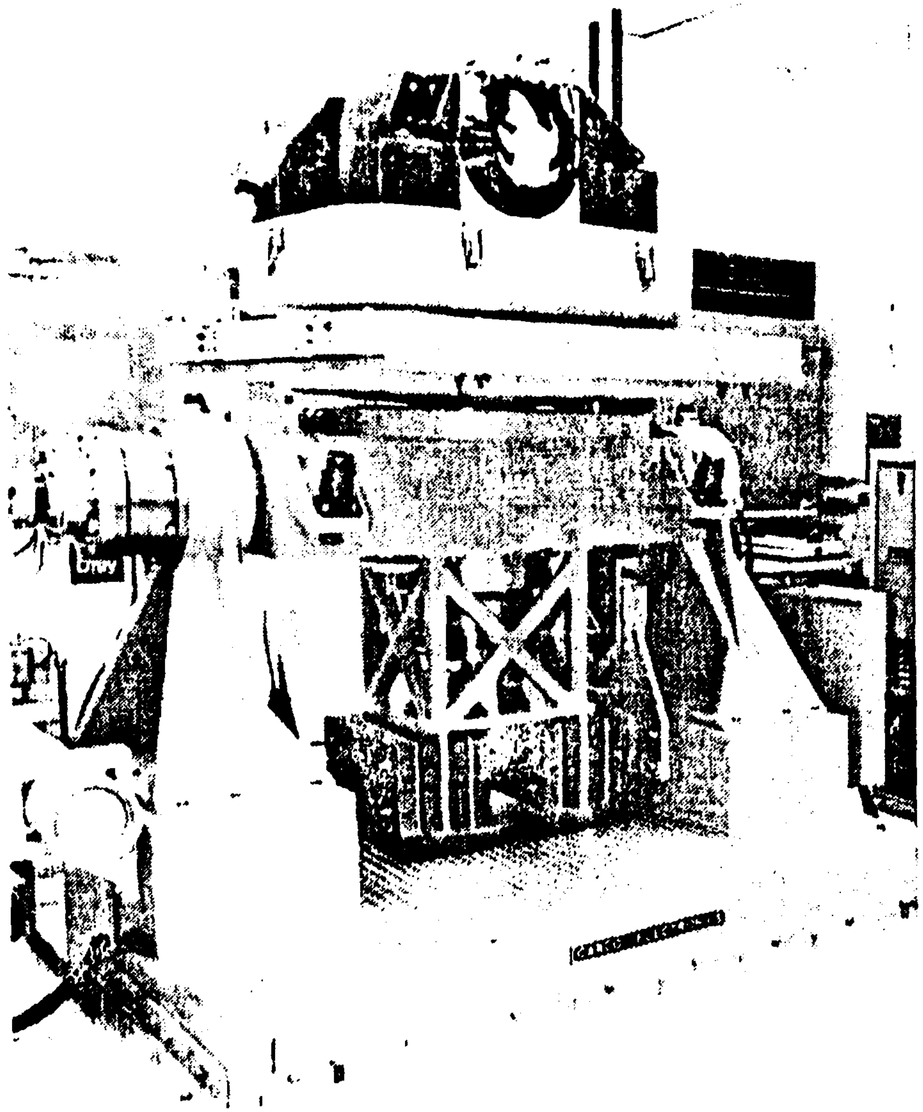

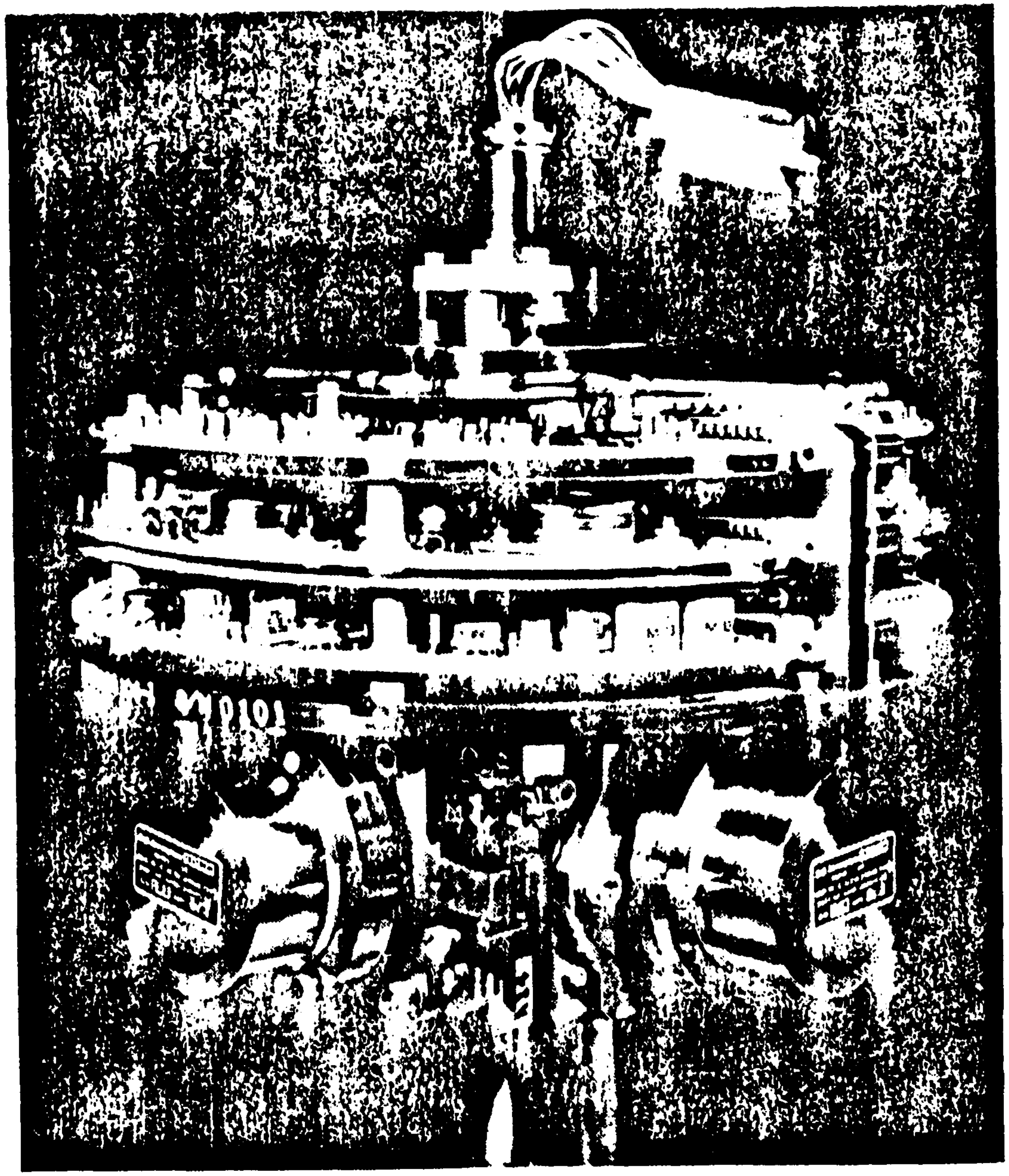

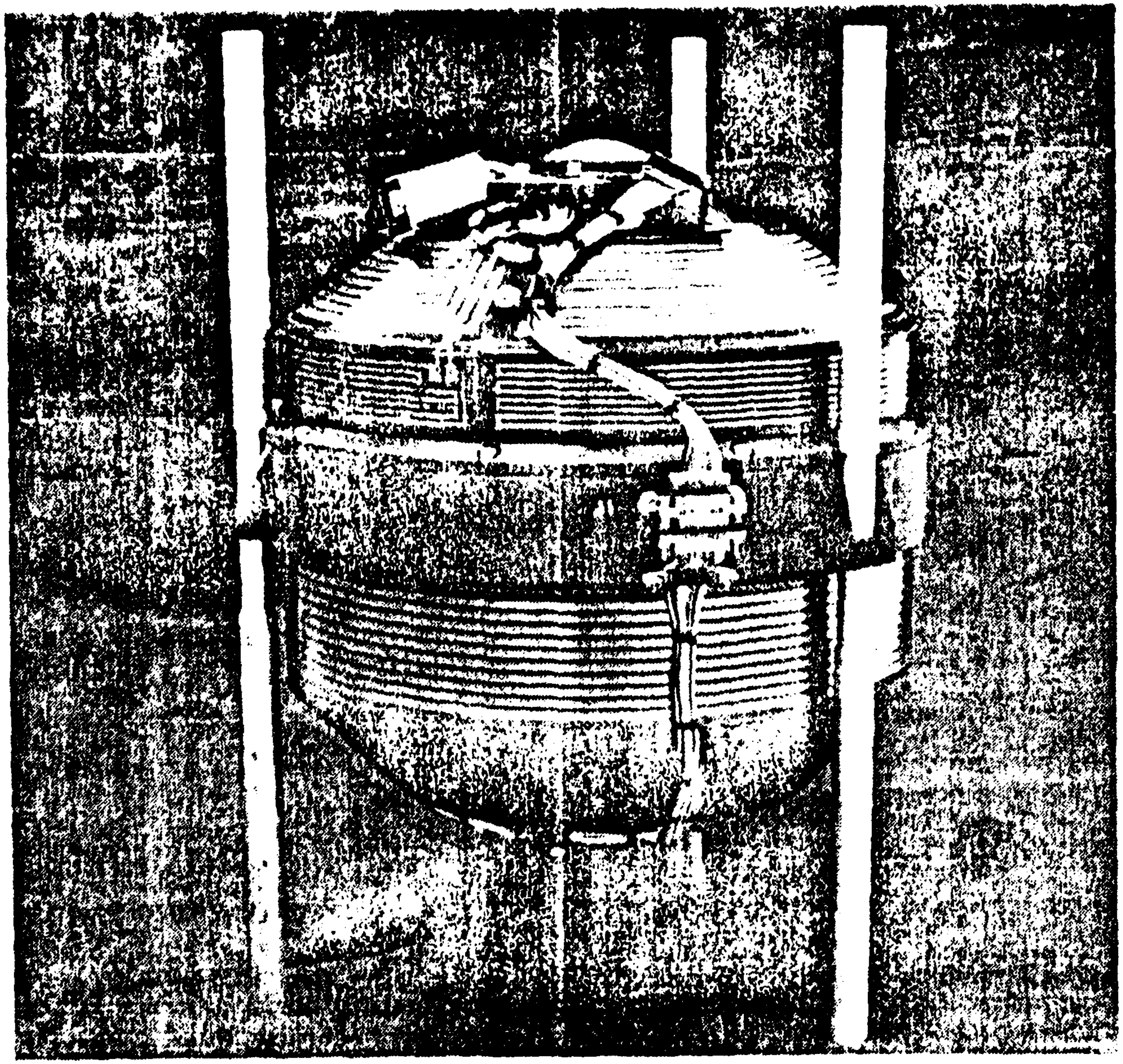

System Laboratory Testing
March Through June 1986

- SYSTEM MODES IMPLEMENTATIONS
  - GYROCOMPASS, GPS AIDED
  - GYROCOMPASS, FIXED COORDINATE AIDED
  - GYROCOMPASS, FIFTH WHEEL AIDED
  - GIMBAL CAGED
  - PURE INERTIAL
- ACCELEROMETER AND GYRO CALIBRATIONS
- GRAVITY GRADIOMETER INSTRUMENT CALIBRATIONS
- PLATFORM SELF GRADIENT CALIBRATION
- GRAVITY GRADIOMETER INSTRUMENT NOISE PERFORMANCE
  - STATIC
  - SCORSBY DYNAMIC

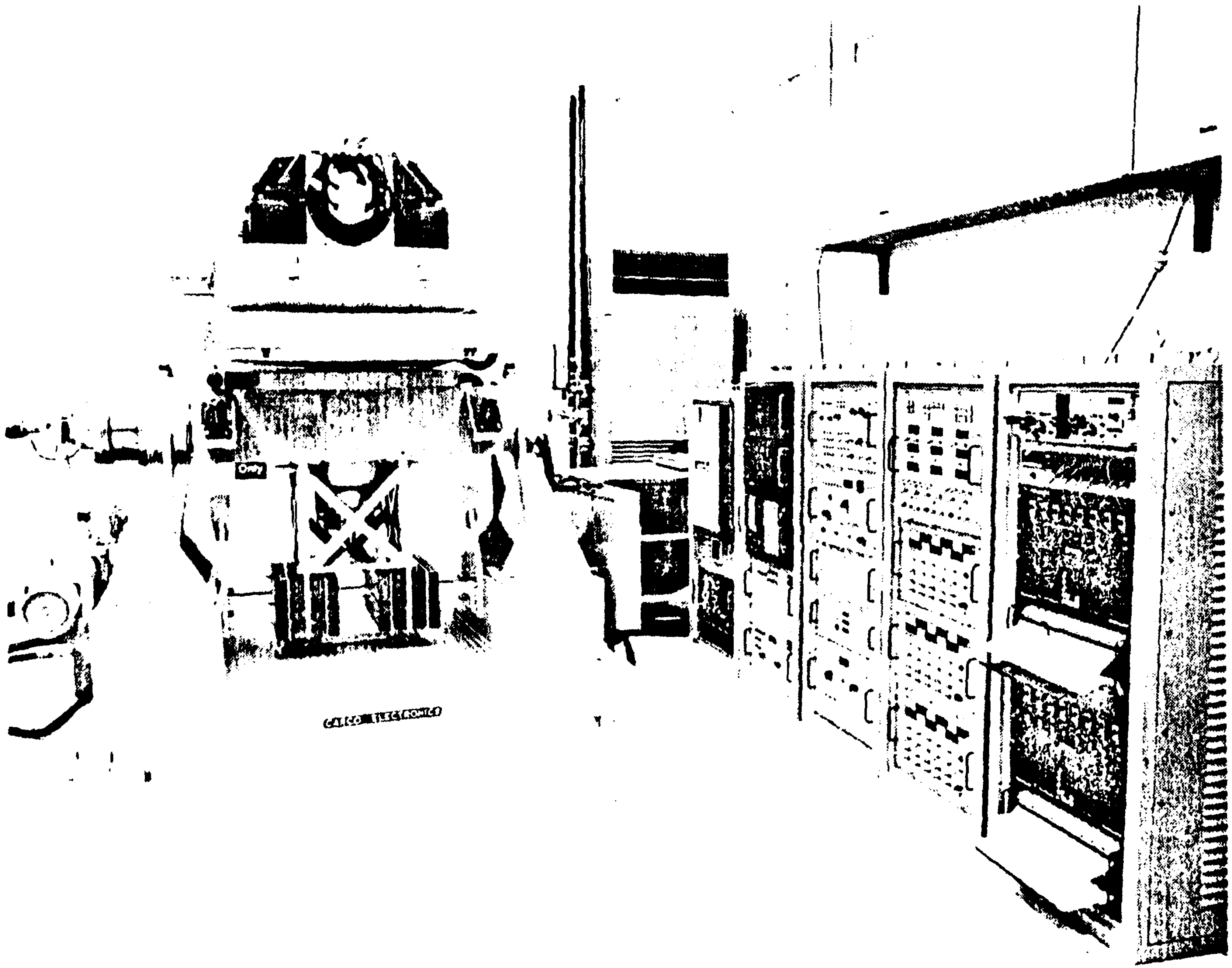
CARCO ELECTRONICS

Land Vehicle Installation July & August 1986

- EQUIPMENT BOLT IN
- INTERCONNECTING CABLES
- GPS ANTENNA
- AIRCRAFT INTERFACES AND POWER
- STATIC PERFORMANCE VERIFICATION

GGSS-Land Vehicle Installation

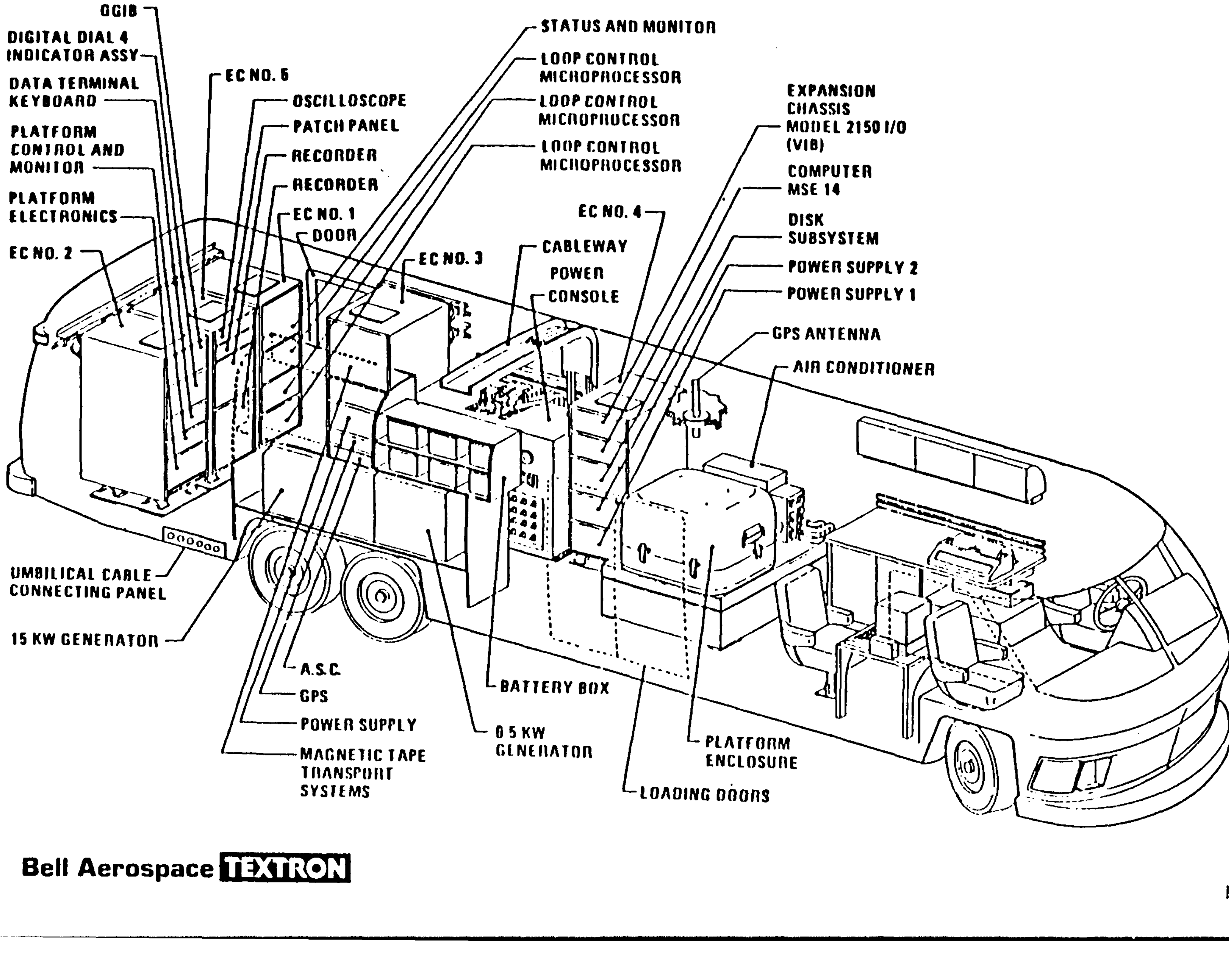

Bell Aerospace TEXTRON

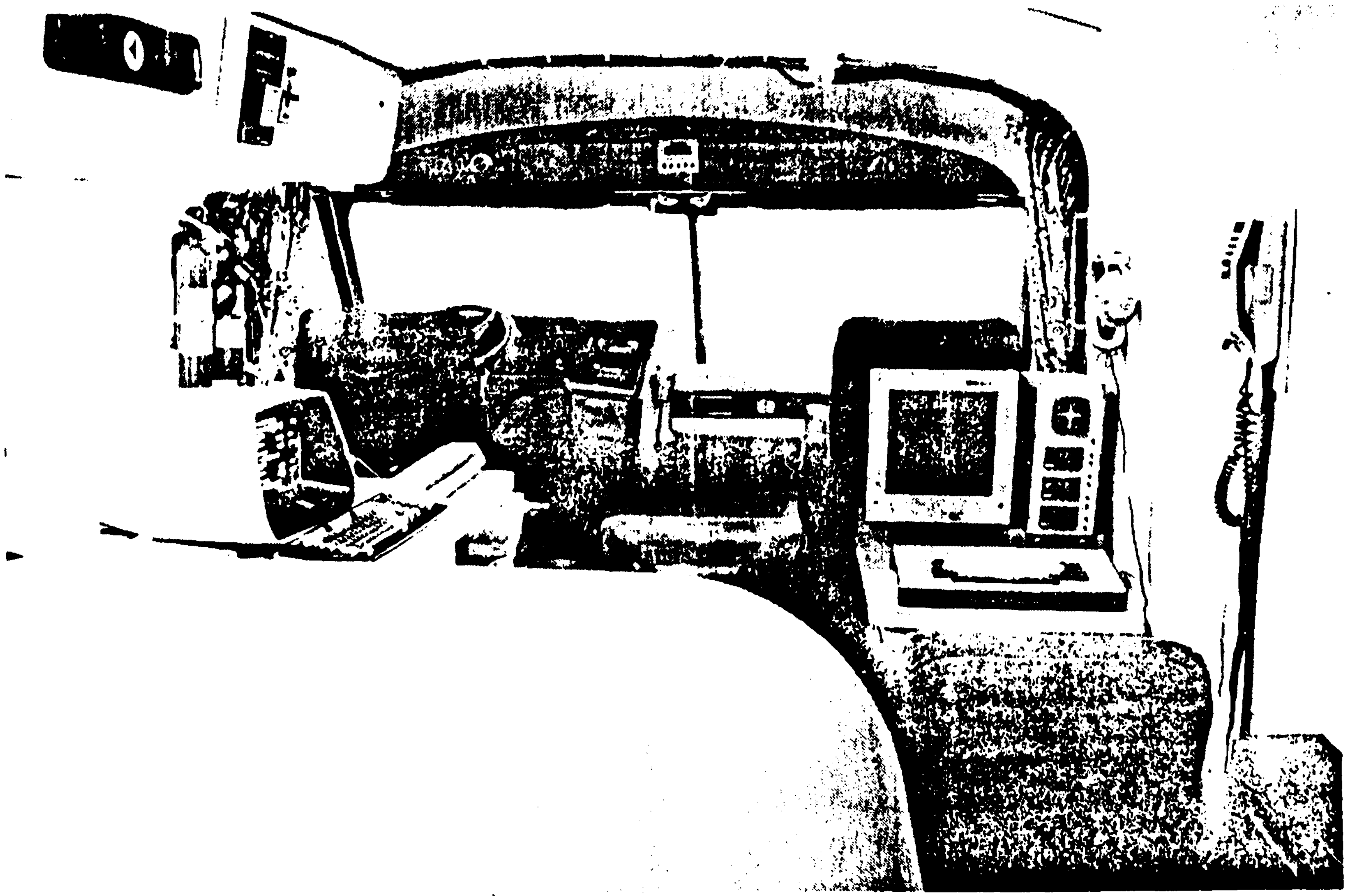

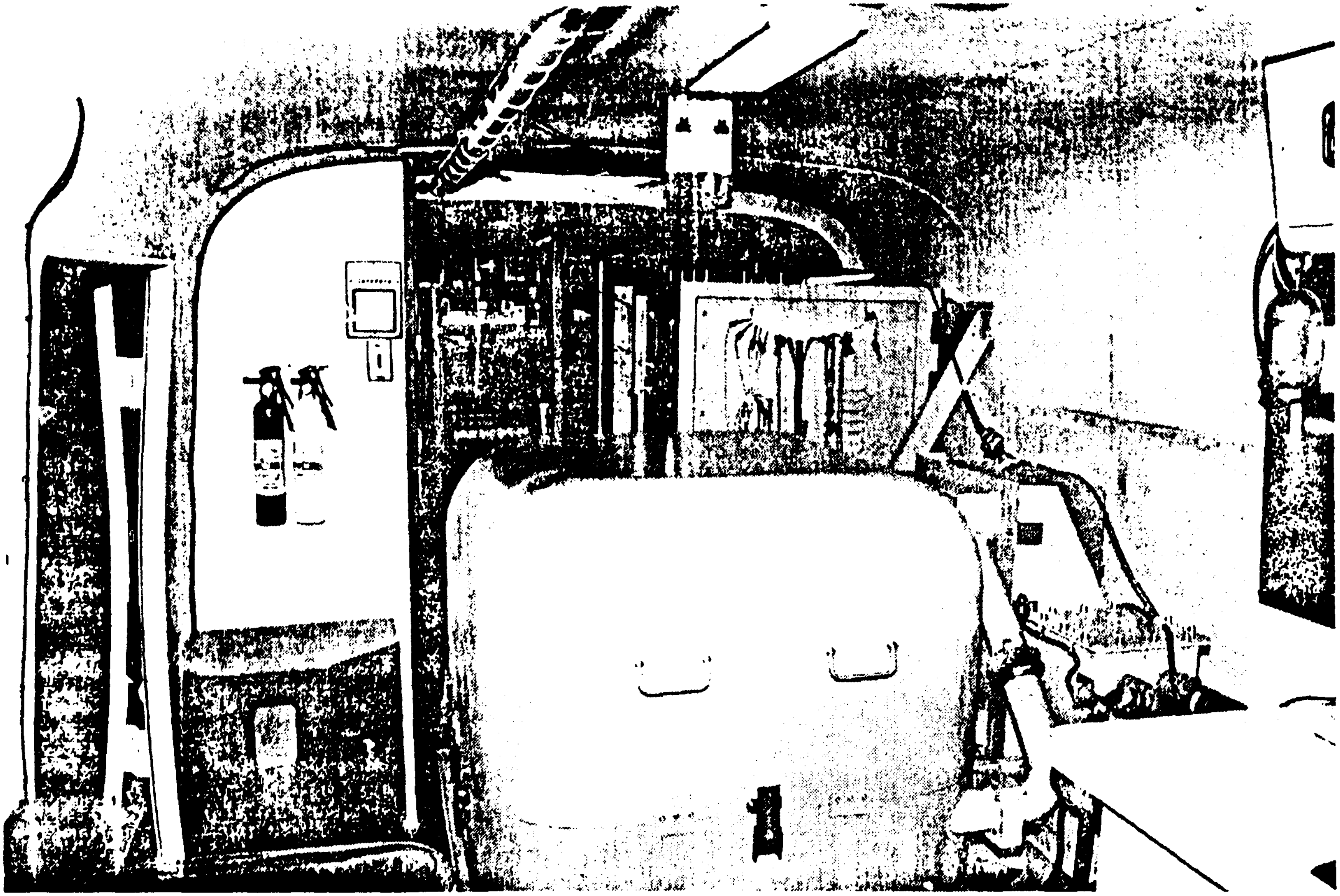

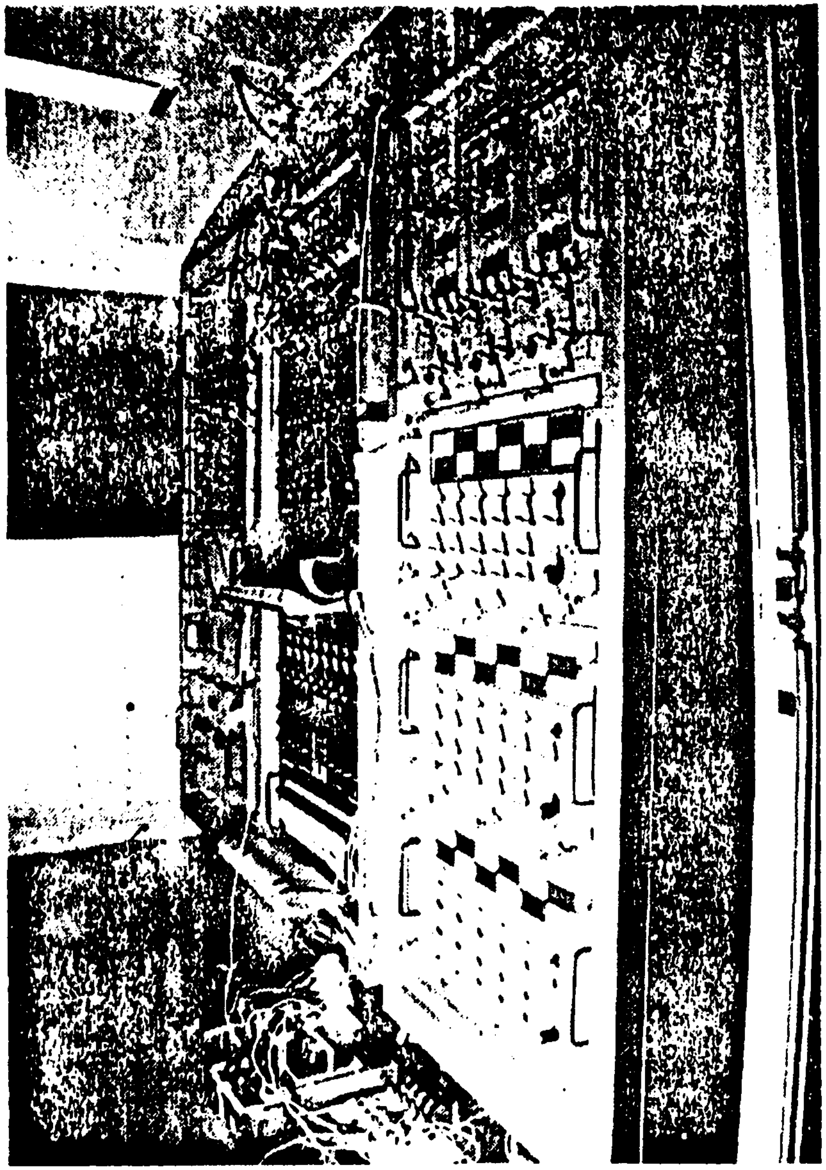

GGSS Installation In C-130 Aircraft & Flight Control Shake Down
September Through November 1986

- C130 AIRCRAFT MODIFICATIONS AT SOUTHERN AIR TRANSPORT
  - SIGNAL AND POWER INTERFACES
  - UMBILICALS TO GGSS VAN
  - COCKPIT DISPLAY INSTALLATIONS
- NEW AUTOPILOT INSTALLATION (COLLINS FCS 105)
- LOADING RAMP DESIGN AND FABRICATION
- DRIVE-ON/TIE DOWN VERIFICATION
- SIGNAL AND POWER HOOKUP AND CHECK OUT
- PRELIMINARY SHAKE DOWN FLIGHTS
- AIRCRAFT GRADIENT CALIBRATION
- FLIGHT PATTERN CONTROL TEST FLIGHTS
- C-130 LINEAR ACCELERATION ENVIRONMENTAL APPRAISAL
- GPS AIRBORNE OPERATION

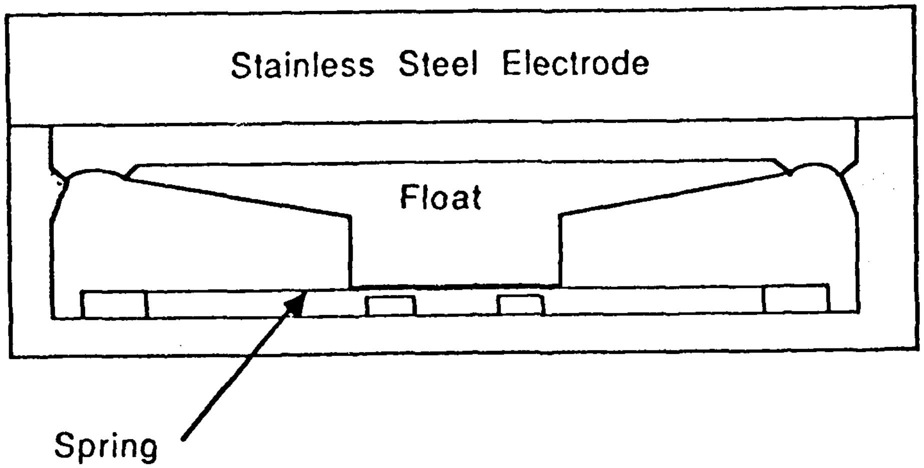

Fig. 7

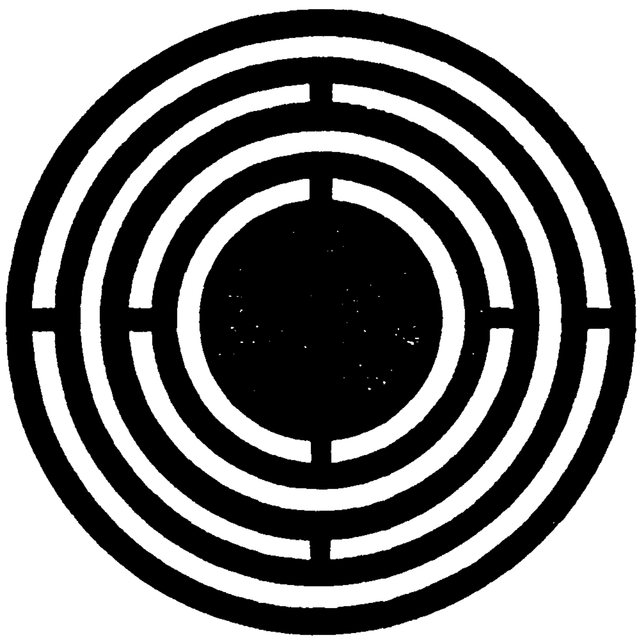

Spring etched from 0.001" sheet

Fig. 8

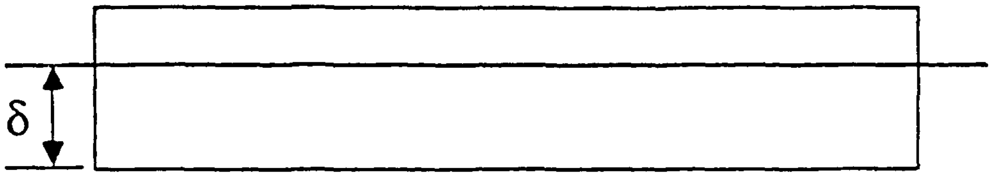

Normal flotation level δ

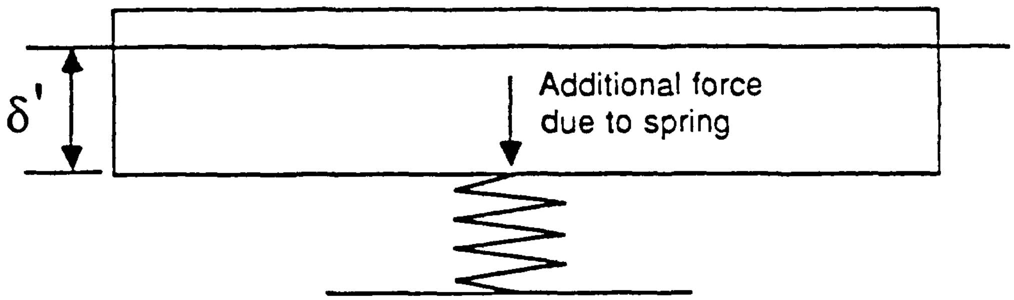

Flotation level with spring δ'

Required spring constant < 0.14 Nm^{-1}

Fig. 9

TITLE OF PAPER: A Mercury Manometer Gravity Gradiometer

SPEAKER: G. Ian Moore

QUESTIONS AND COMMENTS:

1. Question: Jean-Paul Richard

Sensitivity of capacitance detection?

Response:

10^{-7} times the gap = 2×10^{-8} mm.

BELL AEROSPACE GRAVITY GRADIOMETER SURVEY SYSTEM (GGSS) PROGRAM REVIEW

by

Mr. Ernest H. Metzger
Mr. Louis L. Pfohl

Bell Aerospace Textron
P.O. Box One
Buffalo, NY 14240

ABSTRACT

A review of GGSS program activities in 1986 includes system lab testing, land vehicle and aircraft installations, electrical power and signal interfacing, and shakedown cruises. Among the significant accomplishments were system output noise determination in the laboratory, platform and aircraft self-gradient calibrations, and implementation of automated flight pattern control via GGSS navigator and computer linked to the C-130 autopilot.

MOVING BASE GRAVITY GRADIOMETER REVIEW

Gravity Gradiometer Survey System (GGSS) Program Review

AIR FORCE ACADEMY

Report No. 6501-927173 • FEBRUARY 11/12, 1987

Bell Aerospace TEXTRON
Division of Textron Inc

1986 GGSS Activities

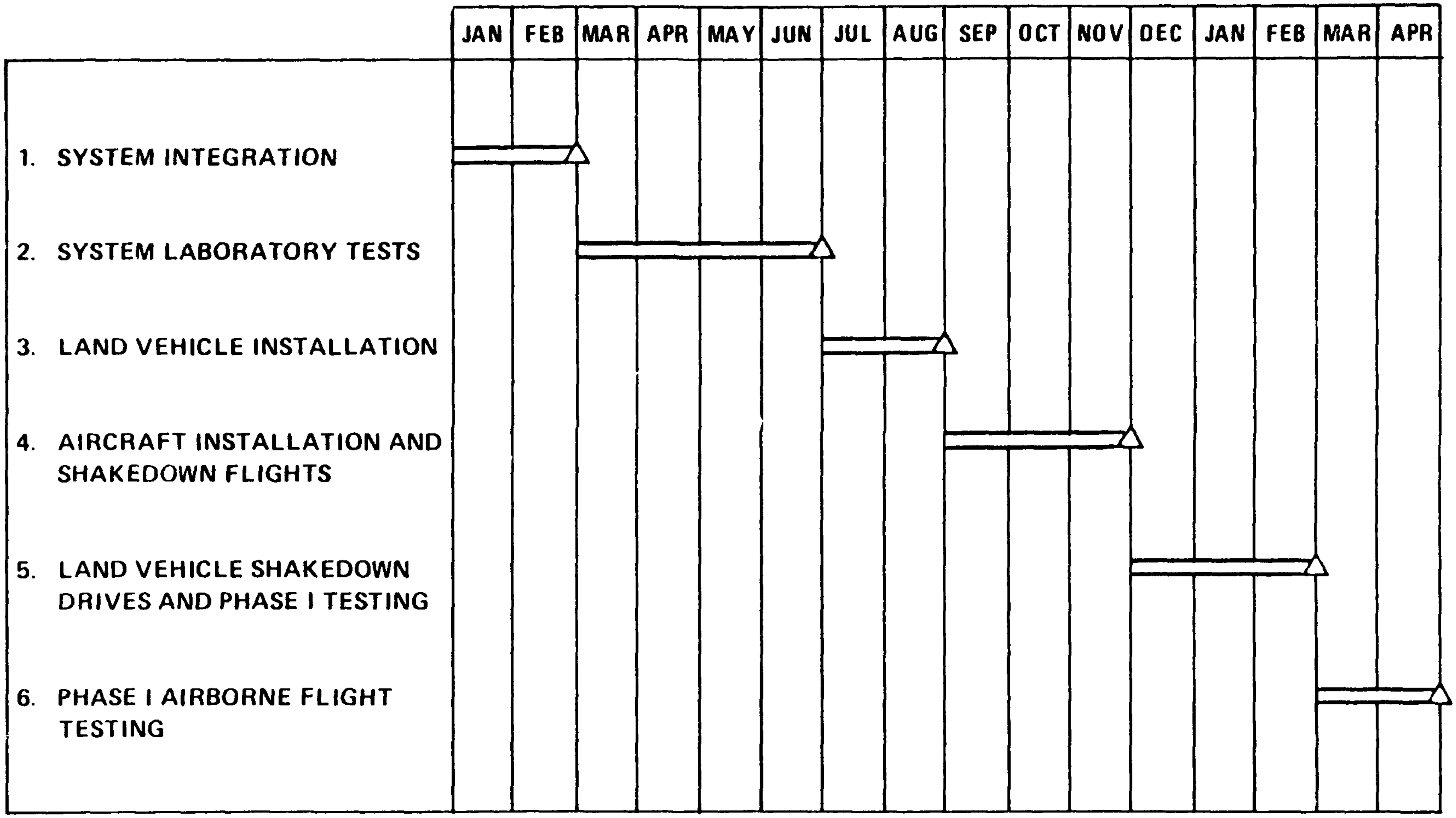

Bell Aerospace TEXTRON

GGSS Functional Block Diagram

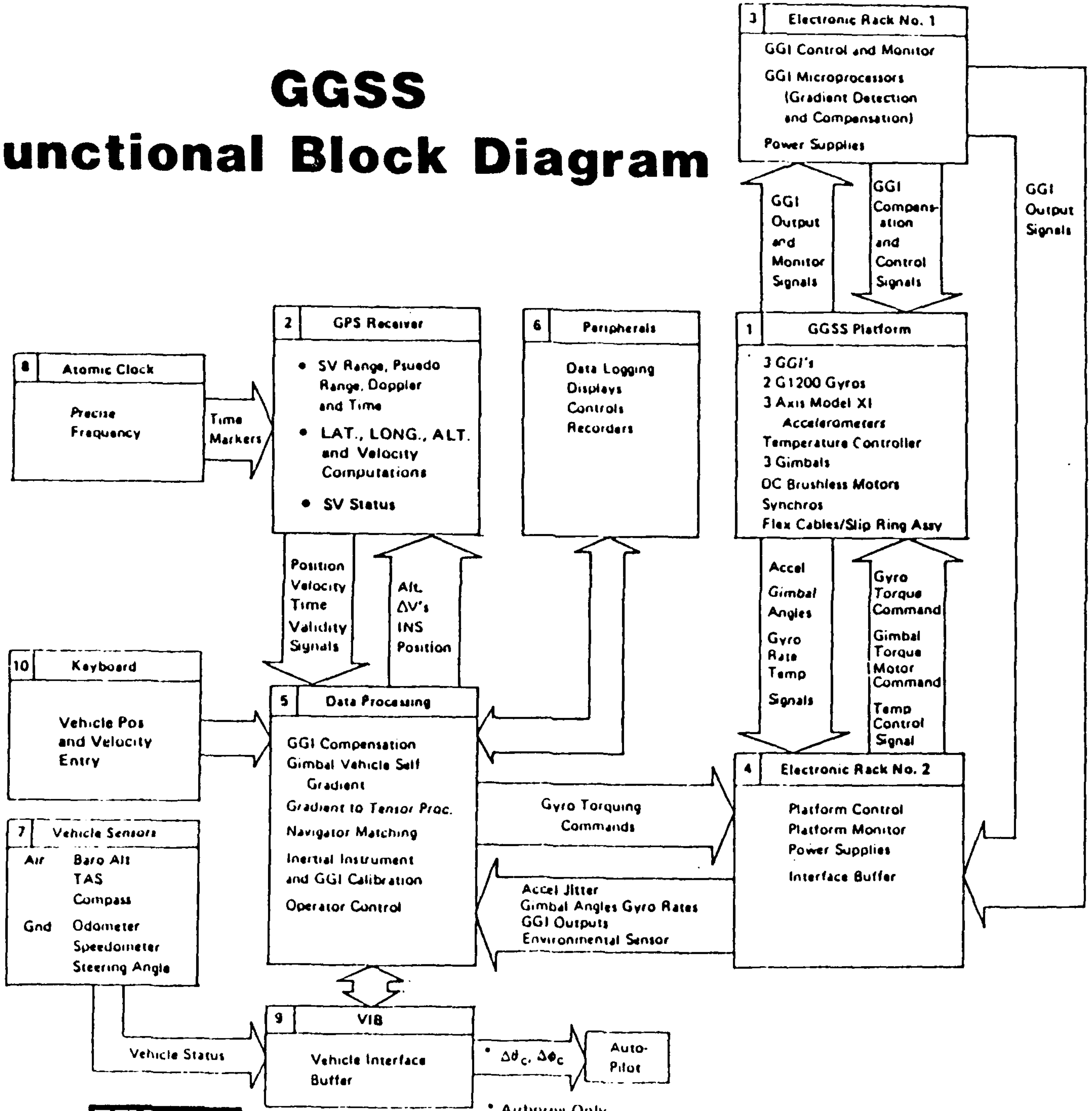

Bell Aerospace TEXTRON

SOLUTION OF MEASUREMENT INTEGRALS WITHOUT MATRIX INVERSIONS

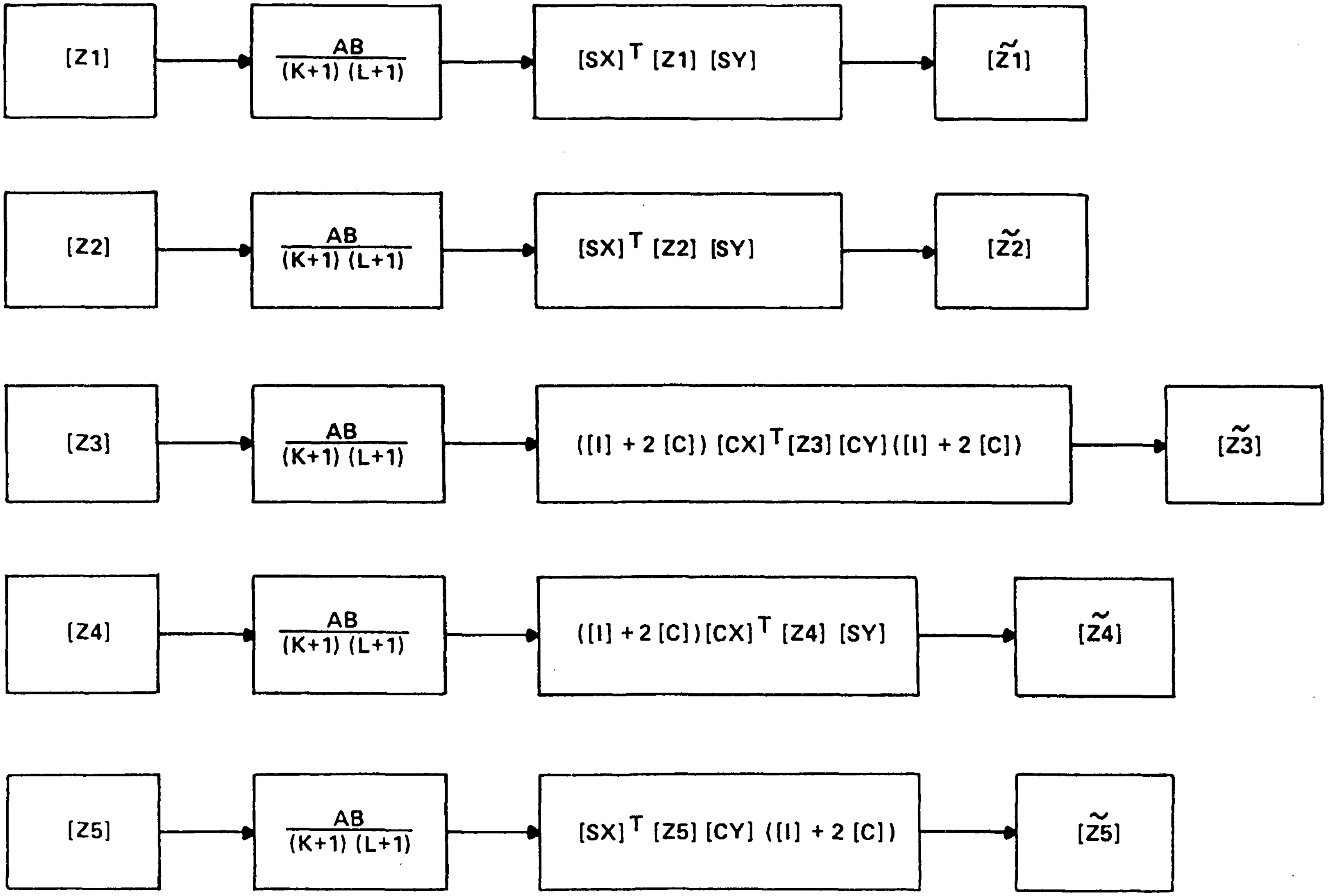

APPLIED SCIENCE ANALYTICS, INC.

OPTIMAL ESTIMATE OF KARHUNEN-LOEVE COEFFICIENTS

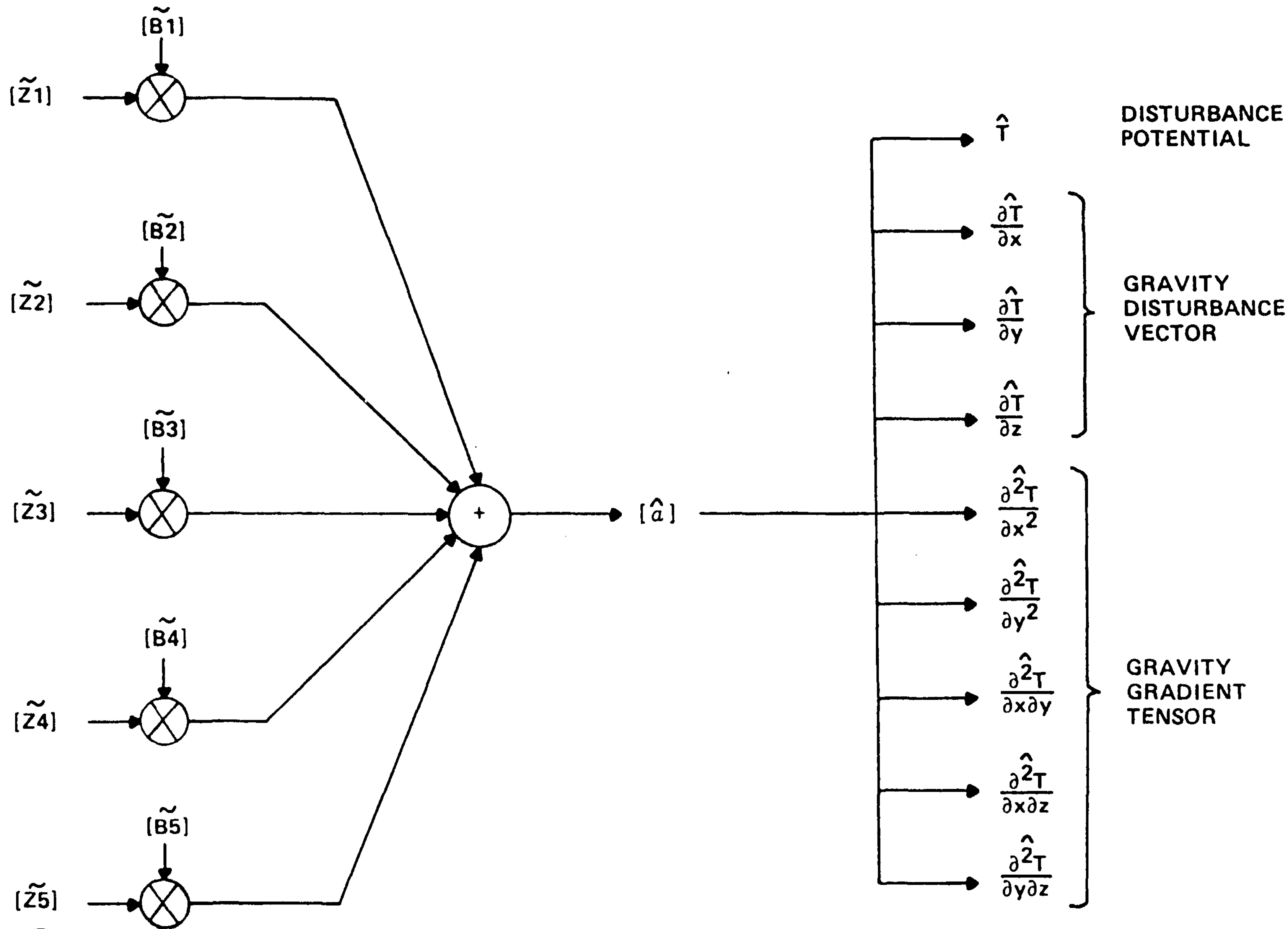

APPLIED SCIENCE ANALYTICS, INC.

GRAVITY VECTOR EXPRESSED IN TERMS OF K–L COEFFICIENT ESTIMATES

$$\begin{bmatrix} \hat{T}(x,y,h) \\ \frac{\partial \hat{T}}{\partial x}(x,y,h) \\ \frac{\partial \hat{T}}{\partial y}(x,y,h) \\ \frac{\partial \hat{T}}{\partial z}(x,y,h) \end{bmatrix} = \sum_{m=1}^{\infty} \sum_{n=1}^{\infty} \hat{a}_{mn} \begin{bmatrix} \sin a_m x \sin b_n y \left\{ \underbrace{\frac{2}{\sqrt{AB}} \; e^{-c_{mn}|h-D|}}_{\gamma_{mn}^{s1}} \right\} \\ \cos a_m x \sin b_n y \left\{ \underbrace{\frac{2}{\sqrt{AB}} \; a_m e^{-c_{mn}|h-D|}}_{\gamma_{mn}^{s2}} \right\} \\ \sin a_m x \cos b_n y \left\{ \underbrace{\frac{2}{\sqrt{AB}} \; b_n e^{-c_{mn}|h-D|}}_{\gamma_{mn}^{s3}} \right\} \\ \sin a_m x \sin b_n y \left\{ \underbrace{\frac{-2\,\mathrm{sgn}(h-D)}{\sqrt{AB}} \; c_{mn} e^{-c_{mn}|h-D|}}_{\gamma_{mn}^{s4}} \right\} \end{bmatrix}$$

AD-A252 128 PROCEEDINGS OF THE ANNUAL GRAVITY GRADIOMETRY 3/3
CONFERENCE (15TH) HELD IN COLORADO SPRINGS COLORADO ON
FEBRUARY 11 - 13 1987 VOLUME 1(U) GEOPHYSICS LAB (AFSC)
UNCLASSIFIED HANSCOM AFB MA V V NEVREKAR 13 FEB 87 NL

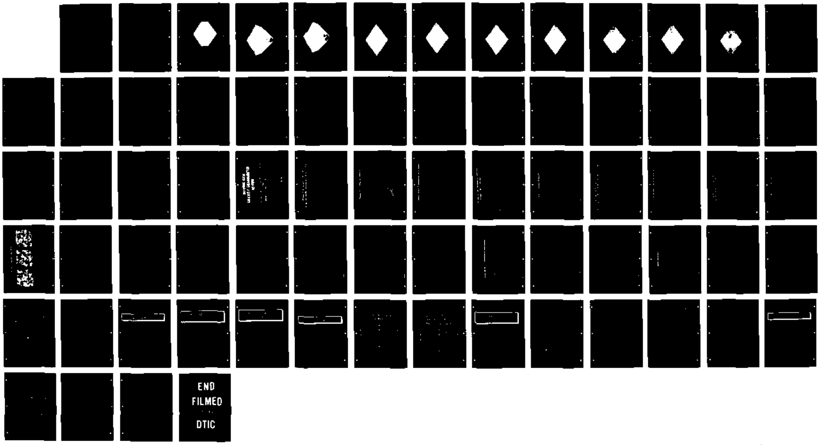

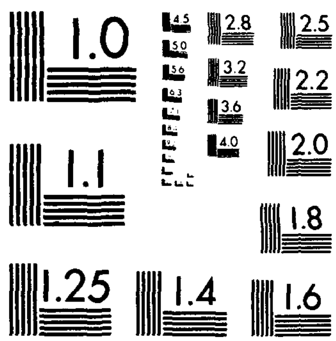

MICROCOPY RESOLUTION TEST CHART
NATIONAL BUREAU OF STANDARDS-1963-A

INTERPOLATED AND DOWNWARD CONTINUED 2D GRID ESTIMATES OF GRAVITY VECTOR

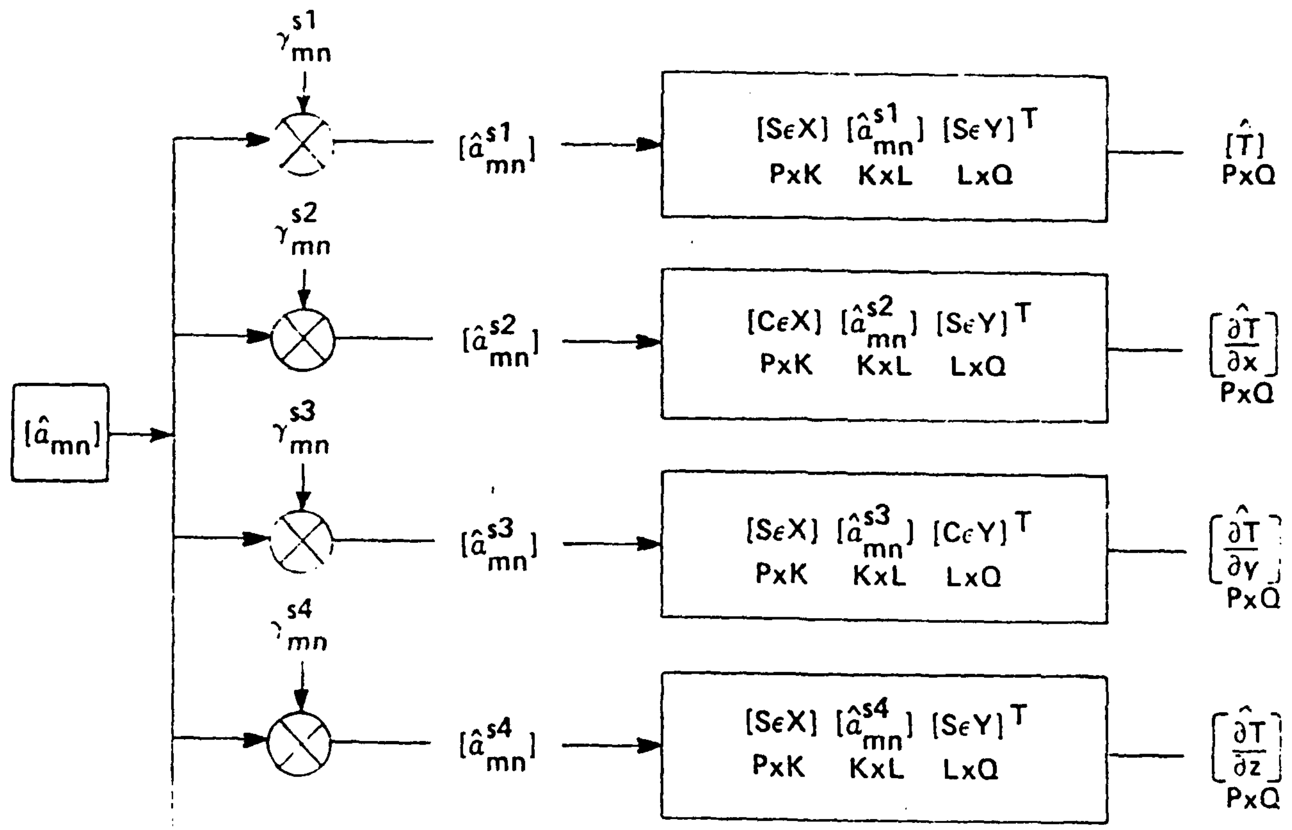

$$A = \epsilon X(P+1)\ ,\quad B = \epsilon Y(Q+1)$$
$$\epsilon X < \Delta X \qquad \epsilon Y < \Delta Y$$

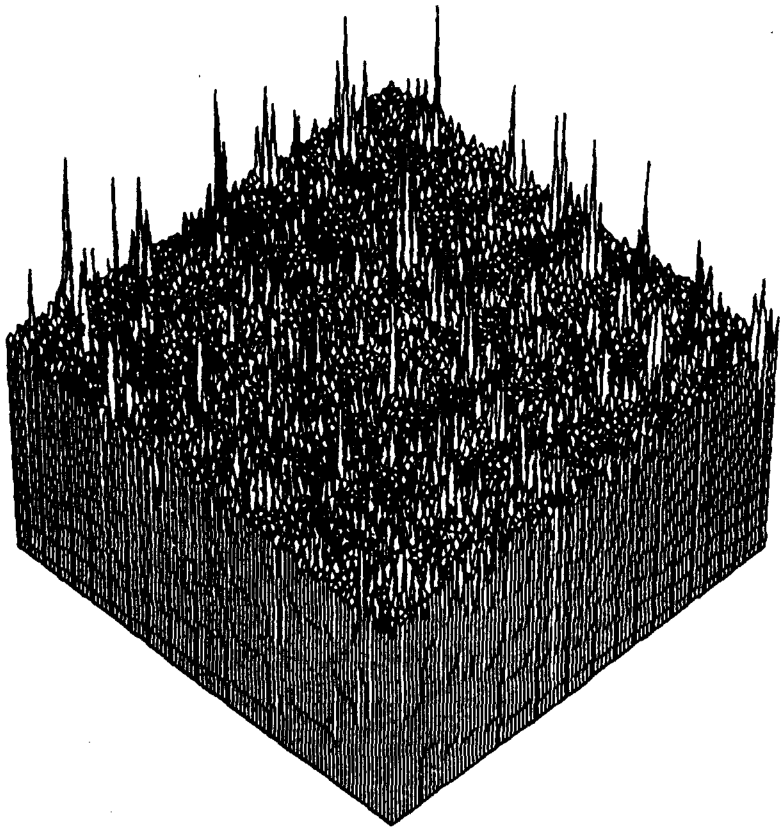

$$\frac{\partial^2 T}{\partial x \partial y} + V$$

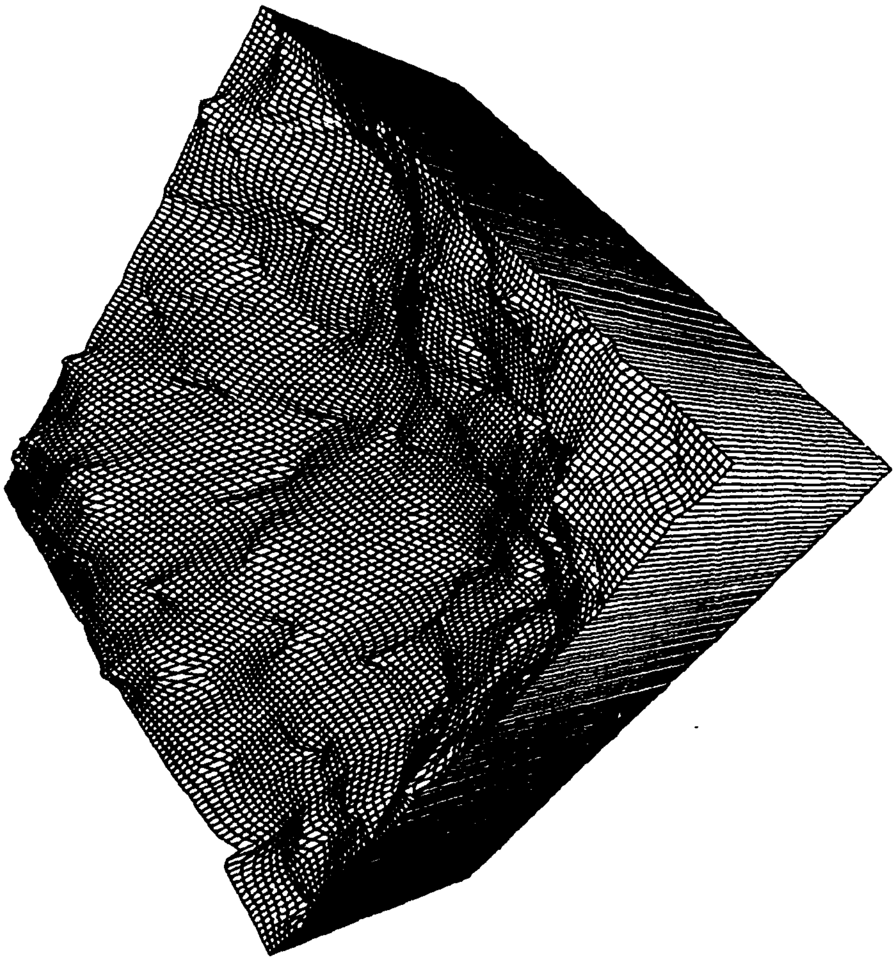

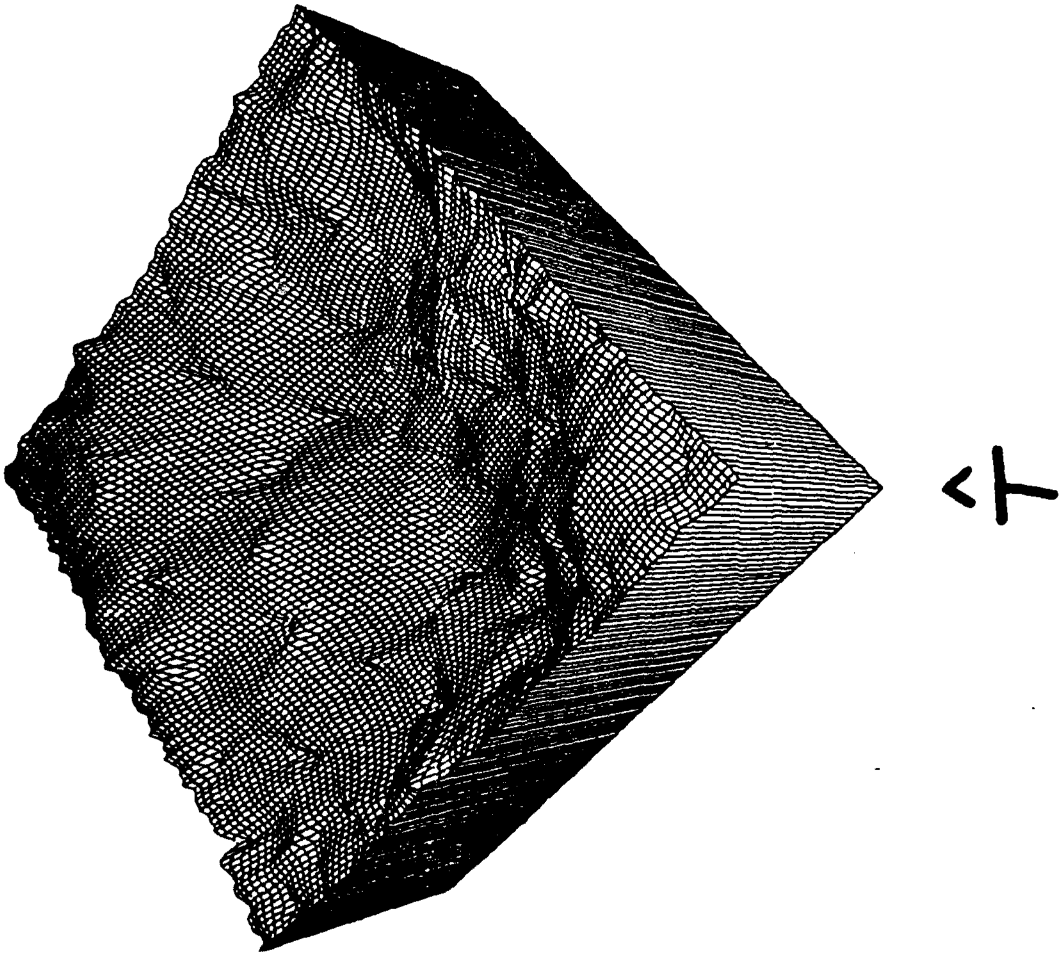

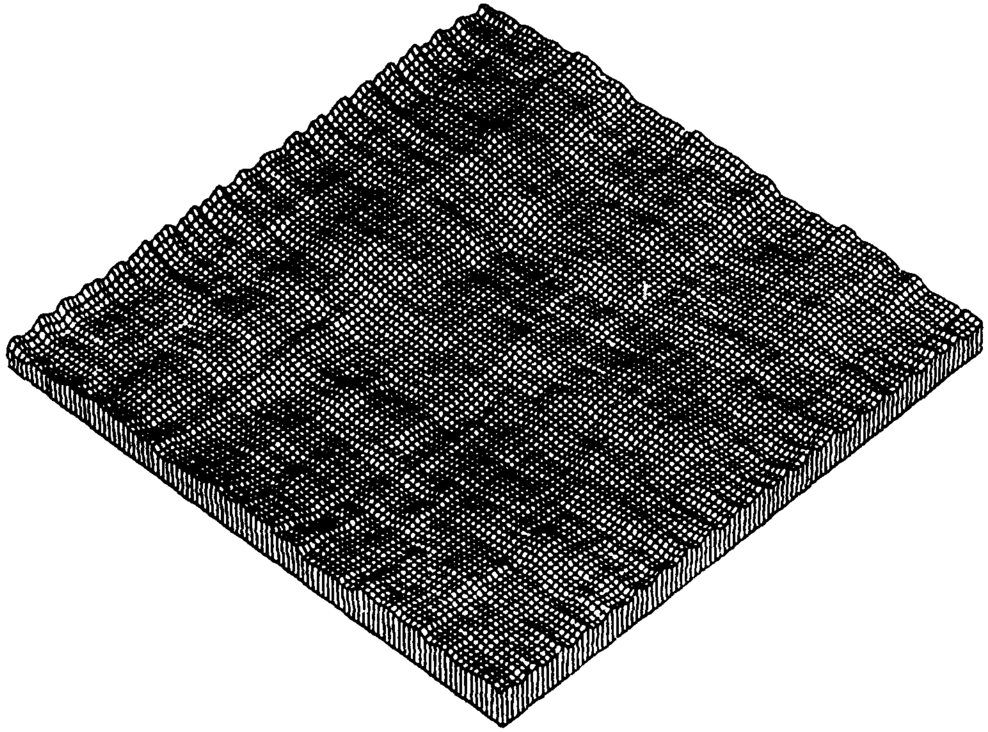

$T - \hat{T}$

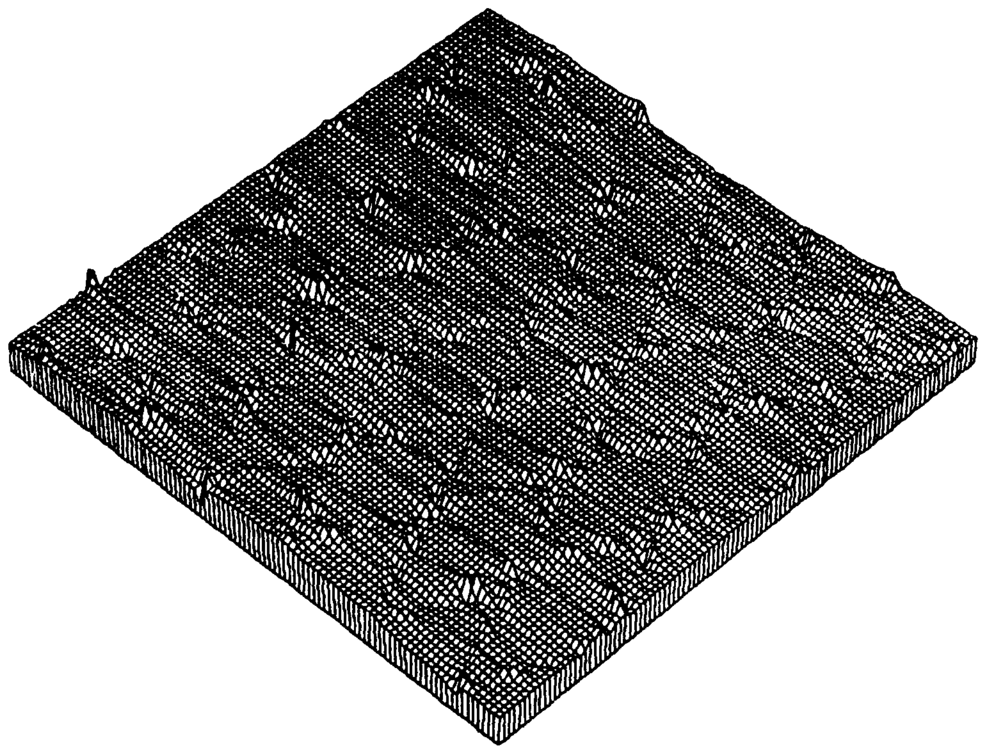

$\frac{\partial T}{\partial x}$

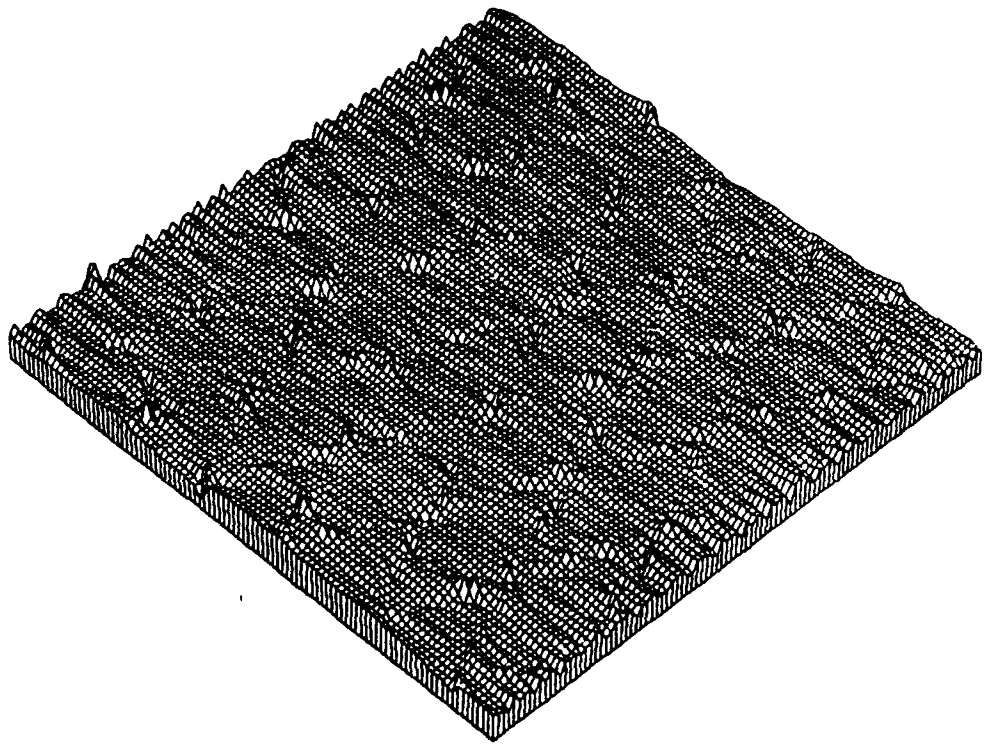

$\frac{\partial T}{\partial x}$

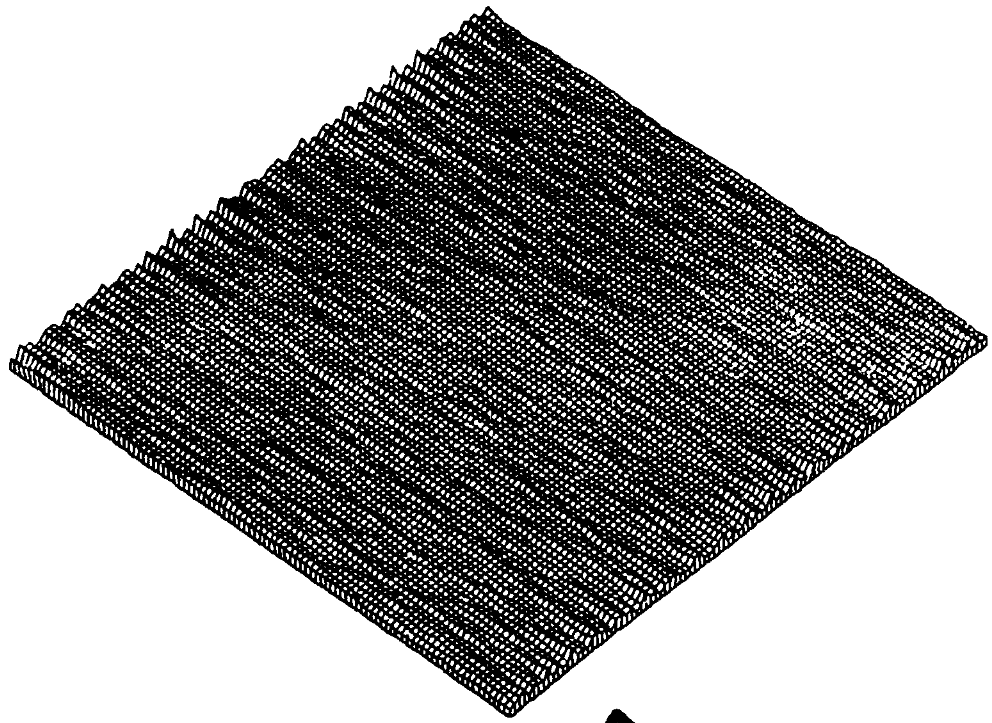

$$\frac{\partial T}{\partial x} - \widehat{\frac{\partial T}{\partial x}}$$

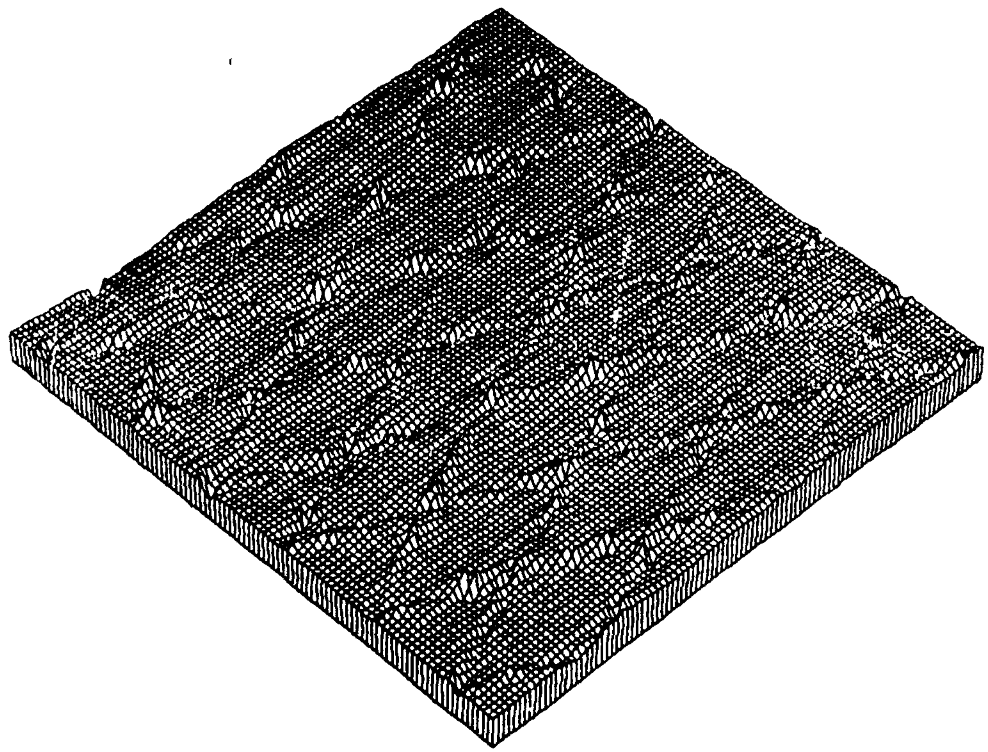

$\frac{\partial T}{\partial y}$

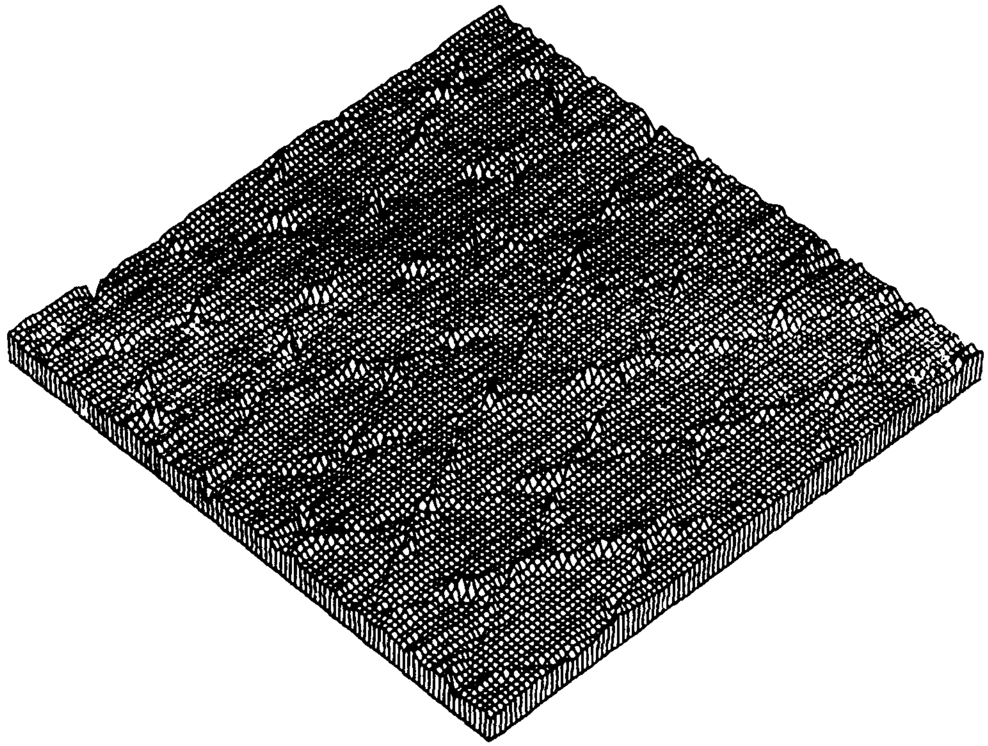

$\widehat{\frac{\partial T}{\partial y}}$

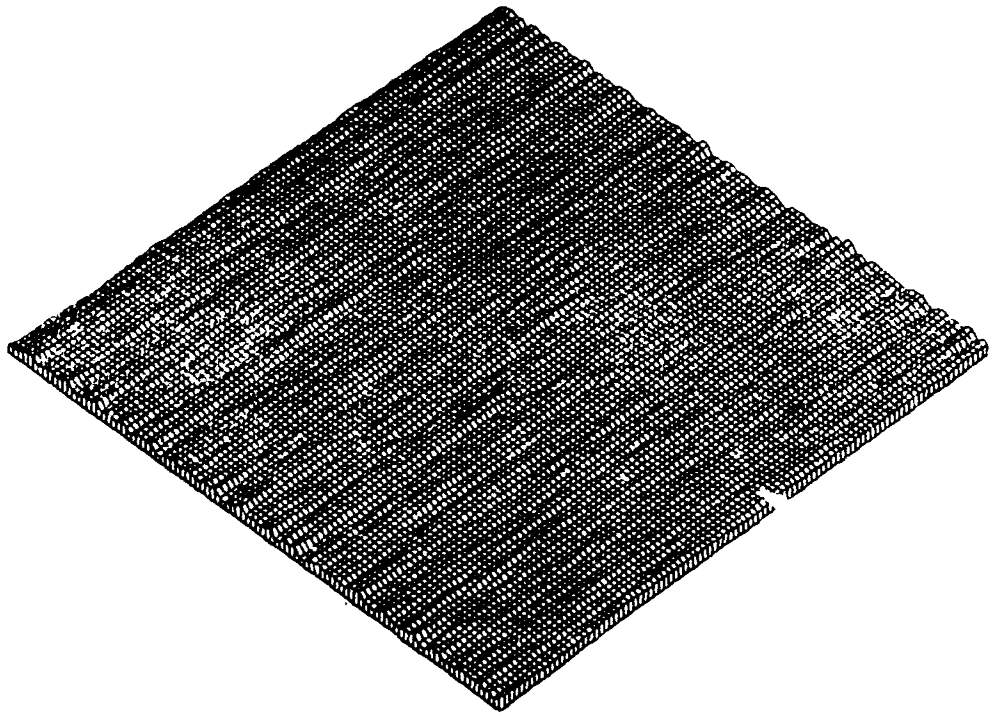

$$\frac{\partial T}{\partial y} - \frac{\partial \hat{T}}{\partial y}$$

TITLE OF PAPER: Gravity Gradiometer Data Processing Using the Karhunen-Loeve Method

SPEAKER: Sam C. Bose

QUESTIONS AND COMMENTS:

1. Question: Ted Sims

   Will the method presented accomodate data taken at differing altitudes?

   Response:

   Yes.

2. Question: Hans Baussus von Luetzow

   How do you consider gravity gradiometer red noise?

   Response:

   Red noise and white noise effects are integrated in one error variance.

3. Question. Anthony R. Barringer

   I am not clear on your survey pattern of flying. Do you have a viewgraph?

   Response:

   No. My analysis is based on an orthogonal grid.

NUMERICALLY DERIVING THE KERNELS OF AN INTEGRAL PREDICTOR YIELDING SURFACE GRAVITY DISTURBANCE COMPONENTS FROM AIRBORNE GRADIENT DATA

by

David M. Gleason
Geodesy and Gravity Branch
Earth Sciences Division
Air Force Geophysics Laboratory
Hanscom AFB, MA 01731-5000

ABSTRACT

C. Jekeli (1986) developed an integral estimator which, when used in conjunction with a set of airborne gradient observations, yields gravity disturbance component differences between a desired collection of actual disturbance component values on the ground and a corresponding collection of least-squares collocation predicted values that are based on a small, given set of disturbance component tie point values, also on the ground, which provide needed long-wavelength gravity information. (Thus the desired actual values can be estimated by adding back the differences to the tie point-implied values). This paper shows how all 18 possible kernels of the integral estimator can be easily and accurately approximated via two dimensional discrete inverse Fourier transforms. Armed with such a set of kernel values, a few tie points and a set of airborne gradient values implied by a mass layer gravity model for northern Texas, the RMS error of a set of predicted ground disturbance components, referenced to "true" values implied by the same model, is less than 1 mgal. A flat earth approximation is employed in this exercise using (X, Y, Z) (east, north, and down) coordinates.

NUMERICALLY DERIVING THE KERNELS OF AN INTEGRAL PREDICTOR YIELDING SURFACE GRAVITY DISTURBANCE COMPONENTS FROM AIRBORNE GRADIENT DATA.

- FOR A DETAILED EXPLANATION OF THE NSWC MASS LAYER LOCAL GRAVITY MODEL FOR NORTHERN TEXAS, SEE WHITE (1984) (TASC/AFGL-TR-85-0037).

I. GETTING INITIAL LSC/TIE POINT PREDICTIONS:

IF $\underline{U}$ CONTAINS A FEW GIVEN TIE POINT DISTURBANCE COMPONENT VALUES ON THE GROUND, I.E.,

$$\underset{(N_T \text{ by } 1)}{\underline{U}} = T_J \quad (J = X, Y \text{ OR } Z)$$

WE CAN ALWAYS PREDICT A VECTOR $\underline{W}$ OF OTHER GROUND DISTURBANCE COMPONENTS VIA THE LSC EQUATION

$$\underset{(N_P \text{ BY } 1)}{\underline{W}} = [P]\,\underline{U} \qquad (1)$$

WHERE THE N_P BY N_T ESTIMATOR MATRIX

$$[P] = \underset{(N_P \text{ BY } N_T)}{[C_{\underline{WU}}]} \cdot \underset{(N_T \text{ BY } N_T)}{[[C_{\underline{UU}}] + [D]]^{-1}} \qquad (2)$$

II. ESTIMATING THE (ACTUAL-LSC) DISTURBANCE COMPONENT DIFFERENCES:

C. JEKELI (1986) SHOWS IF

(1) THE VECTOR $\underline{Y}$ CONTAINS A SET OF FAIRLY DENSE AND INFINITELY EXTENDED AIRBORNE GRADIENTS AT SOME CONSTANT ALTITUDE H ABOVE THE PLANE EARTH (THE OBSERVATIONS MAY OR MAY NOT BE REGULARLY GRIDDED)

(2) THE VECTOR $\underline{U}$ CONTAINS A FEW TIE POINT DISTURBANCE COMPONENT VALUES ON THE GROUND AT POINTS $(X_K, Y_K, 0), K=1, N_T$

(3) WE ASSUME THE GRAVITY SIGNAL TO BE STATIONARY AND THE COVARIANCES TO BE FUNCTIONS ONLY OF THE DISTANCE BETWEEN A PAIR OF POINTS (P_1, P_2)

THEN THE DIFFERENCES BETWEEN THE ACTUAL DISTURBANCE COMPONENT VALUES ON THE GROUND AND THE CORRESPONDING VALUES IMPLIED BY THE LSC PREDICTOR OF SECTION I., AT THE PREDICTION POINT $(X_0, Y_0, 0)$, CAN BE EXPRESSED AS

$$\underline{W}(X_0,Y_0,0) = \int_{-\infty}^{\infty}\int_{-\infty}^{\infty}[B(X_0-X,Y_0-Y,0)]\cdot\underline{V}(X,Y,H)dXdY \qquad (3)$$

WHERE EACH INDIVIDUAL KERNEL ELEMENT IN THE MATRIX [B] CAN BE EXPRESSED AS A SIMPLE LINEAR COMBINATION OF THE CONTINUOUS TWO-DIMENSIONAL INVERSE FOURIER TRANSFORMS OF THE SPECTRUMS

$$[\beta_1(\omega_X,\omega_Y)] = [\Phi_{\underline{WV}}(\omega_X,\omega_Y)]\cdot[\Phi_{\underline{VV}}(\omega_X,\omega_Y)]^{-1} \qquad (4)$$

AND

$$[\beta_2(\omega_X,\omega_Y)] = [\Phi_{\underline{UV}}(\omega_X,\omega_Y)]\cdot[\Phi_{\underline{VV}}(\omega_X,\omega_y)]^{-1} \qquad (5)$$

WHERE $[\Phi_{\underline{WV}}]$, $[\Phi_{\underline{UV}}]$ AND $[\Phi_{\underline{VV}}]$ CONTAIN THE (CROSS)-PSD FUNCTIONS BETWEEN THE $\underline{W}$ PREDICTED, $\underline{V}$ OBSERVED AND $\underline{U}$ TIE POINT QUANTITIES.

NOTES:

(1) EQUATION (3), VIZ.,

$$\underline{W}(X_0, Y_0, 0) = \int_{-\infty}^{\infty} \int_{-\infty}^{\infty} [B(X_0 - X, Y_0 - Y, 0)] \cdot \underline{V}(X, Y, H)\, dX dY \quad (3)$$

IS OUR INTEGRAL PREDICTOR. EACH INDIVIDUAL KERNEL ELEMENT IN [B] CAN BE THOUGHT OF AS A "WEIGHT" SINCE IT IS A FUNCTION ONLY OF THE DISTANCE BETWEEN THE PREDICTION POINT $(X_0, Y_0, 0)$ AND THE VARYING OBSERVATIION POINTS (X,Y,H=C). HENCE, ELEMENTS IN [B] ARE CIRCULARLY SYMMETRIC WRT THE ORIGIN AND MONOTONICALLY DECREASE IN MAGNITUDE AS YOU MOVE AWAY FROM THE ORIGIN.

(2) EQUATION (3) WILL BE NUMERICALLY EVALUATED, BASED ON THE FINITE LENGTH AND DISCRETE DATA SPACING OF THE OBSERVATIONAL GRADIENT SURVEY AREA.

(3) THE (CROSS)-PSD MATRICES IN EQUATIONS (4)-(5), VIZ.,

$$[\beta_1(\omega_X,\omega_Y)] = [\Phi_{\underline{WY}}(\omega_X,\omega_Y)]\cdot[\Phi_{\underline{YY}}(\omega_X,\omega_Y)]^{-1} \tag{4}$$

AND

$$[\beta_2(\omega_X,\omega_Y)] = [\Phi_{\underline{UY}}(\omega_X,\omega_Y)]\cdot[\Phi_{\underline{YY}}(\omega_X,\omega_Y)]^{-1} \tag{5}$$

WILL BE EXPRESSED IN TERMS OF

1) THE FREQUENCY DOMAIN TRANSFER FUNCTIONS WHICH LINK THE DISTURBING POTENTIAL ON THE GROUND, T_0, TO THE GROUND COMPONENTS IN $\underline{W}$ AND $\underline{U}$ AND TO THE AIRBORNE GRADIENTS IN $\underline{Y}$,

2) THE PSD FUNCTION OF T_0, $\Phi_{T0,T0}(\omega_X,\omega_Y)$, WHICH WE'LL ASSUME TO BE ISOTROPIC, I.E., $\Phi_{T0,T0} = \Phi_{T0,T0}(\omega)$, AND IS BASED ON THE DEFINING PARAMETERS OF THE LOCAL GRAVITY MODEL USED AND

3) THE PSD OF THE WHITE NOISE IN THE GRADIENT OBSERVATIONS GIVEN BY

$$\eta = [4E^2/(9/25KM^2)] = 1.11X10^{-11}S^{-4}/(CY/M)^2$$

THE NINE TRANSFER FUNCTIONS THAT ARE APPLICABLE TO THIS STUDY ARE:

QUANTITY (AT HEIGHT h):	F.D. TRANSFER FUNCTION LINKING THE QUANTITY TO T_0:
T_X	$i\omega_x e^{-\omega h}$
T_Y	$i\omega_y e^{-\omega h}$
T_Z	$-\omega e^{-\omega h}$
T_{XX}	$-\omega_x{}^2 e^{-\omega h}$
T_{XY}	$-\omega_x \omega_y e^{-\omega h}$
T_{XZ}	$-i\omega\omega_x e^{-\omega h}$
T_{YY}	$-\omega_y{}^2 e^{-\omega h}$
T_{YZ}	$-i\omega\omega_y e^{-\omega h}$
T_{ZZ}	$\omega^2 e^{-\omega h}$

WHERE $\omega = (\omega_X{}^2 + \omega_Y{}^2)^{1/2}$.

SUPPOSE WE WANTED TO PREDICT $\underline{W}(X_0,Y_0) = (T_X,T_Y,T_Z)$ AT EACH OF THE GGSS GROUND GRID POINTS, USING ALL 6 GRADIENT OBSERVATIONS AT EACH OF THE AIRBORNE GRID POINTS, I.E., $\underline{V}(X,Y,H) = (T_{XX},T_{XY},T_{XZ},T_{YY},T_{YZ},T_{ZZ})$. THEN $[\beta_1(\omega_X,\omega_Y)]$ WILL BE THE 3 BY 6 MATRIX HAVING THE STRUCTURE

$$\begin{bmatrix}
\overset{(X,XX)}{\dfrac{-i\omega_X^{3}N}{D}} & \overset{(X,XY)}{\dfrac{-i\omega_X^{2}\omega_Y N}{D}} & \overset{(X,XZ)}{\dfrac{-\omega\omega_X^{2}N}{D}} & \overset{(X,YY)}{\dfrac{-i\omega_X\omega_Y^{2}N}{D}} & \overset{(X,YZ)}{\dfrac{-\omega\omega_X\omega_Y N}{D}} & \overset{(X,ZZ)}{\dfrac{i\omega^{2}\omega_X N}{D}} \\
\overset{(Y,XX)}{\dfrac{-i\omega_X^{2}\omega_Y N}{D}} & \overset{(Y,XY)}{\dfrac{-i\omega_X\omega_Y^{2}N}{D}} & \overset{(Y,XZ)}{\dfrac{-\omega\omega_X\omega_Y N}{D}} & \overset{(Y,YY)}{\dfrac{-i\omega_Y^{3}N}{D}} & \overset{(Y,YZ)}{\dfrac{-\omega\omega_Y^{2}N}{D}} & \overset{(Y,ZZ)}{\dfrac{i\omega^{2}\omega_Y N}{D}} \\
\overset{(Z,XX)}{\dfrac{\omega\omega_X^{2}N}{D}} & \overset{(Z,XY)}{\dfrac{\omega\omega_X\omega_Y N}{D}} & \overset{(Z,XZ)}{\dfrac{-i\omega^{2}\omega_X N}{D}} & \overset{(Z,YY)}{\dfrac{\omega\omega_Y^{2}N}{D}} & \overset{(Z,YZ)}{\dfrac{-i\omega^{2}\omega_Y N}{D}} & \overset{(Z,ZZ)}{\dfrac{-\omega^{3}N}{D}}
\end{bmatrix}$$

WHERE $N = e^{-\omega h}\,\Phi_{T0,T0}(\omega)$ (6)

AND $D = \eta + e^{-2\omega h}\,\Phi_{T0,T0}(\omega)\,(3\omega^4 - \omega_X^2\omega_Y^2)$. (7)

$$
\begin{bmatrix}
\overset{(X,XX)}{\dfrac{-i\omega_X^{3}N}{D}} & \overset{(X,XY)}{\dfrac{-i\omega_X^{2}\omega_Y N}{D}} & \overset{(X,XZ)}{\dfrac{-\omega\omega_X^{2}N}{D}} & \overset{(X,YY)}{\dfrac{-i\omega_X\omega_Y^{2}N}{D}} & \overset{(X,YZ)}{\dfrac{-\omega\omega_X\omega_Y N}{D}} & \overset{(X,ZZ)}{\dfrac{i\omega^{2}\omega_X N}{D}} \\
\overset{(Y,XX)}{\dfrac{-i\omega_X^{2}\omega_Y N}{D}} & \overset{(Y,XY)}{\dfrac{-i\omega_X\omega_Y^{2}N}{D}} & \overset{(Y,XZ)}{\dfrac{-\omega\omega_X\omega_Y N}{D}} & \overset{(Y,YY)}{\dfrac{-i\omega_Y^{3}N}{D}} & \overset{(Y,YZ)}{\dfrac{-\omega\omega_Y^{2}N}{D}} & \overset{(Y,ZZ)}{\dfrac{i\omega^{2}\omega_Y N}{D}} \\
\overset{(Z,XX)}{\dfrac{\omega\omega_X^{2}N}{D}} & \overset{(Z,XY)}{\dfrac{\omega\omega_X\omega_Y N}{D}} & \overset{(Z,XZ)}{\dfrac{-i\omega^{2}\omega_X N}{D}} & \overset{(Z,YY)}{\dfrac{\omega\omega_Y^{2}N}{D}} & \overset{(Z,YZ)}{\dfrac{-i\omega^{2}\omega_Y N}{D}} & \overset{(Z,ZZ)}{\dfrac{-\omega^{3}N}{D}}
\end{bmatrix}
$$

WHERE $N = e^{-\omega h}\,\Phi_{TO,TO}(\omega)$ (6)

AND $D = \eta + e^{-2\omega h}\,\Phi_{TO,TO}(\omega)\,(3\omega^{4} - \omega_X^{2}\omega_Y^{2})$. (7)

<u>NOTES:</u>

(1) ONLY 7 OF THE 18 SPECTRUMS HAVE TO BE SUBJECTED TO A 2D IFT PROCESS (THE REST ARE DIRECTLY ATTAINABLE FROM THE 7).

(2) DUE TO THE MAKE-UP OF THE DENOMINATOR , D, NONE OF THE 18 SPECTRUMS ARE ISOTROPIC WHICH MEANS THE 2D IFT PROCESS CAN <u>NOT</u> BE SIMPLIFIED INTO A 1D HANKEL PROCESS.

(3) THE STRUCTURE OF THE SPECTRAL MATRIX $[\beta_2(\omega_X,\omega_Y)]$ WILL BE A SUBSET OF THE ABOVE $[\beta_1]$.

C. JEKELI (1986) SHOWS THAT IF

$\underline{V} = (T_{XZ}, T_{YZ}, T_{ZZ})$ AT EACH AIRBORNE SURVEY POINT AND

$\underline{W} = T_Z$ AT EACH GROUND SURVEY POINT

THEN EACH ELEMENT IN THE RESULTING 1 BY 3 SPECTRAL MATRIX $[\beta_1]$ WILL HAVE THE <u>ISOTROPIC</u> DENOMINATOR OF

$$D = \eta + 2\omega^4 e^{-2\omega h} \Phi_{T0,T0}(\omega) \qquad (8)$$

AND THE 2D IFT PROCESS ON $[\beta_1]$ AND $[\beta_2]$ <u>CAN</u> BE SIMPLIFIED TO A 1D HANKEL PROCESS IN TERMS OF THE J_0 AND J_1 BESSEL <u>FUNCTIONS OF THE FIRST KIND.</u>

SIMILARLY, IF $\underline{V} = (T_{XZ}, T_{YZ}, T_{ZZ})$ AND $\underline{W} = (T_X, T_Y, T_Z)$ THEN THE 2D IFT PROCESS ON THE RESULTING 3 BY 3 $[\beta_1]$ AND $[\beta_2]$ MATRICES <u>CAN</u> BE SIMPLIFIED TO A 1D HANKEL PROCESS IN TERMS <u>OF THE J_0, J_1 AND J_2 BESSEL FUNCTIONS.</u>

<u>NOTES:</u>

(1) THE ALGEBRAIC MANIPULATIONS YIELDING THE 1D INVERSE HANKEL TRANSFORMS ARE VERY METICULOUS.

(2) CHRIS NUMERICALLY EVALUATED THE INVERSE HANKEL PROCESS VIA SERIES EXPANSIONS GIVING A POSSIBLE $\sigma=10\%$.

TO OBTAIN N EQUALLY SPACED B(X,Y) VALUES ALONG EACH HORIZONTAL PROFILE (ΔX = INCREMENT) AND M EQUALLY SPACED B(X,Y) VALUES ALONG EACH VERTICAL PROFILE (ΔY = INCREMENT) WE CAN RELATE THE l^{th} ANGULAR FREQUENCIES TO THE INTEGER FREQUENCY COUNTERS l_X AND l_Y VIA

$$\omega_{X_l} = \frac{2\pi \cdot l_X}{N\Delta X} \quad \text{RADIANS/METER} \quad \text{AND}$$

$$\omega_{Y_l} = \frac{2\pi \cdot l_Y}{M\Delta Y} \quad \text{RADIANS/METER}$$

(15)

AND THEN THE DISCRETE INVERSE FOURIER TRANSFORM CAN BE APPROXIMATED BY

$$B(n\Delta X, m\Delta Y) = \frac{1}{MN\Delta X\Delta Y} \sum_{l_Y=\frac{-M}{2}}^{\frac{M}{2}} \sum_{l_X=\frac{-N}{2}}^{\frac{N}{2}} \beta(\omega_{X_l}, \omega_{Y_l}) e^{2\pi i\left(\frac{l_X n}{N} + \frac{l_Y m}{M}\right)}$$

(16).

NOTES WRT EQUATION (16) VIZ.,

$$B(n\Delta X, m\Delta Y) = \frac{1}{MN\Delta X\Delta Y} \sum_{l_Y=\frac{-M}{2}}^{\frac{M}{2}} \sum_{l_X=\frac{-N}{2}}^{\frac{N}{2}} \beta(\omega_{X_l}, \omega_{Y_l}) e^{2\pi i\left(\frac{l_X n}{N} + \frac{l_Y m}{M}\right)} \qquad (16).$$

(1) CLEARLY THE B ESTIMATES OF (16) APPROACH THE DESIRED CONTINUOUS IFT VALUES AS $(M,N) \Rightarrow \pm\infty$ AND AS $(\Delta X, \Delta Y) \Rightarrow 0$.

(2) THE IMSL "CANNED" SUBROUTINE FFT3D CAN COMPUTE 2D DISCRETE INVERSE FOURIER TRANSFORMS BY COMPUTING SUMS OF THE FORM

$$X(I+1, J+1) = \sum_{P=0}^{M-1} \sum_{L=0}^{N-1} A(L+1, P+1) e^{2\pi i\left(\frac{IL}{N} + \frac{JP}{M}\right)} \qquad (17)$$

(3) THE "2 SIDED" SUMS OF (16) CAN BE MADE AMENABLE TO THE IMSL "1 SIDED" SUMS BY PROPER SHIFTING OF THE SUMMATION OPERATORS.

(4) FFT3D REQUIRES THE USE OF THE 2D MATRIX [A] IN (17) WHICH CAUSES STORAGE PROBLEMS EVEN IF VIRTUAL MEMORY IS INVOKED. THE DOUBLE SUM OF (17) CAN BE WRITTEN AS

$$X(I+1,J+1)=\sum_{L=0}^{N-1} G(L+1,J+1)e^{2\pi iIL/N} \tag{18}$$

WHERE

$$G(L+1,J+1)=\sum_{P=0}^{M-1} A(L+1,P+1)e^{2\pi iJP/M} \tag{19}$$

(5) ONE CAN A) TRANSFORM ALL OF THE VERTICAL PROFILES VIA (19), B) ASSIGN INTEGER TAG NUMBERS ONLY TO THOSE RETURNING TRANSFORMED COMPLEX NUMBERS WHICH CORRESPOND TO THE HORIZONTAL PROFILES OF THE GGSS SURVEY GRID, C) SORT THE TAGGED NUMBERS, AND THEN D) TRANSFORM THE HORIZONTAL PROFILES VIA (18).

(6) DUE TO THE RADIAL SYMMETRY OF THE DESIRED WEIGHT MATRIX [B], ONLY ONE GGSS QUADRANT OF [B] VALUES ARE NEEDED.

(7) WITH THE EXCEPTION OF THE SENSITIVE $B_{Z,ZZ}$ KERNEL, THE DOMINANT KERNEL VALUES NEAR THE ORIGIN BEGIN TO CONVERGE WITH "EFFICIENT" CHOICES OF N,M,ΔX AND ΔY.

NUMERICAL RESULTS

SCENARIO:

(1) $\underline{V}$ CONTAINS (T_{XZ},T_{YZ},T_{ZZ}) SIMULATED GRADIENTS AT ALL NODES OF THE GGSS AIRBORNE GRID AT ALTITUDE OF H = 600M.

(2) $\underline{W}$ CONTAINS PREDICTED T_Z COMPONENTS ALONG THE 5 N-S TRACKS OF X = -10,-5,0,5,10 KMS., SPACED EVERY 5 KMS. FOR ALL Y ε (-100 KM, 100 KM) (205 = 5(41) TOTAL PREDICTIONS)

(3) $\underline{U}$ CONTAINS SIMULATED T_Z GROUND TIE POINT VALUES AS FOLLOWS:

CASE I: 2 TIE POINTS AT (0,-100) AND (0,100)
CASE II: 3 TIE POINTS AT (0,-100),(0,0) AND (0,100)
CASE III: 4 TIE POINTS AT (-100,-100),(-100,100),(100,-100) AND (100,100)

CASE	MAX ABS ERROR		MEAN ERROR		RMS ERROR	
	HANKEL	2D DISCR.	HANKEL	2D DISCR.	HANKEL	2D DISCR.
I.	3.40	3.18	0.98	0.89	1.39	1.33
II.	2.54	2.26	-0.65	-0.47	1.17	0.91
III.	3.71	3.51	1.13	0.99	1.49	1.36

CONCLUDING PROS, INCONVENIENCES AND CONS:

PROS:

(1) CHRIS' METHOD OF REDUCING THE AIRBORNE GRADIENTS IS QUITE CAPABLE OF HANDLING GGSS-SIZED SURVEYS.

(2) THE 2D DISCRETE INVERSE FOURIER TRANSFORM APPROACH OF EVALUATING THE KERNELS ALLOWS ALL 6 GRADIENT OBSERVATIONS TO PLAY A ROLE IN THE REDUCTION PROCESS.

(3) ASSUMING A LOCAL $\Phi_{TO,TO}$ PSD MODEL IS AVAILABLE, THE PRE-DATA REDUCTION TASK OF EVALUATING THE KERNELS CAN EASILY BE DONE.

(4) NEITHER THE PREDICTION POINTS, OBSERVATION POINTS NOR TIE POINTS NEED TO BE REGULARLY GRIDDED.

INCONVENIENCES:

(1) FOR N = M = 5,056 AND $\Delta X = \Delta Y$ = 500 METERS, EACH 2D DISCRETE IFT PROCESS WOULD TAKE ABOUT 2 HOURS OF CPU TIME ON CDC/CYBER. (THUS FOR EACH SURVEY AREA, THE 7 NEEDED IFTs WOULD TAKE AROUND 14 HOURS.)

(2)TO RIGOROUSLY DETERMINE ERROR ESTIMATES OF THE PREDICTED SURFACE DISTURBANCE COMPONENTS REQUIRES

$$[E_{\underline{WW}}] = [C_{\underline{WW}}] - 2[[A_1] \quad [A_2]] \cdot \begin{bmatrix} [C_{\underline{YW}}] \\ [C_{\underline{UW}}] \end{bmatrix}$$

$$+ [[A_1] \quad [A_2]] \cdot \begin{bmatrix} [C_{\underline{YY}} + D_{\underline{Y}}] & [C_{\underline{YU}}] \\ [C_{\underline{UY}}] & [C_{\underline{UU}} + D_{\underline{U}}] \end{bmatrix} \cdot \begin{bmatrix} [A_1] \\ [A_2] \end{bmatrix}$$

WHERE $[A_1] = [B]\Delta X \Delta Y$

AND $[A_2] = [C_{\underline{WU}}][C_{\underline{UU}} + D_{\underline{U}}]^{-1} = [P]$ OF SECTION I.

<u>CONS:</u>

(1) DUE TO THE FINITE LENGTH OF THE GRADIENT OBSERVATION GRID, PREDICTIONS NEAR THE PERIMETER OF THE SURVEY AREA WILL BE LESS ACCURATE. (CORNER TIE POINTS CAN HELP).

(2) A $\Phi_{TO,TO}$ LOCAL PSD MODEL MUST BE DEVELOPED FOR EACH SURVEY AREA.

(3) ALL AIRBORNE OBSERVATIONS MUST BE MADE AT THE SAME HEIGHT.

STAGE II SIMULATION RESULTS USING THE NSWC SYNTHETIC GRAVITY FIELD

by

Dr. W. John Hutcheson
Bell Aerospace Textron
P.O. Box One
Buffalo, NY 14240

ABSTRACT

The GGSS data reduction can naturally be broken down into two stages. Stage I, characterized as being high frequency and temporal, consists of deterministic compensations, demodulation and associated filtering. Stage II processing is spatial and therefore two dimensional in nature and consists of synchronous sampling of the gradients passed from the Stage I software, gridding, terrain corrections, integration, track-crossing adjustments, astrogeodetic tie point adjustment, downward continuation and two dimensional smoothing.

This paper contains an overview of the Stage II algorithms and a brief description of the salient operations involved. The main results presented here are from a simulation study where the NSWC synthetic field was used to drive the Stage II software. The effects of algorithm error, gradiometer noise and different tie point configurations are demonstrated.

MOVING BASE GRAVITY GRADIOMETER REVIEW

Stage II Simulation Results Using The NSWC Synthetic Gravity Field

AIR FORCE ACADEMY

Report No. 6501-927173 ● FEBRUARY 11/12, 1987

Bell Aerospace TEXTRON
Division of Textron Inc.

Stage II Simulation Results
Using The NSWC Synthetic Gravity Field

- GGSS DATA PROCESSING OVERVIEW
- STAGE II DATA PROCESSING
  - TRACK CROSSING ADJUSTMENT
  - INTEGRATION AND GRIDDING
  - ASTRO DATA ADJUSTMENT
  - TRUTH DATA COMPARISON
  - INTERPOLATION/SMOOTHING
- SIMULATION RESULTS USING NSWC SYNTHETIC FIELD

Phase II Testing Geometry

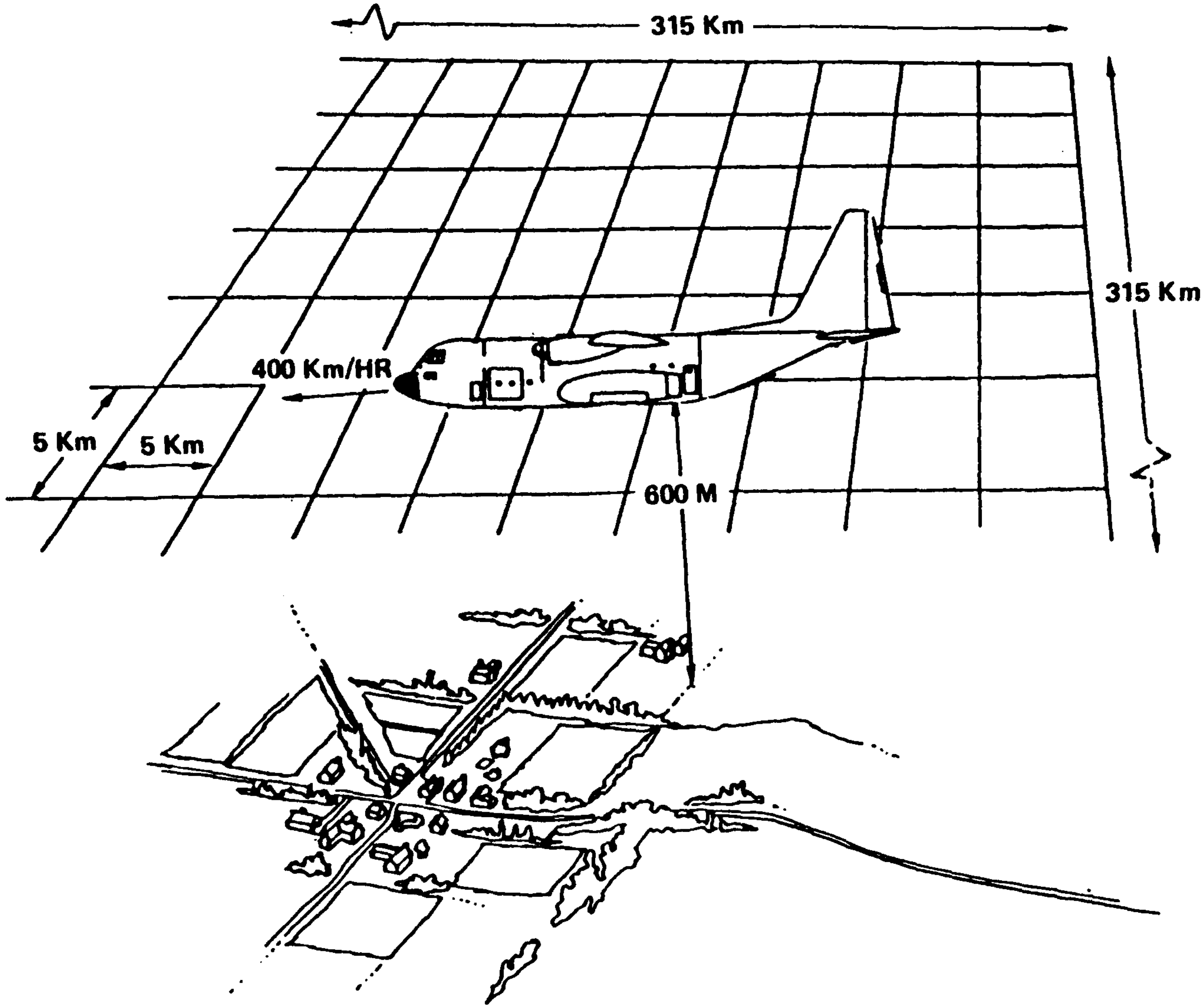

GGSS Data Processing Overview

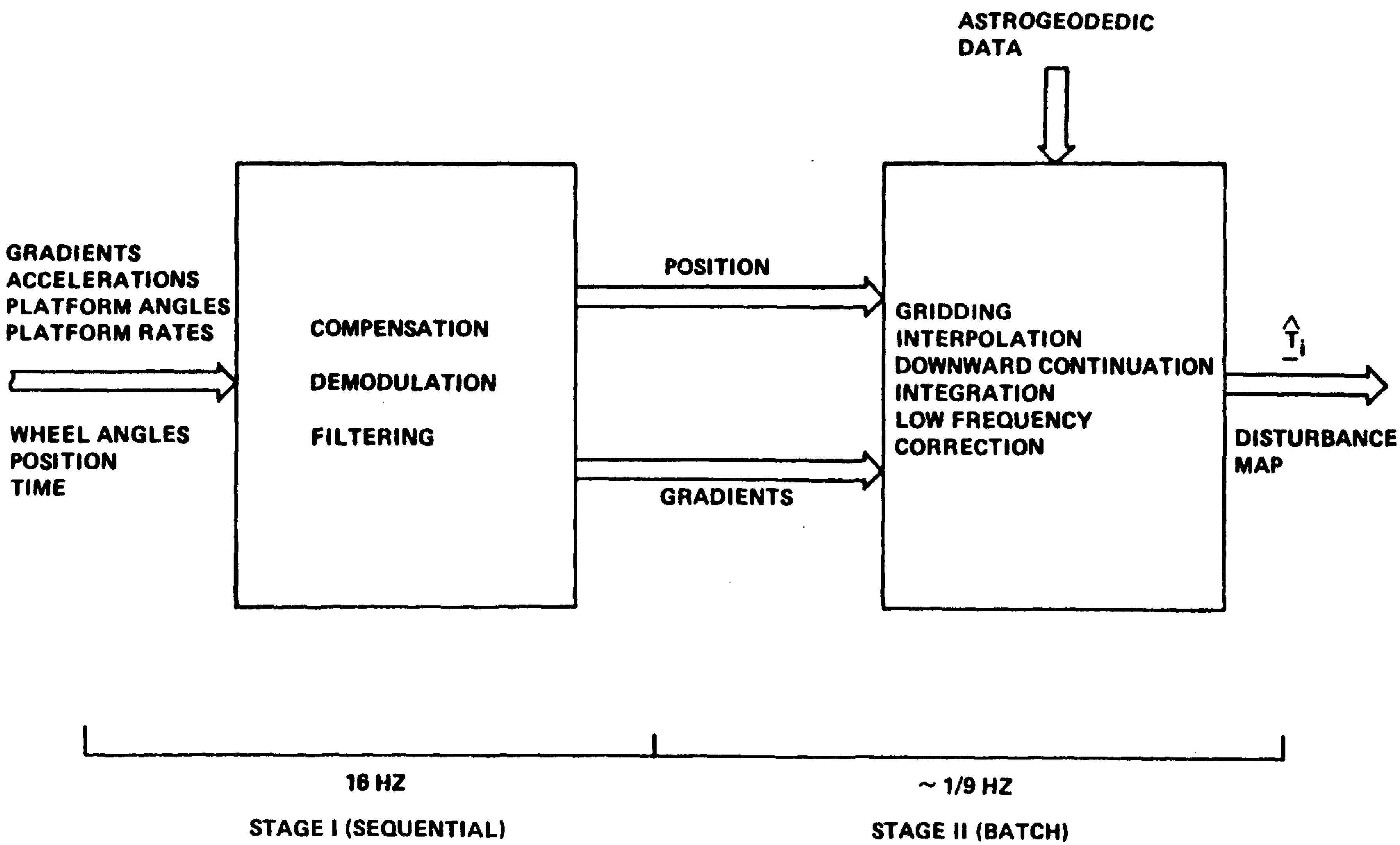

Bell Aerospace TEXTRON

Airborne Gradiometer Survey
Stage II Data Reduction

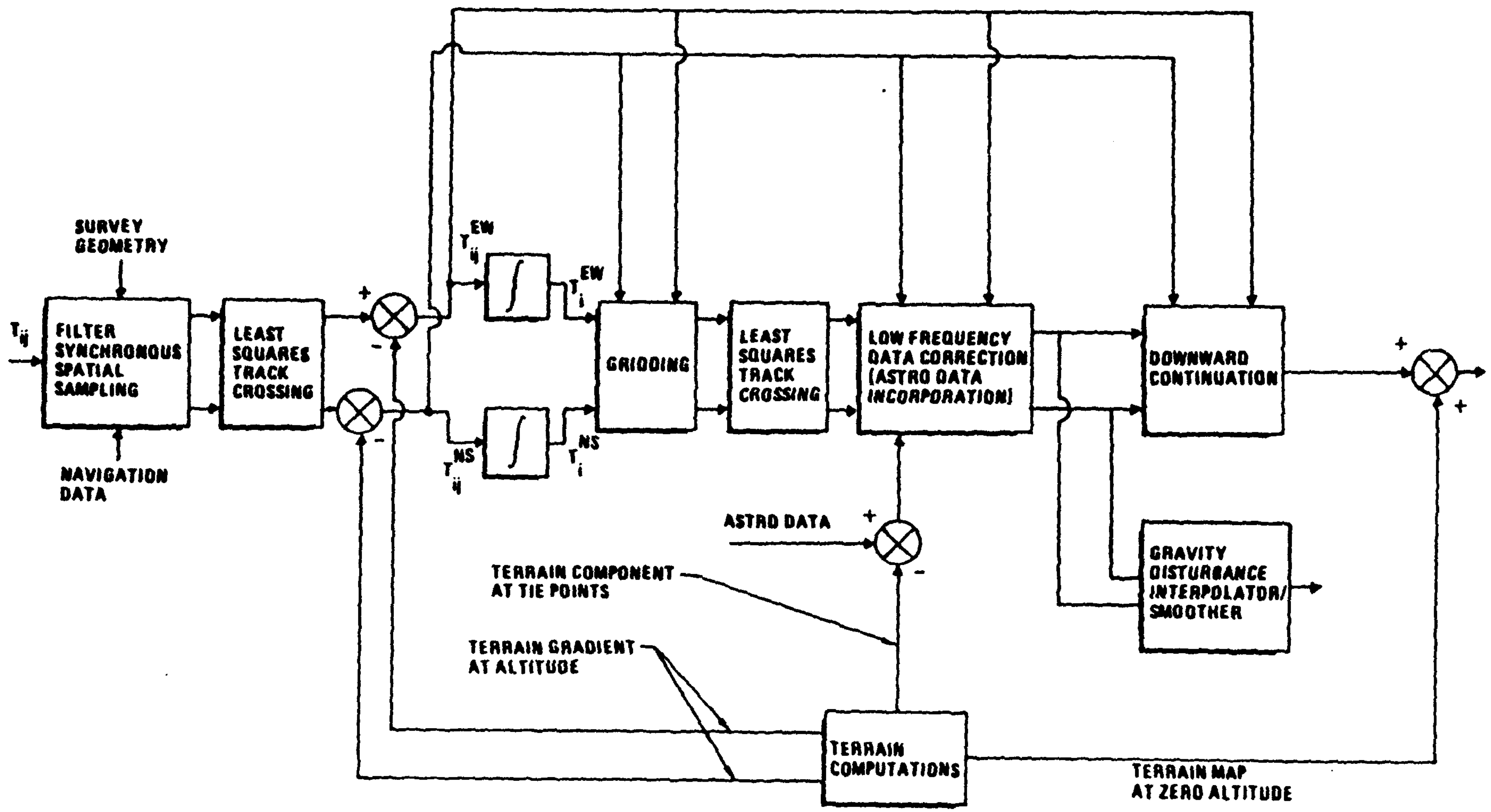

Bell Aerospace TEXTRON

Track Crossing Adjustment

- MODEL CORRELATED NOISE AS A POLYNOMIAL
- OBSERVABLES: $Z_{ij} = \left| g_i^{EW} [(j-1)\,\delta] - g_j^{NS} [i-1]\,\delta] \right| \quad \begin{matrix} i = 1,64 \\ j = 1,64 \end{matrix}$
- NUMBER OF UNKNOWNS = (ORDER OF POLYNOMIAL + 1) X 64 X 2
- PROBLEM IS UNDERDETERMINED
- RESULTING ERROR CURVE IS 2-DIMENSIONAL POLYNOMIAL THE SAME ORDER AS THAT FITTED TO THE NOISE.

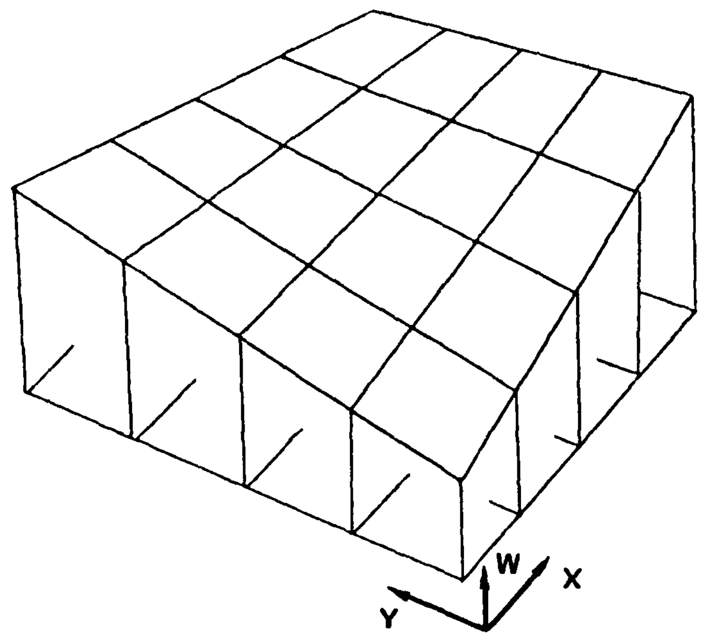

Ex. $W = a + bx + cy + dxy$

Suitability Of Represenatation Of Integrated Noise Realization By Polynominal

INVESTIGATION METHOD: SIMULATE GGI NOISE ALONG 315 Km TRACK, PASS THROUGH LSC OPTIMAL INTEGRATOR AND FIT A RAMP, QUADRATIC AND A CUBIC.

NOMINAL NOISE MODEL $S(\omega) = \frac{10^{-5}}{\omega^2} + 50\ E^2/RAD/S$

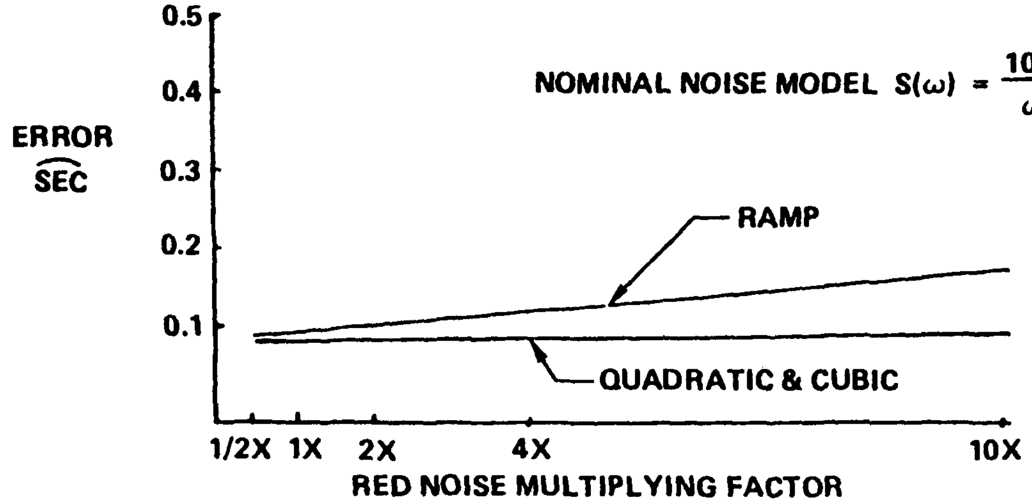

EFFECT OF RED NOISE

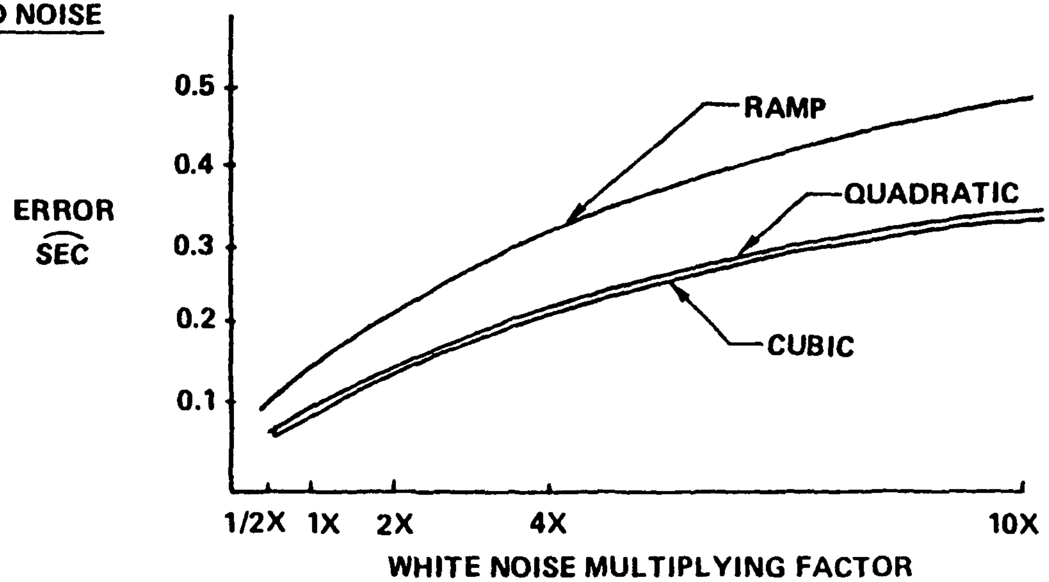

EFFECT OF WHITE NOISE

Integration And Gridding

1) RESOLVE T_{ij}^{NED} INTO COORDINATE SET ALIGNED ALONG AIRCRAFT PATH, T_{ij}^{P}

VIZ $T_{ij}^{P} = C_{NED}^{P}\ T_{ij}^{NED}\ C_{p}^{NED}$

2) INTEGRATE ALONG PATH USING OPTIMAL LSC $T_{i}^{P} = \sum_{K=1}^{256} T_{ij}^{P}(k)\ \delta_k$

3) RESOLVE T_{i}^{P} BACK TO NED, $T_{i}^{NED} = C_{p}^{NED}\ T_{i}^{P}$

4) CONTRACT T_{i}^{NED} ONTO TRACK GRID USING GRADIENTS, VIZ $\overline{T}_{i}^{NED} = N_{i}^{NED} + N_{ij}^{NED} \cdot \underline{\delta}$

5) RESOLVE DISTURBANCE VECTOR INTO GRID COORDINATES.

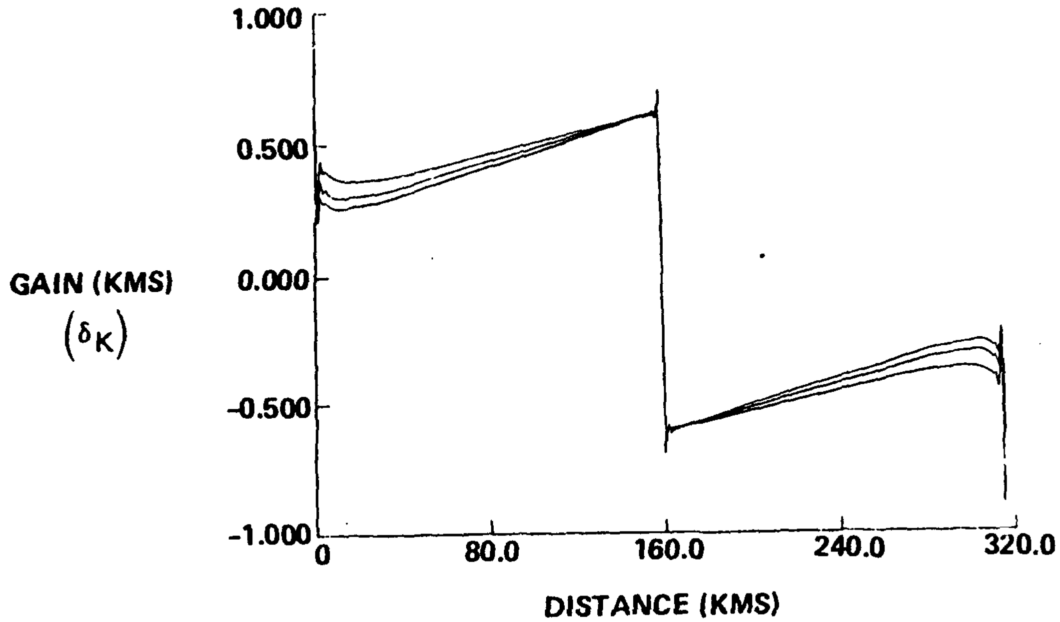

OPTIMAL LSC INTEGRATION KERNEL FOR CENTER POINT.

Tie Point Incorporation And Truth Data Comparison

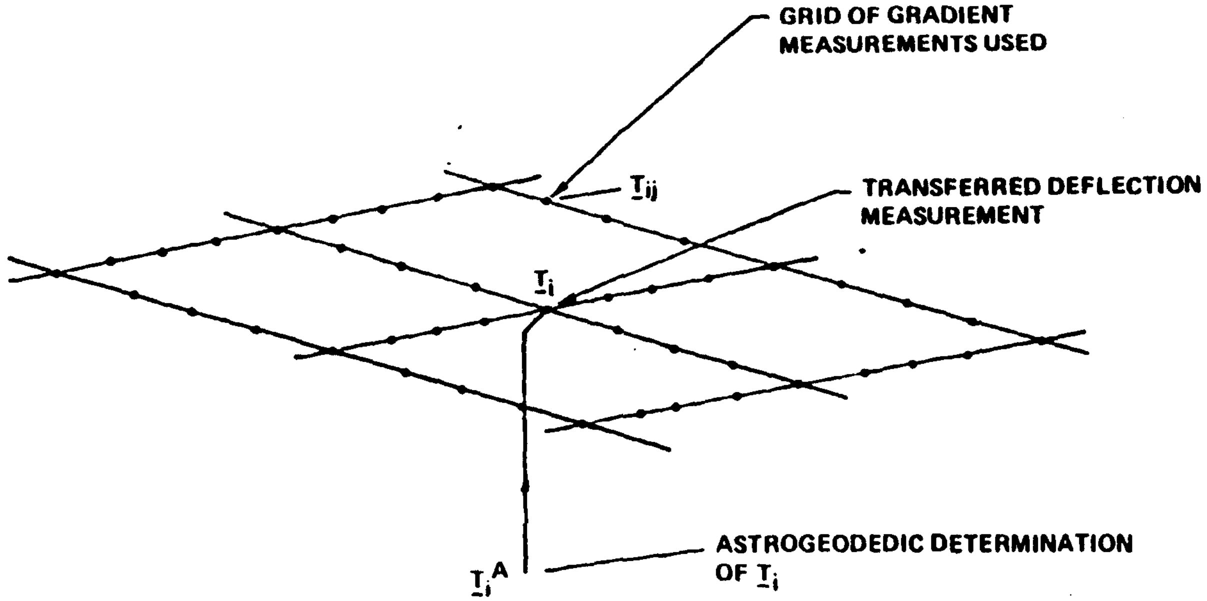

- THE APPROPRIATE GRADIENTS AT ALTITUDE LYING WITHIN A NEIGHBORHOOD OF THE TIE POINTS ARE USED TO TRANSFER THE TIE POINTS UP TO THE SURVEY ELEVATION.
- THE TRANSFERED TIE POINTS ARE SUBTRACTED FROM THE MAP VALUES AND A 2-D POLYNOMIAL SURFACE (THE SAME ORDER AS THAT USED TO MODEL THE INTEGRATED NOISE ALONG THE TRACKS) IS FITTED AND SUBTRACTED FROM THE MAP.
- THE GRADIENTS AT ALTITUDE LYING WITHIN A NEIGHBORHOOD OF THE TRUTH POINT ARE USED TO TRANSFER THE NEAREST MAP VALUE OF $\hat{T}_1$ DOWN TO THE TRUTH POINT.

Interpolation And Smoothing

APPROACH: EXPLOIT REGULAR GRID AND USE FREQUENCY DOMAIN TECHNIQUES

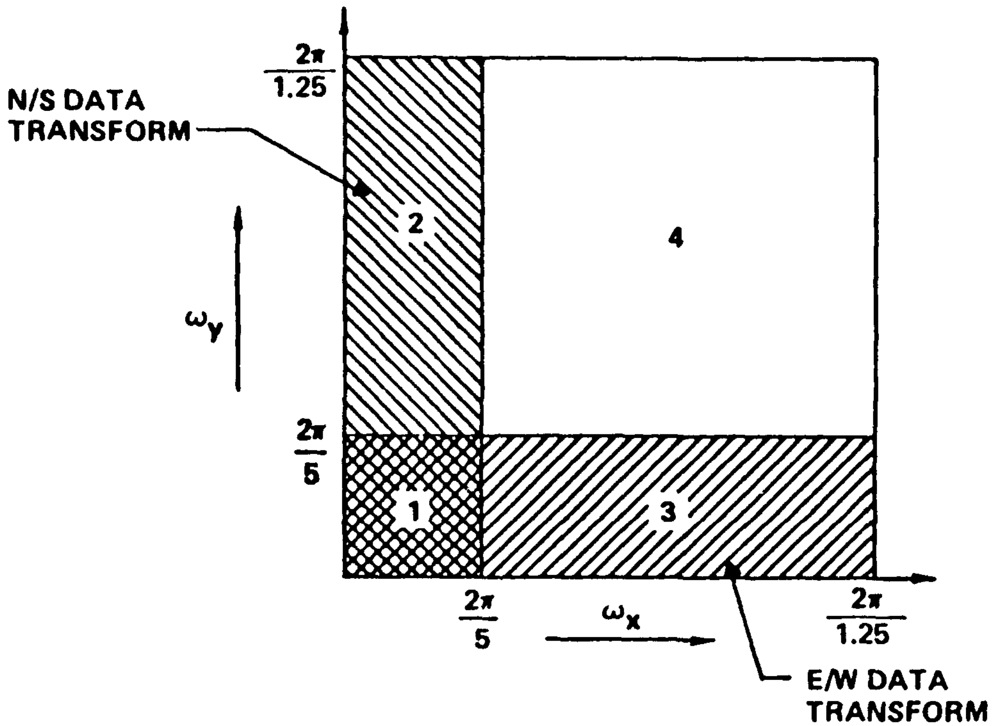

FREQUENCY DOMAIN AVERAGING

REGION 1 $T_i(\omega_x, \omega_y) = \frac{1}{2}\left[T_i^{EW}(\omega_x, \omega_y) + T_i^{NS}(\omega_x, \omega_y)\right]$

REGION 2 $T_i(\omega_x, \omega_y) = T_i^{NS}(\omega_x, \omega_y)$

REGION 3 $T_i(\omega_x, \omega_y) = T_i^{EW}(\omega_x, \omega_y)$

REGION 4 $T_i(\omega_x, \omega_y) = 0$

Bell Aerospace TEXTRON

Central Area Of NSWC Synthetic Field

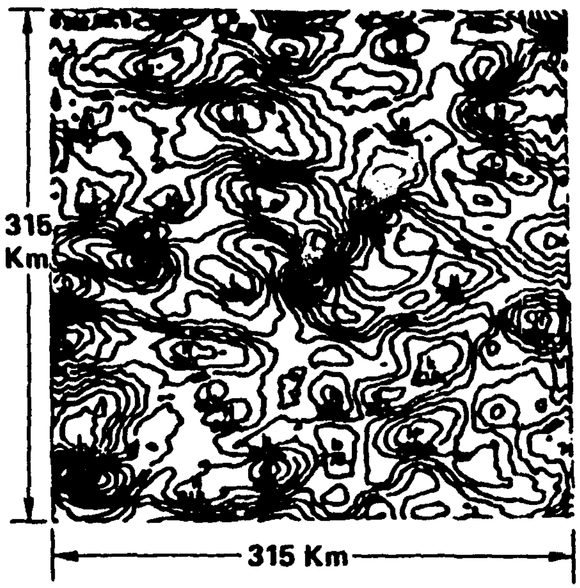

T_x

CONTOUR INTERVAL 1.4 $\widehat{SEC}$

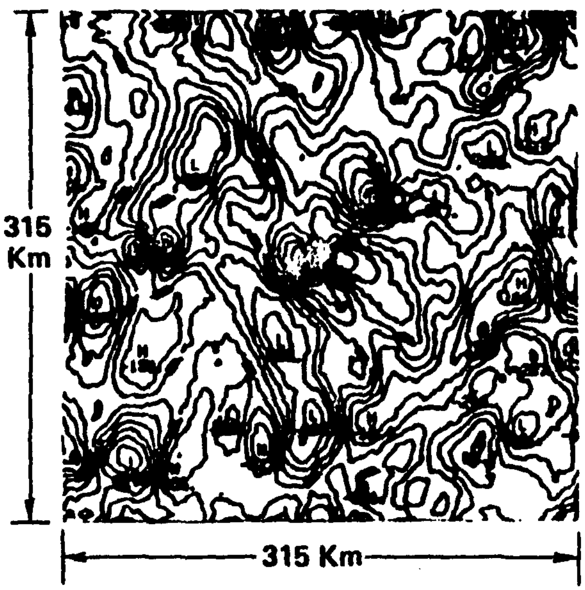

T_y

CONTOUR INTERVAL 1.4 $\widehat{SEC}$

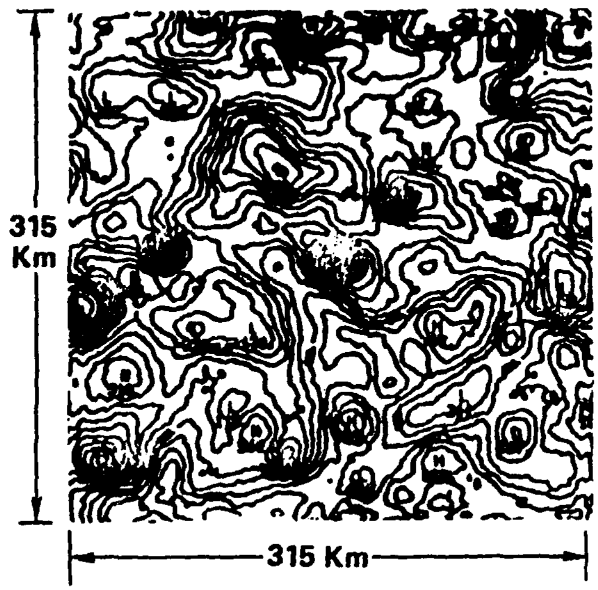

T_z

CONTOUR INTERVAL 7 M GALS

GGI NOISE MODEL $S(\omega) = \frac{10^{-5}}{\omega^2} + 50\ E^2/RAD/SEC$

Bell Aerospace TEXTRON

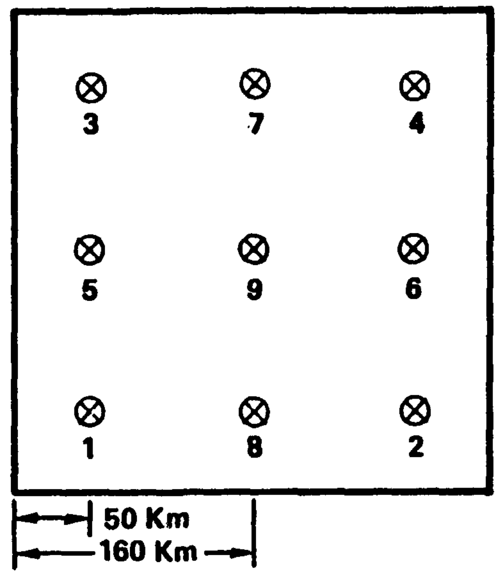

ASTROGEODEDIC TIE POINT GEOMETRY

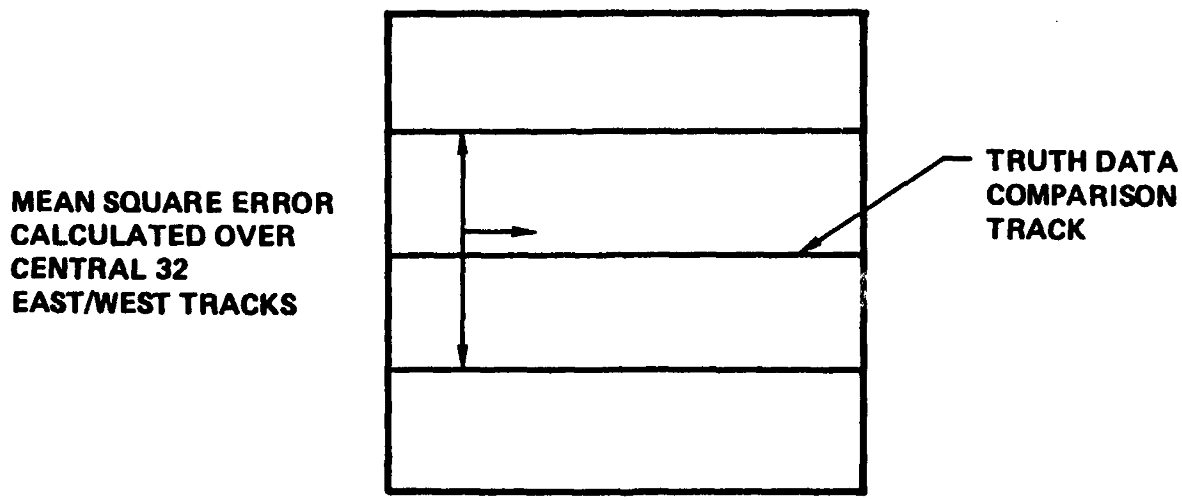

TRUTH/ESTIMATE COMPARISON

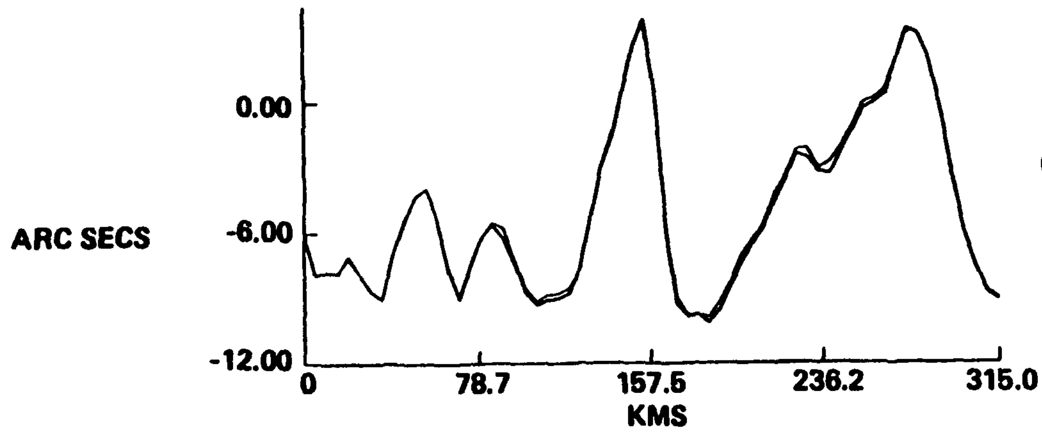

CENTER EAST/WEST TRACK TX
TRUTH AND ESTIMATE

CENTER EAST/WEST TRACK TY
TRUTH AND ESTIMATE

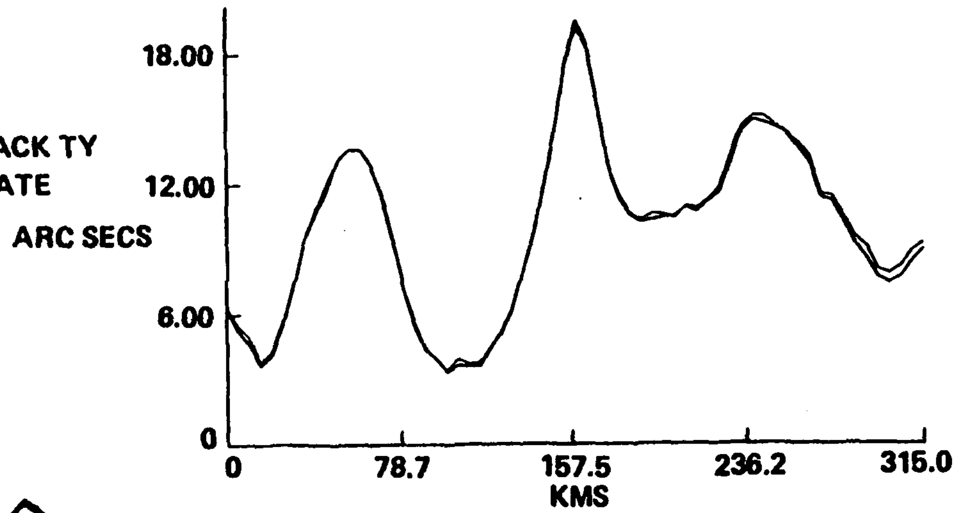

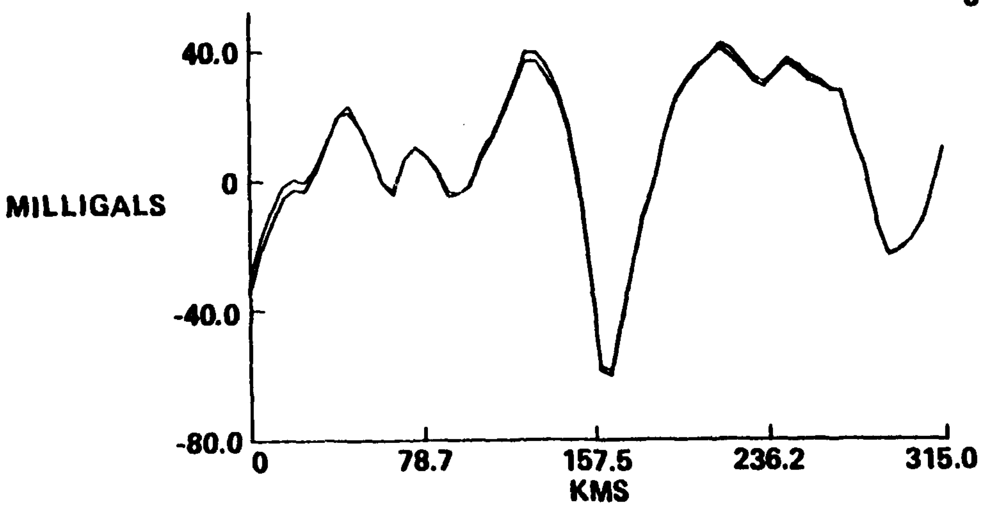

CENTER EAST/WEST TRACK TZ
TRUTH AND ESTIMATE

SIMULATION RESULTS USING
ASTROGEODEDIC TIE POINTS 1–9

Bell Aerospace TEXTRON

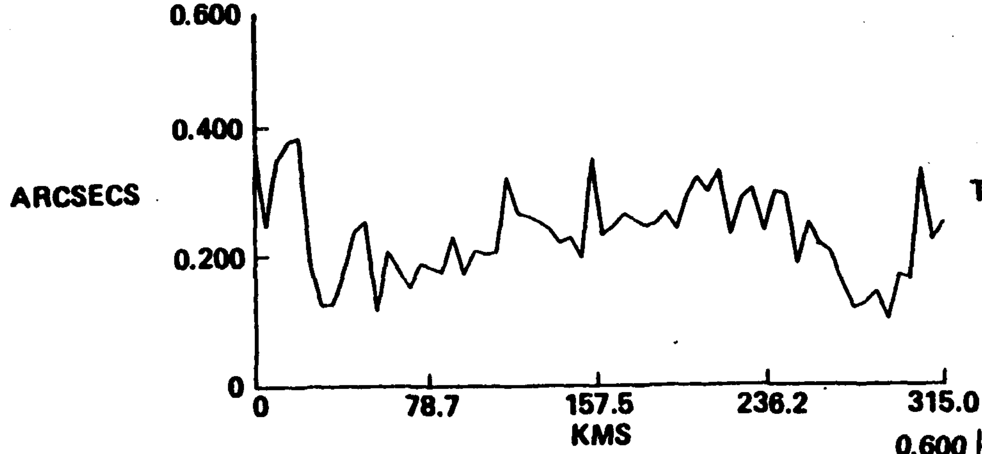

TX: ROOT MEAN SQUARED ERROR FOR CENTER 32 EAST/WEST TRACKS

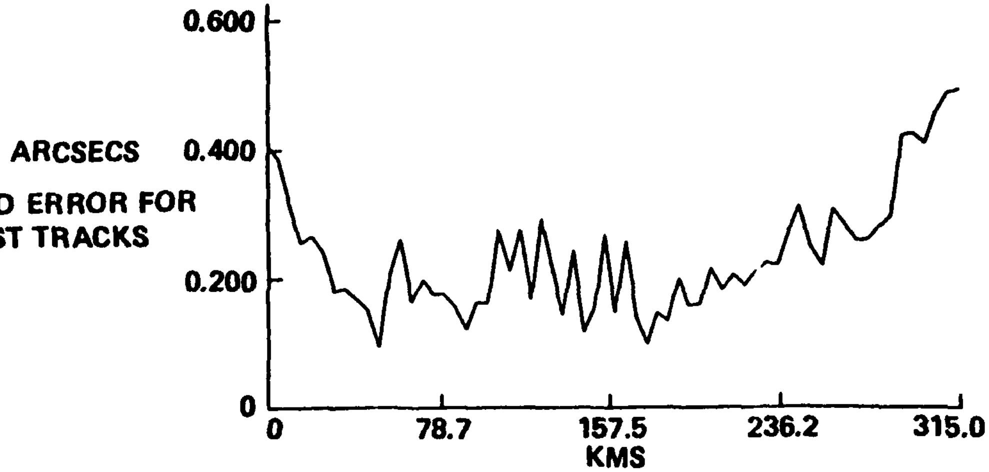

TY: ROOT MEAN SQUARED ERROR FOR CENTER 32 EAST/WEST TRACKS

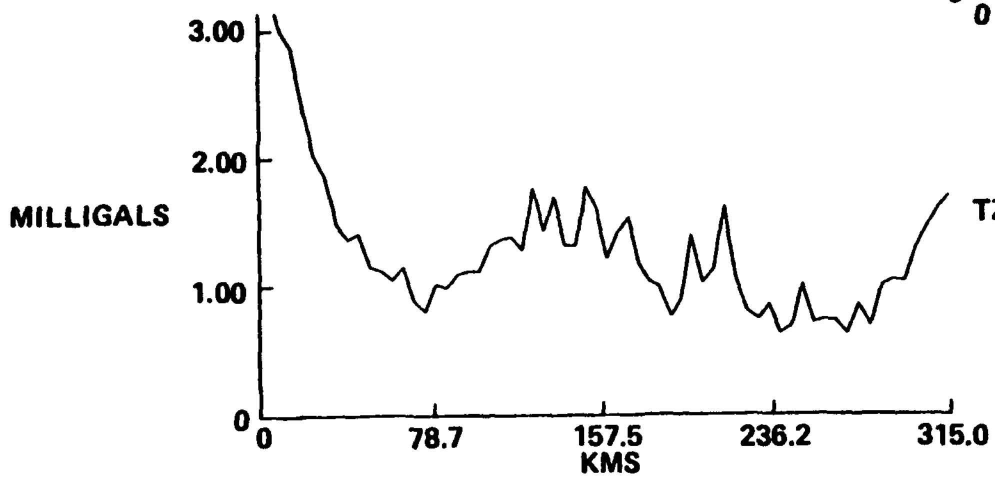

TZ: ROOT MEAN SQUARED ERROR FOR CENTER 32 EAST/WEST TRACKS

SIMULATION RESULTS USING
ASTROGEODEDIC TIE POINTS 1–9

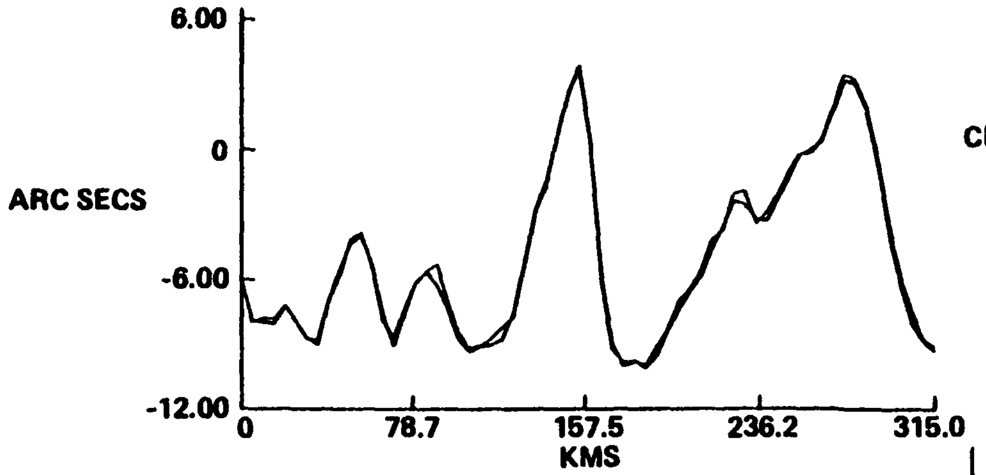

CENTER EAST/WEST TRACK TX
TRUTH AND ESTIMATE

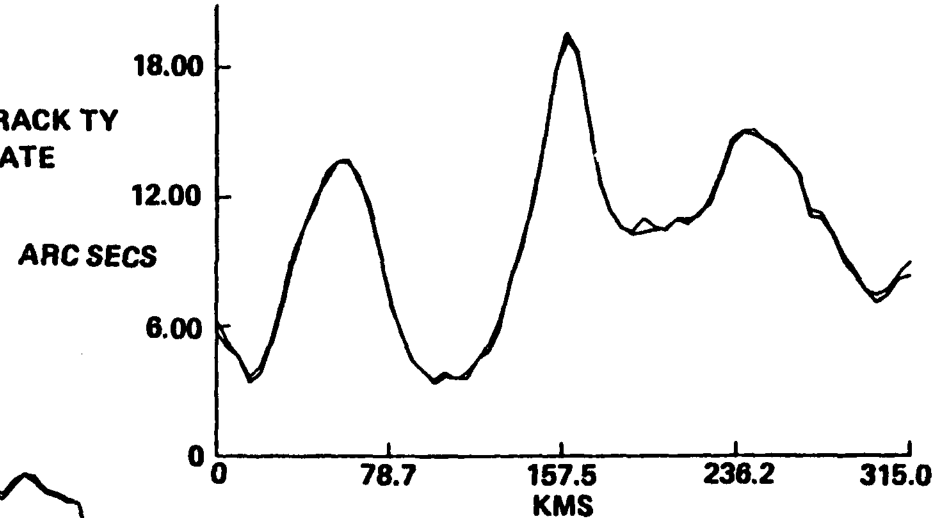

CENTER EAST/WEST TRACK TY
TRUTH AND ESTIMATE

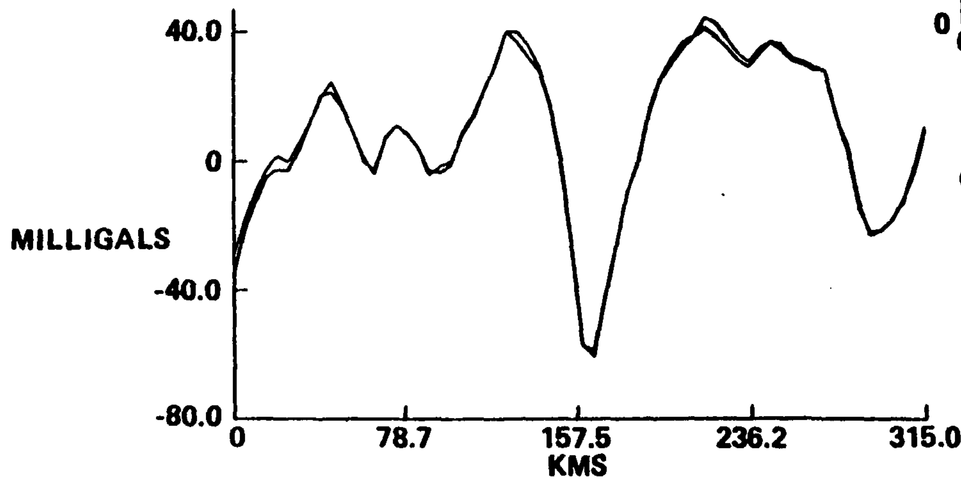

CENTER EAST/WEST TRACK TZ
TRUTH AND ESTIMATE

SIMULATION RESULTS USING
ASTROGEODEDIC TIE POINTS 1–8

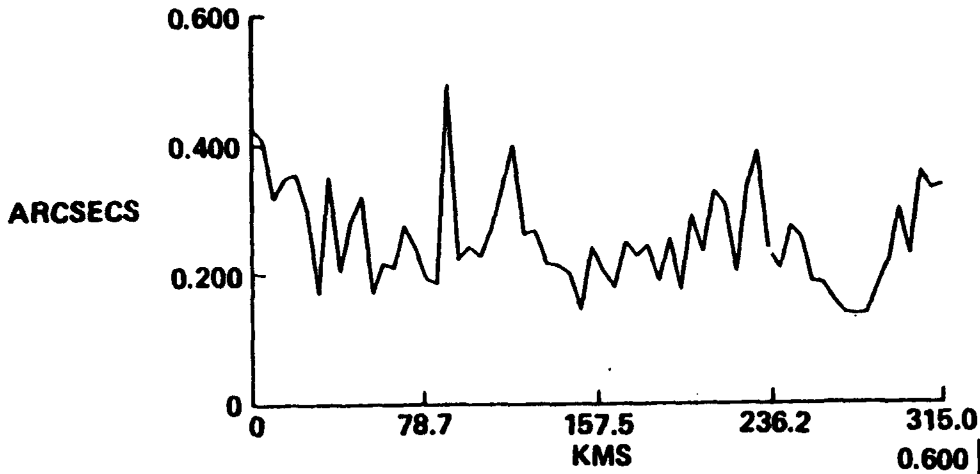

TX: ROOT MEAN SQUARED ERROR
FOR CENTER 32 EAST/WEST TRACKS

TY: ROOT MEAN SQUARED ERROR
FOR CENTER 32 EAST/WEST TRACKS

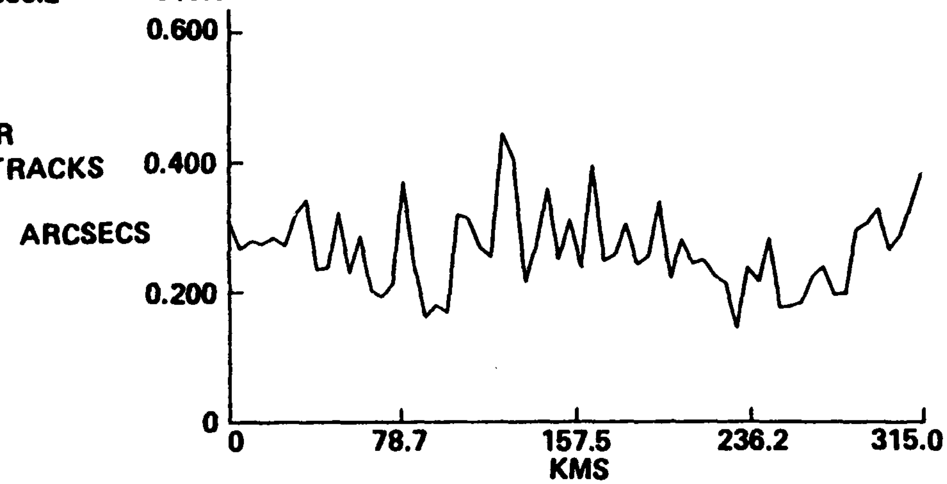

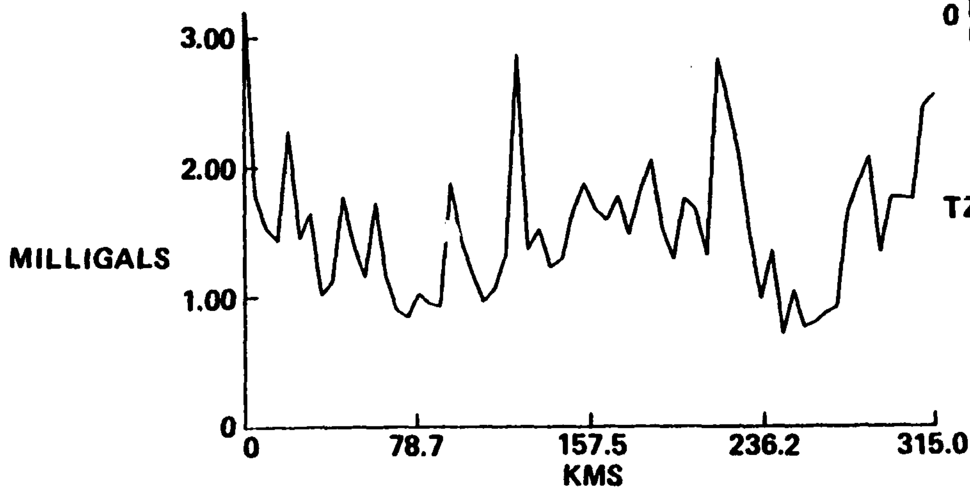

TZ: ROOT MEAN SQUARED ERROR
FOR CENTER 32 EAST/WEST TRACKS

SIMULATION RESULTS USING
ASTROGEODEDIC TIE POINTS 1–8

Bell Aerospace TEXTRON

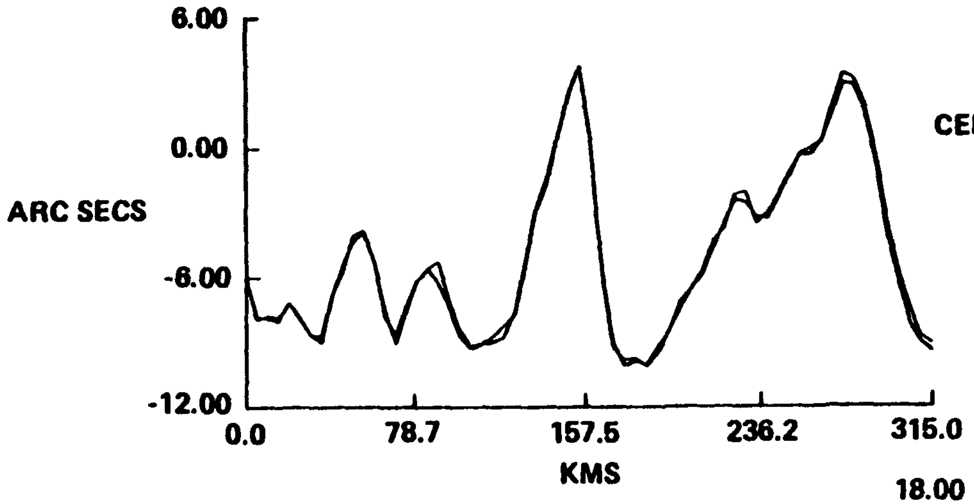

CENTER EAST/WEST TRACK TX
TRUTH AND ESTIMATE

CENTER EAST/WEST TRACK TY
TRUTH AND ESTIMATE

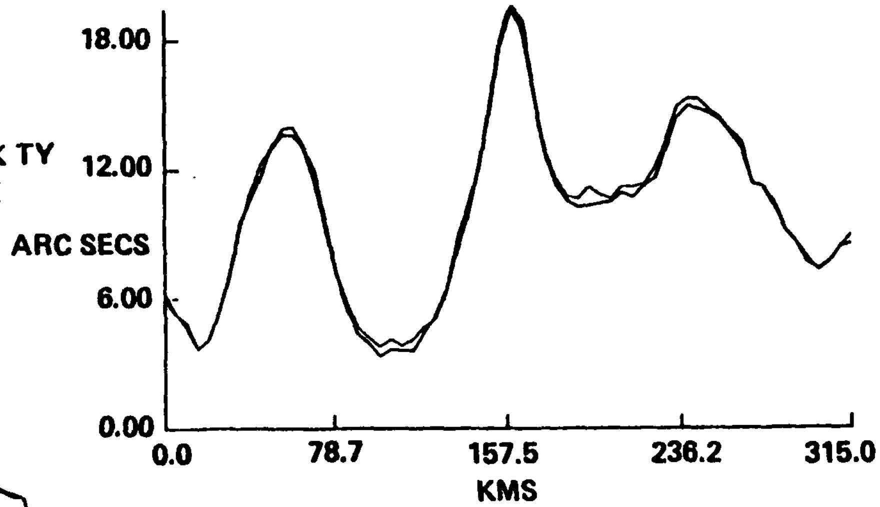

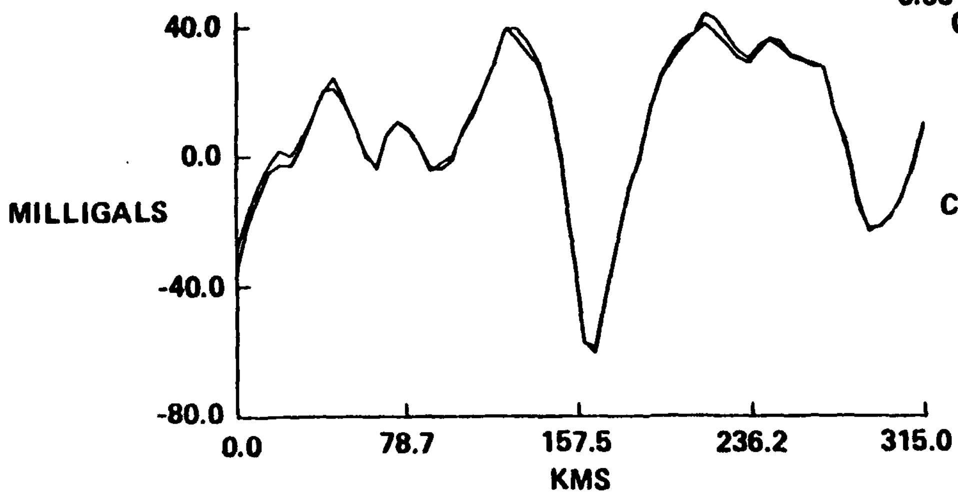

CENTER EAST/WEST TRACK TZ
TRUTH AND ESTIMATE

SIMULATION RESULTS USING
ASTROGEODEDIC TIE POINTS 1–4

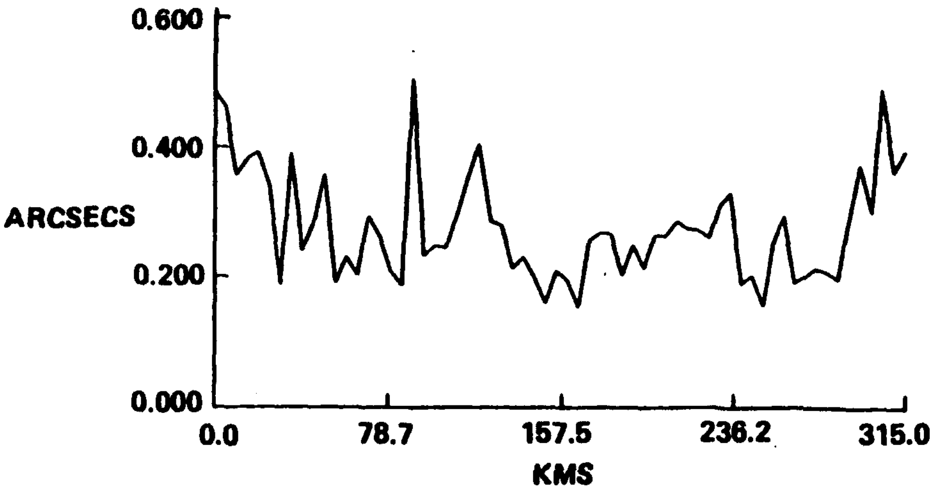

TX: ROOT MEAN SQUARED ERROR FOR CENTER 32 EAST/WEST TRACKS

TY: ROOT MEAN SQUARED ERROR FOR CENTER 32 EAST/WEST TRACKS

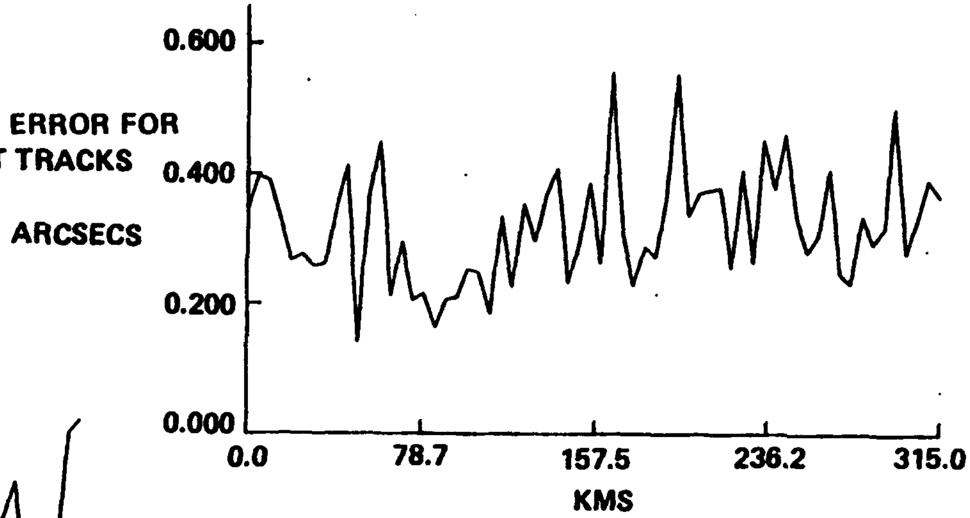

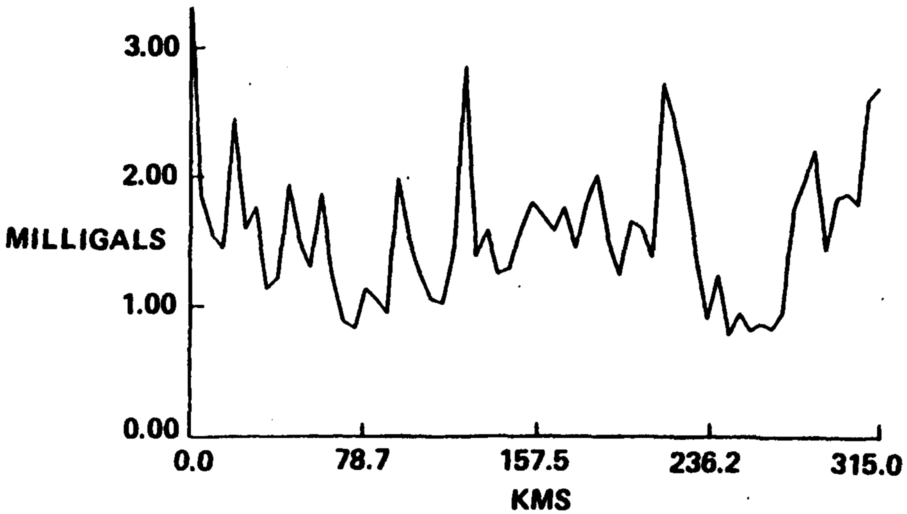

TZ: ROOT MEAN SQUARED ERROR FOR CENTER 32 EAST/WEST TRACKS

SIMULATION RESULTS USING ASTROGEODEDIC TIE POINTS 1–4

Bell Aerospace TEXTRON

Overall Error Standard Deviation

NUMBER OF ASTROS USED	T_x	T_y	T_z
9	.24"	.25"	1.46 gal^{-3}
8	.26"	.27"	1.63 gal^{-3}
4	.28"	.33"	1.67 gal^{-3}

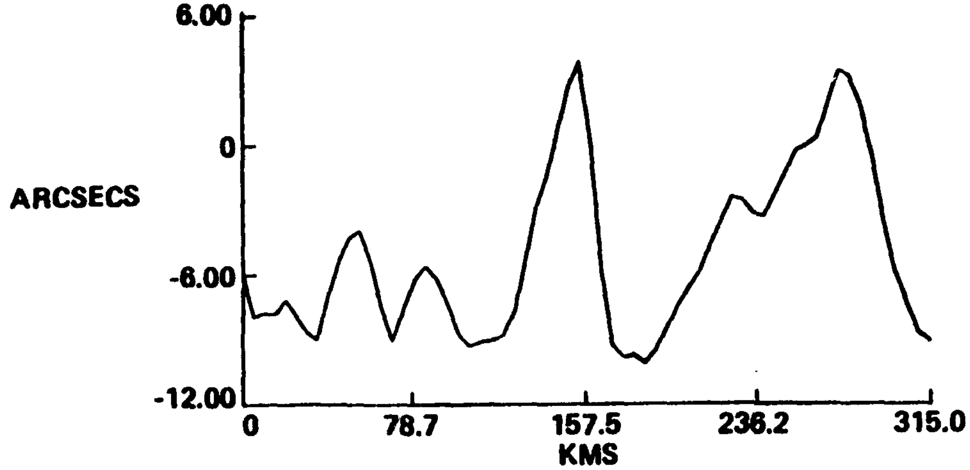

CENTRAL EAST/WEST TRACK TX
TRUTH AND ESTIMATE

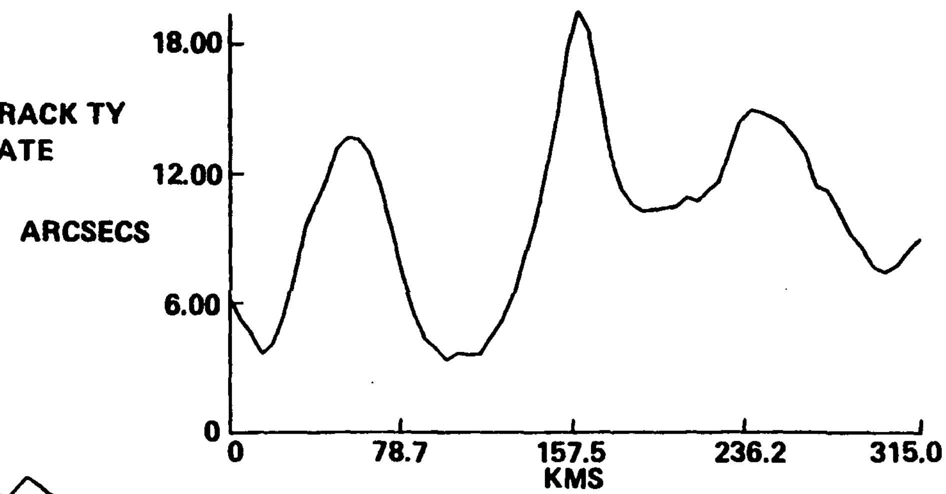

CENTRAL EAST/WEST TRACK TY
TRUTH AND ESTIMATE

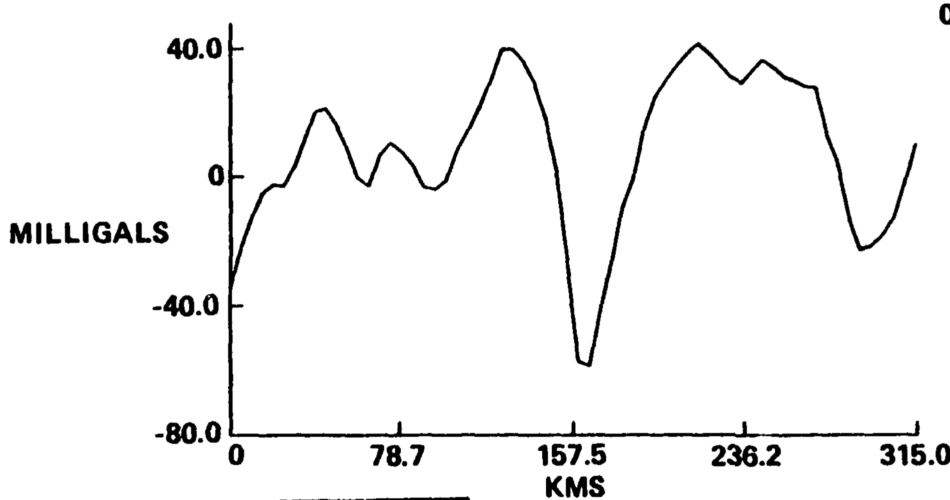

CENTER EAST/WEST TRACK TZ
TRUTH AND ESTIMATE

SIMULATION RESULTS USING
ASTROGEODEDIC TIE POINTS 1–8
AND ZERO GRADIOMETER NOISE

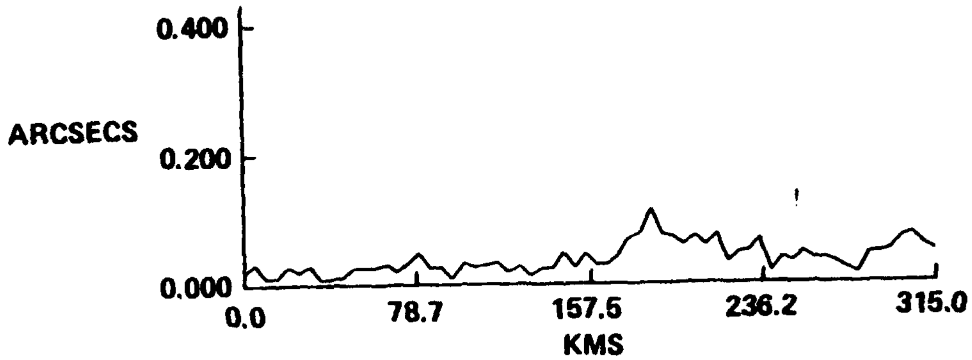

ROOT MEAN SQUARED ERROR
IN TX ESTIMATE OVER CENTRAL 4
EAST/WEST TRACKS

ROOT MEAN SQUARED ERROR
IN TY ESTIMATE OVER CENTRAL 4
EAST/WEST TRACKS

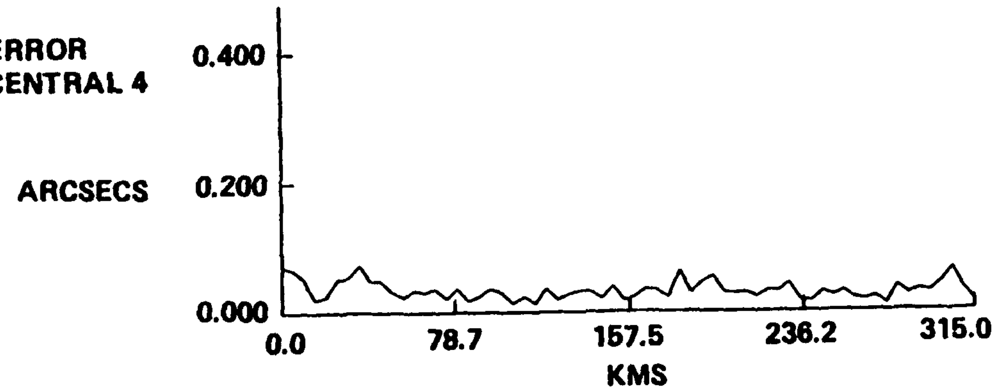

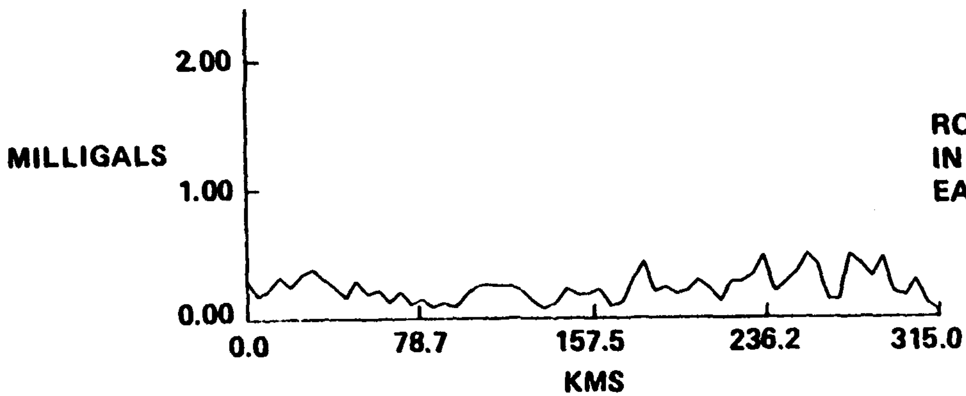

ROOT MEAN SQUARED ERROR
IN TZ ESTIMATE OVER CENTRAL 4
EAST/WEST TRACKS

SIMULATION RESULTS USING
ASTROGEODEDIC TIE POINTS 1–8
AND ZERO GRADIOMETER NOISE.

Main Results

- STAGE II ALGORITHMS APPEAR TO BE ROBUST TO MODEL MISMATCH BETWEEN TEXAS 7 TERM CORRELATION MODEL AND NSWC SYNTHETIC FIELD.
- ERROR IS IN THE ~~2.5~~ 0.25 ARC SEC RANGE FOR T_x AND T_y AND THE 1.5 MILLIGAL RANGE FOR T_z AT THE TRACK CROSSING POINTS.

TITLE OF PAPER: Stage II Simulation Results Using the NSWC Synthetic Gravity Field

SPEAKER: Al Jircitano

QUESTIONS AND COMMENTS:

1. Question: Chris Jekeli

What was the white noise of the gradiometer?

Response:

50 E^2/Hz

2. Question: Alan Rufty

Were all tracks of predicted answers coincident with the given data tracks?

Response:

Yes, but the answers degrade minimally as one goes away from the raw data tracks.

3. Question: Richard Rapp

What was the accuracy of the tie points?

Response:

Approximately 0.1 arcsec for deflections and 0.1 mgal for disturbances.

4. Question: John Brozena

Are the tie point data used to constrain the least squares track adjustments?

Response:

Yes.

GRADIENT INFORMATION IN NEW HIGH DEGREE SPHERICAL HARMONIC EXPANSIONS

by

Dr. Richard H. Rapp
Ohio State University
Department of Geodetic Science and Surveying
1958 Neil Avenue
Columbus, Ohio 43210-1247

ABSTRACT

Spherical harmonic expansions can be used to describe the earth's gravitational field. The resolution of these fields depends on the highest degree in the field. In the past year several fields to degree 180 (OSU81), 200 (GPM2), 250 (OSU86C/D) and 360 (OSU86E/F) have become available. Such fields are needed to compute geoid undulations, deflections of the vertical, etc., or to provide a reference field for reductions of local data, such as altimeter or gradiometer data. This presentation will consider the gradient information in these new fields and will compare solution differences with formal accuracy estimates to assess the accuracy of these new fields.

Gradient Information in New High Degree Spherical Harmonic Expansions

Richard H. Rapp

15th Gravity Gradiometry Conference

February 1987

Abstract

Spherical harmonic expansions can be used to describe the earth's gravitational field. The resolution of these fields depends on the highest degree in the field. In the past year several fields to degree 180 (OSU81), 200 (GPM2), 250 (OSU86C/D) and 360 (OSU86E/F) have become available. Such fields are needed to compute geoid undulations, deflections of the vertical, etc., or to provide a reference field for reductions of local data, such as altimeter or gradiometer data. This presentation will consider the gradient information in these new fields and will compare solution differences with formal accuracy estimates to assess the accuracy of these new fields.

High Degree Fields

Recent Developments

- OSU81
- GPM2 - 1985
- OSU86C/D
- OSU86E/F

New High Degree Fields

OSU86C, OSU86D

- June 1986 1 x 1 Terrestrial Anomalies
- 1985 1 x 1 Altimeter Derived Anomalies
- GEML2' Potential Coefficients
- OSU86D Uses Geophysically Predicted Anomalies
- OSU86C Excludes Geophysically Predicted Anomalies
- Least Squares Combination Followed By Rigerous Optimal Estimation To n=250

New High Degree Fields

OSU86E, OSU86F

- August 1986 30'x30' Terrestrial Anomalies
- 1985 30'x30' Altimeter Derived Anomalies
- Solutions Made By Forcing Mean of 30'x30' Values to Agree with Adjusted 1 Values
- OSU86E - No Geophysical Anomalies
- OSU86F - Includes Geophysical Anomalies
- Coefficient to n=360 by Quadratures (HARMIN)

Solution Comparisons

- Accuracy Estimates
- Anomalies
- Gravity Disturbances
- Deflections of the Vertical
- Gradients

RMS Values *Implied By OSU86F Field

	To 180	To 360
Anomaly (mgal)	± 24. 6	±26.9
Disturbance (mgal)	± 30. 3	±32.3
Deflection (secs)	± 6. 0	± 6.4
Undulation (m)	± 30. 4	±30.4
Gradient (Tzz)(E)	± 3. 4	± 5.5
Gradient (Txx)(E)	± 1. 7	± 2.8

* on the surface of a sphere of radius 6371 km

Comparison of RMS Values *Implied By OSU86F and GPM2 to Degree 180

	OSU86F	GPM2
Anomaly (mgal)	± 24. 6	±26.8
Disturbance (mgal)	± 30. 3	±32.2
Deflection (secs)	± 6. 0	± 6.4
Undulation (m)	± 30 . 4	±30.5
Gradient (Tzz)(E)	± 3. 4	± 4.1
Gradient (Txx)(E)	± 1 . 7	± 2.1

* on the surface of a sphere of radius 6371 km

Applications in Gradiometry

Provide Long Wavelength Information

- Definition of Long Wavelength (>500 km)
- Corresponding Degree About 80
- Gravity Disturbances of Prime Interest?
- Accuracy of OSU86D
- Comparison of OSU86F and GPM2

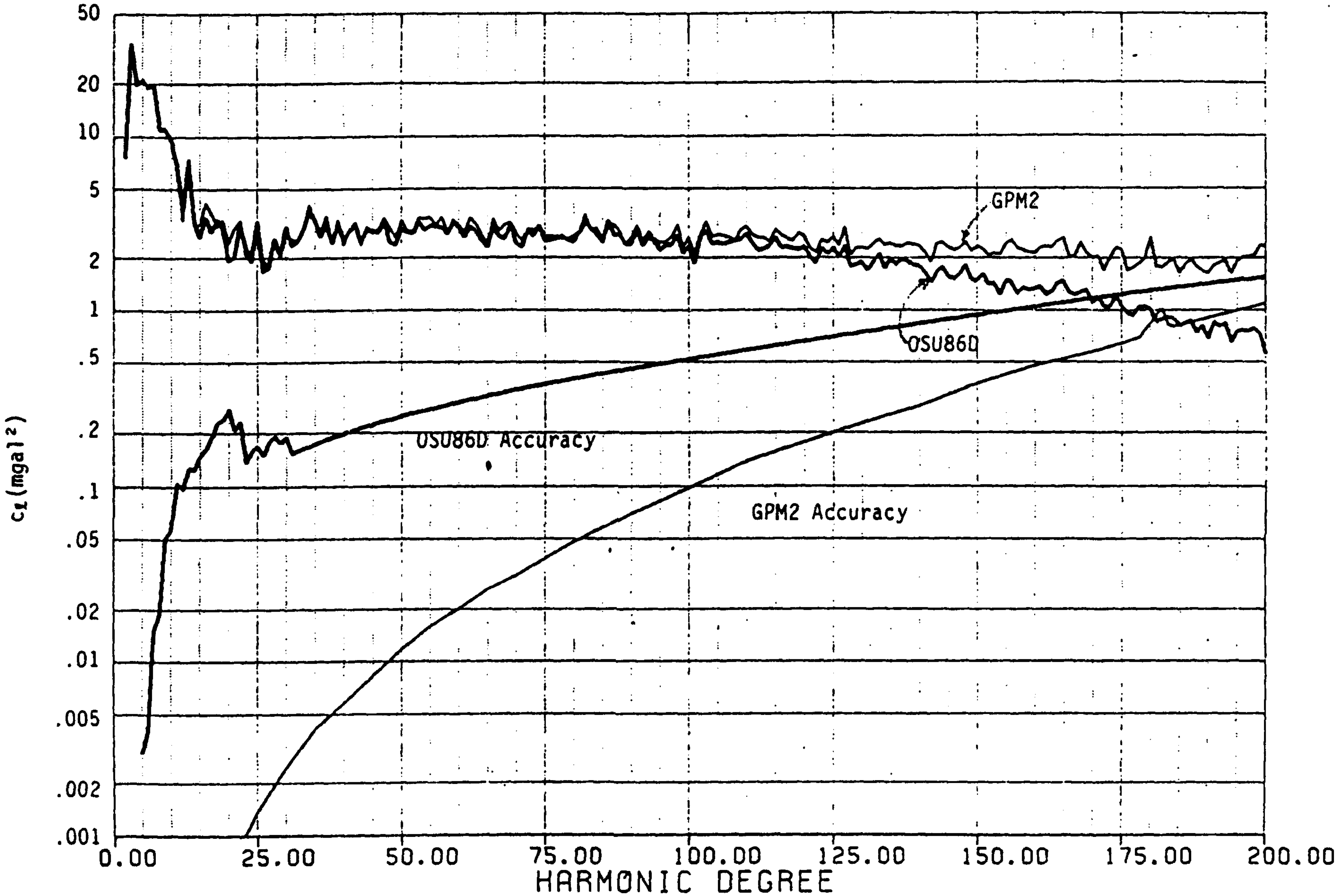

Anomaly Degree Variances and Their Accuracy

Gravity Disturbance Accuracy: OSU86D solution
Gravity Disturbance Difference: OSU86F - GPM2

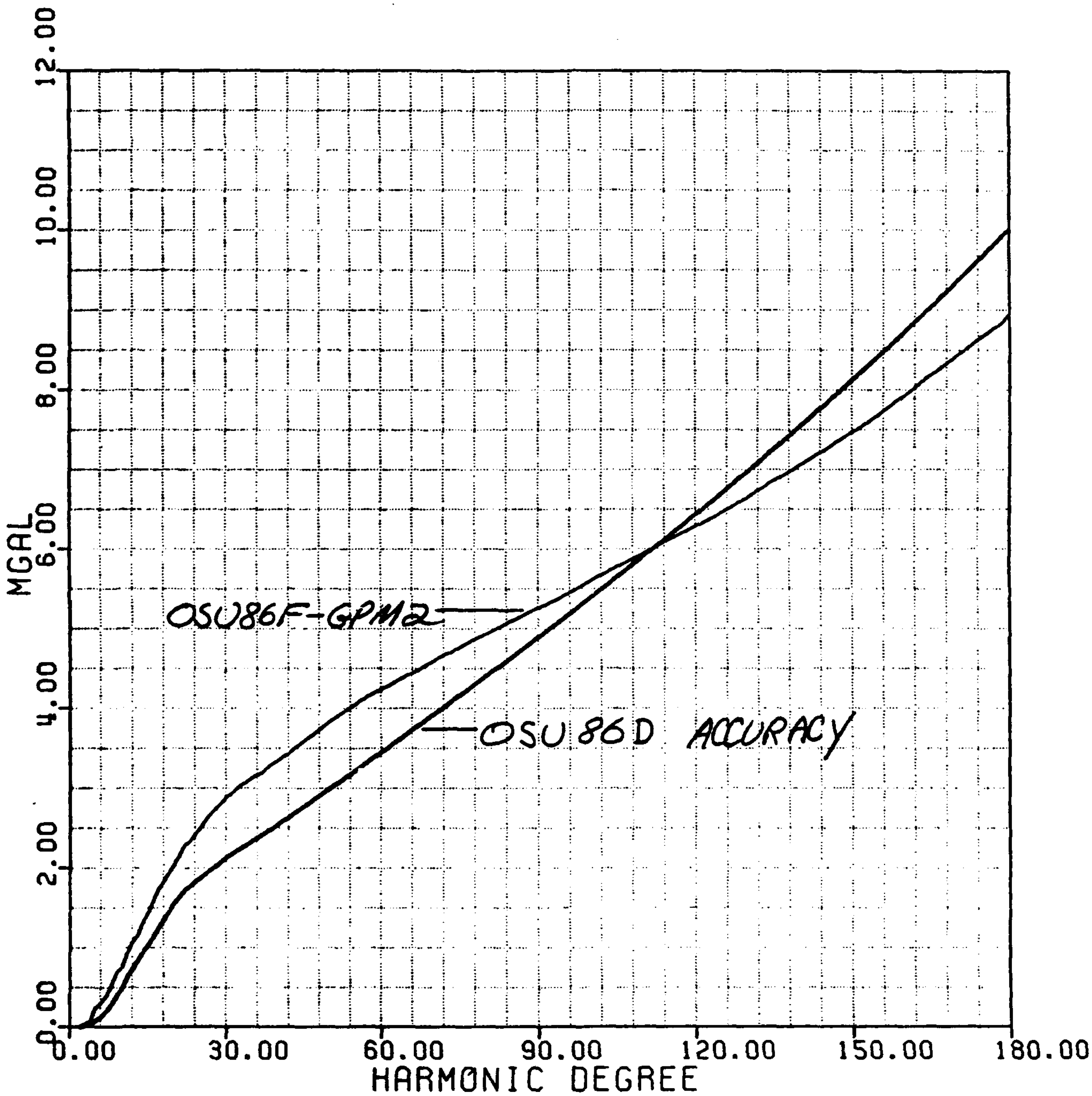

Gravity Disturbance Accuracy: OSU86D solution
Gravity Disturbance Difference: OSU86F - GPM2

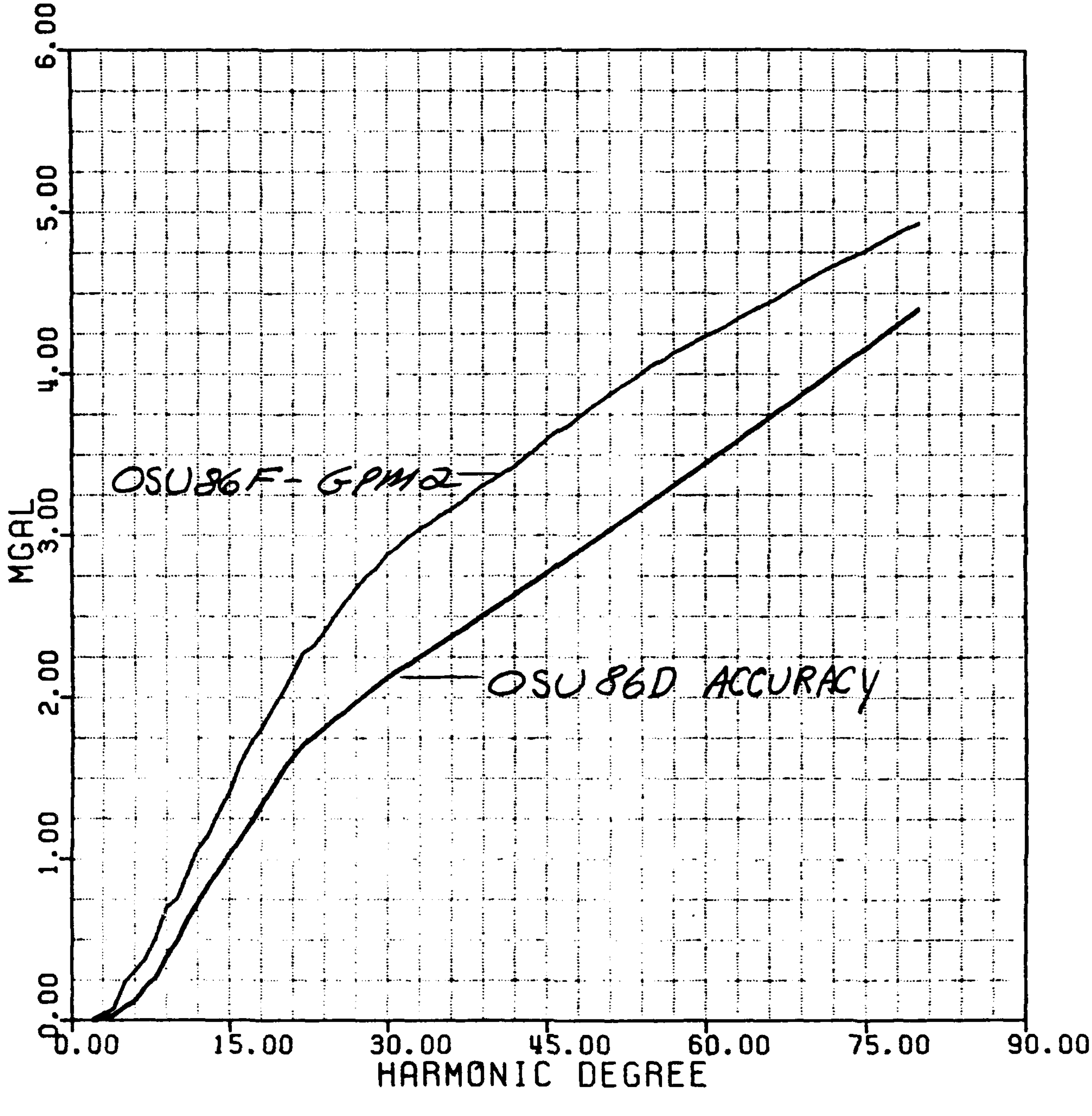

Deflection Accuracy: OSU86D solutions
Deflection Difference: OSU86F - GPM2

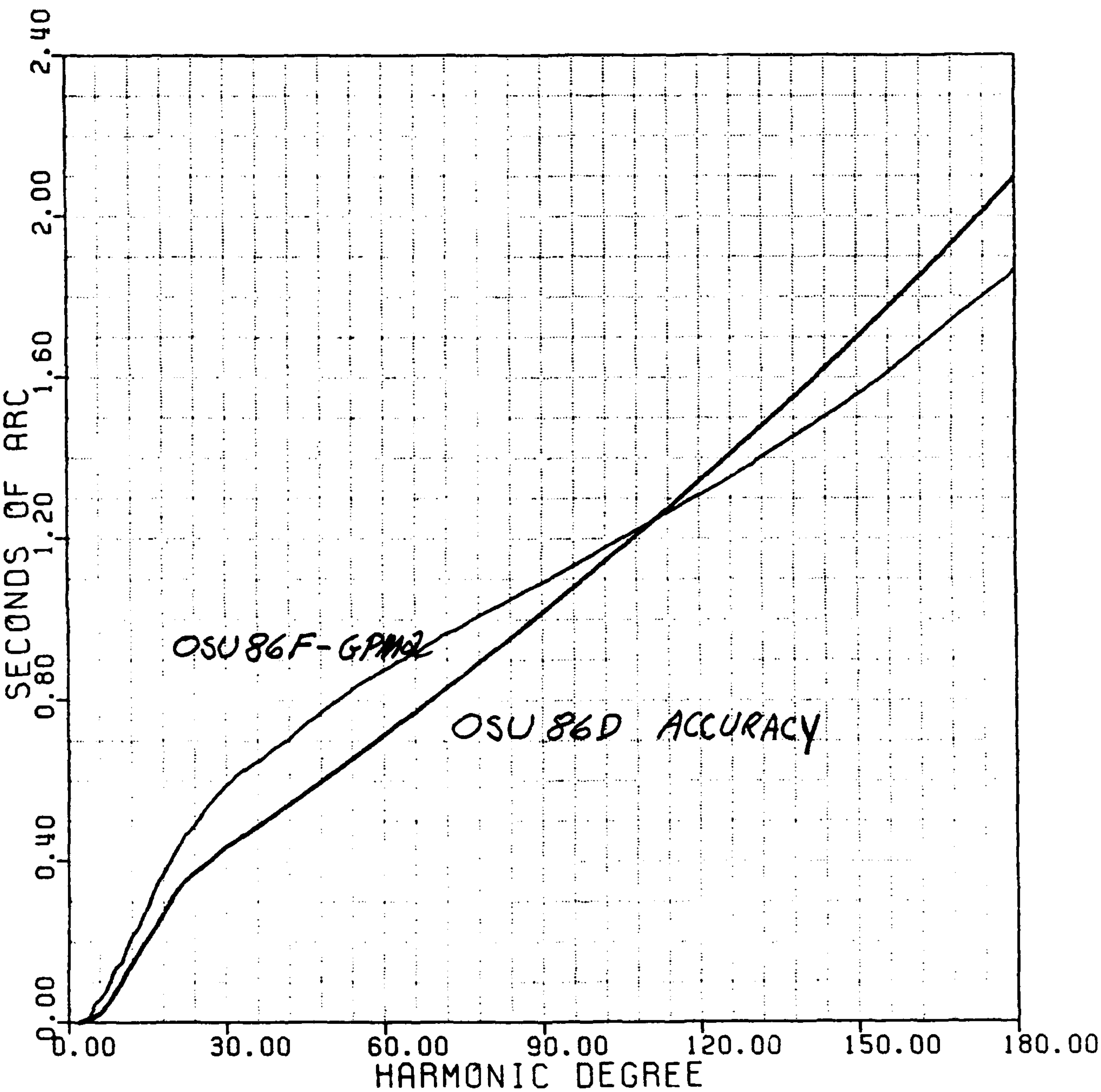

Conclusions

- Improved High Degree Fields Exist
- RMS Disturbance Accuracy is 4.3 mgal
- RMS Disturbance Difference in the U.S. Between OSU86 and GPM2 is 2.5 mgal
- RMS Global Disturbance Difference is 4.8 mgal
- RMS Total Deflection Accuracy is 0.9 secs
- RMS Total Deflection Difference is 1.0 secs
- All above values for degrees 2 to 80

Gravity Disturbance Differences (OSU86F-GPM2)

1 mgal contour interval

RMS Difference : 2.5 mgal

MAX Difference : -10.7 mgal

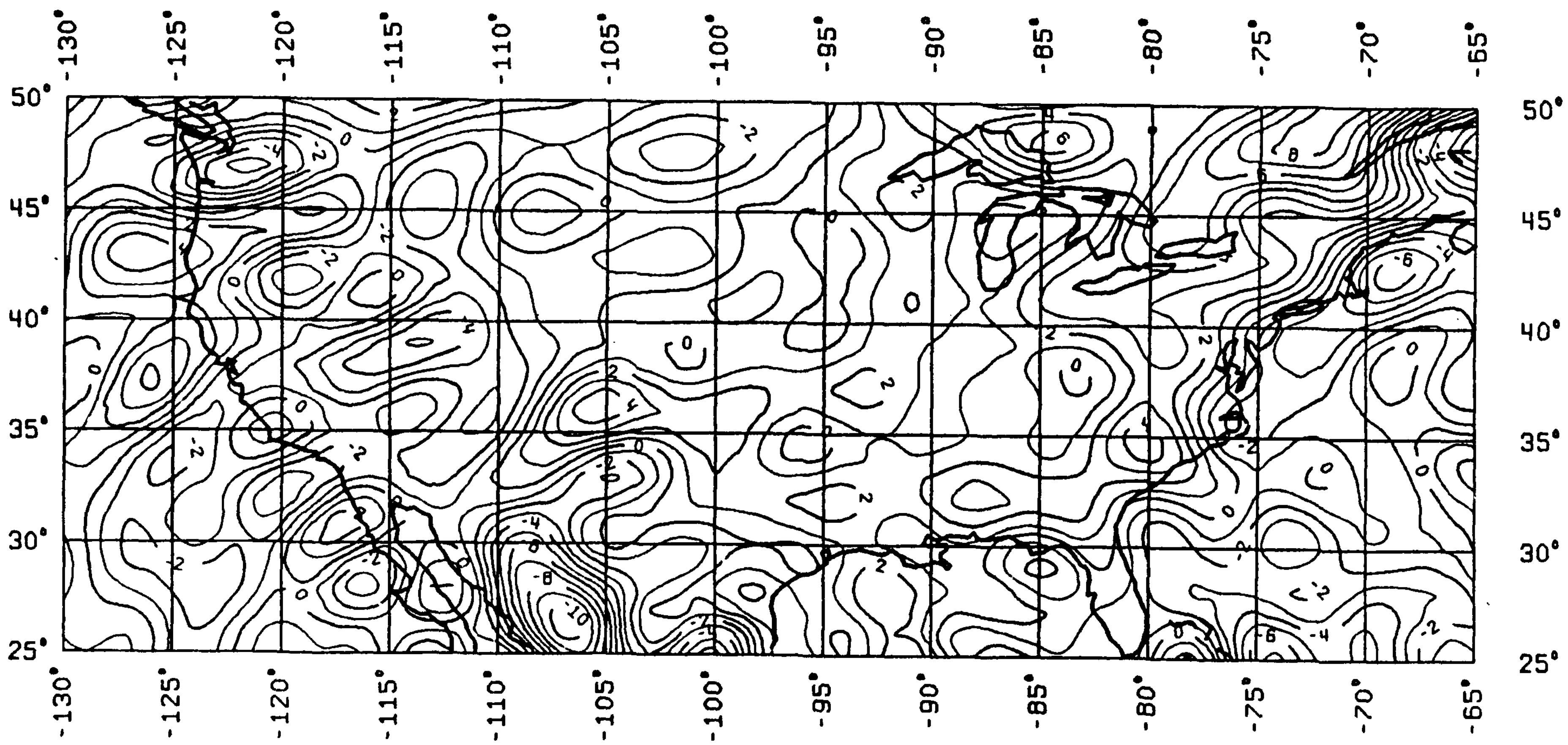

Deflection Accuracy: OSU86D solutions
Deflection Difference: OSU86F - GPM2

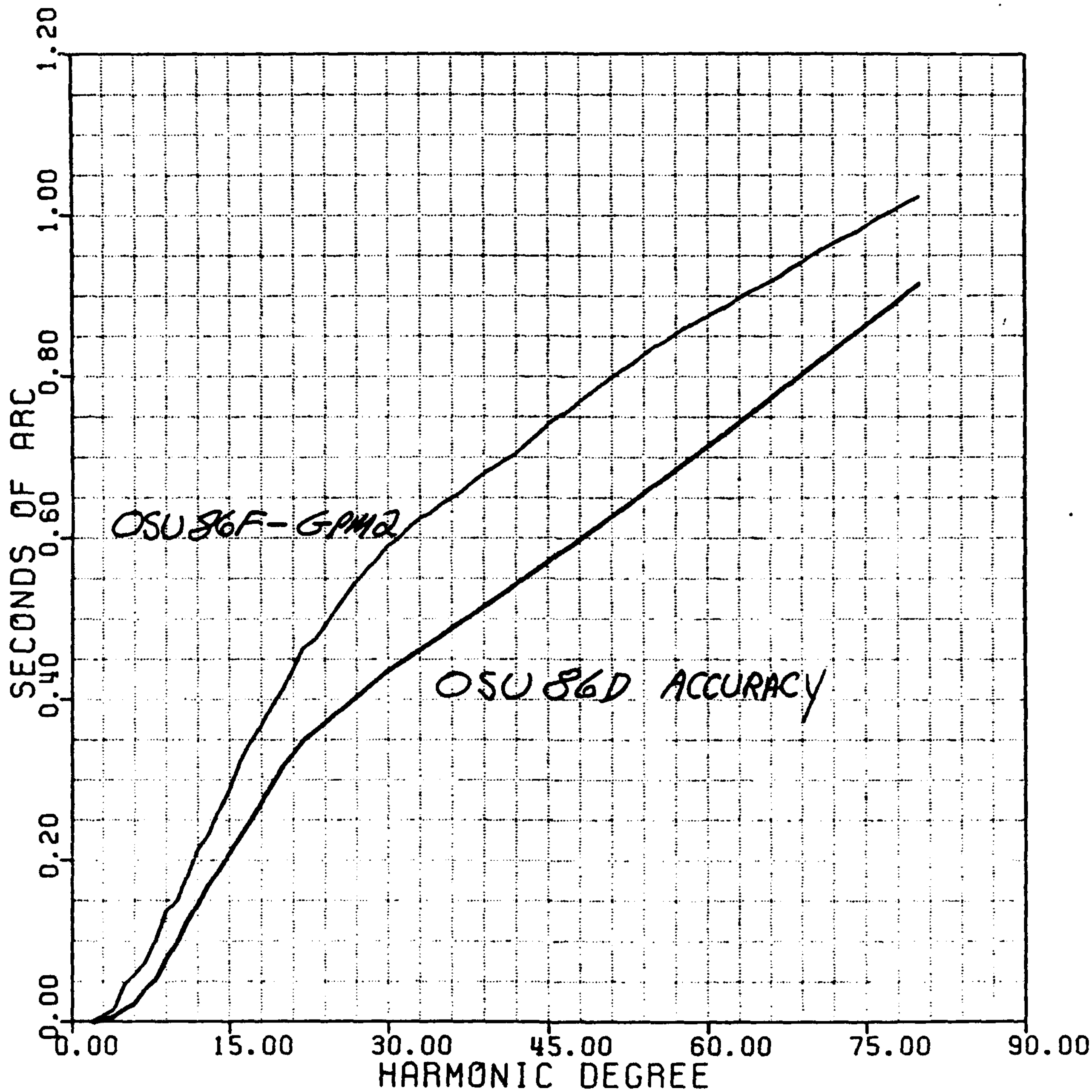

TITLE OF PAPER: Gradient Information in New High Degree Spherical Harmonic Expansions

SPEAKER: Richard H. Rapp

QUESTIONS AND COMMENTS:

1. Question: Charles F. Martin

To what extent is the observational data powerful enough to support harmonic expansion up to degree and order 360°?

Response:

It depends on the quality of data over the areas of interest, i.e., U.S., Central Europe, Marianas Trench. Input data of high quality and harmonic field above 180° provides significant information.

2. Question: Al Jircitano

Is accuracy of gravity data better in ocean areas or land areas?

Response:

Generally better in land areas. In the US and Europe, the accuracy is about 2-3 mgal in 1° squares; in ocean areas it is about 6-7 mgal in 1° squares.

3. Question: Warren Heller

What do you see as the primary error sources driving the approximately 4 mgal of error in harmonics through degree 80?

Response:

Primarily surface data quality and data omission. (Some discussion of advantages of considering local areas where data is good; also discussion of correlation between satellite and terrestrial gravity measurement errors).

4. Question: Jim Lowrey

Are there any plans to extend the model out beyond 360°?

Response:

Curently there are none; however, an extension out to 720 would be possible although the need for this is questionable.